THERMODYNAMICS-BASED DESIGN OF STIRLING ENGINES FOR LOW-TEMPERATURE HEAT SOURCES

A thesis submitted in partial fulfilment
of the requirements for the Degree of
Doctor of Philosophy
in
Mechanical Engineering

by
Benedikt Hoegel

University of Canterbury

2014

Contents

List of Figures

Introduction

Simulation of Stirling engines

Identification of a suitable LTD design

Thermodynamic optimisation of the LTD

Mechanical efficiency

Implications for LTD design

Comparison of ORC and Stirling machinery

Appendix

List of Tables

Acknowledgements

First, I would like to thank my supervisory team at the University of Canterbury (in order of appearance): Dr Michael Gschwendtner for constant support, discussion, enthusiasm and energy which made this project a success against all odds. Dr Alan Tucker not only for constant input and interest throughout the project but also for chasing down every last semicolon proofreading the thesis; despite his well-deserved retirement he was one of the constants during my stay in New Zealand. Dr David Aitchison for taking over Alan's role as senior supervisor and contributing new perspectives and his expertise. Dr Mathieu Sellier for advice and spicing up the thesis and publications. Last but not least Dr Dirk Pons for always having an open door and time for discussions, general guidance through Canterbury's administrative system, the best meeting minutes ever, and his famous Kaiapoi honey.

I would also like to thank my examiners, Professor Khamid Mahkamov and Professor John Raine, who provided detailed and constructive feedback. Their expertise and hands-on experience was much appreciated for the final version of the thesis.

This project was possible only with the generous support from Mighty River Power Ltd who funded my scholarship amongst other, more popular, topics at the University of Canterbury. Special thanks to Joe Gammon for his enthusiasm and for pushing the project in its early stages which made it possible at all. Michael Rock and later Andrew Marsh provided helpful input and insights for the understanding of the geothermal heat source and its peculiarities.

Many thanks to Professor Henrik Carlsen from the Technical University of Denmark and to Dr Tor-Martin Tveit from Single Phase Power AS for sharing experimental data which helped to validate the thermodynamic model.

Also essential for the success of this endeavour were my friends here and overseas who helped me to establish a proper work-life balance. Thanks to 'every each one' of you!

Last but not least, special thanks to my family and to my partner for their constant support and understanding for most of my plans and ideas, silly or not.

Abstract

Large amounts of energy from heat sources such as waste-heat and geothermal energy are available worldwide but their potential for useful power-generation is largely untapped. This is because they are relatively low temperature difference (LTD) sources, in the range from 100 to 200 °C, and it is thermodynamically difficult, for theoretical and practical reasons, to extract useful work at these temperatures. This work explores the suitability of a Stirling engine (SE) to exploit these heat sources. Elsewhere much work has been done to optimise Stirling engines for high temperature heat sources, but little is known about suitable engine layouts, and their optimal design and operational aspects at lower temperature differences. With the reduced temperature difference, changes from conventional engine designs become necessary and robust solutions for this novel application have to be identified.

This has been achieved in four major steps: identification of a suitable engine type; thermodynamic optimisation of operating and engine parameters; optimisation of mechanical efficiency; and the development of conceptual designs for the engine and its components informed by the preceding analysis. For the optimisation of engine and operating parameters a model was set up in the commercial Stirling software package, Sage, which also has been validated in this thesis; suitable parameter combinations have been identified.

This work makes key contributions in several areas. This first is the identification of methods for better simulating the thermodynamic behaviour of these engines. At low temperature differences the performance of Stirling engines is very sensitive to losses by fluid friction (and thus frequency), adiabatic temperature rise during compression, and the heat transfer from and to the surroundings. Consequently the usual isothermal analytical approaches produce results that can be misleading. It is necessary to use a non-isothermal approach, and the work shows how this may be achieved.

A second contribution is the identification of the important design variables and their causal effects on system performance. The primary design variable is engine layout. For an engine having inherently low efficiency due to the low temperature difference it is important to choose the engine layout that provides the highest power density possible in order to minimise engine size and to save costs. From this analysis the double-acting alpha-type configuration has been identified as being the most suitable, as opposed to the beta or gamma configurations. Another key design variable is working fluid, and the results identify helium and

hydrogen as suitable, and air and nitrogen as unsuitable. Frequency and phase angle are other design variables, and the work identifies favourable values. A sensitivity analysis identifies the phase angle, regenerator porosity, and temperature levels as the most sensitive parameters for power and efficiency. It has also been shown that the compression work in low-temperature difference Stirling engines is of similar magnitude as the expansion work. By compounding suitable working spaces on one piston the net forces on the piston rod can be reduced significantly. In double-acting alpha-engines this can be achieved by choosing the Siemens as opposed to the Franchot arrangement. As a result friction and piston seal leakage which are two important loss mechanisms are reduced significantly and longevity and mechanical efficiency is enhanced. Design implications are identified for various components, including pistons, seals, heat exchangers, regenerator, power extraction, and crankcase. The peculiarities of the heat source are also taken into account in these design recommendations.

A third key contribution is the extraction of novel insights from the modelling process. For the heat exchangers it has been shown that the hot and cold heat exchangers can be identical in their design without any negative impact on performance for the low-temperature difference situation. In comparison the high temperature applications invariably require different materials and designs for the two heat exchangers. Also, frequency and phase angle are found to be quite different (lower frequency and higher phase angle) from the optimum parameters found in high temperature engines. Contrary to common belief the role of dead volume has been found to play a crucial and not necessary detrimental role at low temperature differentials.

Taken together, the work is positioned at the intersection of thermodynamic analysis and engineering design, for the challenging area of Stirling engines at low temperature differences. The work extracts thermodynamic insights and extends these into design implications. Together these help create a robust theoretical and design foundation for further research and development in the important area of energy recovery.

Nomenclature

Roman Symbols

Symbol	Units	Description
A	$\mathrm{m}^3, \mathrm{m}^2$	volume amplitude, area
B_n	$-$	Beale number
c_p	$\mathrm{kJ\,kg^{-1}\,K^{-1}}$	specific heat capacity
D	m	piston diameter
E	$-$	efficiency
f	Hz	frequency
h	$\mathrm{W\,m^{-2}\,K^{-1}}, \mathrm{m}$	heat transfer coefficient, radial clearance
k	$-$	constant; volume ratio
L	m	(characteristic) length
m	kg	gas mass
M	$\mathrm{kg\,mol^{-1}}$	molar mass
N	$-$	number
p	Pa	pressure
P	W, $-$	power, porosity
Q	J	heat
r	$-$	ratio
R	$\mathrm{J\,kg^{-1}\,K^{-1}}$	specific gas constant
s	$\mathrm{J\,K^{-1}\,kg^{-1}}$	specific entropy
T	K	temperature
V	m^3	volume
W_n	$-$	West number, normalized work
W	J	work

Greek Symbols

Symbol	Units	Description
α	$^\circ$	phase angle
γ	-	adiabatic index
η	$-$	efficiency
θ	$^\circ$, rad	crank angle
λ	$\mathrm{W\,m^{-1}\,K^{-1}}$	thermal conductivity
μ	$\mathrm{Pa\,s}, -$	gas viscosity, coefficient of friction
ρ	$\mathrm{kg\,m^{-3}}$	density

Indices

Symbol	Description
c	compression, cylinder
C	cell
d	dead volume, displacer
e	expansion
eff	effective
el	electrical
gen	generator
h	hot heat exchanger
ind	indicated
k	cold heat exchanger
$mech$	mechanical
p	piston
r	regenerator
s	swept
us	unswept

Acronyms

Symbol	Description
AIP	air independent power
CFD	computational fluid dynamics
CHP	combined heat and power
FP	free-piston
GWP	global warming potential
HEPA	heat exchanger piston alternator assembly
HTD	high temperature difference engine
HX	heat exchanger
IC	internal combustion
ISEC	International Stirling Engine Conference
LTD	low temperature difference engine
MPP	maximum power point
MRP	Mighty River Power Ltd
NoC	number of cylinders
ODP	ozone depletion potential
ORC	Organic Rankine Cycle
RK	Redlich-Kwong
SE	Stirling engine
WWII	World War 2

Chapter 1

Introduction

Increasing energy demand and shrinking fossil resources make it necessary to improve the efficiency of existing power-consuming processes and to tap into energy sources that have not been used widely until now. Low temperature heat sources such as waste heat and geothermal energy in the range from 100 to 200 °C are widely available and their potential is largely untapped. In addition large amounts of heat are rejected to the atmosphere every day by industry, wasting exergy. The rising cost of energy creates a need for society to be more efficient with energy, and in-house power generation using this waste heat is an interesting option.

In 2009 a group of students investigated 15 different thermodynamic cycles as their final year project at the University of Canterbury together with Mighty River Power (MRP) [1]. The heat source considered in this project was geothermal energy at low temperatures - between 120 and 200 °C - and the conclusion reached was that Stirling engines (SE) are both economically and thermodynamically interesting and technically mature. As a consequence, this PhD project was initiated as a further development, with industry support. However, the low temperature is a challenging operating regime for the SE and the thermodynamics need to be investigated in further detail to explore its possibilities and restrictions.

1.1 Low temperature heat sources

1.1.1 The geothermal energy source and power plants

Geothermal energy has been exploited for power generation for over a hundred years. The first plants built used the hot dry steam released by the earth directly to drive a steam engine or, later, steam turbines. This convenient way of power generation is only possible as long as the reservoir temperature is high enough. Unfortunately only few sites in the world allow the direct use of dry steam. Most of these fields are already fully developed, or, if not, then their lack of development has been for good reasons, mostly conservatory or environmental. As temperatures drop, the utilisation of the geothermal energy source becomes more difficult and more elaborate technology is necessary. Down to a certain temperature wet steam can still be used to directly power the turbines but the liquid and vapour phases have to be separated prior to the turbine. This process is utilised in so-called Flash Power Plants. As long as steam comes to the surface no additional pumps are needed to exploit the reservoir. These reservoirs having exploitable temperatures above 150 °C are referred to as high temperature resources [2].

As the temperature in the reservoir drops further, steam is no longer available to drive turbines. However, the geothermal fluid, the so-called brine which is used to extract the heat from the low temperature underground resource, is predominantly water containing all sorts of chemical compounds dissolved from surrounding rock beds. As there is no longer enough steam generated to supply the plant with heat, the hot brine has to be pumped to the surface prior to power generation. Usually the used brine is re-injected into the geothermal system to keep the contamination of the atmosphere with dissolved gases (e.g. CO_2 and CH_4) low and to replenish, if necessary, the system. In these circumstances the turbine working fluid has to be replaced by one with a lower boiling point that can be expanded far enough without reaching the wet vapour zone. Although different

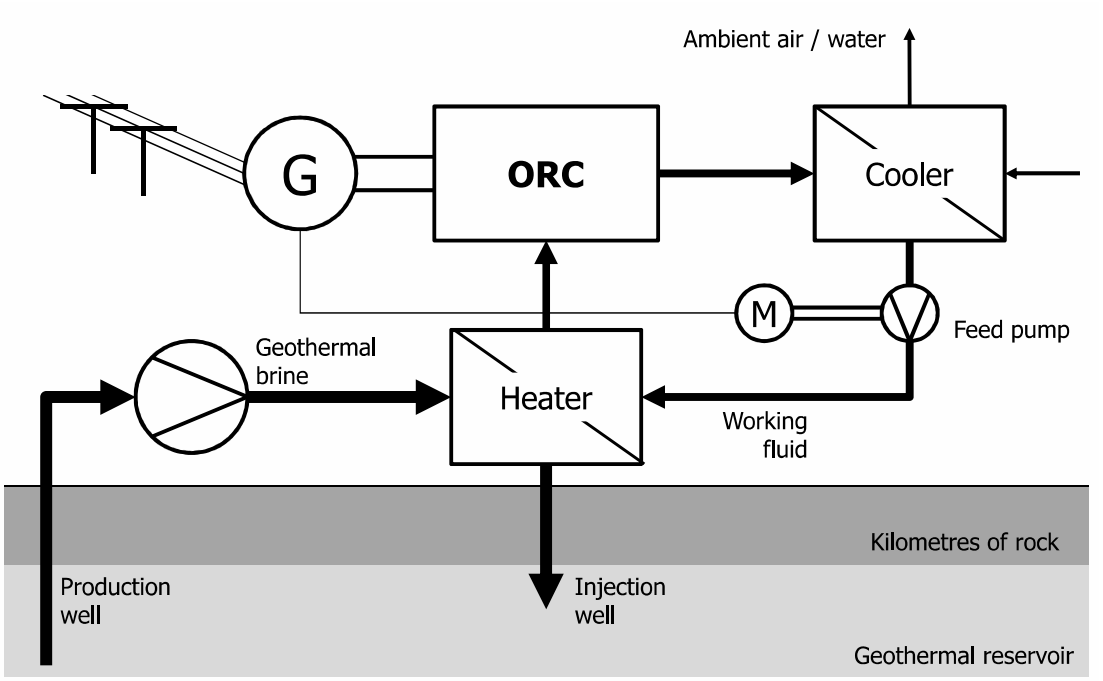

Figure 1.1: Binary cycle power plant for geothermal power generation

organic substances are possible candidates, most plants use pentane. Obviously the organic fluid is not pumped through the soil but kept in a closed system and is heated and evaporated in heat exchangers by the circulating brine [3]. Such binary cycle plants are not only used as stand-alone plants for low temperature heat resources, but are used also as bottoming cycles[1] for other geothermal power plants to improve the overall plant performance. Figure 1.1 shows a schematic diagram of a stand-alone power plant. Irrespective of the machine used to expand the working fluid the process is referred to as Organic Rankine Cycle (ORC). The heated and gaseous working fluid expands in a turbine or a similar device which drives a generator to produce electricity. It is then condensed in the cooler. Back in its liquid state it is compressed by the feed pump and moved back to the heater where it is evaporated again.

[1]Cascaded heat utilisation is a common principle to improve the efficiency of power plants. At least two power generating cycles are combined where the heat rejected from one cycle is the heat source of the next cycle. Another example is the Combined Cycle Gas Turbine (CCGT) where the exhaust gases from a gas turbine power a steam turbine [4].

An alternative to the ORC is the Kalina cycle [5, 6]. Here, a mixture of water and ammonia is heated and then separated; the ammonia expands in a turbine which drives the generator. After expansion the two working fluid streams are mixed again. The system uses a number of heat exchangers and recuperators to improve its efficiency which add to the complexity and cost of the system. Kalina cycle plants are especially suitable for heat source temperatures below 100 °C [7, 8]. However, a comparison between the Kalina cycle and the ORC by DiPippo suggests that efficiency improvements achievable with the Kalina cycle are only marginal [9]; even for small temperature differences the ORC appears to become the standard solution since the number of units installed is growing whereas the Kalina cycle remains a more exotic choice.

The lower the temperature and thus the exergy[2] the larger is the geothermal exploitable potential that exists worldwide, but the equipment to do so gets much more expensive, up to the point where economics prevent plant construction. Also, binary cycles using a turbine usually are not economical for small scale power generation (<1 MW) [10]. Unable to compete at high power ratings of tens or hundreds of megawatts, a reciprocating engine could be advantageous for smaller systems. Lund [11] gives several examples for small scale geothermal power plants using temperature levels as low as 81 °C up to 250 °C, producing net power outputs ranging from 20 kW to 5 MW. The lowest temperature of a geothermal heat source currently used to generate electricity is 74 °C [12–15]. The plant location is in Chena, Alaska, and around 400 kW_e can be produced with a heat sink temperature of 4 °C.

Every geothermal field has different characteristics. Not only do the temperature levels vary from site to site and well to well but so do flow rates. Well

[2] In a thermodynamic system the exergy is the maximum useful work possible. The higher the temperature difference between two systems, the higher the exergy. Thus a geothermal system with a large amount of energy but at low temperatures (50-100 °C) is not well suited for power generation, but can be interesting as an energy source for district heating or industrial heat.

head pressure, porosity of the underground, well design, thermal conductance of the surrounding rock, chemistry and other factors influence the well performance. Franco and Villani [16] propose 20 to 120 $\mathrm{kg\,s^{-1}}$ brine mass flow per MW installed plant power to be economically viable.

Another peculiarity of brine from geothermal sources is that large amounts of minerals are dissolved in the fluid. If their limit of solubility is reached at a certain temperature they come out of solution and aggregate on surfaces. Calcium carbonate scaling is usually not a problem for the power plant components, as its solubility increases with decreasing temperature, but silica scaling is a major factor to be considered in the utilisation of geothermal fluids. Surfaces cooler than the brine become clogged with quartz-like structures. Heat transfer is then much diminished in the case of heat exchangers. Therefore silica scaling has to be controlled either chemically or mechanically, and heat exchangers have to be designed for that special environment, requiring that they be easy to clean and accessible for maintenance. However, the biggest challenge with scaling is silica deposition in the wells. Inaccessible for manual removal the well clogs over time and becomes unproductive; new wells have to be drilled which is rather costly [17–19].

1.1.2 Waste heat

Many industrial processes are extremely energy consuming, either in the form of fossil fuels or electrical power. Increasing energy demand and costs as well as the shrinking fossil resources make it necessary to improve the efficiency of these existing energy consuming processes. Different approaches are possible: one is to save power, e.g. by replacing old and inefficient electrical equipment; another is to recycle heat internally or, if not possible, to use this waste-heat to generate power. This in-house power generation using the waste heat can be a financially interesting option [20]. Temperatures range with the process and industry, and as

for geothermal energy the lower the temperature the more waste-heat potential can be tapped. For temperature regimes similar to geothermal energy identical equipment can be used as shown in [21]. As available thermal power also varies with the industry and application, power outputs can be found in the kilowatt- as well as in the gigawatt-range. Smaller power outputs might be suitable for reciprocating power converters too. The advantage of industrial waste-heat as opposed to geothermal energy is that the heat carrier used can be much cleaner and less corrosive and prone to clogging than the geothermal brine. Pure water, steam or a thermo-oil can be used in a closed cycle which is less demanding on the heat exchangers. The generated power can be used directly on site and reduce the energy costs or, depending on current price and demand, fed into the grid.

Waste heat and geothermal energy present similar working conditions for power generation. Identical machinery can be used to convert this heat to power. At lower heat source temperatures (below 200 °C) usually ORC binary cycle plants are in operation. As an alternative to such equipment Stirling engine technology is proposed, especially as an option for smaller capacities (<1 MW).

1.2 Stirling Engines

1.2.1 Working principle

The basic working principle behind a Stirling engine is the thermal expansion or the increase in pressure of a gas when heat is applied, and compression or decrease in pressure when cooled, as is formulated in the ideal gas law:

$$pV = mRT \tag{1.1}$$

If a specific gas volume is sealed in a cylinder, pressure and volume are only affected by a change in temperature as the gas mass and the gas constant remain

unchanged.

$$pV = kT \tag{1.2}$$

Figure 1.2 illustrates this principle. A sealed cylinder is filled with a gas. If heat is applied the pressure increases; if the cylinder is cooled the pressure decreases. Applying heating and cooling alternatingly is not feasible for an engine that runs at a certain speed since heat transfer is not instantaneous and the cylinder wall possesses a certain heat capacity. Therefore one side of the cylinder is constantly heated and the other side is constantly cooled. In order to achieve a pressure change a device is needed that moves the gas from the heated to the cooled zone and vice versa. Using pistons, two possible options are commonly found. The first is to use a displacer-piston that moves within the sealed cylinder. The second possibility is to seal the cylinder on both sides using pistons and to move these pistons in parallel. Either way the gas volume is heated and cooled alternately and the pressure changes accordingly. So far no volume is changed and therefore no power output can be generated. Some modifications are still needed in order to obtain a working engine.

1.2.2 The Stirling cycle and its realisation

The ideal thermodynamic cycle consists of two isothermal processes where heat is added and rejected, and two isochoric[3] processes where heat is stored and recovered. Figure 1.3 shows the change of state of the working fluid in a pressure-volume ($p-V$) as well as in a temperature-entropy ($T-s$) diagram: Isothermal expansion (1-2), isochoric cooling (2-3), isothermal compression (3-4), and isochoric heating (4-1). This cycle provides the theoretical boundaries for all real Stirling machines. Many different principles have been proposed to perform this cycle. Among these are diaphragms, liquid pistons, acoustic machines, pistons driving cranks, and

[3] A constant volume process, the volume remains constant, pressure and temperature change.

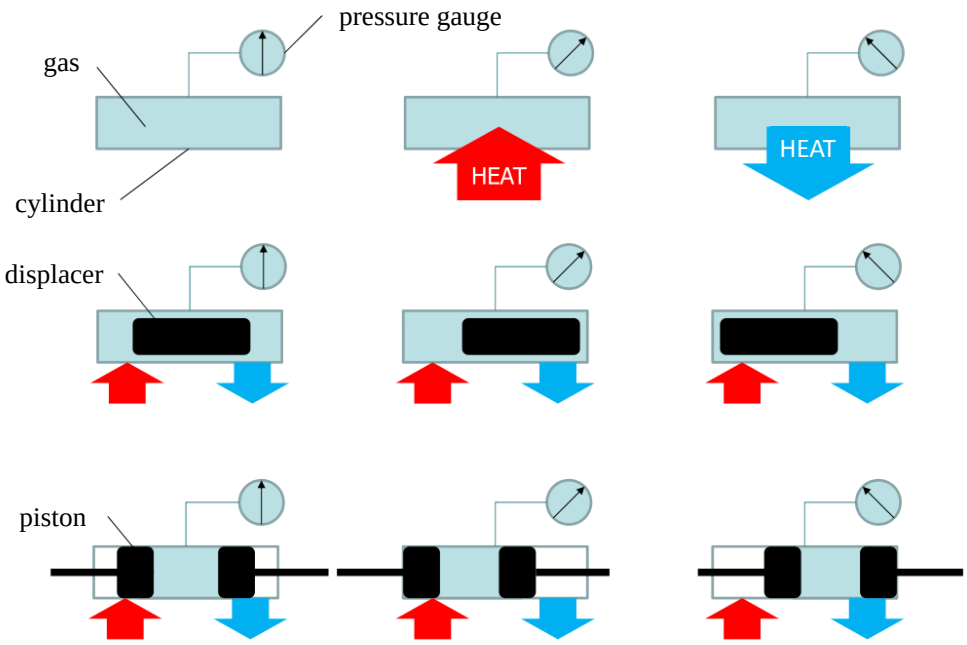

Figure 1.2: The working principle of Stirling engines

free-pistons. On a larger scale, however, reciprocating engines with conventional pistons and/or displacers are the only known realisation [22–24].

The two-piston device from Figure 1.2 can be used to describe a theoretical engine working on the Stirling cycle. Hot and cold heat exchangers are added to the device to increase the heat transfer rate as can be seen in Figure 1.3. Between the two heat exchangers a regenerator is installed which is a very important part if high efficiencies are desired. It can be thought of as a thermal sponge: when heated gas leaves the hot heat exchanger and passes through the cold regenerator it transfers part of its heat to the regenerator matrix before entering the cold heat exchanger. On the way back the now cold gas is preheated in the regenerator by the previously stored energy. The ideal cycle can be approximated as follows:

- 1-2 Isothermal expansion during which the compression piston remains at its upper dead point. The expansion piston travels to its lower dead point. While heat is added the gas expands and work is produced.

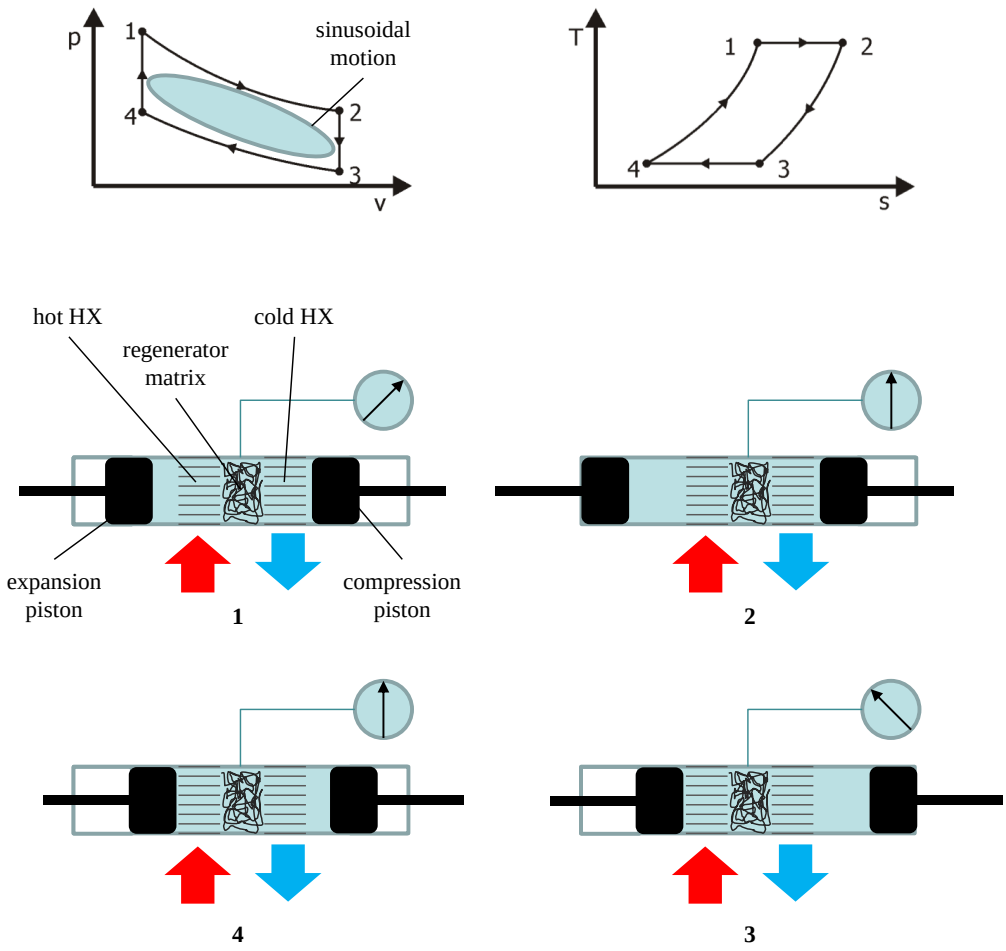

Figure 1.3: The ideal Stirling cycle and its realisation

- 2-3 Isochoric cooling during which both pistons travel in parallel from left to right. The hot gas from the expansion space heats the regenerator and is then further cooled down in the cold heat exchanger.

- 3-4 Isothermal compression in which the expansion piston remains at its upper dead point, the compression piston compresses the cold gas, work has to be added externally.

- 4-1 Isochoric heating during which both pistons move in parallel from right to left. The cold working gas is heated as it passes the regenerator matrix. The cycle is completed and can start again.

In physical engines pistons cannot move at infinite speeds or discontinuously as they are usually connected to a crank mechanism and therefore move in a more or less sinusoidal manner. This sinusoidal movement reduces the area enclosed by the $p - V$ plot to a more bean-shaped silhouette as depicted in Figure 1.3.

The example shown is just one possibility of realising a Stirling engine. Three different basic types of SE can be distinguished [24]:

- Alpha engines: The enclosed gas volume is expanded and compressed between two pistons, as shown. More information on alpha-type specific thermodynamics can be found in Section 3.1.1.
- Beta engines: A displacer shuttles the working gas between hot and cold areas of a cylinder. A power piston within the same cylinder compresses and expands the fluid (see Section 3.1.2 for details).
- Gamma engines: Similar to beta engines, but piston and displacer are not located in the same cylinder (for details refer to Section 3.1.3).

1.2.3 Efficiency limits of Stirling engines

As is the case for every other heat engine the Stirling engine has to conform to the basic laws of thermodynamics. No heat engine will produce more power than the heat it is supplied with but, necessarily, even less. The Carnot efficiency (η_{Carnot}) is the theoretical limit for every heat engine, depending on the temperature levels of the heat sink and source at which heat is added and rejected:

$$\eta_{Carnot} = 1 - \frac{T_{sink}}{T_{source}} \tag{1.3}$$

From the equation for the Carnot efficiency plotted in Figure 1.4 over the heat source temperature for different sink temperatures it can easily be seen that at

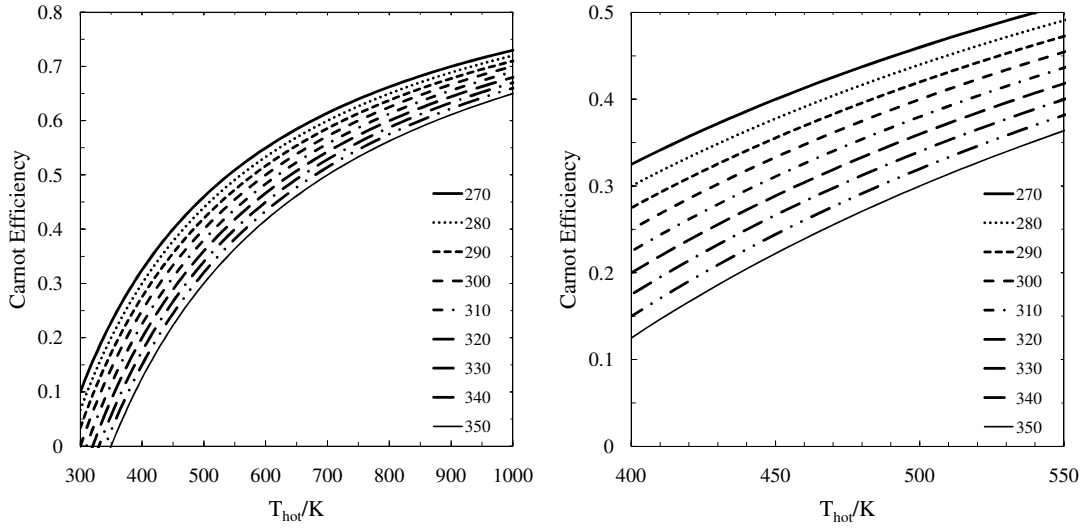

Figure 1.4: Carnot efficiency vs. source temperature at different sink temperatures

temperatures between 400 to 550 K (130 to 280 °C) the temperature of the heat sink plays an even more important role than at higher temperatures. For example, at 400 K source temperature and 300 K sink temperature a change of 10 K in the heat sink changes the Carnot efficiency by 10 % of the value (at 1000 K only by 1.5 %). Daily or seasonal changes in the rejection temperature can have a large impact on the achievable efficiency; the lower the sink temperature the higher the efficiency. Providing effective cooling is mandatory when designing an actual Stirling engine for geothermal power generation or other low-temperature heat sources.

Every engine that is heated externally such as the SE and, in fact, every engine that passes through a Reitlinger cycle[4] operating between a high and low temperature will not reach these limits with its working fluid. In fact there has to be a temperature gradient to drive the heat flow in and out. A very slow running engine is able to get closer to these temperature extremes and thus is capable of reaching higher efficiency (see above), but at a small power output. For a fast

[4]A Reitlinger cycle describes a thermodynamic cycle consisting of two isotherms and regeneration between the two other states. If regeneration is complete, Carnot efficiency can be reached [22, 25].

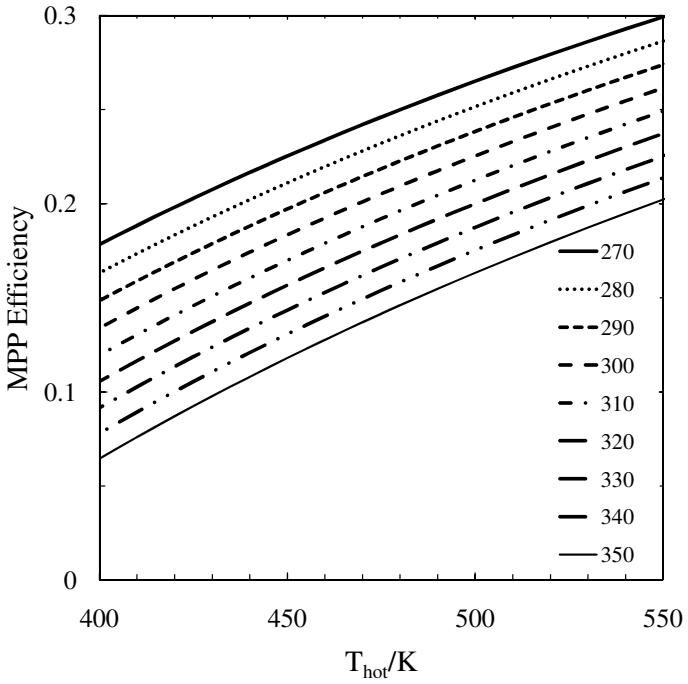

Figure 1.5: Maximum power point efficiency vs. heat source temperature for different sink temperatures

running engine the Carnot efficiency deteriorates but power output increases with frequency. There is an optimum for the power output in between. Curzon and Ahlborn[5] [27] showed that the efficiency at this maximum power point (η_{mpp}) is only a function of the heat sink and source temperatures:

$$\eta_{mpp} = 1 - \sqrt{\frac{T_{sink}}{T_{source}}}, \tag{1.4}$$

and therefore independent of the heat transfer in the heat exchangers. It can be observed from the plot (Figure 1.5) that the heat sink temperature still plays the same predominant role for efficiencies and, of course, that obtainable efficiencies are much lower now.

Comparing Figures 1.4 and 1.5, it can be seen that Figure 1.5 is about 50 % of the Carnot efficiency. This corresponds to Walker's empirical observation that the efficiency in a real SE is found to be between 0.4 and 0.5 of the theoretical Carnot

[5]The same principle was also shown earlier by Novikov and simultaneously Chambadal [26].

value [22]. Differences between observation and theory can be attributed mostly to mechanical losses and other irreversibilities. Thus, the theoretically obtainable efficiency at the output shaft at maximum power point (η_{shaft}) can be expressed as

$$\eta_{shaft} = \eta_{mpp}\eta_{mechanical}, \tag{1.5}$$

with $\eta_{mechanical}$ being the mechanical efficiency of the engine. An engine using geothermal energy or waste heat to generate power should be designed for maximum power point operation and not for maximum efficiency to keep the engine and thus capital cost as small as possible and specific power output high.

1.2.4 Power output of Stirling engines

Based on an observation made by Beale, Walker found an empirical correlation for the power output (P), using the operating frequency (f), the mean pressure (p_m), and the volumetric change (ΔV) of the working gas (maximum minus minimum volume) [22]:

$$P = B_n f p_m \Delta V \tag{1.6}$$

with B_n being the so-called Beale number, a dimensionless constant of about 0.15. West [28] refined this correlation by including the prevailing temperature limits to

$$P = W_n f p_m \Delta V \frac{T_{source} - T_{sink}}{T_{source} + T_{sink}}, \tag{1.7}$$

which was later confirmed by Senft [29]. Iwamoto [30] and Prieto [31,32] made further efforts to predict the engine performance based on a group of non-dimensional parameters.

The West equation is a guideline to estimate the engine size for a desired power output, as well as to validate the engine performance. If, for a given engine with a specific power output, the value for the West number (W_n) is found to

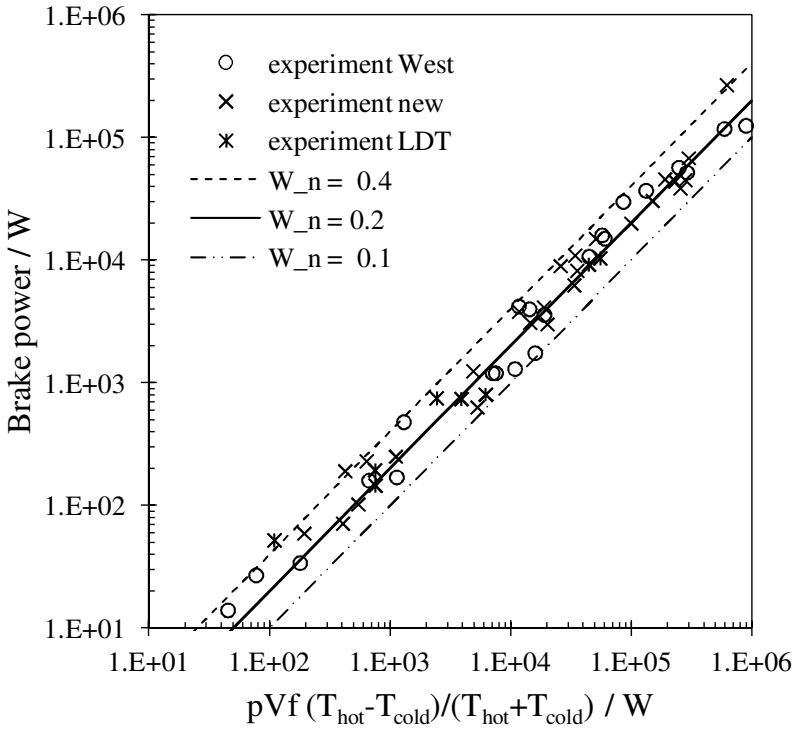

Figure 1.6: Prediction of the brake power as a function of the engine parameters (pressure, swept volume, frequency, temperature levels) using the West number, and including the available low-temperature experimental data

be around 0.2 and beyond, sound thermodynamic and mechanical design can be assumed. It has to be mentioned, however, that the data set used to established this correlation includes only engines with heat source temperatures higher than 340 °C (610 K), which is far above the temperatures considered in this work. Since 1986, when a corrected West number (W_n=0.25) was published [24], a small number of low temperature difference engines were built and information about their performance was published [30, 33–37]. Figure 1.6 shows the correlation of the brake power and the engine parameters, where the prediction made by the West number is plotted as the solid line and the circles (o) represent the original data set used to establish the correlation. The other markers (x) represent experimental low temperature difference Stirling engines from the references listed above and additional experimental data made available since the first publication. The underlying data set is given in Table A.1.

When the correlation was originally established the West-number was not estimated by evaluating a proper fit to the data set but simply by computation of the arithmetic mean of the West number for each of the data points. If a proper linear fit were added, a West number of 0.17 would have resulted. By including the newly available data a new West number is found to be around 0.21. The West number concept proves to be as accurate for low temperature engines as it is for high and medium temperature engines, which means that it offers a simple tool for a rough estimation of the swept volume needed to reach a specific power output for a given temperature difference. The level of pressurisation and the operating frequency have to be chosen in a reasonable range, as shown in Chapter 4. Care has to be taken when calculating the swept volume for alpha engines, as opposed to displacer type engines where only the power piston contributes to the volumetric change, since both pistons and their phase angle influence the volume change (see Section 3.1.1). In Appendix B the derivation of the effective swept volume for a given phase angle is shown. For alpha engines the power of an engine with two cylinders of volume V_{swept} can be estimated to be:

$$P = 0.2 f p_m \Delta V^* V_{swept} \frac{T_{source} - T_{sink}}{T_{source} + T_{sink}}, \tag{1.8}$$

with values of ΔV^* as found in Table B.1 or by solving Equation B.13 for the desired phase angle. Suitable phase angles start at 90° for high temperature engines and increase with decreasing temperature difference, as it is shown in Chapter 4.

From Equation 1.7 and Equation 1.8 it can be seen immediately that if the temperature difference decreases frequency, mean pressure, and swept volume have to be compensated if a high power output is needed. Since the frequency is limited in low temperature differential devices only pressure and swept volume can be increased which directly influences the capital costs of a LTD engine since a large engine built for high pressure is needed to generate high power outputs.

1.2.5 History of the Stirling Engine

Stirling or hot gas engines are reciprocating machines that convert heat input to mechanical work output. Their working gas (air, nitrogen, helium, and hydrogen are the most common) is sealed inside the machine and heated by an external heat source. Hot air engines have been known for almost two hundred years. They were invented as a safer alternative to steam engines, which were notorious for boiler explosions at that time. Since hot gas, as opposed to steam, is the working fluid of choice, material failures had less fatal effects. In 1815 the Stirling brothers presented their first hot air engine [25]. The most important feature of their invention is an internal heat regenerator, that economises fuel consumption and enhances power output [38].

Until the beginnings of the 20th century when internal combustion engines became the dominating prime mover, hot gas engines were widespread in use, but relatively inefficient. They were even less efficient than their ancestor as the beneficial effect of the regenerator was neglected [38]. It was not until the 1940s when the Dutch company Philips refocused their research on Stirling's invention, in response to the need for a small and silent power generator to power radios during WWII. New materials and manufacturing methods made higher pressures and thus power outputs possible. Also a fundamental understanding of the processes inside the engine was developed by a constant process of trial and error. A good insight into the company's activities and also the preceding history can be found in Hargreaves' monograph on the history of Stirling engine development at Philips in Eindhoven, Netherlands [23].

Fundamental work was carried out there, so when other companies became interested in hot gas engines they were dependent on Philips' know-how and licenses. General Motors, Ford, MAN and DAF all held licenses to develop engines for automotive propulsion in the 1960s and 1970s. Due to the continuous combustion process, noise levels are low and exhaust gas components are much easier to

control so that unburnt hydrocarbons, nitrogen oxide (NO_x) and carbon monoxide (CO) levels could be much better controlled than in internal combustion engines at that time. Schreiber reports ten percent less fuel consumption than spark ignition engines and emission levels ahead of the times [39]; other authors give a less positive result [40]. Sealing problems as well as the much higher production costs compared to Diesel engines ended research and development work sooner or later [22].

The invention of the free-piston Stirling machine by William Beale [41] as well as the thermo-mechanical generator by Cooke-Yarborough [42] brought SE to new levels of longevity and simplicity. Omitting a lubricated crankcase and hermetically sealing made it a maintenance-free device and allowed reported continuous operation for more than ten years. The high reliability made it a premium prime mover for remote operation without maintenance. Combined with the ability to run on almost any heat source at good efficiencies, even in the absence of oxygen, outer space seems a natural application. Indeed there has been ongoing research at NASA's research centre since the 1970s [43, 44]. Even double-acting multi-cylinder engines with free pistons have been demonstrated to be feasible, with fewer tuning issues than single cylinder engines [45]. Other configurations are currently under investigation [46, 47].

Solar energy cannot only power space applications but also prime movers on earth. So-called Dish-Stirling units consist of a SE in the focal point of a large parabolic mirror. Other solar thermal power systems using turbines to generate power do not allow either small-scale power generation (up to a few hundred kilowatts) when they are in the form of solar power tower plants, or sufficiently high concentration and temperatures - and hence high thermal efficiencies - when solar troughs are the form of solar energy collection[6] [48].

[6]Solar power tower plants use a number of tracked mirrors to concentrate solar radiation on a small surface on top of the tower. Air is heated and circulated and a heat exchanger transfers the heat to the working fluid of a steam turbine. Due to the high concentration ratio

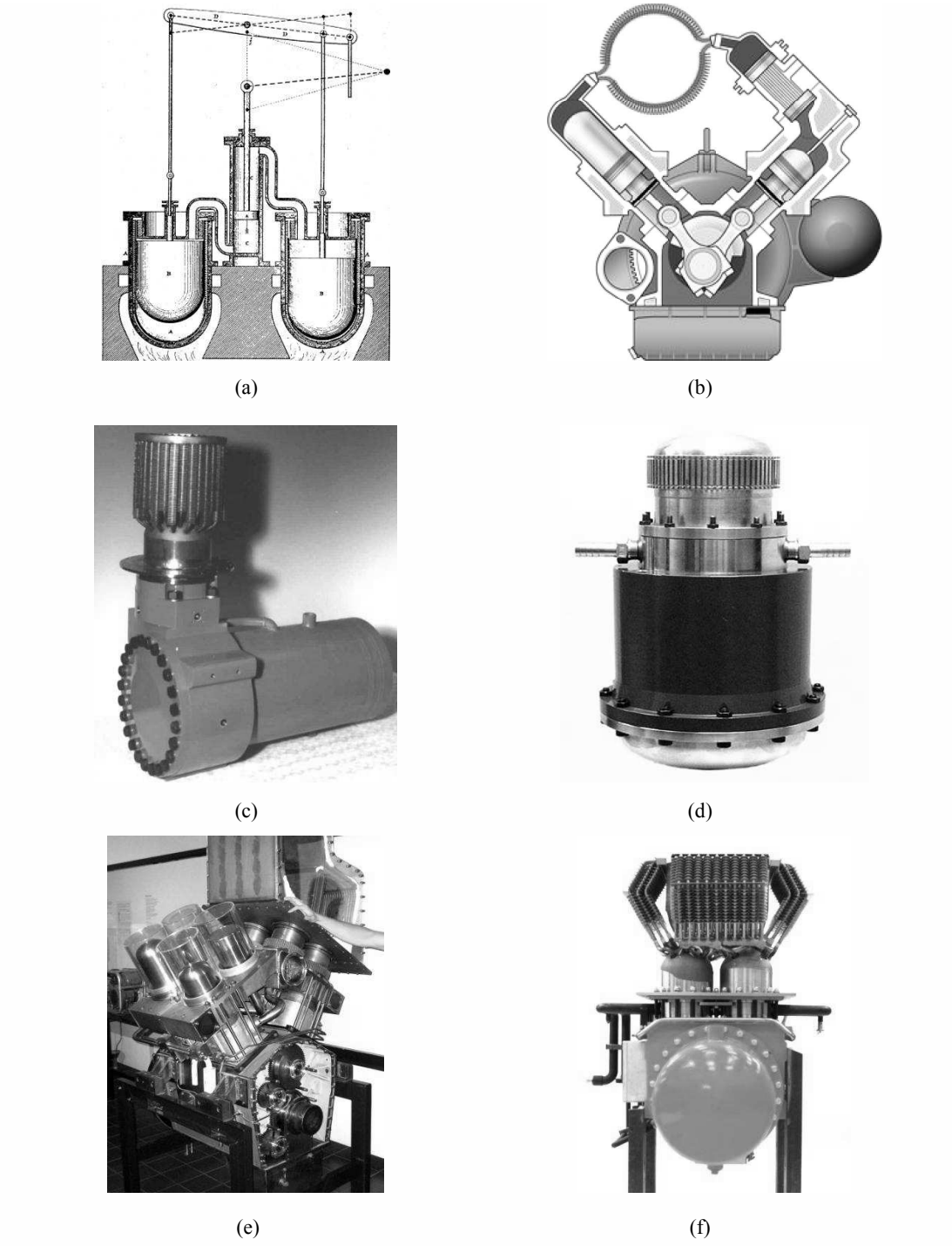

Figure 1.7: Examples of SEs built in different configurations: (a) An early SE built by the Stirling brothers in 1843, a double-acting engine of the gamma-type [23]. (b) A single-acting alpha design; expansion piston (left) and compression piston (right) share a common crank-pin. The heat exchangers can be identified clearly. Design by SOLO, now Cleanergy [49]. (c) A single cylinder engine of the beta-type developed at the University of Denmark [50]. (d) Sunpower's P2A, a free-piston engine of the gamma-type [51]. (e) A double-acting 4-cylinder engine of the alpha-type intended for the use in submarines, V-configuration. (f) A double-acting four cylinder engine with parallel pistons for the use with biomass CHP [52]

The possibility of a smoothly and silently running engine also caught military interest. Submarine manufacturers such as the Swedish company Kockums use SEs since the 1980s as air-independent power generators (AIP) [53, 54]. Infinia is developing multi-fuel generators for in-field usage for the US army [55]. But quiet operation is not only interesting for military purposes. Domestic combined heat and power systems (CHP) using SE can be installed in the living areas of houses without high noise penalties, as the gas-fired Whispergen system demonstrates [56]. Other companies have followed their lead, see below. The ability to use a variety of heat sources made the SE popular for biomass CHPs from domestic power and heat demands up to a hundred kilowatts [57–59]. Figure 1.7 shows examples of SEs of different shapes and sizes that have been built over the years.

The same basic cycle, in reverse, can be used as a heat-removal device for refrigerating applications. Externally driven, SEs can work as (cryo-)coolers or heat pumps reaching very low temperatures (below 80 K) at high efficiencies, which is difficult to obtain by other technologies [60]. Free-piston and kinematic machines are commercially available for different power and temperature ranges [61–63].

Since Stirling engine technology is comparatively cost-intensive, only niche applications can be found today. There is no indication that SEs will ever be competitive with internal combustion engines or another technology that makes reasonably good use of an existing heat-source at a competitive price. However, exotic heat sources, environmental issues or financial reasons can justify their implementation.

high temperatures are reached in the focal point. Solar trough plants use parabolic mirrors to concentrate solar radiation on a tubular absorber. The used heat carrier is oil, so high concentration ratios and thus high temperatures and high thermal efficiency are not feasible due to the temperature limits of the heat carrier. A standard steam turbine is used to generate power in both cases, thus a certain plant size is required to be economically justifiable.

1.2.6 Stirling engines today - recent activities

A number of companies have brought Stirling engine technology to a commercial stage but today only a few companies are building and selling engines. The biggest volume of engines sold can be found in the residential co-generation market. Here, two different systems were available: the kinematic Whispergen from EHE [56,64] and the free-piston system by Microgen [65]. The electrical power output of these systems is about 1 kW and the heat source is gas. Some thousand engines have been produced until now and are mainly installed in European homes. By the end of 2012 EHE had to file for bankruptcy and the Whispergen is no longer available [66,67]. Microgen's single cylinder engine is still available from a number of home appliance manufacturers integrated in micro-CHP units [68–73].

Engines for solar dishes have been developed further with a greater focus on mass production and can be found in various test facilities, provided by different manufacturers. At the moment Infinia is building a 1.5 MW field consisting of around 450 Dish-Stirling units in Utah, USA and larger projects are planned in the Mediterranean [74]. In September 2013 Infinia filed for bankruptcy [75] and was then bought by the Israeli company Qnergy [76]. The free-piston engines used have a relatively small power output of only 3 kW, whereas the competing systems from Cleanergy (formerly SOLO) [49] and Ripasso [77] use much larger kinematic engines (11 and 30 kW) but have fewer units and capacity installed so far. The latter engine uses technology developed by Kockums which is still producing engines for submarines; with 75 kW the most powerful engine in production today [54]. A similar device has been developed recently at the automotive company MAHLE but the development was stopped [78].

Two different engines for biomass CHP were available until recently, one from Stirling DK [52, 79] the other from Stirling Biopower [80], both in the 40 kW region. Stirling DK is no longer producing Stirling engines, Stirling Biopower bought Stirling Energy Systems (SES) and changed the company name to Stirling

Power, the engine development is ongoing. Table 1.1 gives an overview on the most recent commercial activities involving Stirling engines.

Table 1.1: Recent commercial Stirling engines activities ($^+$ no longer available)

company	power	type	NoC	heat source	references
EHE-Whispergen$^+$	1 kW	piston	4	gas	[56, 81, 82]
Microgen	1 kW	displacer (FP)	1	gas	[65, 83]
Qnergy (Infinia)	3 kW	displacer (FP)	1	solar	[74, 76]
Cool energy	3 kW	piston	6	various	[84]
Sunpower	7.5 kW	displacer (FP)	1	various	[85]
Cleanergy	11 kW	piston	2	various	[49]
MAHLE$^+$	25 kW	piston	4	solar	[78]
Ripasso	30 kW	piston	4	solar	[77]
Stirling DK$^+$	35 kW	piston	4	biomass	[52]
Stirling (Bio)Power	43 kW	piston	4	various	[80]
Kockums	75 kW	piston	4	diesel	[53, 54]

1.2.7 Design features of Stirling engines

Independent of the engine configuration and size, the heat exchangers and the regenerator are the most crucial components in SE design. Since the reinvention of the SE by Philips in the 1940 the basic physical designs of these components have not changed much. However, with more sophisticated simulation tools becoming available the thermodynamic and fluid-dynamic layout could be improved.

Hot heat exchanger

Two types of heat exchangers are commonly found in Stirling engines: tubular heat exchangers and the annular gap type. Combinations of the two are possible but rare. Figure 1.8 shows the two basic designs for the heater. Tubular heaters (a) are usually located around the heat source and the hot flue gases (in the case of combustion) pass the tubes twice. The bend of the tube allows for their thermal expansion without stressing the connections to adjacent components too much, which is necessary as the increase in temperature of several hundred degrees

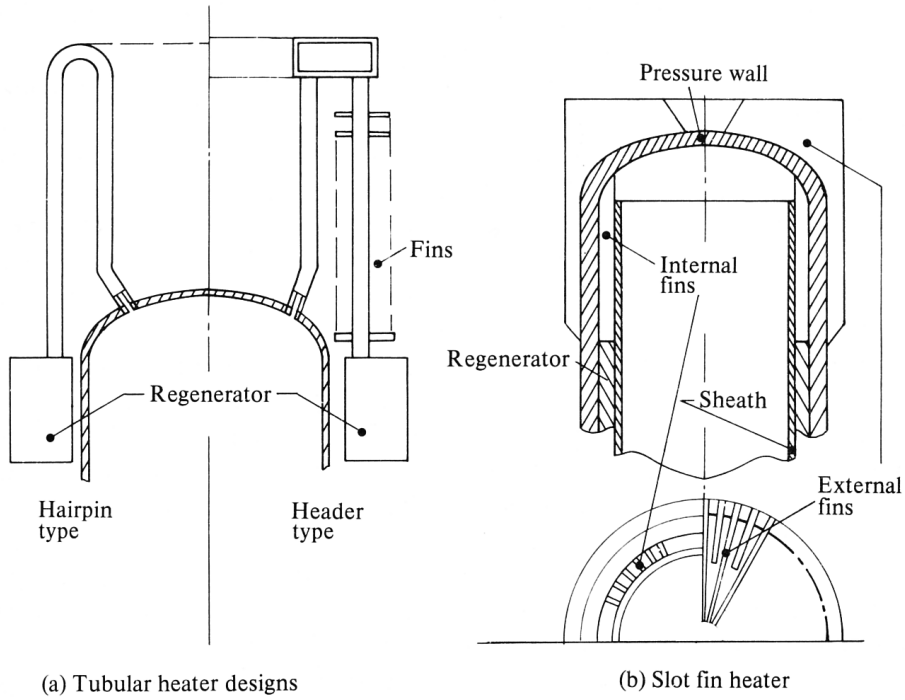

Figure 1.8: Tubular (a) and annular gap type (b) heat exchangers [22]

would increase the stress significantly. The addition of external fins to increase the heat transfer can be done relatively easily. The annular gap type heat exchanger (b) consists of a cavity formed between the cylinder liner on the inside and the pressure wall on the outside. Often fins are added on the inside and also on the outside, depending on the application.

From these two basic designs a great multitude of variations have been produced over the years but the concepts have remained largely unchanged. Figure 1.9 shows a number of selected examples for the engine heaters. Comparing the tubular type on the left hand side with the annular type on the right hand side a few differences become obvious. The heat transfer area can be adjusted more easily in the case of the tubular heat exchanger as tube length and number can be changed; it is therefore easier to generate a larger surface area compared to the annular type. A clear disadvantage is the manufacturing cost as more time and well-trained workers are needed to produce leakage-free heaters. Each tube

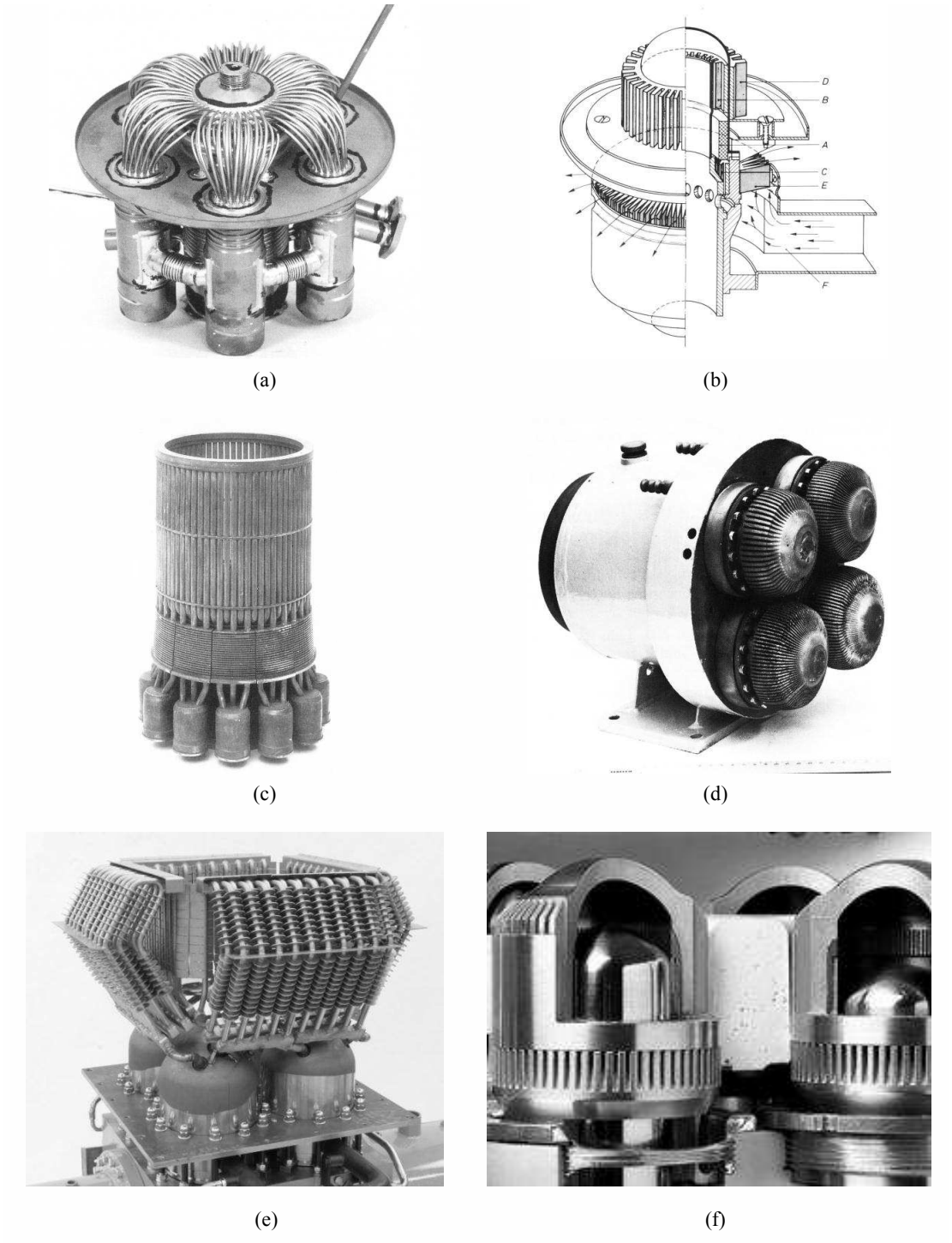

Figure 1.9: Tubular (left) and annular gap type (right) heat exchangers. (a)-(d) various Philips heater designs; (a) bend single piece tube, (b) annular gap with internal and external fins for heat transfer augmentation, (c) straight tubes with manifold at top and bottom, (d) annular gap external view [23], (e) Stirling DK tubular heat exchanger with external fins and multiple manifolds for reduced pressure losses [52], (f) Whispergen external and internal fins [56]. Heaters (a)-(c) are for single cylinder beta, (d)-(f) are for four cylinder double-acting alpha engines.

joint bears the potential of leakage. This weak point is omitted in the annular gap design since the heater head is made from one piece (cast or machined) and connected to the housing via a flange or thread. As the wall of the heater head is the pressure wall of the cylinder at the same time, the wall thickness of the heater is much larger than for the tubular type and hence heat transfer is worse.

Regenerator

The function of the regenerator is to store and release heat internally in order to make the whole process more efficient. The regenerator material is heated when hot gas passes from the hot heat exchanger to the cold side. When the direction of the flow changes and the now-cooled gas passes the regenerator again, the heat is released back to the fluid. This internally recycled heat allows for smaller heat exchangers with less volume on both sides for an identical power output. Being positioned between the hot and cold heat exchangers the regenerator can also help to reduce conductive losses between the two components and hence increase the efficiency further. The presence of a regenerator increases the pumping losses in the system which reduces the power output; finding a suitable design is therefore always a trade-off between the pressure losses on the one hand and the regenerator performance on the other.

In its simplest and least effective form a regenerative effect can be achieved by an annular gap in the cylinder; the heat capacity of the duct wall is used to store and release the heat. More common and efficient designs rely on the addition of a solid material of a certain porosity in this annular gap or packed in an external canister. Figures 1.9 (a) and (c) give examples for the canister type where the regenerator is packed in an external tube between the heat exchangers. The remaining figures show examples for the annular type which can be seen best as component A in Figure 1.9 (b). Common regenerator matrix structures are random fibre and stacks or rolls of woven-wire sheets (wire mesh); more exotic

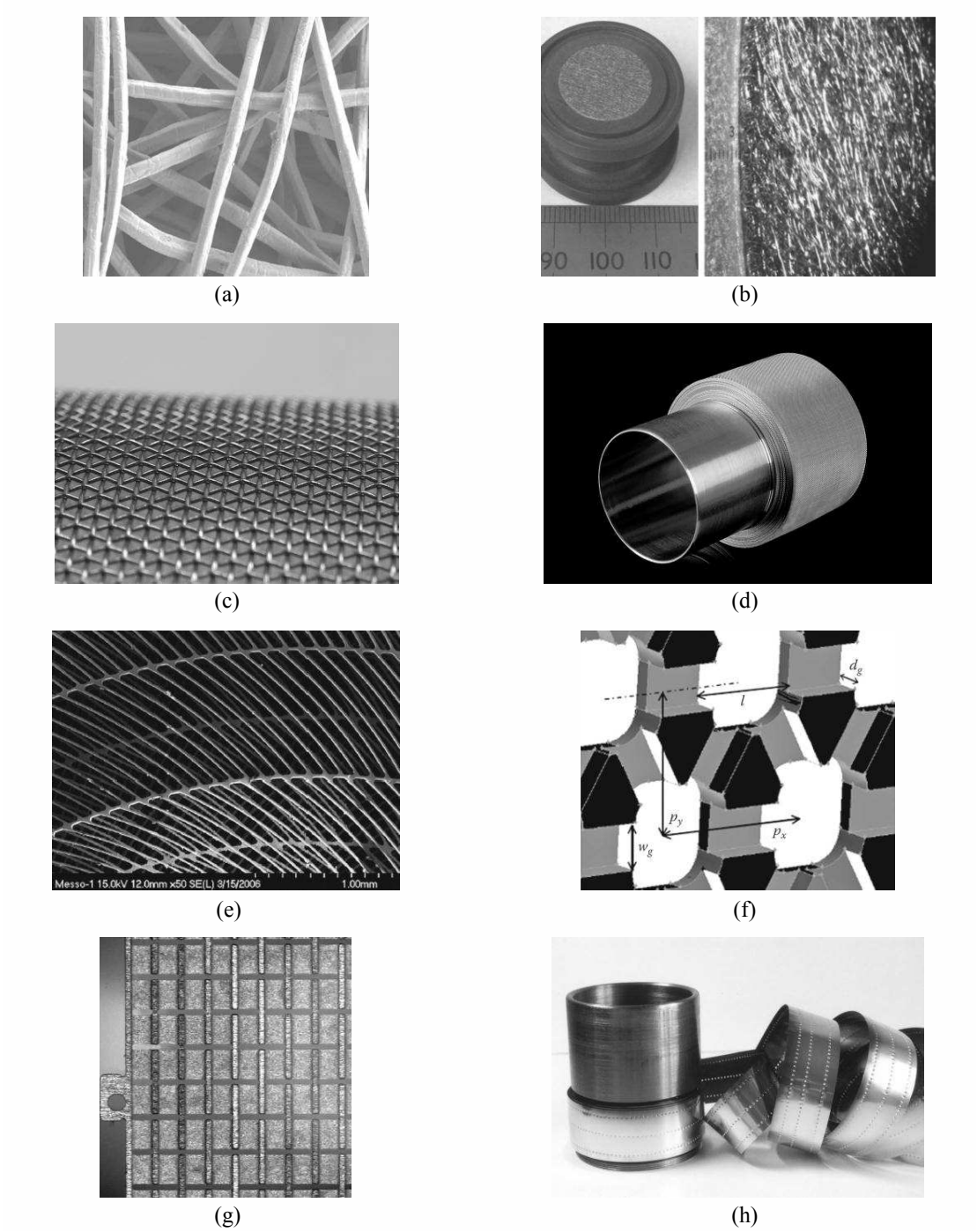

Figure 1.10: Regenerator matrix structures. (a) Random fibre close-up [86]. (b) Random fibre in canister assembly [86]. (c) Wire mesh. (d) Wound wire mesh stripe for annular regenerator [56]. (e) Microfabricated segmented-involute-foil regenerator with flow normal to the foil [86]. (f) Etched mesh sheet with flow normal to the sheet [87]. (g) Etched foil with flow parallel to the foil [88]. (h) Wound foil with dimples for even spacing [89]

structures include wrapped foils with parallel ducts and foils or sheets with delicate surface structures. Other structures are possible too but more suitable for cooling applications or acoustic machines [86, 90]. Figure 1.10 gives examples of the different structures.

Figures 1.10 (a) and (b) show a random fibre matrix. To create such a regenerator the desired geometric shape is cut out of a raw material (felt) with wire diameters as small as 10 µm. Depending on the desired thickness, multiple layers can be stacked on top of each other and are then compressed to the desired porosity and measurement. To prevent the material from losing single fibres to the engine where they can cause increased wear and failure, and to make the whole unit more stable, these raw stacks are often sintered. The result is a cost-effective solution using widely available raw materials of a performance similar to other types. Due to the random fibre nature of the material it is more challenging to create matrices with evenly distributed porosity and flow [86].

One possibility of creating regenerators with a more homogeneous matrix is to use wire mesh material. Such material, as can be seen in Figure 1.10 (c), is usually cut to size and then stacked in layers one on top of the other, similar to a stack of pancakes. In the case of the annular regenerator there is also the option of rolling the mesh around the cylinder liner, which is a very simple and cost effective method. Figure 1.10 (d) illustrates this design. A similar design is shown in Figure 1.10 (h) where the wire mesh is replaced by a metal foil. In order to generate passage ways for the oscillating working fluid, dimples are formed in the foil which form parallel ducts when the foil is wound around the cylinder liner [89].

Modern manufacturing techniques have led to a variety of new regenerator designs. In all cases the basic concept is to create a surface structure on a foil or a thin screen which then creates channels when stacked on top of each other. Figure 1.10 (e-g) gives examples of such structures. Detailed description of struc-

ture (e) developed by NASA can be found in [86, 91–93]. The etched structure (f) was developed at the National Defense Academy in Japan [87, 94–96]. A similar process is also used to create structure (g) which results in parallel channels when stacked [88]. None of these sophisticated regenerator designs can be found in the commercial engines discussed above. Test results published so far do not show any substantial improvement in regenerator performance [86].

For single cylinder engines and engines using annular gap heat exchangers the annular type seems to be the best choice as it allows for a simple and robust design. One shortcoming of this design is that the outer diameter of the pressure vessel is increased which increases the thickness of the regenerator wall at the same time. This leads to higher conductive losses from the hot side of the regenerator to the cold side. In a canister design with identical regenerator cross-section these losses are reduced since the wall thickness can be reduced. In multi-cylinder arrangements another advantage of the canister type is that the cylinders can be placed closer together which allows for more compact engines with shorter crankshafts, if applicable.

Cold heat exchanger

For the cold heat exchanger two types are common, depending on the regenerator design. In the case of an annular regenerator the cold heat exchanger is located below the regenerator around the cylinder liner. Usually a water jacket is used as the heat sink. Not only the working fluid is cooled in this configuration but also the cylinder and the piston rings. Such a heat exchanger can be found in Figure 1.9 (b) labelled as part C, here air-cooled. Figures 1.9 (d-f) all incorporate such an annular design. In addition to the finned annulus design a tube bundle can be used as a cold heat exchanger which is quite common - despite the additional costs involved - since the tubes increase the surface area highly. The engines (c)

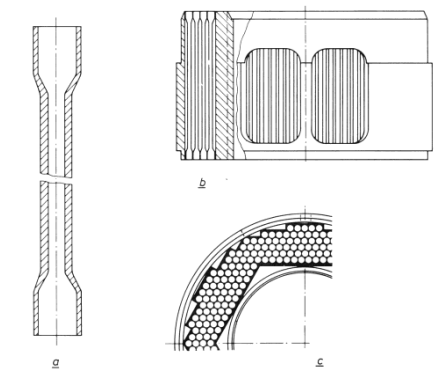

(a)

(b)

(c)

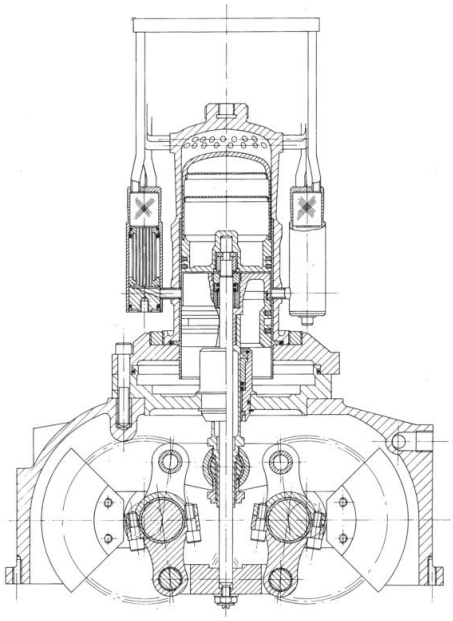

(d)

Figure 1.11: Cold heat exchangers: (a) detail of an annular heat exchanger using tubes. The ends of the tubes are flared so that they can be brazed together directly omitting the need for drilled end-plates [23]. (b) A flat-plate heat exchanger using parallel ducts for piston-engines of small power output [97]. (c) Tubes and regenerator from a canister style heat exchanger with the shell removed [23]. (d) The same heat exchanger combination installed in several canisters around the single-cylinder of a beta engine [98].

and (f) in Figure 1.7 also incorporate such a design. A detailed drawing is given in Figure 1.11 (a).

Regenerators of the canister type are usually followed by a shell and tube heat exchanger on the cold side. The engines in Figure 1.7 (b) and (e) as well as in Figure 1.9 (a) and (c) feature such designs. Figure 1.11 (c) is a close-up of the regenerator and tube components of such a configuration, with the shell removed. Figure 1.11 (d) shows their location in a single-cylinder displacer-engine.

In small engines of the piston type another variation of the cold heat exchanger can be found: a series of parallel straight ducts, separated by fins serve as the cooler, as can be seen in Figure 1.11 (b). Due to the flat-plate style construction this design is not particularly well suited for high levels of pressurisation [89,97,99].

1.3 Summary of this research

1.3.1 Objectives

A Stirling engine has been proposed as a means of generating power from a low temperature heat source such as geothermal energy or industrial waste heat. This research explores this possibility on different levels; the thermodynamic processes at low-temperature operation and the resulting practical design issues are under investigation. This work is intended to create a broad base of knowledge for the future building and operation of a low-temperature difference engine. As the obtainable power is very limited for the low temperature situation a sound understanding of the thermodynamic side is mandatory to be able to design an efficient engine. In a second step the thermodynamic insights gained can be used to identify design features which allow to translate these insights into a feasible design.

1.3.2 Unique and novel aspects

To date not much research has been undertaken to develop a Stirling engine for a moderate temperature heat source such as geothermal energy or waste heat. Most previous research has focused on the temperature difference extremes, as small as 0.5 K [100] and as high as heat exchanger materials can withstand (around 800 °C). Findings from the well observed high and ultra-low temperature differentials engines cannot be adapted without restrictions. Ultra-low temperature difference engines can be treated as mere toys, even though their study brings valuable insights into the Stirling cycle. Their actual design and the lack of usable power output make changes in design very necessary. High temperature engines, though thermodynamically favoured, have to deal with different, much more demanding constraints. All their design problems arise from the high temperatures which cause thermal stress, fatigue, lubrication and sealing problems. These acknowledged 'Achilles heels' of many Stirling engine designs will be much less extreme at the moderate temperatures of geothermal heat sources or waste heat.

For moderate temperature differences in the range of 100 to 200 K, which are typical for geothermal and waste-heat applications, only few references could be found. Kolin, a pioneer in low delta-T Stirling engines describes the possibility of using SE for geothermal power generation [101]. At the university of Saitama, Japan, a research group focuses on low temperature SEs [102]. Different single-cylinder prototypes have been constructed ranging from 100 W to 1 kW, see e.g. Figure 1.12 (a) [34, 103, 104]. These designs have been refined at Suction Gas Engine where a prototype with two cylinders and 10 kW power output was built, shown in Figure 1.12 (c) [35–37, 105]. Kongtragool showed the importance of proper thermodynamic and mechanical design [106]. His solar-powered (T_{hot} = 420 K) engine, shown in Figure 1.12 (b), achieved efficiencies between 0.004 and 0.005. The Carnot efficiency for 420 K is almost 0.3, about 70 times the measured value.

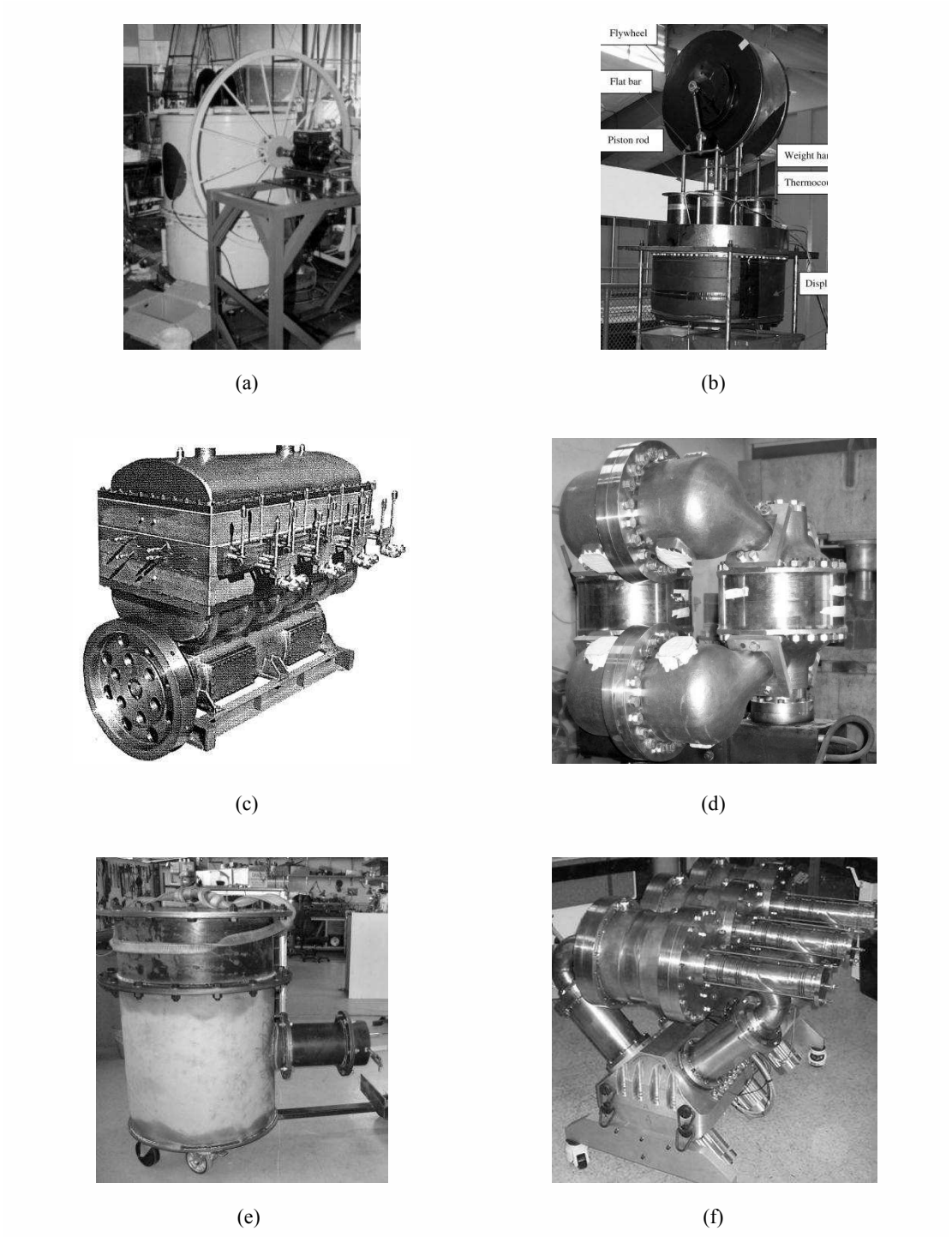

Figure 1.12: Low-temperature Stirling engine prototypes. (a) A 300 W engine of the gamma type (Saitama University) [34, 103]. (b) A 6 W engine of the gamma type showing very low efficiencies (King Mongkut's University) [106]. (c) A 10 kW double cylinder engine for 300 °C source temperature (Suction Gas Engine) [37]. (d) A double-acting engine of the Franchot type (Single Phase Power) [107]. (e) A gamma type engine, development paused (University of Canterbury) [108, 109]. (f) A 3 kW single-acting alpha type multi-cylinder engine (Cool Energy) [84].

Ongoing research and development activity regarding low temperature Stirling engines can be found in the USA and Europe. At Cool Energy a 3 kW engine (Figure 1.12 (f)) for solar thermal power generation using non-concentrating collectors or waste-heat is currently under development and the design of a 20 kW engine has been started resently [84]. Infinia presented a study for a megawatt class free-piston engine, which has not been realised until today [74, 110]. The Norwegian company Single Phase Power (SPP) is at an early stage of their development of low-temperature Stirling engines for waste heat recovery. Figure 1.12 (d) shows the second prototype [107, 111–113].

No evidence has been found that SEs operating at the intermediate temperatures of geothermal heat sources or waste-heat exist in an advanced design. From the specific literature covering the desired temperature range available, which is sparse, it seems that attempts to design a LTD have been made without a detailed analysis of the underpinning thermodynamics and mechanical loss mechanisms. As a result the designs are non-efficient and often complicated. The approach taken for this study is thus to start back at the fundamentals to create a sound thermodynamic base and then to use these findings to generate a suitable physical design unbiased by any personally favoured engine type, piston set-up, drive mechanism, philosophy, etc. In the next section this approach is described in detail. Each of these steps roughly corresponds to one chapter.

1.3.3 Methodology

Literature research (Current chapter)

Even though specific literature for low-temperature Stirling engines is very limited, the amount of general Stirling engine literature is vast. In a first step relevant literature and key publications have been sorted and are cited throughout this work where appropriate. Specific low-temperature literature is listed in the preceding

section. The wide range of experience with SEs as well as other reciprocating machinery available was used to gather an understanding for the project.

Simulation model and software validation (Chapter 2)

Nowadays highly sophisticated simulation tools are available to predict SE performance. Such tools are valuable to make realistic models of the low temperature device, to explore the design space, and optimise a variety of parameters. The alternative of building a machine and then optimising it empirically is not efficient and does not permit a thorough exploration of the solution space. Sage, a commercial Stirling engine simulation software was selected for this project. Together with a common numerical analysis tool it was validated against test data from a real engine under different working conditions in order to be able to demonstrate the reliability and applicability of the two models.

Identification of a suitable engine set-up (Chapter 3)

As mentioned above SEs can be realised using different set-ups. The large variety of possible set-ups has been compared at a highly idealised level. A simple simulation model has been developed based on an isothermal analysis. This largely idealised, non-dimensional analysis allows the examination of the volume and pressure variations and the resulting power output and efficiency for different engine configurations. A deeper insight into the thermodynamics of Stirling engines is gained as a result of this modelling. The two most promising designs are then modelled in greater detail with Sage to identify the single most promising engine configuration.

Thermodynamic optimisation of a LTD with sensitivity analysis (Chapter 4 and Chapter 5)

For the engine configuration showing the highest specific power output, geometric as well as operating parameters are optimised. What is theoretically achievable from a thermodynamic perspective is then regarded as a performance benchmark for the low-temperature operation. For these optimised configurations, sensitivities to parameter variations are examined to provide insights into the restrictions as well as the freedoms faced with the low temperature design. Two popular physical layouts of thermodynamically identical set-ups are then compared with regard to mechanical efficiency, leakage, and loads to identify the best concept.

Generation of design concepts (Chapter 6)

The findings from the thermodynamic optimisation and other insights gained are then used to inform the search for suitable design solutions. Existing SE designs as well as design solutions from related technologies are discussed for their applicability in LTDs. Design concepts for components such as the heat exchangers and the regenerator as well as the engine as a whole are discussed with respect to the thermodynamic performance and technical feasibility.

Comparison of SE and ORC technology (Chapter 7)

Finally suitable SE designs, optimised for the specific heat source, are compared to commercially available ORC plants. Different operating temperature regimes are under investigation, 150 and 200 °C, the typical range of geothermal and waste-heat applications. In addition the individual components of the two systems are discussed in detail.

Chapter 2

Simulation of Stirling engines

2.1 Classification of simulation models

Early Stirling engines (1816) were built without the help of any thermodynamic theory except the observation that air expands when heated and compresses when cooled. In 1971 the first (known) attempt was made to describe a hot air engine mathematically. Since then theories have been improved and refined to a high level of sophistication. Modern computer equipment allows for fast and detailed simulation of the whole engine. After Martini [114] the different simulation approaches are classified from first-order to third-order models according to the degree of detail. It should be clarified that the term 'order' does not refer to the numerical order of the discretisation of space and time, as will be explained below.

2.1.1 First-order modelling

The simplest form of Stirling engine analysis was introduced by Schmidt in order to describe Lehmann's machine, an engine of the displacer type [115]. The gas temperatures in different areas of the engine are assumed to be isothermal, hence the theory is also known as isothermal analysis. It is closely related to the ideal

Stirling cycle but the sinusoidal piston motion and the resulting working gas distribution is taken into account. For sinusoidal piston and displacer motion a closed form solution is available which allows predictions to be made according to the swept volume, the temperature ratio, phase angle and the pressure.

Finkelstein improved the isothermal model by assuming adiabatic or partially adiabatic cylinders and shifting the heat transfer from the cylinders to the heat exchangers [116]. No closed-form solutions are available for the 'adiabatic theory' and numerical methods have to be used for solving the power prediction.

First-order models are highly idealised as heat transfer is assumed to be without losses and no internal pumping losses are considered. The power and efficiency predictions are therefore highly optimistic. Specific design insights, such as for the layout of the regenerator or the heat exchanger, cannot be obtained from such simple modelling. Especially for the low-temperature difference case, the assumption of ideal heat transfer is very unrealistic, especially at higher frequencies where pumping losses also become an important loss mechanism.

However, first-order modelling is a good starting point to get insights into the Stirling cycle and to evaluate different concepts at a very basic level. The isothermal analysis is explained below in greater detail as it is used for comparison and identification of promising engine concepts.

2.1.2 Second-order modelling

The two analysis methods mentioned above can be used as the basis for more accurate calculations. For second-order simulations usually a prediction with a first-order model is made. From the values obtained different losses are then subtracted to correct the idealized predictions. These parasitic power losses are calculated independently of each other. Pressure losses, limited heat transfer in

the heat exchangers, heat conduction, mechanical friction, seal leakage and other losses can be taken into account.

At the moment two second-order simulation programs are commercially available: SNAPpro (Stirling Numerical Analysis Program) [117, 118] by Altman and PROSA (PROgram for Second-order Analysis) [119–121] developed by Thomas.

Although good results can be achieved if validated models for the different loss mechanisms are used, second-order models cannot provide the same level of insight obtainable from a third-order model.

2.1.3 Third-order modelling

One-dimensional flow

The aim of third-order modelling is to provide a more realistic representation of the state of the working fluid using a resolution in time and space. Usually the resolution in space is only one-dimensional, but higher orders are possible too (see below). The different components of the engine are divided into a number of finite cells which are then connected by the corresponding number of nodes. Each of these cells represents a gas volume of a certain temperature, volume, pressure and mass. A series of differential equations for each cell is established. These are conservation of mass, momentum (e.g. viscous and pressure forces) and energy. Energy, mass and momentum can be transferred between the cells via the nodes. Heat flow into and out of cells to solid bodies can be added as boundary conditions to model heat exchangers or parasitic losses. Not only the heat transfer is simulated but also the fluid-dynamics of the working fluid at the same time.

No closed-form solution is available, and numerical methods have to be applied to solve the system. Empirical correlations are necessary for some of the heat transfer and flow phenomena in order to gain valid results. The hardware

requirements are much higher than for the lower-order approaches but a standard desktop computer will find a solution for a specified model within a reasonable time, depending on the solution algorithm. Urieli et al. describe the fundamentals of most third-order analysis named 'quasi steady flow model' in detail [122, 123].

An overview and a discussion of the simulation model techniques and programs in the early 1980's is given by Chen [124]. Since then models have been refined and improved, but the underlying ideas have not changed. At the moment the only commercially available third-order model software is Sage by Gedeon Associates [125–127], which is described below in greater detail. Other third-order models used for academic purposes can be found for example in Garcia-Granados as well as Andersen's work [128, 129].

Third-order models are very well suited for mapping and general engine optimisation purposes. Important engine design variables can be found as well as suitable working conditions. Existing designs can be optimised thermodynamically and fluid-dynamically or new engines can be designed from scratch. A typical shortcoming of one-dimensional models is that they are less accurate for non axis-symmetric engines (beta-type engines are typically axis-symmetric). When a gas circuit contains branching accuracy can be affected and the introduction of 2D and 3D modelling approaches can help to improve the predictions. Generally 2D and 3D CFD modelling provides a good addition to refine engine designs obtained from an one-dimensional model further.

Two- and three-dimensional CFD modelling

Third-order analysis can provide deep and accurate insights into the Stirling cycle in a short time. However, it might be desired to know the temperature and pressure distribution in the working fluid in even greater detail with a discretisation in space in two or even three dimensions. Computational fluid dynamics (CFD) have

been applied mainly by two research groups, one at Durham University [130, 131] and the other at NASA [132, 133].

Computing a whole engine over a complete cycle is a highly resource-intensive task and cannot be done on a standard desktop machine. In 2008 a 32 processor machine ran between one and eight hours for the calculation of an engine and it took weeks to generate a suitable mesh which had to be done mainly manually [134]. The results obtained are reported to be very accurate. With the large amount of preparation work necessary it becomes clear that CFD modelling of the Stirling engine is (at least today) only suitable for a mature stage in the design process and that an experienced user is needed.

A less detailed CFD model can however be useful in order to find and reduce pressure losses or to optimise the gas flow paths in the engine once a design with a lower-order model has been chosen.

2.2 Isothermal analysis

A simple analysis is required not only to understand the processes involved in Stirling engines but also to understand fundamental (inherent and design-independent) differences in the performance of different configurations. The first theoretical approach to predict the behaviour of hot gas engines was made by Schmidt in 1871, e.g. in the book by Urieli [123]. When the Stirling engine was revived at Philips in the 20th century, isothermal analysis was the first mathematical tool used for the engine development [135]. A good overview of the evolution of mathematical models for Stirling engines can be found in Organ and Finkelstein's book [38] on air engines. The latter is also the author of a paper [136] on the optimization of SE using isothermal theory. Other important papers were published by Kirkley [137] and Walker [138] showing results in a more selected and straightforward approach.

Even today papers based on the isothermal analysis are published on a regular basis [139, 140].

In the simple isothermal analysis, gas is moved between two volumes (one hot; one cold) connected via another volume at intermediate temperature representing the heat exchangers and other unswept volumes. All volume changes are constrained to sinusoidal piston and displacer movements. Furthermore, flow losses, heat transfer processes, geometrical constraints and the presence of a regenerator are not taken into account. Thus the calculated efficiency tends to be too low (due to the lack of internal regeneration) and the calculated work output to be too high (due to the perfect heat exchange). It is not possible to optimise the heat exchangers or the regenerator, as ideal heat exchange is assumed which leads to a contradiction: In the analysis the heat exchangers seem to be dispensable as they only contribute to the dead volume, whereas in a real engine they represent a vital part. Thus dead volume, or volume for the heat exchangers, has to be generated in the model to represent a more realistic set-up.

Nevertheless isothermal analysis can be a valuable tool to familiarize oneself with SE operation and to gain a basic understanding of the cyclic variations inside the SE[1]. A basic comparison of different configurations with each other is possible as the same assumptions are made for each case.

[1]In a sense, the value of such isothermal analysis is similar to the role that the limiting reversible cycle analysis plays in gaining an understanding of the relative importance of different operational parameters in thermodynamic processes and cycles generally.

The isothermal model

To simplify Stirling engine analysis for the isothermal case some assumptions are necessary:

- heat exchange between working fluid and heat source and sink is perfect (no temperature gradient)
- no thermal short-cutting; thus wall thickness or geometrical constellation have no impact on performance
- the ideal gas law predicts the working fluid's behaviour
- there is no regeneration, due to internal heat storage and recycling. Nevertheless the temperature change of the gas in the regenerator shows the same temperature gradient as a real regenerator.
- the gas pressure is equal throughout the different volumes at each time step; there are no pressure losses.
- the cyclic mean pressure acts on the backside of the pistons at all times (for single gas cycle engines)
- constant gas mass throughout the cycle
- sinusoidal displacer and piston motion (if not stated otherwise)
- temperatures in the different spaces are constant
- engine speed is constant and has no influence on performance
- steady state operation
- kinetic and potential energies are neglected
- the total swept volume (V_{swept}) is identical for different configurations

The engine is divided into five volumes: The cold compression space (V_c) and the cold heat exchanger (V_k), the regenerator (V_r) at an intermediate temperature, the hot expansion space (V_e) and the hot heat exchanger (V_h). Only the compression and expansion volumes change, heat exchanger and regenerator volume remain constant and are thus referred to as dead volume (V_d). The total gas volume (V_{gas}) as a function of the crank angle (θ) can then be expressed as:

$$V_{gas}(\theta) = V_c(\theta) + V_k + V_r + V_h + V_e(\theta) = V_c(\theta) + V_d + V_e(\theta). \tag{2.1}$$

Volume changes are constrained to the motions of piston(s) and displacer. As sinusoidal piston motion is assumed, the compression volume can be expressed as:

$$V_c(\theta) = A_c \left(1 + \cos\left(\theta\right)\right) \tag{2.2}$$

and the expansion volume as

$$V_e(\theta) = A_e \left(1 + \cos\left(\theta + \alpha\right)\right), \tag{2.3}$$

with α being the phase angle by which the expansion volume leads the compression volume, and A_x being the amplitude of the corresponding volume. Due to the different geometrical arrangements in alpha-, beta- and gamma engines the equations for the volume change and the resulting thermodynamic phase angles change in each engine and are thus given in the corresponding sections.

The pressure within these spaces changes during the cycle, but the instantaneous pressure is the same throughout the engine as no pressure losses occur:

$$p_{gas}(\theta) = p_c(\theta) = p_k(\theta) = p_r(\theta) = p_h(\theta) = p_e(\theta). \tag{2.4}$$

The gas mass (m_{gas}) is constant within the envelope of the engine for one configuration and is adjusted to define the maximum pressure. According to the

piston and displacer motion as well as to the temperature distribution the mass distribution changes during the cycle. Thus:

$$m_{gas} = m_c(\theta) + m_k(\theta) + m_r(\theta) + m_h(\theta) + m_e(\theta). \tag{2.5}$$

Applying the ideal gas law,

$$pV = mR_{gas}T, \tag{2.6}$$

with R_{gas} being the specific gas constant of the working fluid and T the temperature. Rearranged to

$$m = \frac{pV}{R_{gas}T} \tag{2.7}$$

for each volume leads to the instantaneous gas mass distribution:

$$m_x(\theta) = \frac{p_{gas}(\theta)V_x(\theta)}{R_{gas}T_x}. \tag{2.8}$$

Inserted into Equation 2.5 for each volume leads to:

$$m_{gas} = \sum_x \frac{p_{gas}(\theta)V_x(\theta)}{R_{gas}T_x} \tag{2.9}$$

and thus:

$$m_{gas} = \frac{p_{gas}(\theta)}{R_{gas}} \left(\frac{V_c(\theta)}{T_c} + \frac{V_k}{T_k} + \frac{V_r}{T_r} + \frac{V_h}{T_h} + \frac{V_e(\theta)}{T_e} \right). \tag{2.10}$$

The cyclic pressure variation can be found by rearranging Equation 2.10 to:

$$p_{gas}(\theta) = m_{gas}R_{gas} \left(\frac{V_c(\theta)}{T_c} + \frac{V_k}{T_k} + \frac{V_r}{T_r} + \frac{V_h}{T_h} + \frac{V_e(\theta)}{T_e} \right)^{-1}. \tag{2.11}$$

The constant terms for cooler, regenerator and heater can be combined, so that

$$p_{gas}(\theta) = m_{gas}R_{gas} \left(\frac{V_c(\theta)}{T_c} + \frac{V_d}{T_d} + \frac{V_e(\theta)}{T_e} \right)^{-1}, \tag{2.12}$$

where the dead volume's representative temperature is calculated assuming a logarithmic temperature profile in the regenerator, so that

$$T_d = \left(\frac{x_k}{T_k} + \frac{x_r \ln \frac{T_h}{T_k}}{T_h - T_k} + \frac{x_h}{T_h} \right)^{-1} \tag{2.13}$$

with

$$T_k = T_c, T_h = T_e, x_x = V_x / V_d$$

As every piston has two sides, gas forces from both sides act on the piston. While inside the working cylinder $p_{gas}(\theta)$ acts on the piston surface, there is another pressure working in the opposing direction. This can be the ambient pressure if the crank case is open to the atmospheric air, the mean cycle pressure (p_{mean}) if the crank case is sealed or a large buffer space is installed, or the pressure of an adjacent cycle if double-acting pistons are used in multi-cycle engines. Finkelstein [136] derived the mean cycle pressure as the geometric mean:

$$p_{mean} = \sqrt{p_{max} p_{min}}, \tag{2.14}$$

which has also been confirmed numerically with the established model. The effective pressure thus becomes

$$p_{eff}(\theta) = p_{gas}(\theta) - p_{mean}. \tag{2.15}$$

Now the indicated work can be calculated as

$$W_e = \int_0^{2\pi} p_{eff}(\theta) dV_e(\theta) = \oint p_{eff} dV_e \tag{2.16}$$

for the expansion space, and

$$W_c = \int_0^{2\pi} p_{eff}(\theta) dV_c(\theta) = \oint p_{eff} dV_c \tag{2.17}$$

for the compression space. Since the model does not include any further loss mechanisms the total work can be calculated as

$$W = W_e + W_c = \int_0^{2\pi} p_{eff}(\theta) dV_{gas}(\theta) = \oint p_{eff} dV_{gas} \tag{2.18}$$

In order to have more comparable results independent of the maximum pressure and the total volume, the equations should be made non-dimensional. The cyclic pressure from Equation 2.12 can be made non-dimensional by using the maximum cycle pressure:

$$p_{gas,n}(\theta) = \frac{p_{gas}(\theta)}{p_{max}} \tag{2.19}$$

The same can be done for the volume. Equation 2.1 then becomes

$$V_{gas,n}(\theta) = \frac{V_{gas}(\theta)}{V_{total}}. \tag{2.20}$$

with

$$V_{total} = V_{swept} + V_d \tag{2.21}$$

Finally, normalising the indicated work leads to:

$$W_n = \frac{W}{p_{max} V_{total}}. \tag{2.22}$$

Schmidt presented a closed form solution for the indicated work of the Stirling cycle which is only available for sinusoidal piston motion. Numerical solution of the equations above allows also for non-sinusoidal motion, e.g. slider-crank mechanism or discontinuous displacer motion. Originally the efficiency of the isothermal analysis was calculated as the Carnot efficiency. Numerical integration of the heat input and indicated work of the engine allows for a different calculation

of the efficiency which can then be calculated as

$$\eta = \frac{W}{Q_{in}}. \tag{2.23}$$

Isothermal analysis can be a useful tool to make preliminary estimations and to gain an understanding of the volume changes, piston movements and pressure oscillations inside the Stirling engine. It is used below for the identification of a suitable engine type for the low-temperature Stirling engine. An optimisation of the heat exchangers and the regenerator is not possible, as their volumes all represent additional dead volume and are only defined by their volume, not by geometry. Thus, optimisation of those volumes would lead to no regenerator and no heat exchangers. The only way to deal with this problem is to set the three volumes (hot and cold HX, regenerator) to a reasonable size; for the comparative simulations below it was set equal to the swept volume (a size similar to real engines). Furthermore, the coefficient of convective heat transfer in the heat exchangers and the regenerator depends on the phase angle and thus the mass flow rate, as Iwabuchi showed experimentally [141]. This fact is not taken into account in the isothermal analysis, nor are the heat losses by radiation or conduction, and pressure (pumping) losses. Pumping losses and heat transfer are highly dependent on the frequency which is not accounted for in the isothermal model. However, for general comparisons between different engine concepts it is regarded as a valuable tool.

2.3 Sage simulation software

The Sage software is a commercial code that provides a graphic user interface and solver for a validated third-order model with one-dimensional flow (see Section 2.1.3). It is capable of a more in-depth analysis of the Stirling engine than the

isothermal analysis. A specific working fluid with specific characteristics (density, heat capacity, viscosity, etc.) can be chosen from the database as opposed to the isothermal model where different working fluids do not change engine performance for a given pressure (only the amount of gas mass changes). The heat transfer to the gas is modelled according to the physical set-up of the heat exchangers and the regenerator and their consequent flow and surface areas. Heat conduction and radiation between neighbouring parts can be implemented too to create an even more realistic model. Pressure loss in ducts and matrices due to fluid friction is also implemented. In Sage a model for the heat transfer in the solid components of the engine and a fluid- and thermodynamic model of the working gas are coupled in order to describe all thermodynamic and fluid-dynamic loss mechanisms.

Sage [127] has been chosen as a simulation tool for a number of reasons. First of all, it is commercially available and not a company's proprietary code, making it simply obtainable. Some companies such as Philips and MAN used their own code for design purposes in the past, but of course never made that knowledge public [22]. Due to its modular structure Sage is very flexible and can model Stirling machines in the configuration and the level of detail needed, in both direct and reversed mode. The different modules within the code are already validated, so that results gained with Sage are in much better agreement with reality than a mere theoretical model can be, even though the working gas is only discretised in one dimension. This versatility and accuracy makes it the software of choice in the industry. Companies such as Sunpower (where Sage originated), Infinia, and Single-Phase-Power (SPP) use Sage to simulate their Stirling engines but also research institutions such as NASA GRC [86, 92, 107, 142–146]. At the University of Canterbury Sage was applied successfully in a number of projects in cooling and engine applications [147–149]. The structure and underlying models of the program are presented in the following section.

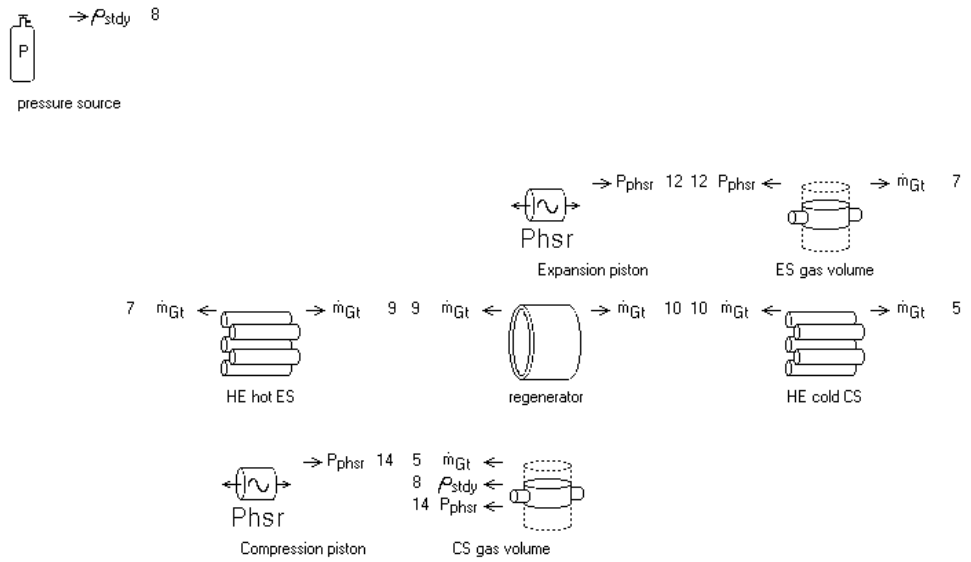

Figure 2.1: User interface of a Sage model of a simplified alpha engine. Not shown are heat sink and source.

2.3.1 Program structure

Figure 2.1 shows a screen shot of the user interface representing an alpha-engine. Each of the icons which can be chosen from a menu represents a distinct part of the engine, usually the working gas and the corresponding pressure wall or other solid bodies in contact with the fluid. As long as the connections are physically meaningful (same property), these icons can be combined freely. Depending on the component to be modelled different sub-models can be included to simulate the desired heat transport phenomena. The individual components (e.g. heat exchanger, cylinder space, etc.) are internally split into a number of connected cells. In Figure 2.2 a flow diagram of an engine is given, showing the established sub-models as well as the individual cells. The individual cells in the different components communicate via the established mass and heat transfer paths with other components. Geometrical parameters which influence e.g. cross-sections, cell length, heat transfer, and pumping losses are specified for each component in the main model and automatically transferred into the sub-models. As usual for

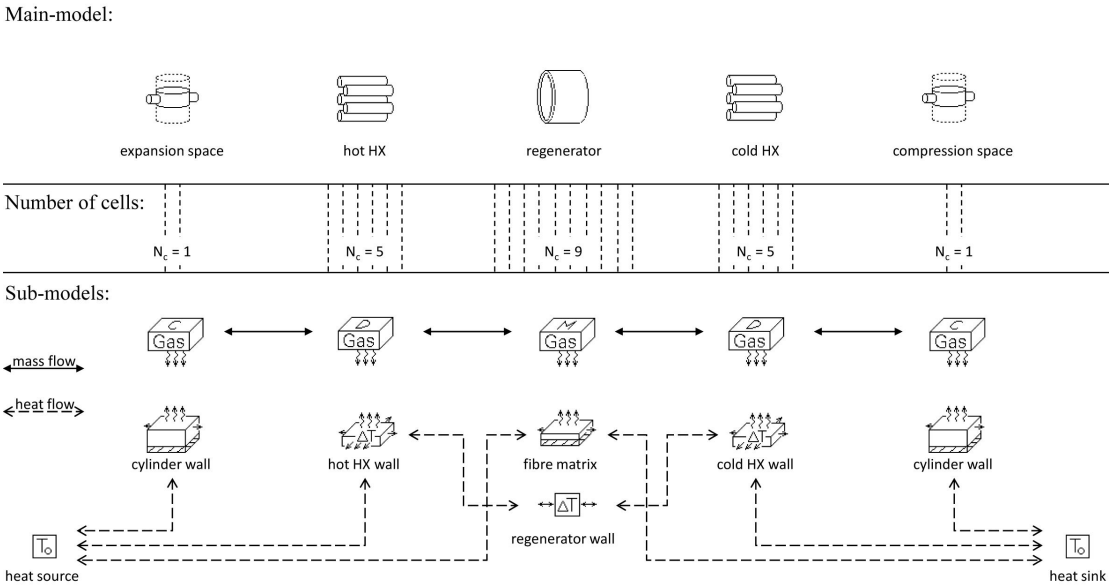

Figure 2.2: Sage model of the alpha-type Stirling engine showing the discretisation in space of the components (N_C), and its sub-models with conductive heat flows (---), gas mass flows ($\longleftrightarrow$), and heat transfer between the surfaces and the working fluid ($\rightsquigarrow$).

third-order models the three equations of conservation (mass, momentum, energy), the internal energy, and an Equation of State have to be solved simultaneously for each singular cell and time step. Detailed information about the thermodynamic and fluid-dynamic model and the solving method can be found in [126, 127]; a short description is given in the following sections.

2.3.2 Underlying models

Gas model

For each of the cells introduced in Figure 2.2 a number of equations has to be established to describe the thermodynamic and fluid-dynamic state of the working fluid for each time step. Each cell is characterised by the geometric information inherited from the main model; the flow area (A) and the length ($dx = l_{component}/N_C$).

The length is fixed for each time step but the area can be variable as is the case for the cylinder spaces which here represents the volumetric displacement caused by the motion of the pistons. The equations needed to characterise each cell are the equations of continuity, an Equation of State, and a definition for the internal energy. General derivations for these equations for three dimensional flow can be found in introductory books on CFD simulation e.g. [150–152]. The equations of continuity can be derived from the general Navier-Stokes equations but have to be modified for the special case of one-dimensional flow or can be found by applying mass, momentum, and energy balances on a single cell (control volume). In Figure 2.3 this derivation of the differential equations is shown.

Following Figure 2.3 (a) the equation for the continuity can be found to be

$$\frac{\partial \rho A}{\partial t} + \frac{\partial \rho u A}{\partial x} = 0 \tag{2.24}$$

with u being the velocity of the fluid and ρ being its density. The net mass flow out of the control volume has to equal the time rate of decrease of mass inside the control volume.

The second quantity which has to be conserved is the momentum. The rate of momentum accumulation in the control volume has to equal the net rate of momentum out plus the sum of forces (i.e. pressure and fluid friction) acting on the control volume. Balancing the forces on the control volume in Figure 2.3 (b) yields the equation for the conservation of the momentum

$$\frac{\partial \rho u A}{\partial t} + \frac{\partial u \rho u A}{\partial x} + \frac{\partial p}{\partial x} A - F A = 0 \tag{2.25}$$

where F represents a viscous flow resistance due to surface shear stress given as a force per unit length per unit flow area. Due to the one-dimensional nature of the model it cannot be resolved directly and is thus modelled separately as a

Continuity

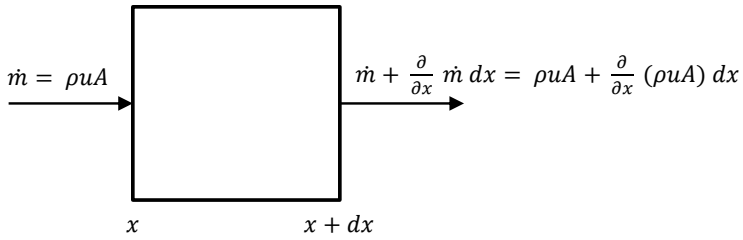

$$\frac{\partial}{\partial t} m = \frac{\partial}{\partial t}(\rho A)\,dx = \rho uA - \left(\rho uA + \frac{\partial}{\partial x}(\rho uA)dx\right)$$

$$\boldsymbol{\frac{\partial}{\partial t}(\rho A) + \frac{\partial}{\partial x}(\rho uA) = 0}$$

(a)

Momentum

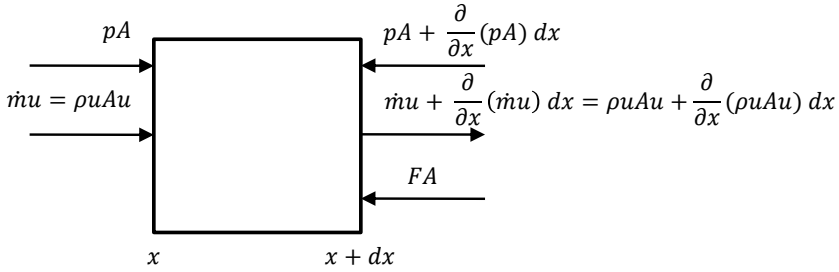

$$\frac{\partial}{\partial t}(\rho uA)dx = -\frac{\partial}{\partial x}(\rho uAu)dx - \frac{\partial}{\partial x}(pA)dx + FA\,dx$$

$$\boldsymbol{\frac{\partial}{\partial t}(\rho uA) + \frac{\partial}{\partial x}(\rho uAu) + \frac{\partial}{\partial x}(pA) - FA = 0}$$

(b)

Energy

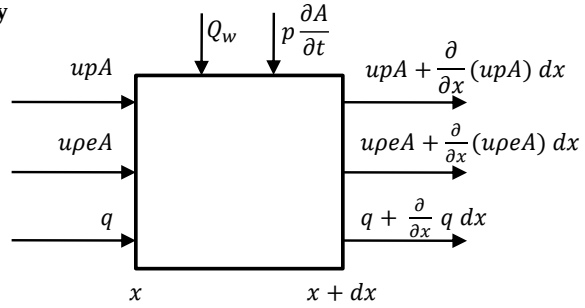

$$\frac{\partial}{\partial t}(\rho eA)dx = -p\frac{\partial A}{\partial t}\,dx - \frac{\partial}{\partial x}(upA)dx - \frac{\partial}{\partial x}(u\rho eA)dx - \frac{\partial}{\partial x}q\,dx + Q_w\,dx$$

$$\boldsymbol{\frac{\partial}{\partial t}(\rho eA) + p\frac{\partial A}{\partial t} + \frac{\partial}{\partial x}(upA) + \frac{\partial}{\partial x}(u\rho eA) + \frac{\partial}{\partial x}q - Q_w = 0}$$

(c)

Figure 2.3: Derivation of the differential equations for the finite cells approach used in Sage; (a) continuity, (b) momentum, (c) energy.

frictional pressure gradient. E.g. for a heat exchanger F is calculated by

$$F = -(f/d_h + k/l)\rho u|u|/2 \tag{2.26}$$

with the Darcy friction factor (f) and loss coefficient (k) obtained from published empirical correlations; d_h is the hydraulic diameter ($d_h = 4A/S$, S the wetted perimeter) of the duct and l its length.

The conservation of energy is the third differential equation needed to describe the volume element. The rate of energy gain of the control volume is defined by the $p - V$ work done on the wall, the change of gas energy flux (internal energy, pressure, axial conduction), and heat transferred to or from the wall, as can be seen in Figure 2.3 (c). Thus the equation becomes

$$\frac{\partial \rho e A}{\partial t} + p\frac{\partial A}{\partial t} + \frac{\partial}{\partial x}(u\rho eA + upA + q) - Q_w = 0 \tag{2.27}$$

with empirical terms for the axial conduction in the gas (q) and the film heat transfer (Q_w) between the gas and a solid. As for the frictional pressure drop (F) assumptions for the turbulence of the fluid are included here, depending on the gas domain (cylinder space, heat exchanger, regenerator matrix). A detailed description can be found in [127]. The mass-specific gas energy (e) is defined as

$$e = \epsilon + u^2/2. \tag{2.28}$$

The mass-specific internal gas energy (ϵ) is calculated depending on the Equation of State used for the gas. For the ideal gas equation

$$p = \frac{RT}{v} = \rho RT \tag{2.29}$$

the internal energy becomes

$$\epsilon = c_v T. \tag{2.30}$$

In the case that the Redlich-Kwong equation:

$$p = \frac{RT}{v-b} - \frac{a}{T^{1/2}v(v+b)} \tag{2.31}$$

with gas specific parameters a and b is used, the internal energy becomes

$$\epsilon = \bar{c}_v T - \frac{3}{2}\frac{a}{b}\ln(1+\frac{b}{v})T^{-1/2}. \tag{2.32}$$

The independent variables gained from the differential equations are the mass density (ρ), the mass flow rate (ρuA), and the energy density (ρe) and are used to describe the dependent variables temperature (T) and pressure (p).

Wall model

Thermal solid components (s) which are in contact with the working fluid such as heat exchanger ducts, pressure canisters, or regenerator matrices are discretised on the same spatial and time grid as the corresponding gas component. Generally they are modelled by a one-dimensional solid-energy equation as

$$\rho_s c_s A_s \frac{\partial T_s}{\partial t} + \frac{\partial q_s}{\partial x} + Q_w = 0. \tag{2.33}$$

The heat flow (q_s) in axial direction is modelled as

$$q_s = -k_s \frac{\partial T_s}{\partial x} A_s \tag{2.34}$$

with the solid's conductivity k_s and A_s the cross-sectional area.

The surface heat transfer (Q_w) which represents the energetic connection to the gas model in Equation 2.27 is established using empirical correlations. The wall temperature T_w is introduced to formulate Q_w as a function of the temperature difference $T_w - T$, the Nusselt number and hence turbulence, and the geometry of

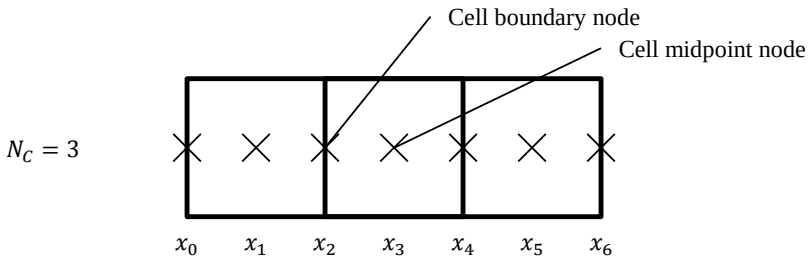

Figure 2.4: Example of a component discretised in three cells ($N_C = 3$) showing the established mid- and boundary nodes

the component. Depending on the modelled surface different approaches are used but go beyond the scope of this introduction.

2.3.3 Solution method

As described above the individual components are divided into a number of finite cells or volumes. Discretisation is in space as well as in time. For a chosen number of cells (N_C), $2N_C+1$ nodes are established on the spatial grid (index i) since each cell receives a centre and two boundary nodes, see Figure 2.4. Together with the discretisation in time (number of time nodes N_T, index j) a matrix is generated for each variable in each component. For a generic variable $f(x,t)$ this matrix has the following form:

$$\begin{pmatrix} f(x_0,t_j) & \cdots & f(x_i,t_j) \\ \vdots & \ddots & \vdots \\ f(x_0,t_0) & \cdots & f(x_i,t_0) \end{pmatrix}$$

The values for ρ, ρuA, and ρe are solved at alternate nodes using a staggered grid logic (only spatial). The mass flow ρuA is solved implicitly on the boundary nodes and interpolated for the mid-point nodes; mass and energy density are solved and interpolated vice versa. Thus solution instability can be avoided. For

approximation the derivatives are replaced with central differences at the spatial node (i)

$$\frac{\partial f}{\partial x} = \frac{f_{i-1} - f_{i+1}}{2dx} \tag{2.35}$$

A periodic solution is expected and assumed for the system. Time differencing is done according to a multipoint backward differencing method similar to the three point backward differencing given by

$$\frac{\partial f}{\partial t} = \frac{3f_j - 4f_{j-1} + f_{j-2}}{2dt}. \tag{2.36}$$

A built-in non-linear solver is used to find an iterative solution to the large system of equations applying the Newton-Raphson method.

2.4 Validation of a Sage model

2.4.1 A 9 kW beta-type high-temperature engine

Even though Sage is well known and wide-spread in use it was important to gain an understanding on how precise the predictions for power output and efficiency are. Therefore test data of a real, well-documented single cylinder beta engine provided by Professor Carlsen of the University of Denmark has been used to validate a Sage model. Further information on the engine can be found in references [50] and [153], on the specific crank mechanism used in [154] and on the engine's regenerator in [155]. It has been used for simulation model validation before [156]. In Figure 1.7 (c) a photo of the engine can be found; Figure 2.5 shows a picture of the thermodynamically relevant parts of the investigated engine. The displacer and the working piston both have a bore of 114 mm and a stroke of 54 mm. The power output is designed to be 9 kW at 1020 rpm with helium as the working gas at a mean pressure of 8 MPa and 700 °C heat exchanger

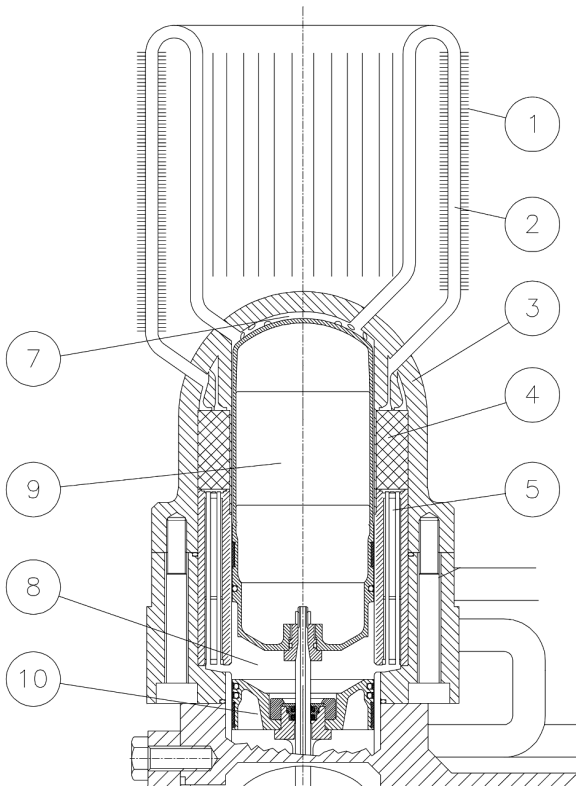

Figure 2.5: Experimental 9 kW Stirling engine of the University of Denmark [50]

temperature. The expansion space (7) is connected to the compression space (8) via the externally-finned tubular hot heat exchangers (1, 2), the wire mesh-filled regenerator (4) and the water-cooled cold heat exchanger (5). The two gas spaces are separated by the elongated displacer (9), which moves the working gas through the heat exchangers. Compression and expansion of the gas volume is made possible by the power piston (10) which also houses the displacer rod seal in the centre. The internal heat conduction paths were determined by examination of the engine drawing. Depending on the temperature difference between adjacent parts and their wall thicknesses the most significant conduction paths have been identified and implemented into the Sage model. As can be seen from the drawing (Figure 2.5) the massive housing (part 3) which directly connects the hot and cold heat exchangers is responsible for the major heat loss. Nevertheless, thermal conduction in the displacer, the regenerator and the cylinder liner is implemented, too. Figure 2.6 shows the simulation model built in Sage.

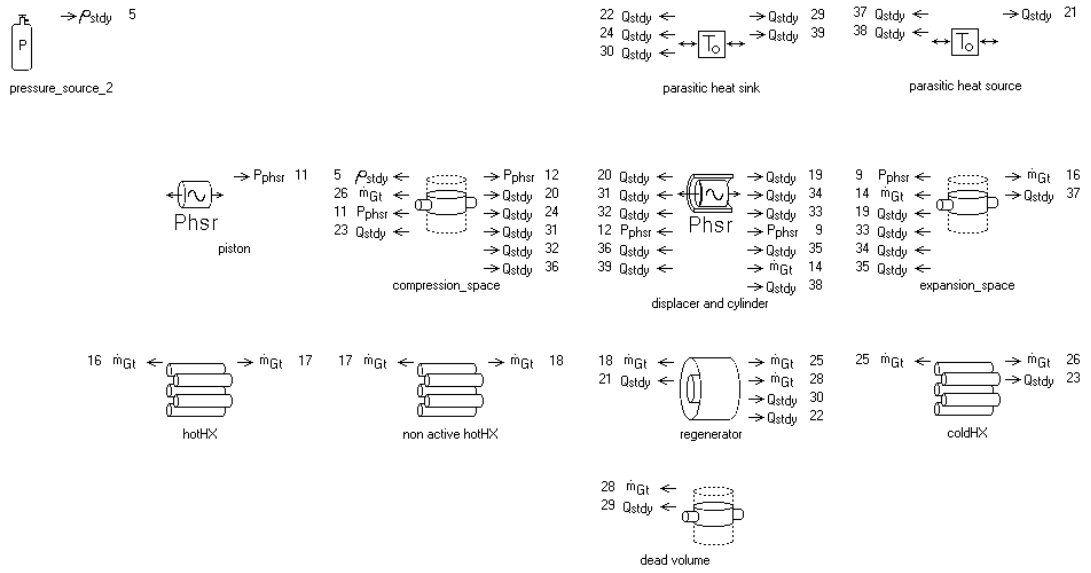

Figure 2.6: Sage model for the validation of the 9 kW Stirling engine

In Sage only the thermo- and fluid-dynamics of the working gas are calculated. The resulting pressure and volume variations, which together represent the indicated power P_{ind}, have to move a crankshaft and a generator if electrical power is to be produced. Since this never happens without losses, the electrical power output can be calculated to

$$P_{el} = \eta_{mech}\eta_{gen}P_{ind}, \tag{2.37}$$

with η_{mech} being the mechanical efficiency of the engine and η_{gen} being the electrical efficiency of the generator. Usually brake power is measured using a dynamometer to estimate engine performance. Due to the hermetically sealed design of this specific engine this is not possible; hence it is measured indirectly by the electrical power output of the generator. The electrical efficiency of the generator was determined at the University of Denmark for each measured working point but not the mechanical efficiency, which had to be estimated in order to connect the Sage model to the 'real world'. Figure 2.7 (left) shows the plots of the

electrical power output for different conditions versus the temperature for both experimental results (x) and Sage (+) modelling. For helium as a working gas three different levels of pressurisation (5.4 MPa (a), 6.2 MPa (c), 8.2 MPa (e)) have been tested and for each pressure level the temperature of the cooling water was varied in three increments (40 °C, 55 °C, 70 °C). Tests with nitrogen as a working gas were conducted too, but only for a heat sink temperature of 40 °C which is shown here at a pressure of 7.8 MPa (e). Each of the tested conditions was reproduced and computed in Sage. Since the mechanical losses were unknown they had to be calculated. As the frequency is constant for all measured working points the mechanical efficiency is considered to be constant, and the losses are expected to be only load-dependent. With the electrical efficiency known from experiments, the mechanical efficiency was used to fit the results from the simulation to the measured performance according to Equation 2.37. A least squares fit of the residuals yields a calculated mechanical efficiency of 0.81 for all set-ups, a reasonable value considering the complexity of the crank mechanism.

In Sage different gas models are available. The working fluid can either be modelled as an ideal gas according to Equation 2.6 or as a real gas using the Redlich-Kwong (RK) equation of state. For helium there is no noticeable difference in the pressure and temperature ranges considered. For nitrogen on the other hand, using the real gas model makes a noticeable difference with a better fit to the experimental data and an even a higher power output, as can be seen in Figure 2.7. When simulating engines charged with nitrogen this should be remembered and the RK gas-model should be used.

Figure 2.7 (right) shows the plots for the electrical efficiency of the engine (η_{el}). It is defined here as

$$\eta_{el} = \frac{P_{el}}{\dot{Q}_{in}} \tag{2.38}$$

with $\dot{Q}_{in}$ being the heat input to the engine. As it was not measured it had to be derived from an energy balance on the engine. It can therefore be calculated to

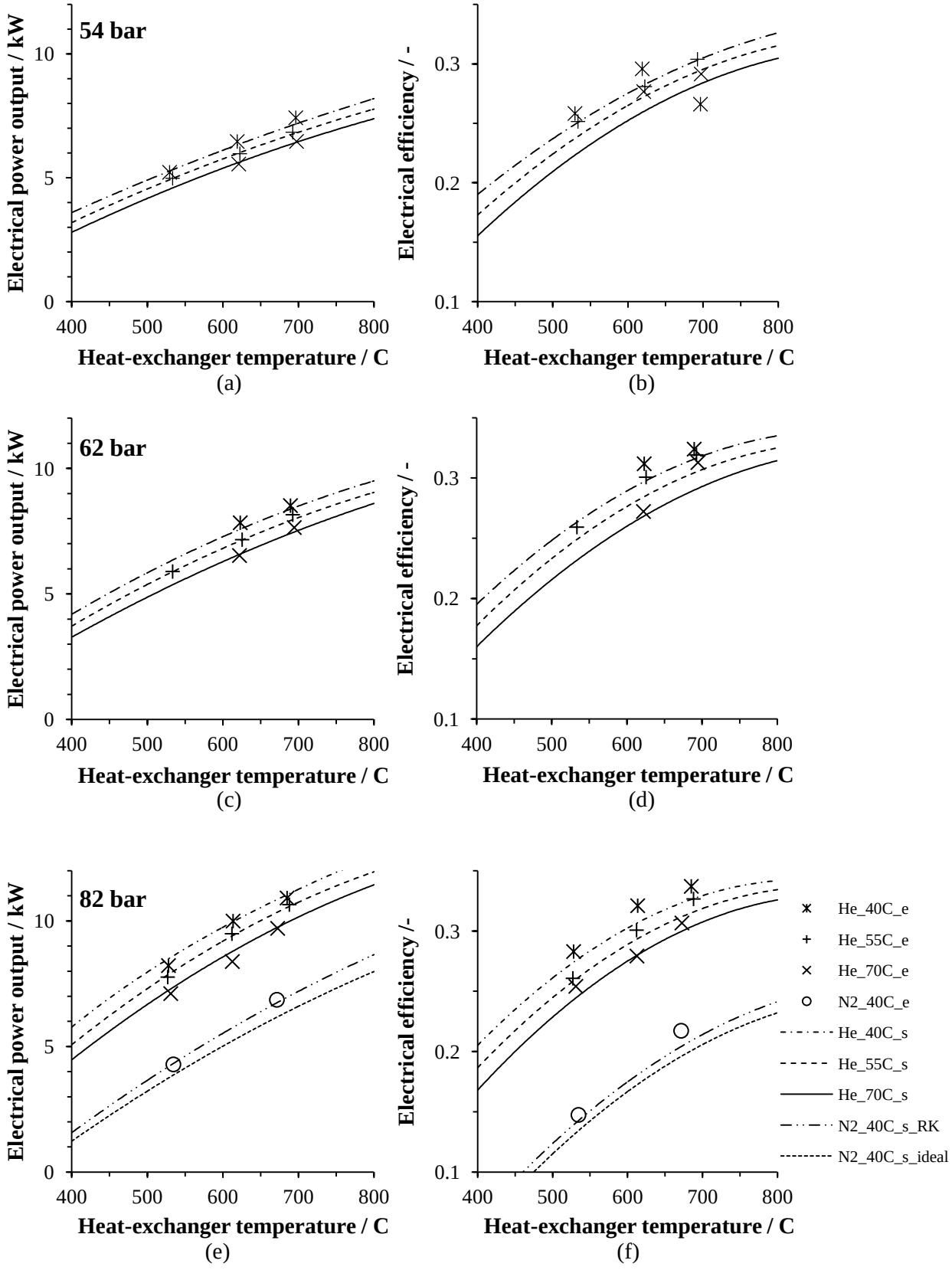

Figure 2.7: Test and simulation results for the 9 kW beta engine: Electrical power output and efficiency (e: experimental, s: Sage simulated)

be

$$\dot{Q}_{in} = P_{el} + \dot{Q}_{out} \tag{2.39}$$

where

$$\dot{Q}_{out} = \dot{Q}_{engine} + \dot{Q}_{generator} + \dot{Q}_{ambient}. \tag{2.40}$$

The thermal output of the cooling water of the engine ($\dot{Q}_{engine}$) and the generator ($\dot{Q}_{generator}$) were measured, whereas the losses to the ambient ($\dot{Q}_{ambient}$) had to be estimated from the engine surface area and its assumed temperature difference to the ambient. Due to the number of experimental values that feed into the calculation of the efficiency the difference between model and experiment is higher than for the power output, and the data points are more scattered. Nevertheless, the efficiency simulation is in good agreement with the experiment. One exception is the data point for helium at 5.4 MPa, 700 °C source and 40 °C sink temperature which appears to be a measurement error. The largest residuals are below 10 % of the measured and the calculated values.

One might argue that the mechanical efficiency is a mere tuning factor to adjust simulation and experiment but without exact measurement of the indicated power, the mechanical efficiency cannot be identified and thus has to be assumed. Nevertheless, the estimated mechanical efficiency allows the residuals of the electrical power output to be minimised. Unaffected by pressure level, working medium and temperatures, the power output is predicted with constant accuracy. Figure 2.8 shows that the difference between the Sage model and the experimental results is less than ±5 %. The confidence in using Sage-simulations for the thermodynamic investigation of SEs is high due to the very satisfying results of this study and the positive results by other authors. It will be used extensively throughout this work.

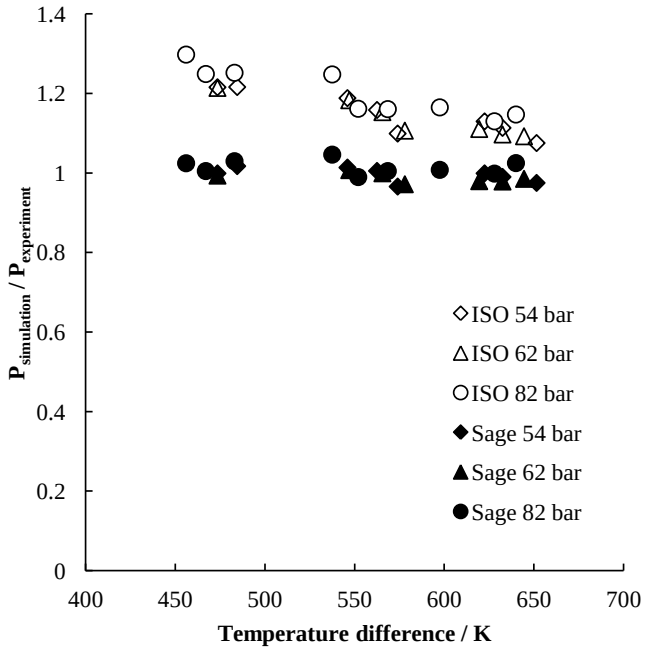

Figure 2.8: Comparison between the predictions for the 9 kW beta engine made by the Sage model (for helium) and by the isothermal model

2.4.2 Sage and low-temperature heat sources

The validation of the beta-type engine in the preceding section confirmed the good agreement of experimental data and the predictions obtained from a model built in Sage. Unfortunately no usable data for a low-temperature engine became available for additional validation. Nevertheless, since the main focus of this project is on Stirling engines for low temperature heat sources, it seems appropriate to discuss the thermodynamic and fluid-dynamic model used in Sage for this specific application.

The finite cell approach used in Sage is a general fluid modelling method not bound to any temperature regime. It is valid for a wide range of operating conditions such as engines at high temperature differences, cooling equipment running at low temperatures ($< 100\,\mathrm{K}$), or heat pumps near ambient conditions. In order to model pressure losses and heat transfer properly it is important to include the properties of the working fluid in the model. The fluid properties of

the used gases are well known over a wide temperature range and are included in the database. It is therefore possible to model engines at low temperature differences as good as at any other temperature provided its properties are known.

As the isothermal analysis is much simpler to implement, it is hoped that it can be used to compare different engine types on a very basic level to find the most promising engine layout. To validate this assumption a comparison between the isothermal model and the Sage simulation is made in Section 2.5 which follows. If it can be shown, that independent of the temperature level, the predictions of the isothermal model show qualitatively the same behaviour as the Sage model for different engine set-ups, even though its prediction may be somewhat optimistic, the isothermal model can be used.

2.5 Comparison of isothermal analysis and Sage simulation

For comparison of the outcomes of the isothermal analysis and the Sage simulation a model was built in Sage. Figure 2.1 shows the set-up of that model. It can be seen that no heat flows between the different parts were considered to allow better comparison with the ideal isothermal model. Connection between the different components is made only by mass flow ($\dot{m}_{Gt}$). The heat exchangers and the regenerator were optimised, so that the power output is maximised for a specific swept volume, phase angle and heat source temperature. The resulting volumes of the hot and cold heat exchangers, as well as the regenerator volume, is then transferred to the isothermal model where the swept volume, the phase angle and the temperature levels have already been implemented. The mean gas pressure acts on the backside of the power piston(s).

Figure 2.9 (a) and (b) show the resulting volume and pressure variations for two different heat source temperatures, 1000 K and 450 K, at a frequency of 30 Hz.

Since the piston motion is sinusoidal in both cases, the volume variations are equal for both simulations. As a result of the large surface needed for heat exchange at the small temperature difference the total volume is higher for the lower heat source temperature. With the maximum pressure for the two different simulations having been set to the same value, the resulting pressure amplitude is higher in the Sage model. Here, adiabatic effects heat and cool the working fluid beyond the temperatures of the heat exchanger walls. The higher temperature amplitude results directly in a higher pressure amplitude. In the isothermal model the gas temperature is always constraint by the temperature of the heat exchangers and the pressure amplitude is thus smaller for otherwise identical conditions. Since no pressure losses are considered in the isothermal the pressure (p_{iso}) is identical in the whole gas domain. In the Sage model pressure losses due to fluid friction reduce the pressure amplitude in the expansion space ($p_{e,sage}$) compared to the compression space($p_{c,sage}$).

In Figure 2.9 (c) and (d) the $p-V$ plots for the expansion and for the compression space are shown. It can be seen that the magnitude of the indicated expansion work (area enclosed by the lines) is in better agreement between the two models than the compression work. Adiabatic effects and fluid friction as modelled with Sage increase the compression power needed. The net work is thus higher for the isothermal model. Despite the higher compression power needed the calculated efficiency is higher for the third-order model. This is a direct result of the higher pressure amplitudes since the area below the $p-V$ plots which corresponds to rejected heat can be reduced.

In Figure 2.9 (e) and (f) the power development of the engine with the mean pressure acting on the backside of the pistons is shown. It can be seen when the pistons produce a usable power output (negative sign) and when power is consumed (positive sign). The higher pressure amplitudes from the Sage model increase also the amplitudes of the power plots compared to the isothermal model.

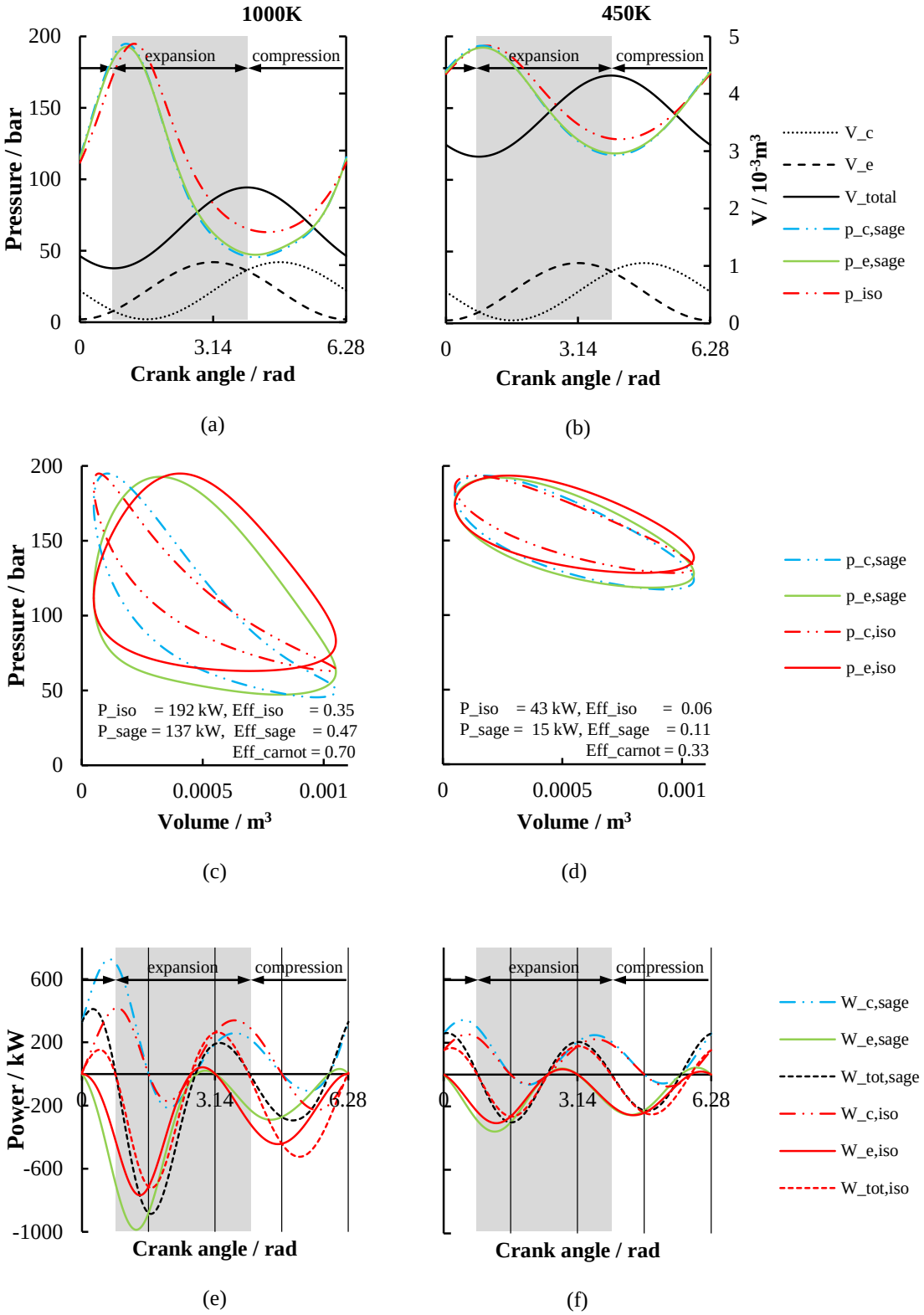

Figure 2.9: Comparison of Sage simulation and isothermal analysis for an alpha engine; operating frequency 30 Hz. Pressure and volume amplitudes for one cycle (a,b). $P-V$ plots representing the indicated work (c,d). Compression, expansion, and total power over one cycle (e,f)

The lower heat source temperature results in more symmetric power outputs in both horizontal and vertical direction compared to the high temperature. This is a direct result of the heating during expansion; whereas in the LTD the pressure and hence the power development is driven largely by the volume variation the larger temperature variation has a more dominant influence in the HTD, especially during expansion. The maximum pressure is also shifted away from the minimum volume (where it would coincide for no temperature difference) towards the maximum expansion volume - away from a compression driven maximum pressure towards a more heat driven maximum pressure.

A beta engine with the same parameters as the alpha engine was modelled in isothermal analysis and in Sage. Table 2.1 gives the ratios of power output for different engine types at different temperatures and frequencies. At high temperatures the difference between the isothermal model and the Sage simulation is much smaller than at low heat source temperatures as the heat transfer is closer to the ideal assumption when the temperature difference in the heat exchangers is large. For the low temperature difference the prediction of the power is about three times the value predicted with the Sage model. If the frequency is reduced (10 Hz) the agreement can be improved. For a specific temperature and frequency the offset seems relatively constant especially for the smaller frequency (where pressure losses are small and where the gas temperature comes closer to the wall temperature). The two different engine types (alpha and beta) perform similar in comparison for the different temperature levels. Especially for the lower frequency the two models rate the performance ratio of the two engines identically.

The 9 kW beta engine was also simulated by means of the isothermal analysis to validate the performance of that modelling tool. Therefore all heat exchangers, void regenerator, piston clearance, and duct volumes were established as dead volume at the corresponding temperature level. The variable cylinder volumes were built according to piston stroke and diameter as well as the phase angle. Iden-

Table 2.1: Comparison isothermal and Sage simulation: ratio of power output for different engines and simulations at different heat source temperatures and frequencies

Power ratio	450 K		1000K
	30 Hz	10 Hz	30 Hz
$alpha_{iso}$ / $alpha_{sage}$	2.7	1.9	1.4
$beta_{iso}$ / $beta_{sage}$	3.2	1.9	1.3
$beta_{iso}$ / $alpha_{iso}$	1.4	1.4	1.6
$beta_{sage}$ / $alpha_{sage}$	1.2	1.4	1.7

tical generator efficiency and mechanical efficiency as for the Sage model were assumed. The deviation from the experimental results can be seen in Figure 2.8. For the considered temperature range the model predicts 10 to 30 % more power than could be observed experimentally (or predicted with Sage). The quality of the isothermal model is highly dependent on the temperature difference as could already be observed in Table 2.1; the higher this difference the better the agreement between the two models. The smaller the temperature difference the more optimistic the isothermal model becomes which makes quantitative predictions for the area of interest of this study, low-temperature differences, unreliable.

From the simulations it can be seen, that even though the results from the isothermal model are not very close to the more realistic Sage model, it is possible to show tendencies and to compare thus different engine concepts for a specific temperature. While not allowing for good quantitative results for the estimation of the power output, it allows to show which engine set-ups makes the most of a given swept volume. Due to the intrinsically small power density of the low temperature engine this is the first step in finding a suitable design for the LTD. In the next chapter isothermal analysis is applied to identify the most promising engine concepts from a large number of possible engine set-ups. The most promising concepts will then be investigated further using more detailed Sage simulation which will result in quantitatively better results.

Chapter 3

Identification of a suitable LTD design

Due to the inherently low thermal efficiency obtainable for low-temperature differences engines are expected to be rather large compared to their power output. In order to minimise costs, different engine set-ups are compared to identify the engine set-ups with the highest power density. First isothermal analysis is applied to reduce the number of possible candidates, which seems appropriate on a comparative level, as it has been shown in the preceding chapter. A more detailed Sage simulation will then be conducted for the most promising candidates to ensure that the simplifications made in the isothermal model do not distort the outcome.

3.1 Single gas circuit engines (Isothermal analysis)

In its simplest form only two reciprocating elements are needed to create a Stirling engine as it has been described briefly in Section 1.2.2. These can be one displacer

and one piston or two pistons. Here, specifics of the resulting configurations are discussed and their resulting performance is compared. The results of the simulations are based on the isothermal analysis described above (see Section 2.2).

3.1.1 Alpha engines

In alpha configurations, two pistons moving with a phase offset generate the volumetric changes and the pressure fluctuations. Figure 3.1 (b) illustrates the movement of the two pistons. The expansion and compression cylinders are connected via the hot and cold heat exchangers, as well as the regenerator, which are depicted by the tubular duct on the left hand side. In Figure 3.1 (a) the trajectories of the piston surfaces are plotted over one cycle as well as the resulting volume changes in the expansion and compression cylinders and the overall volume change. Note that the maximum for the hot (expansion) volume always leads the cold (compression) volume as in every Stirling machine. This is known as the thermodynamic phase angle (α), which here is 0.5 π in contrast to the piston phase angle, which here is 1.5 π. The pressure variation due to the temperature and volume changes is plotted too, and it can be seen that the maximum pressure occurs only shortly after the minimum total volume as a consequence of the mass distribution over different temperature regimes. The working gas is highly compressed and more gas is in the hot expansion space than in the cold compression space. This asymmetry allows the engine to produce more power during expansion than it consumes during compression.

The compression (cold) volume can be calculated to be

$$V_c(\theta) = {}^1\!/_2 V_{s,c}(1 + \cos\theta), \tag{3.1}$$

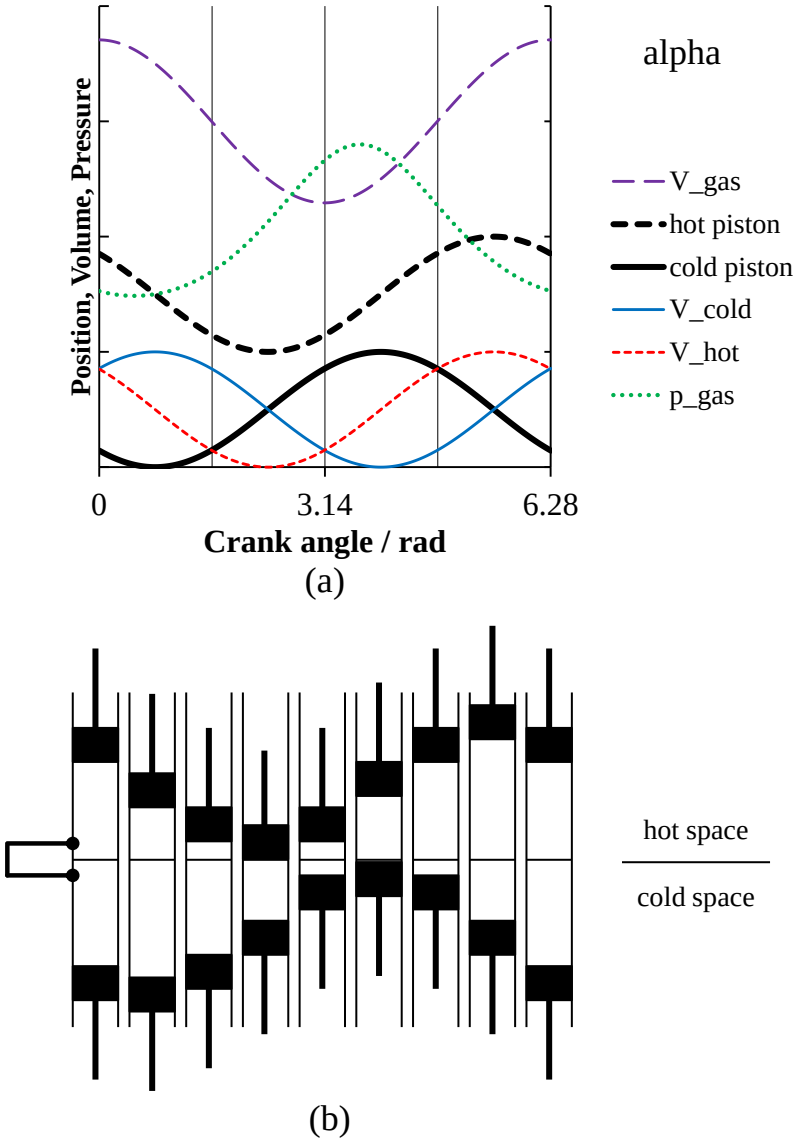

Figure 3.1: Set-up of an alpha engine in which two pistons are used to compress and expand the gas. Here they are phased in a way that the expansion space leads the compression space by 90° (0.5 π). The heat exchangers are depicted on the left (b). The resulting volume and pressure variations are shown above (a).

and, correspondingly, the expansion (hot) volume is

$$V_e(\theta) = 1/2 V_{s,e}(1 + \cos(\theta + \alpha)), \tag{3.2}$$

or with k being the ratio of the two swept volumes

$$k = \frac{V_{s,c}(\theta)}{V_{s,e}(\theta)} \tag{3.3}$$

the expansion volume becomes

$$V_e(\theta) = \frac{1}{2k} V_{s,c}(1 + \cos(\theta + \alpha)), \tag{3.4}$$

where θ is the crank angle, α the phase angle and $V_{s,c}$ being the volume swept by the compression piston and $V_{s,e}$ the volume swept by the expansion piston. Together they represent the swept volume:

$$V_{swept} = V_{s,c} + V_{s,e} \tag{3.5}$$

The gas volume then becomes:

$$\begin{aligned} V_{gas}(\theta) &= V_c(\theta) + V_e(\theta) + V_d \\ &= 1/2 V_{s,c}(1 + \cos\theta) + 1/2 V_{s,e}(1 + \cos(\theta + \alpha)) + V_d. \end{aligned} \tag{3.6}$$

And normalised to the total volume:

$$V_{gas,n}(\theta) = \frac{1/2 V_{s,c}(1 + \cos\theta) + 1/2 V_{s,e}(1 + \cos(\theta + \alpha)) + V_d}{V_{total}} \tag{3.7}$$

Figure 3.2 shows the influence of changes of the phase angle on engine behaviour for two different heat source temperatures. The volume ratio k (of expansion and compression volume) is fixed to unity, as it is close to the optimum value

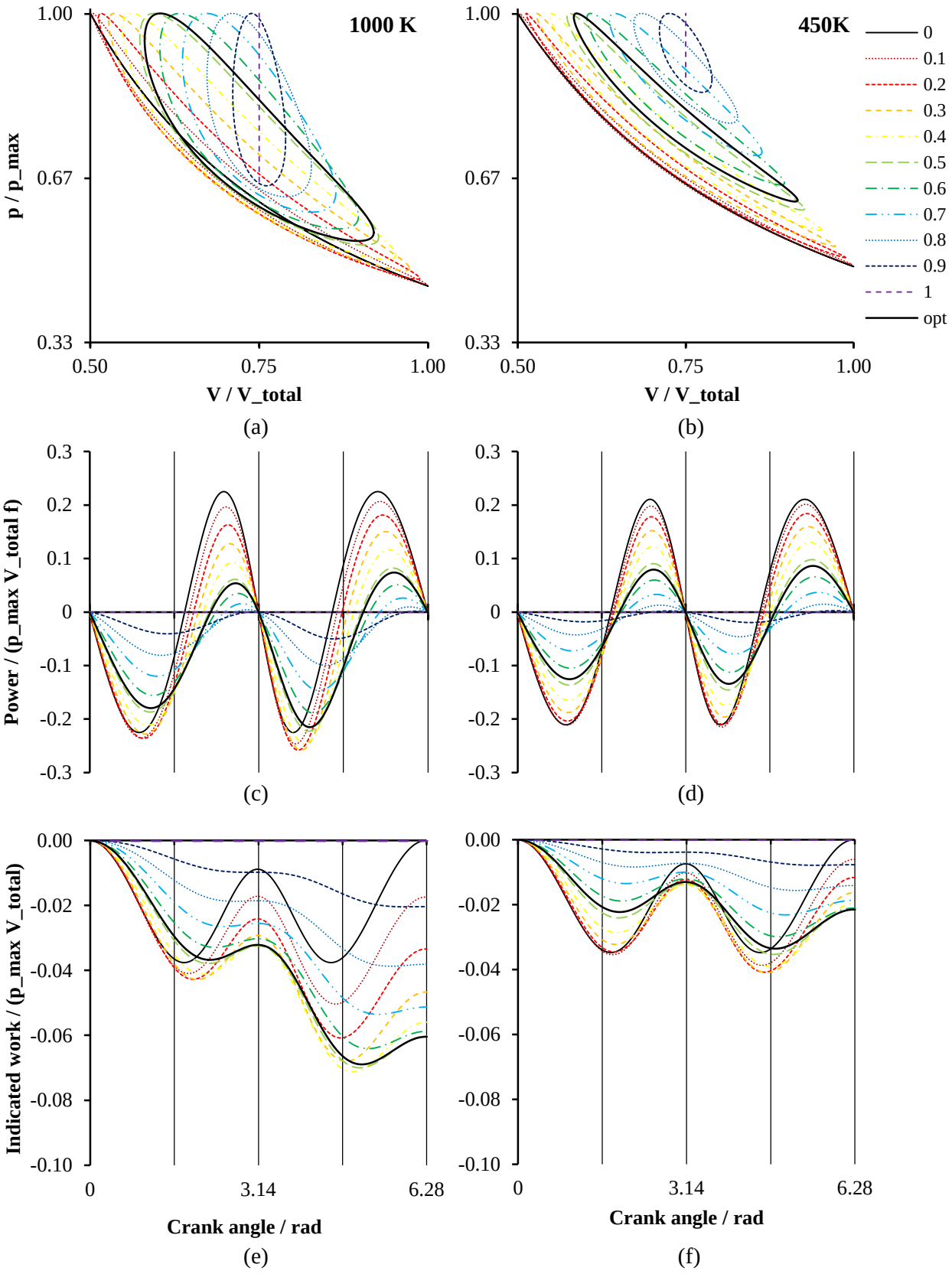

Figure 3.2: Influence of the phase angle on the performance of alpha engines for 1000 K and 450 K. Shown are the $p - V$ plots (a), the reduced power output or work (b), and the indicated work (c) over one complete cycle.

for all cases, for the sake of comparability. The phase angle is given in multiples of π in radians on the right hand side. Figure 3.2 (a) and (b) show the pressure-volume plots, (c) and (d) the power that is produced (negative values) and that is consumed (positive values) over one complete cycle (0 to 2π). Figure 3.2 (e) and (f) show the plots for the indicated work over one complete cycle, which is the integral of the power, so that the value at $\theta = 2\pi$ equals the area of the $p - V$ plot.

If the two pistons move in the opposite direction, the phase angle is zero, and no work is done by the gas volume as cold and hot volumes remain both in their cylinders, being compressed and expanded isothermally. The complete swept volume can be used to generate a pressure change as a result of a volumetric change and not a temperature change. Increasing the phase angle leads to smaller variations in total volume, since now, when the compression piston reaches its lower dead centre and the volume in the corresponding cylinder is maximal the expansion piston has already passed this point and its volume is decreasing and so is the total volume. The larger the phase angle the smaller the resulting total volume and the pressure amplitude. The $p-V$ plots become more vertical, and the expansion work exceeds to the work needed for compression. A more isochoric change of state is reached at the other extreme when the two pistons move in parallel and, as they are not generating any volume change, no work is produced at all. Here, the pressure change is only due to the change in gas temperature when the gas is swept from one temperature level to the other. The larger the phase angle the later the maximum pressure during compression. The pressure peak moves from being coincident with the minimum total volume (maximum compression) to being incident with the maximum expansion volume, from being solely caused by expansion and compression to being solely caused by heat and cooling. A more isochoric state of change can be observed, meaning that only little work has to be added during compression. This can also be observed in plots (e)

and (f) for the indicated work where the lines become straighter with increasing phase angle. Phase angles between π and 2π lead to the reversed thermodynamic cycle representing a heat pump or a cooling unit and are therefore not considered here.

Optimum performance in terms of indicated work (represented by the enclosed area in the $p-V$ plot) can be found in between those two extremes. Regardless of the heat source temperature it is not the phase angle which leads to the highest pressure fluctuation combined with the largest volume variation which performs best, but the one which is balancing positive and negative work output best by sweeping the gas most efficiently, represented by the line of optimum work output (opt) in Figure 3.2.

A reduced heat source temperature obviously reduces the possible pressure amplitude, but not the volume change. Thus the $p-V$ plots become slimmer and flatter. The increased compression work necessary to run the cycle is degrading the performance more strongly than at high temperatures, as can be seen in Figure 3.2 (c) and (d). The influence of changing the ratio of expansion and compression volume (k) is shown in Figure 3.3, for the phase angle fixed to 0.5π (which is close to the value for maximum power output). The two extreme cases are $k = 0$ and $k = \infty$ representing the absence of one of the two pistons (or volume at the other temperature). Thus compression takes place isothermally in the corresponding volume and the dead volume, using the whole swept volume. Optimum operation in terms of indicated work output is found in the case for which the power needed for compression is minimal. This can be seen comparing Figures 3.3 (c) and (d) with the corresponding $p-V$ plot or indicated work plot. If the power is positive mechanical work has to be added; if the power is negative work is done on the piston. This happens when the change in total volume is minimal, close to $k = 1$ where the expansion and compression swept volumes are equal.

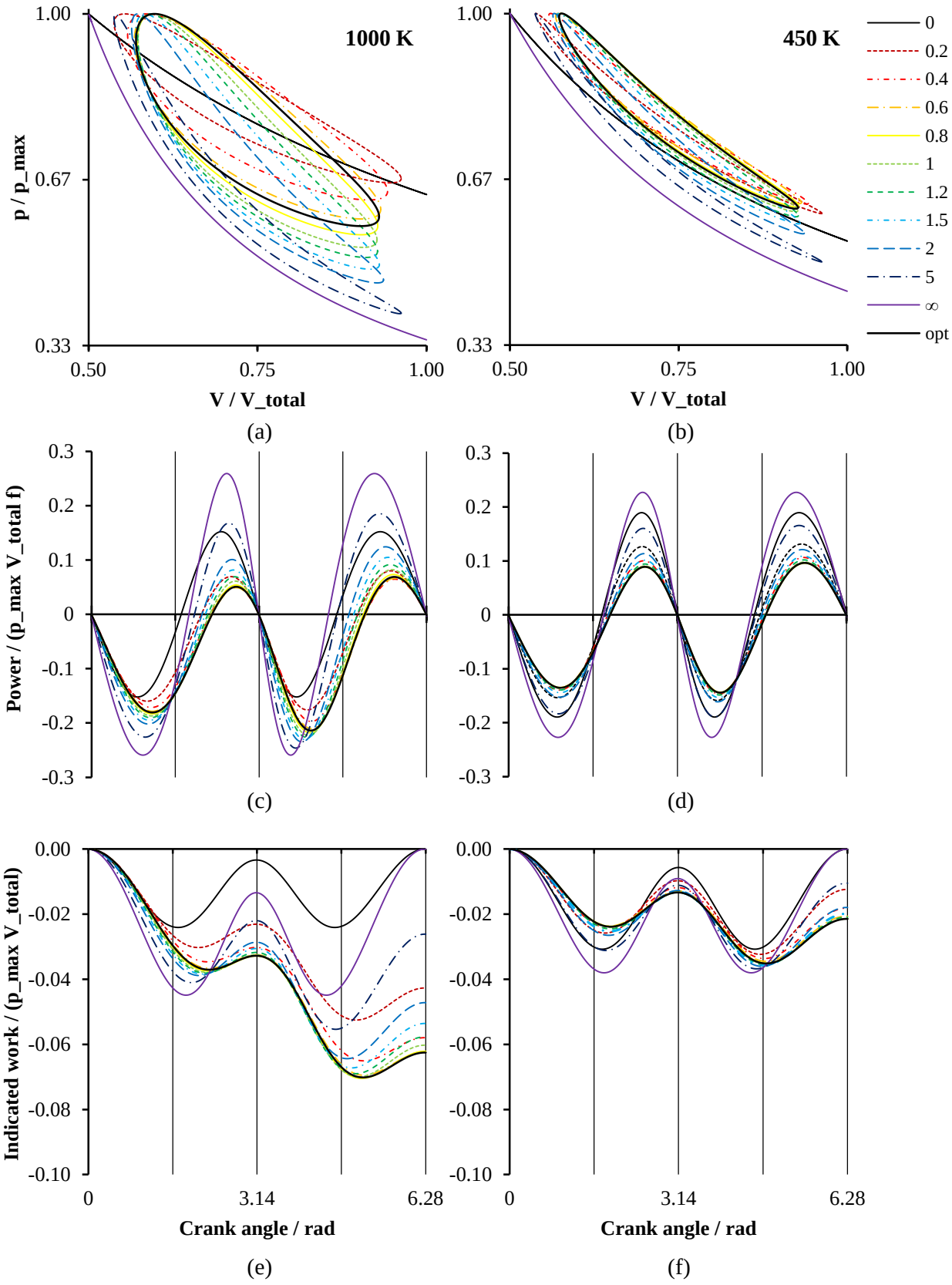

Figure 3.3: Influence of the volume ratio (k) on the performance of alpha engines for 1000 K and 450 K. Shown are the $p-V$ plots (a), the reduced power output or work (b), and the indicated work (c) over one complete cycle.

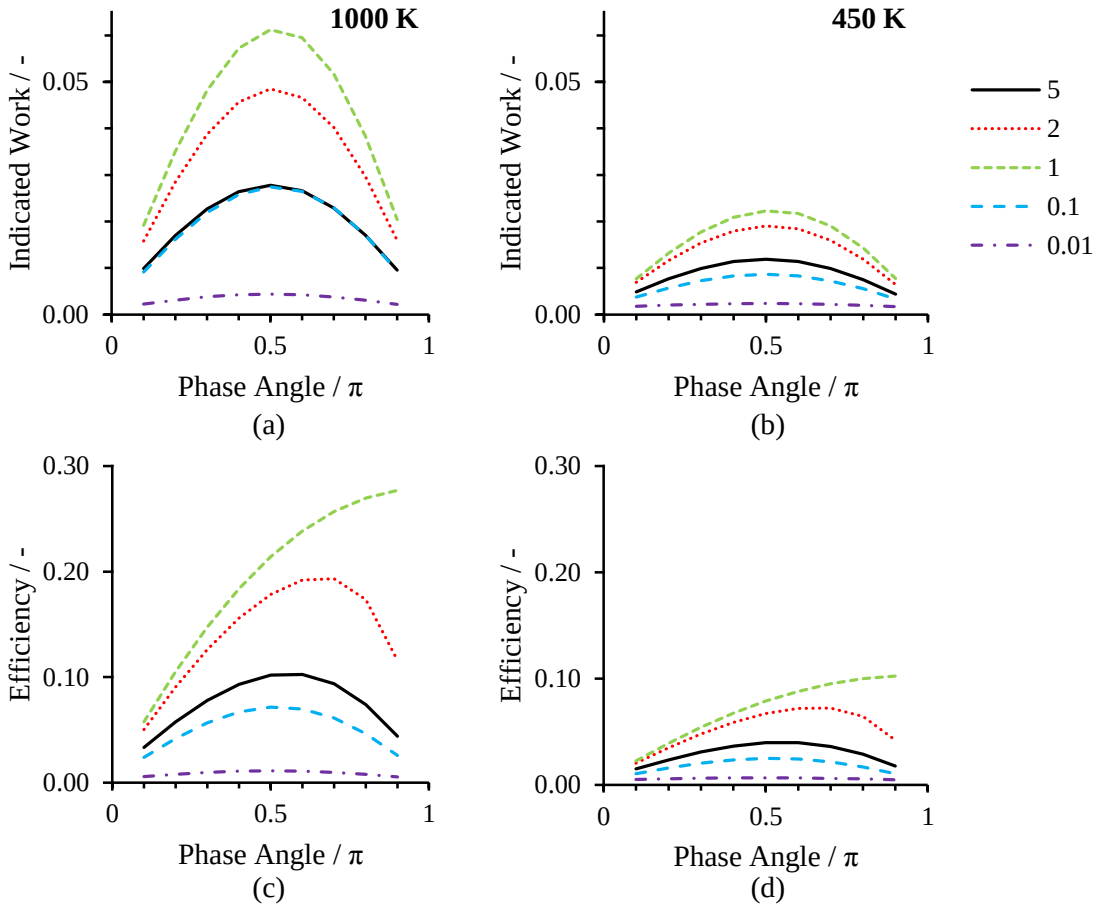

Figure 3.4: Alpha engine: Indicated work and efficiency vs. phase angle for different volume ratios. The optimum phase angle for maximum power is unaffected by the volume ratio.

Figure 3.4 shows the indicated power output and the efficiency over the phase angle for different volume ratios. Looking at the indicated power in Figures 3.4 (a) and (b) it can be seen that, independent of the volume ratio, the optimum phase angle is about 0.5 π. The optimum volume ratio of the expansion and compression space should be at unity ($k = 1$). The best efficiency is also reached with the volume ratio at unity (Figures 3.4 (c) and (d)). The more gas volume that is actually swept between the hot and cold volume (increasing phase angle), the more efficient the engine works but with declining power output. A good way to visualise the changing efficiency and performance is to investigate the $p - V$ plots in Figure 3.2.

3.1.2 Beta engines

In beta engines, as illustrated in Figure 3.5 (b), one displacer[1] (the elongated element) and one piston oscillate in a common cylinder. The displacer moves the gas from the hot to the cold volume and back, whereas the piston is used to compress and expand the gas. The displacer motion leads the piston motion by the displacer phase angle α_d. Due to the phase offset the strokes of both elements can overlap, making a more efficient use of the space available. Looking at the trajectories (thick lines) in Figure 3.5 (a) this overlap can be seen clearly. As for alpha engines the hot volume leads the cold volume[2].

The compression (cold) volume can be calculated to be

$$V_c(\theta) = 1/2 V_{s,e}(1 + \cos(\theta + \alpha_d)) + V_{us,d} - 1/2 V_{s,c}(1 + cos(\theta)), \tag{3.8}$$

with $V_{s,e}$ being the volume swept by the displacer and $V_{s,c}$ the volume swept by the power piston, where the volume unswept by the displacer ($V_{us,d}$) can be found by finding the crank angle (θ_0) where V_c is minimum and displacer and piston meet (found by setting $\frac{dV_c}{d\theta} = 0$):

$$\theta_0 = \arctan \frac{\sin \alpha_d}{k - \cos \alpha_d}(+\pi). \tag{3.9}$$

Then, by setting V_c in Equation 3.8 to zero and inserting (θ_0) $V_{us,d}$ can be found to be

$$V_{us,d} = 1/2 V_{s,c}(1 + \cos(\theta_0)) - 1/2 V_{s,e}(1 + \cos(\theta_0 + \alpha_d)) \tag{3.10}$$

The expansion (hot) volume can easily be calculated as

$$V_e(\theta) = 1/2 V_{s,e}(1 - \cos(\theta + \alpha_d)). \tag{3.11}$$

[1] A displacer or displacer-piston is a device similar to a piston, but with the difference that there is no noticeable pressure difference between its two sides, but a temperature gradient.

[2] In Stirling machines expansion space always leads compression space, regardless of whether it's in direct or in reversed mode.

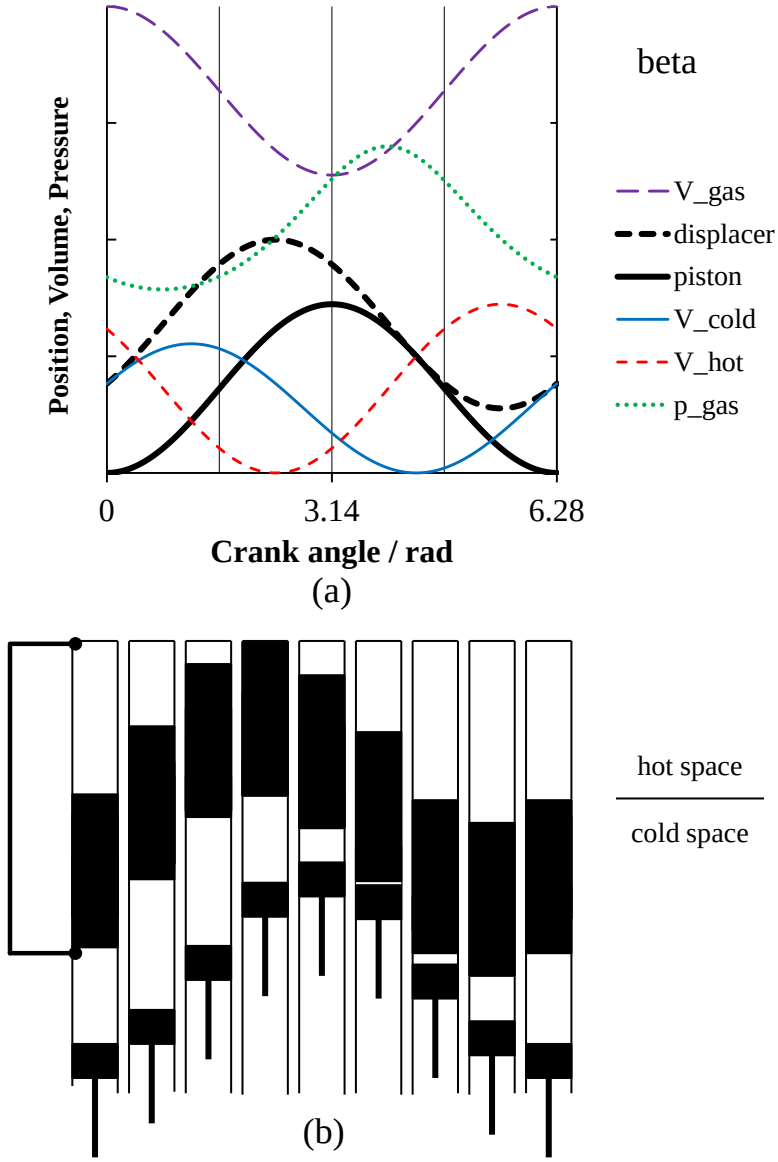

Figure 3.5: Set-up of a beta engine, one piston and one displacer are running in the same cylinder, with the strokes overlapping. Here they are phased in a way that the expansion space leads the compression space by more than 90° (0.5 π). The heat exchangers are depicted on the left (b). The resulting volume and pressure variations are shown above (a).

and the total swept volume as

$$V_{swept} = V_{s,e} + V_{us,d}, \tag{3.12}$$

where θ is the crank angle and α_p the phase angle between displacer and piston. The gas volume and normalised gas volume is then calculated according to Equations 3.6 and 3.7.

Figure 3.6 represents the influence of the change of the displacer phase angle for beta engines on the indicated work. The volume ratio k (here the ratio piston volume amplitude to displacer volume amplitude or simply the ratio of the two strokes) is fixed to one - again for the sake of comparability - and, additionally, it is close to the optimum performing ratio. In this case, in this case zero radians phase angle means that piston and displacer move synchronously; in fact the displacer is sitting on top of the piston as it moves. Therefore no volume is swept between the hot and cold areas, and the hot volume is compressed isothermally taking advantage of the whole swept volume. No work at all is produced. Increasing the phase angle reduces the amplitude of both piston and displacer (equal as $k = 1$) because now they have to compete with each other for a fraction of the swept volume, avoiding collision. If the phase angle becomes π the swept volume is divided equally into a space for the piston and one for the displacer as they are now moving in opposite directions, not allowing any further overlap of their strokes. Maximum performance is reached at relatively low phase angles (around 0.3 π), when the power piston sweeps a larger part of the swept volume and the overlap with the displacer stroke is high. The work needed to compress the gas is minimal in this case (see Figures 3.6 (c) and (d)).

Reducing the temperature has the same very detrimental effect as in alpha engines: The areas become slimmer and more inclined;, therefore the forced work increases, diminishing the already small power output further. Comparing Figures 3.6 (c) and (d) it can be seen that if the source temperature is lowered, not

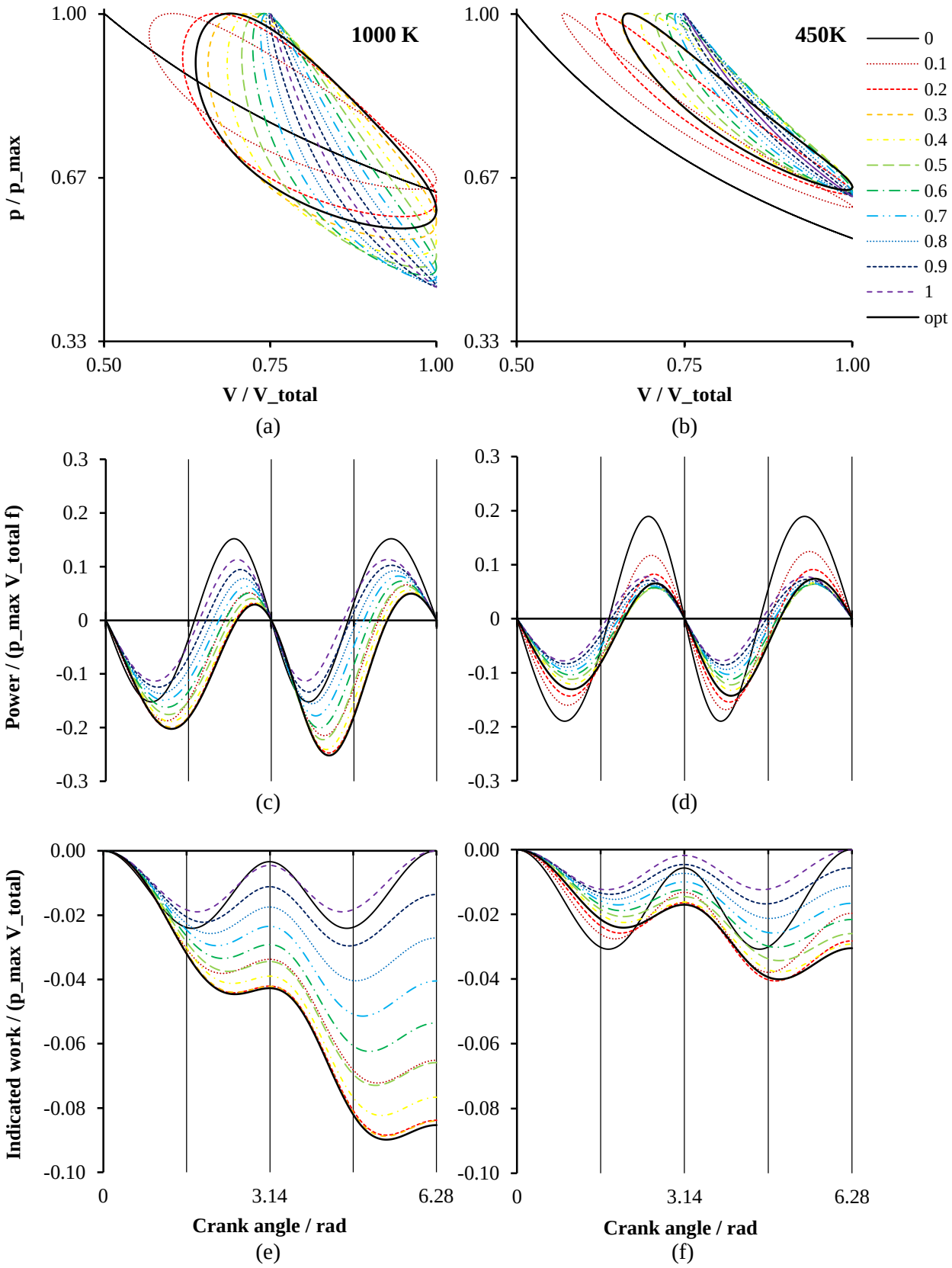

Figure 3.6: Influence of the phase angle, beta engine, normalised, 1000 K and 450 K

only the generated power (negative sign) is diminished but also the work needed for compression is increased. The optimum $p - V$ plots (Figure 3.6 (a) and (b)) shows the following effect: During expansion more heat is transferred to $p - V$ work (area under the curve) for the high temperature as the curve is higher than for low temperature differences. As the gas is expanded to a lower pressure in the high temperature engine (less gas mass in the cycle), during compression less work is needed.

In Figure 3.7 the influence of changing the ratio of the strokes is illustrated. A volume ratio of infinity means there is no displacer motion at all; thus the power piston is compressing and expanding the working fluid isothermally in the cold space (and the dead space). At the other extreme, when the volume ratio becomes very small, the power piston amplitude becomes very small. When it becomes zero and the volume is not changed at all the gas is simply shuttled between hot and cold spaces by the displacer, creating a mere temperature-triggered isochoric pressure change. Since there is no volume change, obviously there is no $p - V$ work. Small volume ratios lead to more rounded and symmetric $p - V$ shapes having only little forced work, but also small areas (indicated work), due to the small volume and pressure amplitude. Best performance is found for values close to unity where the power piston can sweep a large portion of the cylinder and, at the same time, a relatively large amount of gas is moved between the two sides.

Figure 3.8 shows the influence of the phase angle on indicated work and efficiency for different volume ratios. A volume ratio of unity shows best performance in terms of indicated work over the whole variation of the phase angle (Figures 3.8 (a) and (b)). With larger or smaller volume ratios the optimum phase angle moves towards 0.5 π. Best efficiencies are found if the expansion volume is large compared to the compression volume. This is analogous to alpha engines, where the efficiency also increases when more gas is swept from the hot to the cold side and less compression is needed.

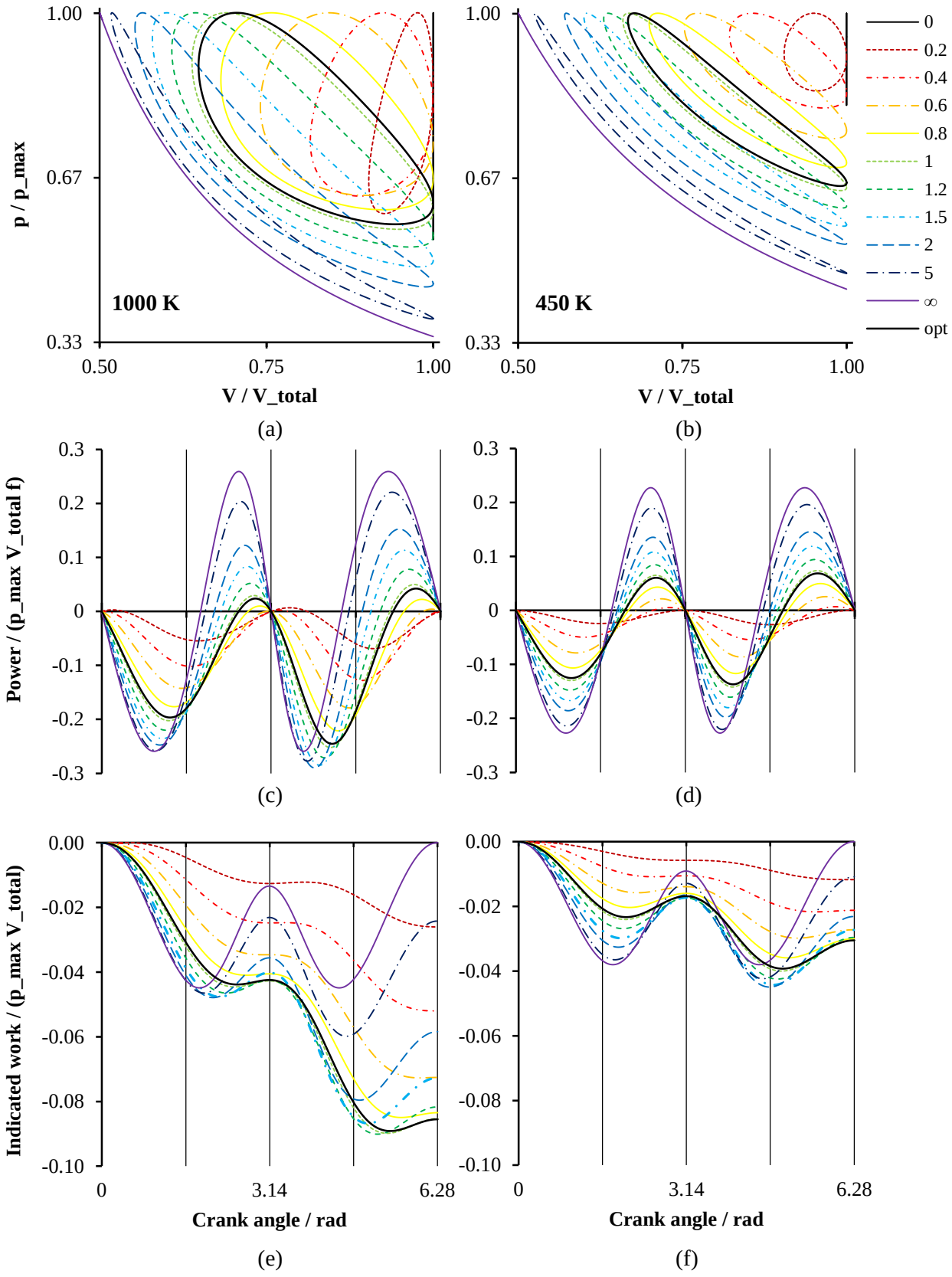

Figure 3.7: Volume ratio, beta engine, normalised, 1000 K and 450 K

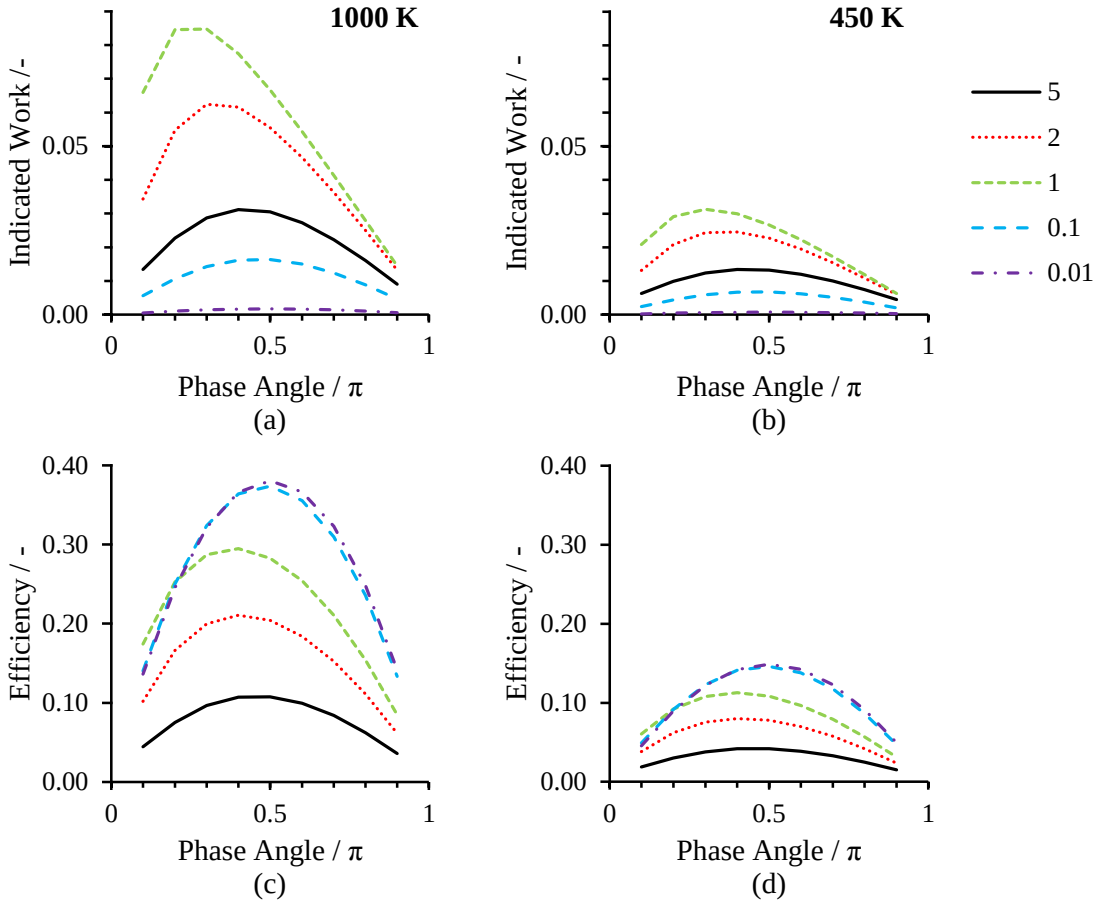

Figure 3.8: Beta engine: Indicated work and efficiency vs. phase angle for different volume ratios

3.1.3 Gamma engines

In a gamma configuration the displacer and piston do not run in the same cylinder. In Figure 3.9 (b) this is depicted by the separating line between the cold displacer volume and the cold piston volume, as well as the heat exchanger with the manifold on the cold hand side. An overlap of the strokes, as in beta engines, is no longer possible and the use of the volume available becomes thermodynamically unfavourable as can be seen below. On the other hand, from a practical point of view, such an arrangement adds some extra degree of freedom in terms of engine design, as the power cylinder can be placed where appropriate. Beta engines usually need to have the displacer rod penetrating the piston which is not necessary in the gamma design.

The volume changes can be calculated similarly as for the beta engine but simpler as no overlap exists. The compression (cold) volume can be calculated from the volumes underneath the displacer and over the power piston to be

$$\begin{aligned} V_c(\theta) &= \tfrac{1}{2}V_{s,e}(1+\cos(\theta+\alpha_d)) + V_{s,c} - \tfrac{1}{2}V_{s,c}(1+\cos(\theta)) \\ &= \tfrac{1}{2}V_{s,e}(1+\cos(\theta+\alpha_d)) + \tfrac{1}{2}V_{s,c}(1-\cos(\theta)), \end{aligned} \tag{3.13}$$

and the expansion (hot) volume from the volume on top of the displacer is

$$\begin{aligned} V_e(\theta) &= V_{s,e} - \tfrac{1}{2}V_{s,e}(1+\cos(\theta+\alpha_d)) \\ &= \tfrac{1}{2}V_{s,e}(1-\cos(\theta+\alpha)), \end{aligned} \tag{3.14}$$

where θ is the crank angle and α_d the phase angle between displacer and piston.

The influence of a change of the phase angle can be seen in Figure 3.10. The volume ratio is kept constant ($k = 1$) and there is no overlap in the strokes of piston and displacer, as they are in separate cylinders. Only the power piston contributes to the volume change. As the volume is divided equally between piston

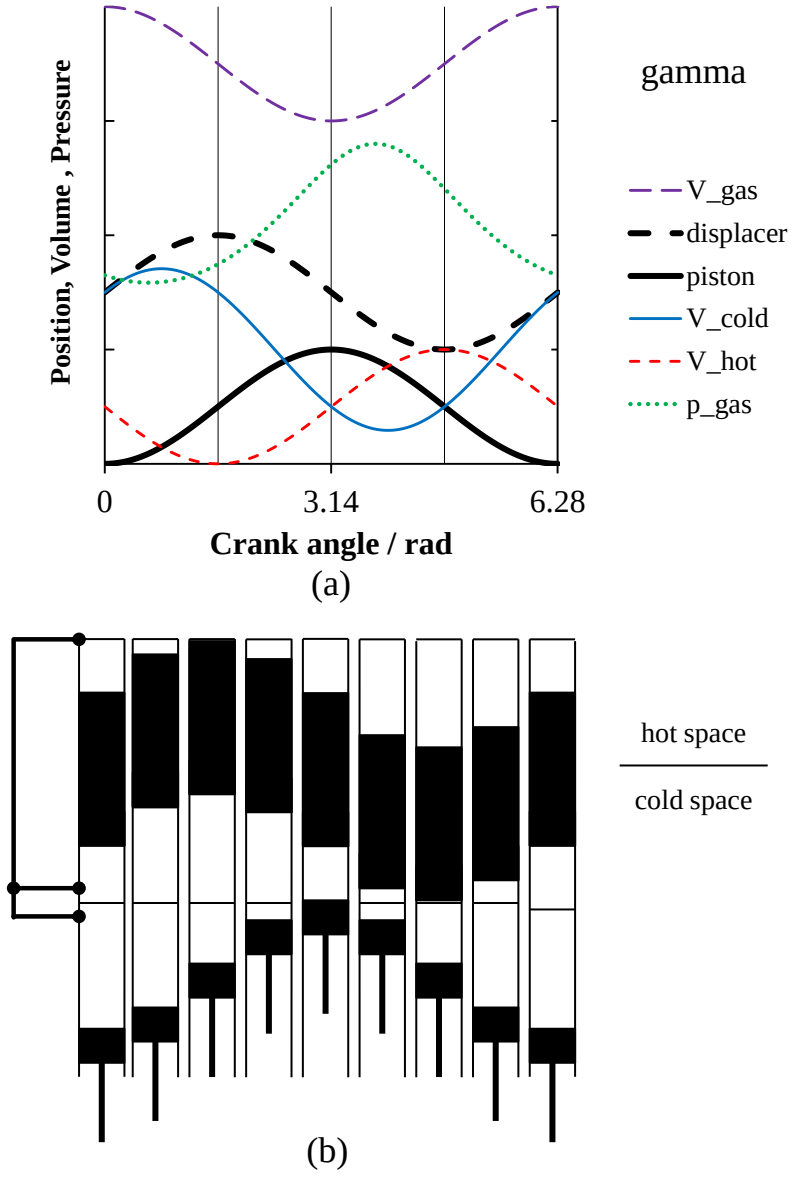

Figure 3.9: Set-up of a gamma engine, one piston and one displacer are running in different cylinders. Here they are phased in a way that the displacer leads the piston by 90°. The heat exchangers are depicted on the left (b). The resulting volume and pressure variations are shown above (a).

and displacer ($k = 1$), here the volumetric change is half of the swept volume. The optimum is found in the middle between the two extremes of parallel and opposed motion of piston and displacer (around 0.5 π).

Figure 3.11 (a) to (f) shows the influence of the volume ratio for gamma engines. As for beta engines $k = 0$ means no piston displacement (the vertical line) and $k = \infty$ no displacer movement, hence the whole volume is swept by the piston at constant gas temperature. An optimum can be found close to unity as for beta-type engines.

The results of the phase angle and volume ratio variations are summarised in Figure 3.12. As for alpha and beta engines the indicated work is maximised for volume ratios at unity (Figures 3.12 (a) and (b)). The optimum phase angle for power and efficiency is around 0.5 π. Optimum efficiency is reached with the same relation to the volume ratio as in beta engines: The lower the volume ratio, the more gas is shuttled between the different temperature levels, the less gas is compressed and the higher the efficiency.

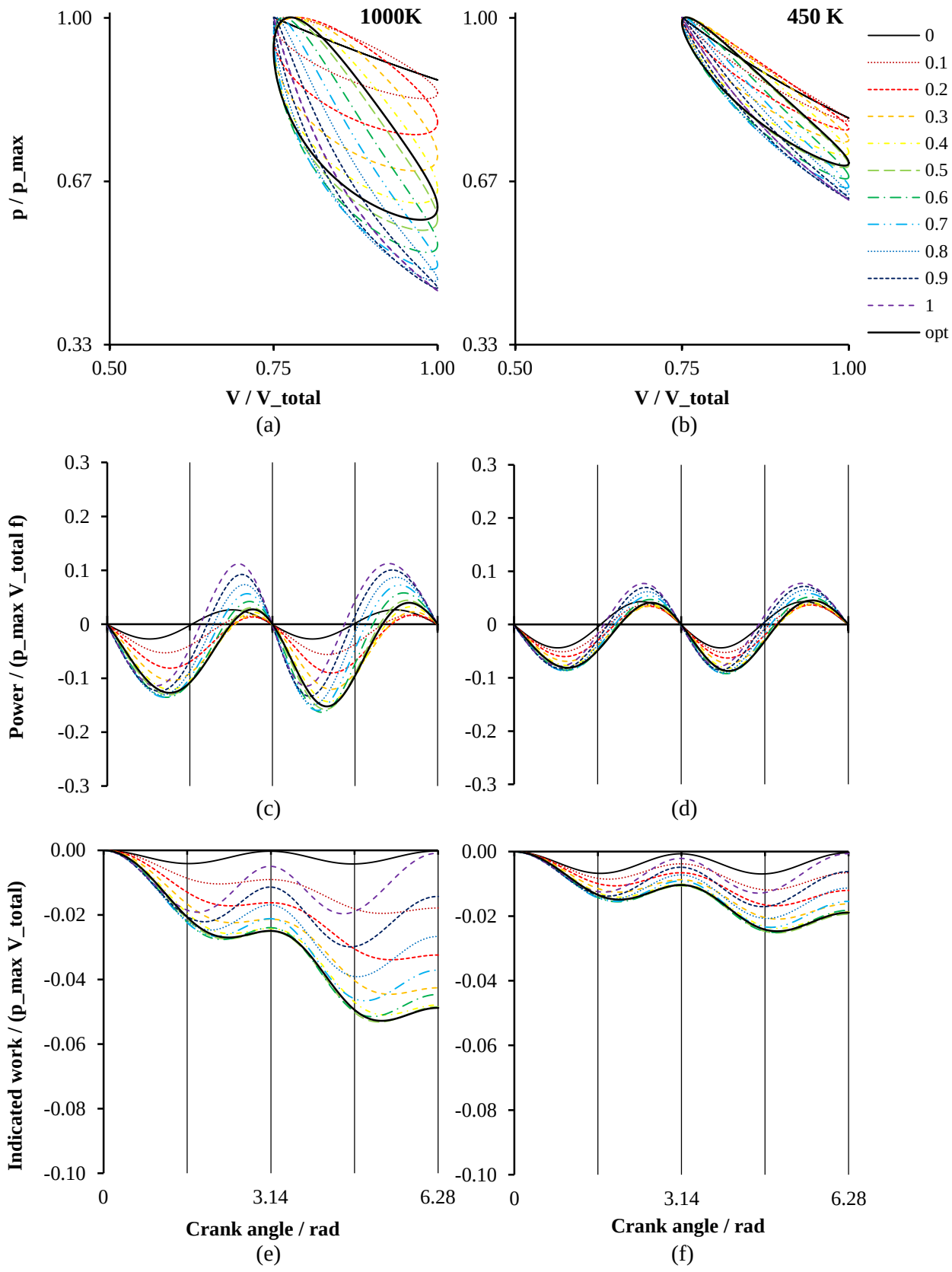

Figure 3.10: Phase angle, gamma engine, normalised, 1000 K and 450 K

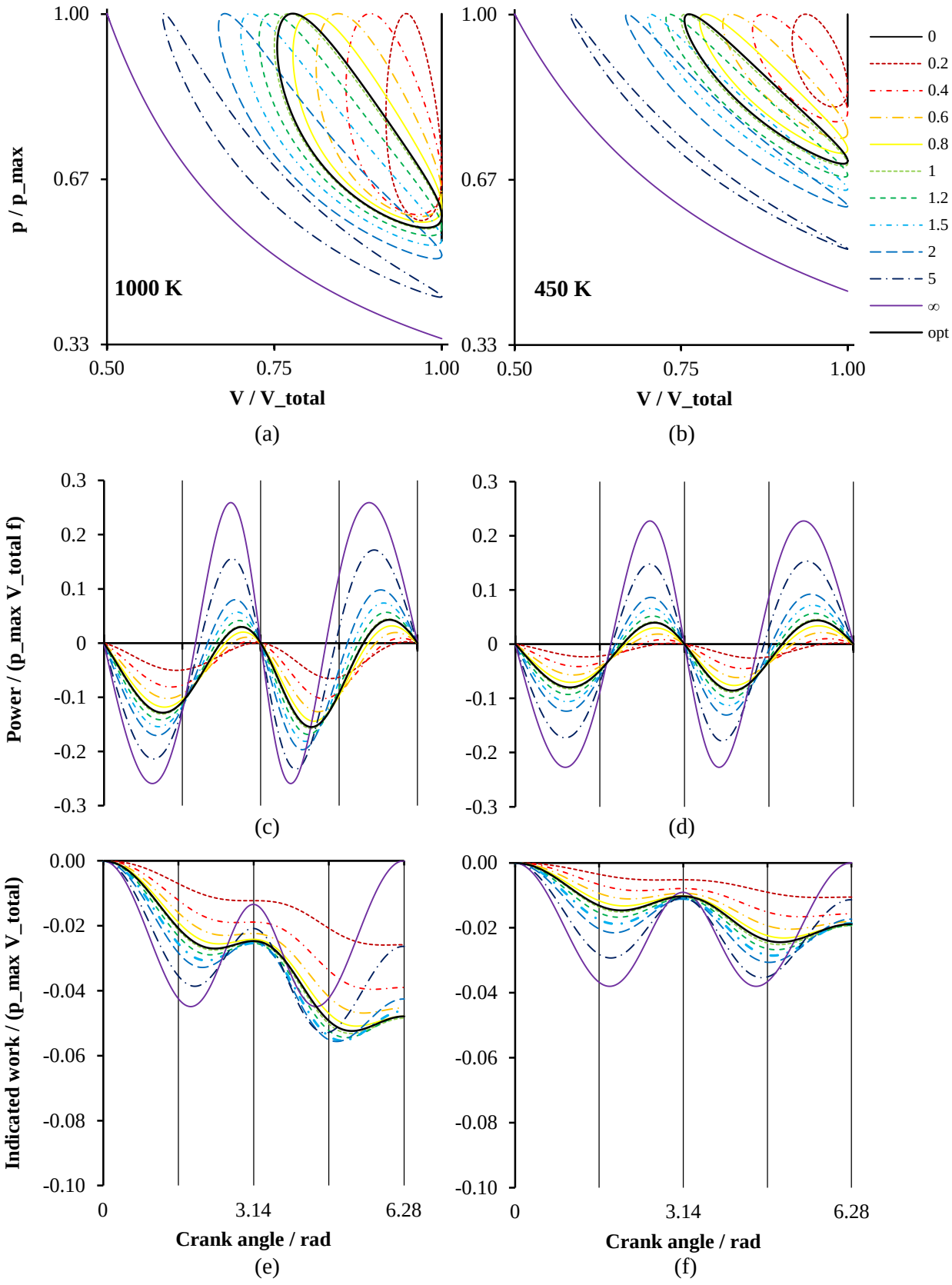

Figure 3.11: Volume ratio, gamma engine, normalised, 1000 K and 450 K

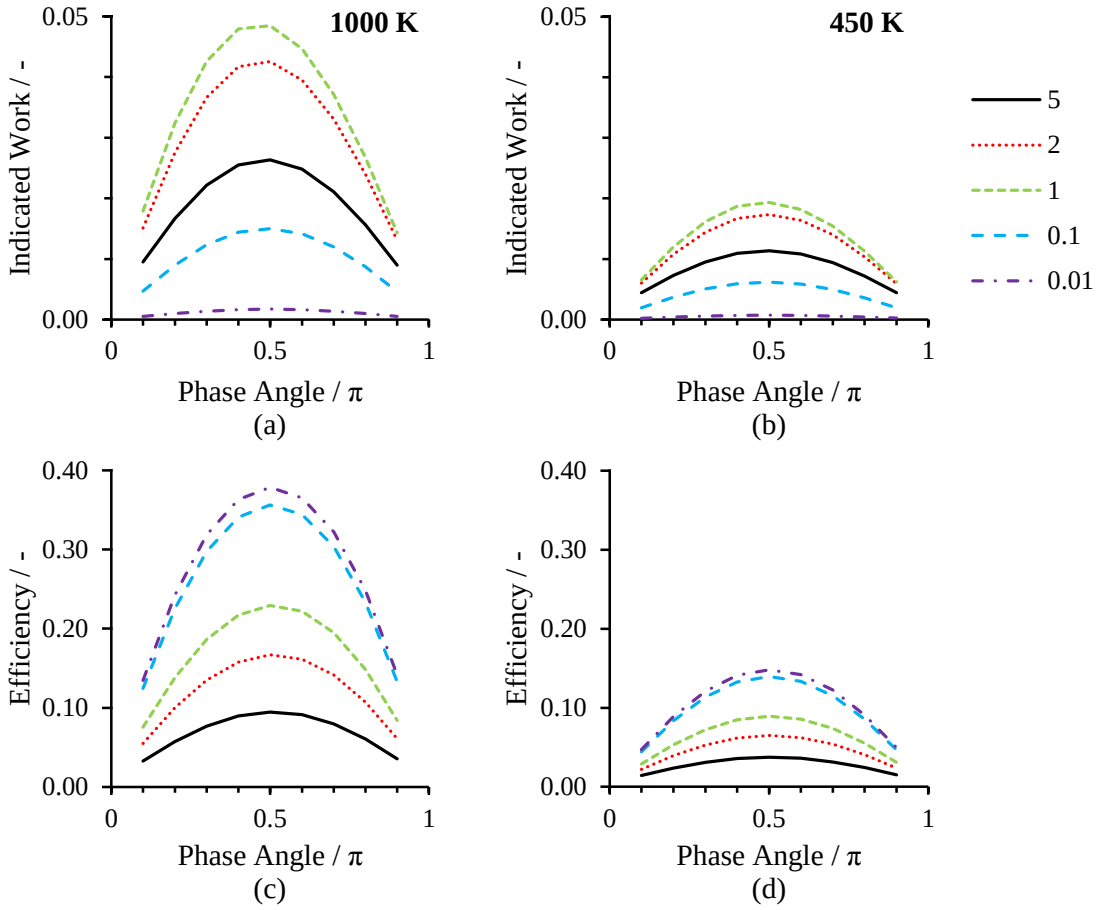

Figure 3.12: Gamma engine: Indicated work and efficiency vs. phase angle for different volume ratios

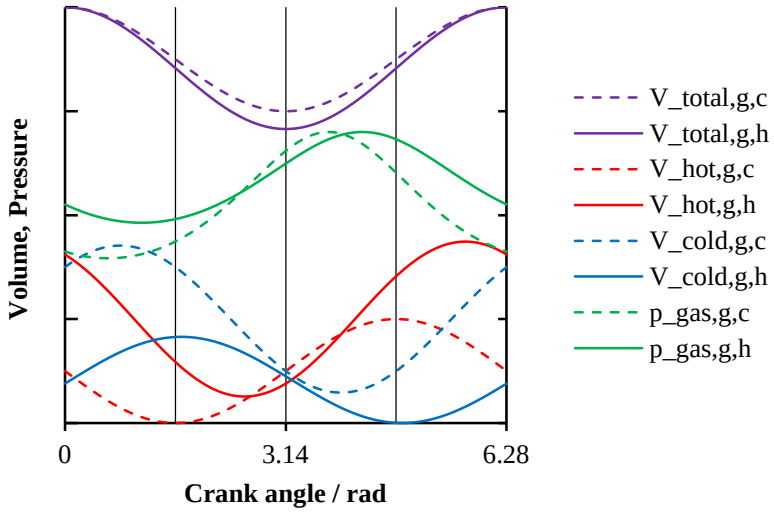

Figure 3.13: Gamma hot piston engine: volume and pressure variation

3.1.4 Gamma hot piston

If in a gamma engine the connection of the piston is moved from the cold side of the displacer to the hot side, engine performance can be improved. This has been shown by different authors, also experimentally [157–161]. The resulting volume variations after optimisation for the two different gamma engine concepts can be seen in Figure 3.13. It can be seen that the phase angle between expansion and compression volume remains unchanged. When unswept volume remained in the cold volume for the standard gamma engine it is now the hot volume that remains unswept by a fraction. During expansion more working fluid is heated while the cold volume reaches its minimum; together this results in a shift of the pressure curve to the right where it results in a higher power output since it makes better use of the volume variation (dV). As the maximum cycle pressure is identical in both cases, the hot piston engine contains less working gas.

Figure 3.14 shows the optimised (for maximum power output) $p - V$ plots (a,b), pressure and work variations (c to f) for gamma engines with the piston

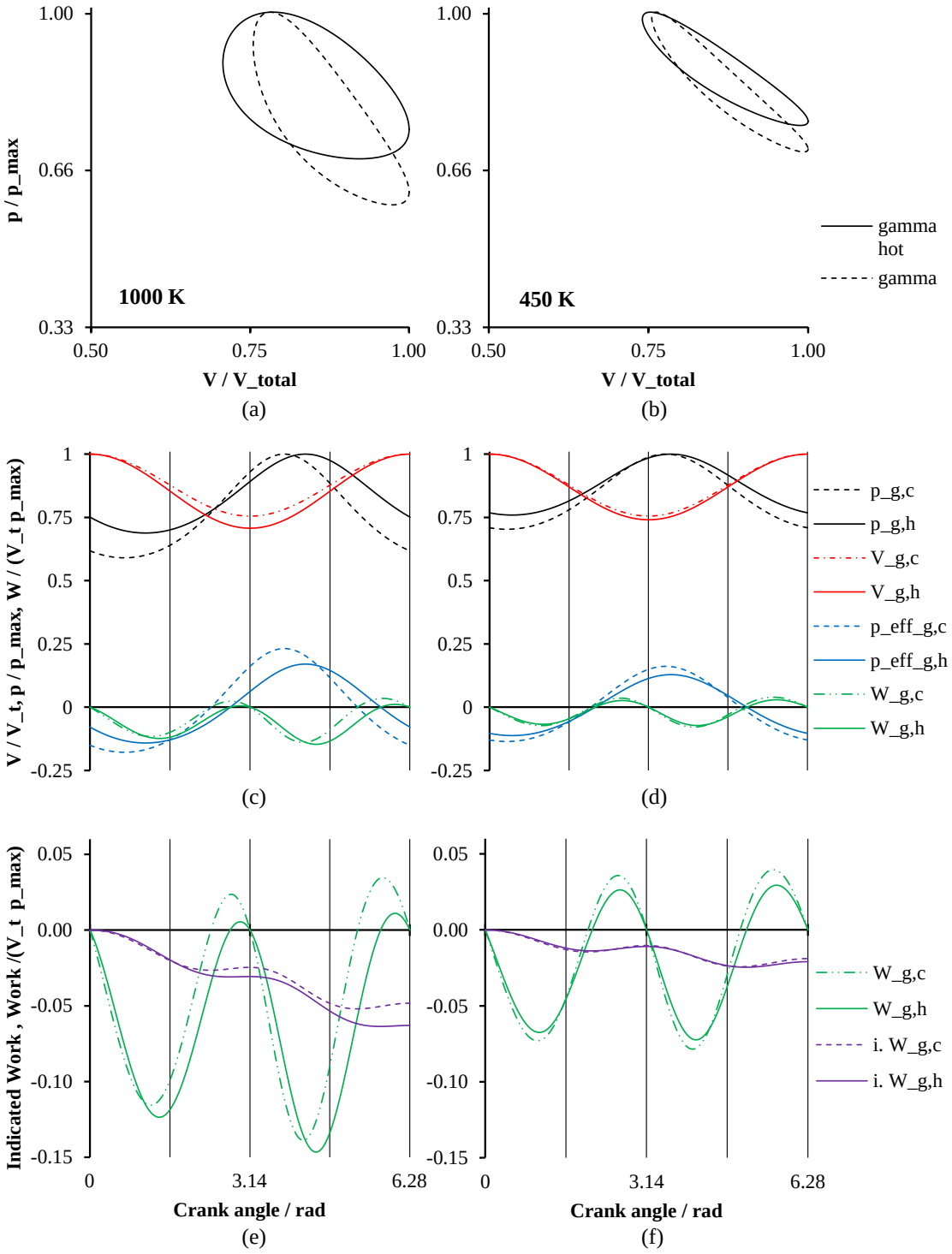

Figure 3.14: Gamma hot piston engine: (a), (b) $p-V$ diagrams for different source temperatures; the improvement can be seen clearly. (c), (d) absolute pressure, effective pressure on the piston with p_{mean} acting on the backside, total volume variation, and power output; the peak pressure in the hot piston engine acts when the volumetric change is higher which results in the higher power output. (e), (f) work and indicated work in detail

space connected to the hot volume for two temperatures; the classic gamma configuration is also plotted for comparison. At 1000 K (300 K heat sink) indicated work is improved by 30 %, at 450 K by 11 %, if the piston is connected to the hot space compared to the indicated work if the piston is connected to the cold end. The smaller improvement for the lower temperature difference is a result of the more similar temperature levels and hence smaller effect of the piston space temperature. Despite the fact that the pressure amplitude is diminished for the piston connected to the hot volume the indicated work is increased. The smaller pressure amplitude is a result of the reduced gas mass in the system (see Figure 3.13). The peak pressure can be used more effectively as it occurs later in the cycle when the volumetric change (dV) is higher, as the work is defined by pressure times volumetric change (see Figure 3.14 (c) and (d)). A larger volume ratio and thus a larger volume variation by the power piston can be achieved during optimisation. This manifests in the larger and flatter-shaped $p - V$ plots.

One might argue that positioning the power piston in the hot zone is not ideal, because then the seals are exposed to the elevated temperature. In fact every alpha engine has to deal with the same challenge, usually solved by forming a very long piston dome, with the seal located close to the expansion space and next to a cooled cylinder wall. It should be mentioned that with such a configuration there are two cylinders with a temperature difference along their longitudinal axis instead of only one with temperature difference and one without. For engines running at moderate temperatures, this design challenge becomes less of a problem.

Swapping hot and cold end in a beta engine has no impact on engine performance at all, as long as swept volume ratio and phase angle are adjusted accordingly. After adjustment the volumetric changes of the expansion and compression space and their phasing is identical to the original state. No practical value can be seen in such a configuration as now two seals have to be protected from the high

temperatures. Even more obviously, swapping the hot and cold cylinders and heat exchangers in an alpha engine does not have an impact either as the engine stays unchanged. One interesting conclusion can be drawn from these considerations: The power piston in a displacer engine can be located in either the expansion or the compression space. Usually it is connected to the compression space to allow the piston rings to operate in a more favourable environment.

3.1.5 Discontinuous displacer motion

Often the text book explanation of the ideal Stirling cycle is given using an opposed piston alpha engine with discrete piston motion (e.g. in [22]). In order to bring real Stirling engine operation closer to that ideal and increase the power output, discontinuous movement of one or both reciprocating devices instead of (quasi-) sinusoidal movement has been considered. Real engines with discrete displacer motion where built and researched by Martini[3] and more recently by Gopal at the University of Canterbury [149, 162, 163].

Figure 3.15 (b) shows an idealised discrete displacer movement for a beta engine; gamma engines are set-up analogously. The movement of the displacer is not steady but is conducted in a way to optimise the thermodynamic behaviour. Moving the two pistons (alpha engine) in parallel or the displacer very quickly while not moving the power piston (beta and gamma engines) creates an isochoric change of state, which is not possible with sinusoidal movement. Thus the indicated work is increased in such engines since the area in the $p-V$ plots is enlarged into the corners of the ideal Stirling cycle. Figure 3.16 shows the $p-V$ plots for a beta engine with sinusoidal and a second engine with discontinuous displacer motion for two different temperatures. The piston stroke[4] and all other parameters are identical.

[3] Hence such devices are also known as Martini displacer. [22] page 456, [24] page 79

[4] Optimum piston stroke for the discontinuous moved displacer engine is somewhat larger, but for comparability the same stroke was chosen to generate the plot

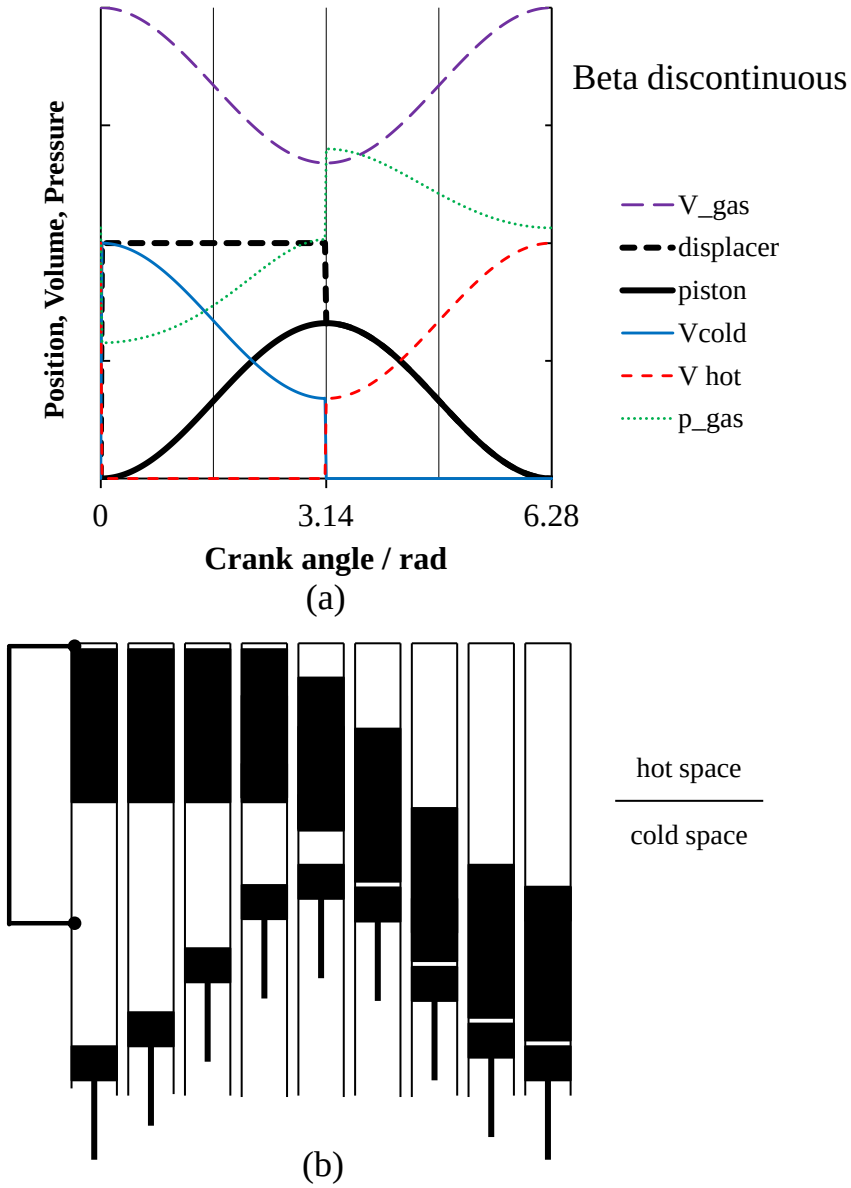

Figure 3.15: Piston movement, displacer movement, volume variations and pressure variations of a beta engine with discontinuous displacer motion

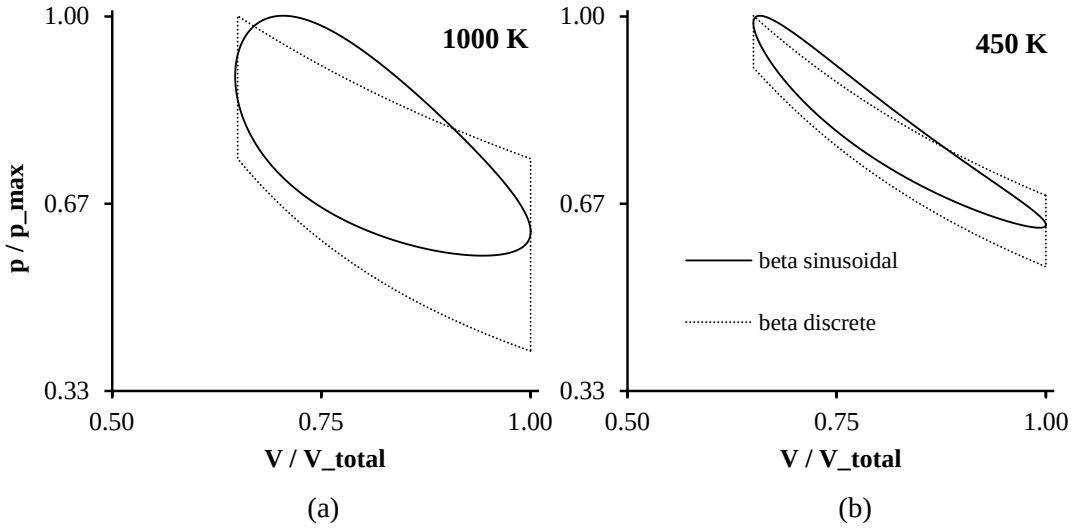

Figure 3.16: Pressure volume variations for a beta engine with sinusoidal and discontinuous displacer motion at two different heat source temperatures. The shape of the $p - V$ plots resemble the ideal Stirling cycle

Controlled movement of displacers is easier to accomplish than controlled movement of pistons, as the power necessary to move the displacer is small compared to a piston, as only little work is done (gas volume is constant, or only slightly changed). Thus the required actuator can be small and of only little electrical power consumption. From the sketch in Figure 3.15 (b) and the corresponding volume plot in Figure 3.15 (a) it can be seen that during compression most of the working gas is cooled in the cold parts of the engine. As soon as the piston starts to expand, the displacer is moved to the piston crown where it travels together with the expanding piston to the lower dead point, with most of the gas in the hot areas. At the lower dead point the displacer is moved back, shuttling the gas to the cold areas. Figure 3.15 (a) shows the resulting pressure oscillation. Heating and cooling the gas by a rapid movement of the displacer leads to a sharp change of pressure. Obviously infinite acceleration of a displacer is not possible for real engines, so that with finite acceleration the power output would be somewhere between the sinusoidal and ideal discontinuous value. Table 3.1 shows the improvement theoretically achievable using discontinuous displacer motion instead

Table 3.1: Improvement of indicated work using discrete displacer motion compared to sinusoidal motion for different temperatures in beta and gamma engines

	simulation		experiment
Temperature / K	$\frac{W_{\text{beta,disc}}}{W_{\text{beta,sin}}}$	$\frac{W_{\text{gamma,disc}}}{W_{\text{gamma,sin}}}$	$\frac{W_{\text{gamma,disc,exp}}}{W_{\text{gamma,exp}}}$ [163]
450	1.4	1.2	-
1000	1.4	1.1	1.2

of sinusoidal. Almost unaffected by the heat source temperature, beta engines deliver up to 40 % more power, gamma engines between 10 and 20 % more which is confirmed by Gopal's experiments.

3.1.6 Comparison of alpha-, beta-, and gamma-type single gas circuit engines

After optimising each type of engine on its own, now the three basic types are compared with each other to show their similarities and highlight the differences. Engines of identical swept volume, dead volume (equals the active volume if not stated otherwise) and maximum pressure are simulated for two different heat source temperatures (1000 K and 450 K) at 300 K heat sink temperature.

Looking at the $p-V$ plots in Figure 3.17 (a) and (b) it becomes obvious that beta engines perform best, followed by alpha engines and then gamma engines (cold piston) according to the size of the area enclosed by the $p-V$ plot independent of the source temperature. This area is the equivalent to the indicated work at the end (2π) of each cycle in Figure 3.17 (e) and (f). It can be seen, that depending on the source temperature, beta engines of comparable size and dimension have about 40 % more output of indicated work than alpha engines and between 80 % (for 1000 K) and 60 % (for 450 K) more than gamma engines.

Figure 3.17 (c) and (d) show how the combination of volume and effective pressure variation define the resulting work over one cycle. The cyclic pressure

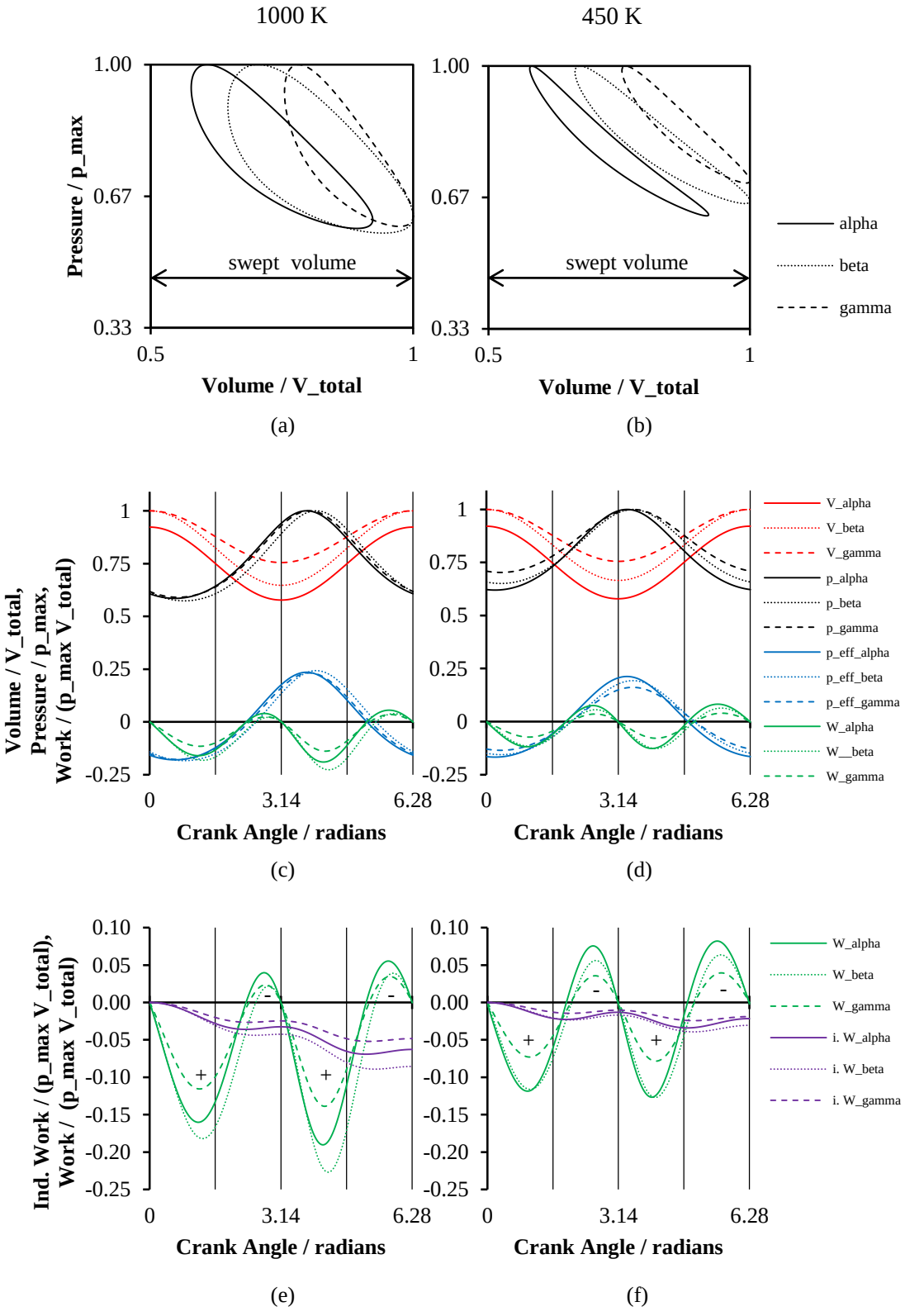

Figure 3.17: Alpha-, beta- and gamma-type engine comparison. (a), (b) $p - V$ plots. (c), (d) absolute pressure, volume, effective pressure, and power. (e), (f) work and indicated work.

combined with the opposing mean pressure result in the effective pressure (p_{eff}) on the piston. If the effective pressure is in accordance with the piston motion, work can be extracted (the sign is negative); if not, mechanical work has to be added to compress the gas (positive sign). Comparing alpha and beta engines in Figure 3.17 (c) and (d) it can be seen that the volume as well as the pressure amplitude are very similar especially for the 1000 K hot end temperature. The reason why beta engines perform so much better is that the maximum pressure occurs later than for alpha engines, namely at a time when the volumetric change of the gas volume is higher, so that the pressure fluctuation can be used more effectively to generate power. On the other hand less mechanical energy has to be added for compression as the gas pressure is smaller during compression.

Despite the fact that all three configurations use the same swept volume, the total volume of the working gas changes between different extremes. Looking at Figure 3.17 (a) and (b) the minimum volume for alpha engines is smaller than for the other two and so is the maximum volume. The two out-of-phase pistons never allow the gas volume to reach the maximum value of the swept volume because if one piston reaches its outer dead point the other is already on its way back in, diminishing the gas volume. On the other hand as both pistons can reduce the enclosed gas volume the minimum volume is smaller than for single piston engines. In beta and gamma engines, where only one piston defines the overall volume, the volume becomes maximal when that piston reaches its outer dead point. The overlap of strokes of displacer and power piston in beta engines makes it possible to increase the volume change. The poor performance of gamma engines results mostly from the fact that the volumetric change is smaller than in the other configurations because there is no overlap of strokes as in beta engines, or a second piston which helps to create a larger change in volume.

A comparison of the indicated work and efficiencies of the reviewed single gas circuit engines is given in Figure 3.18. Both values are normalised to the indi-

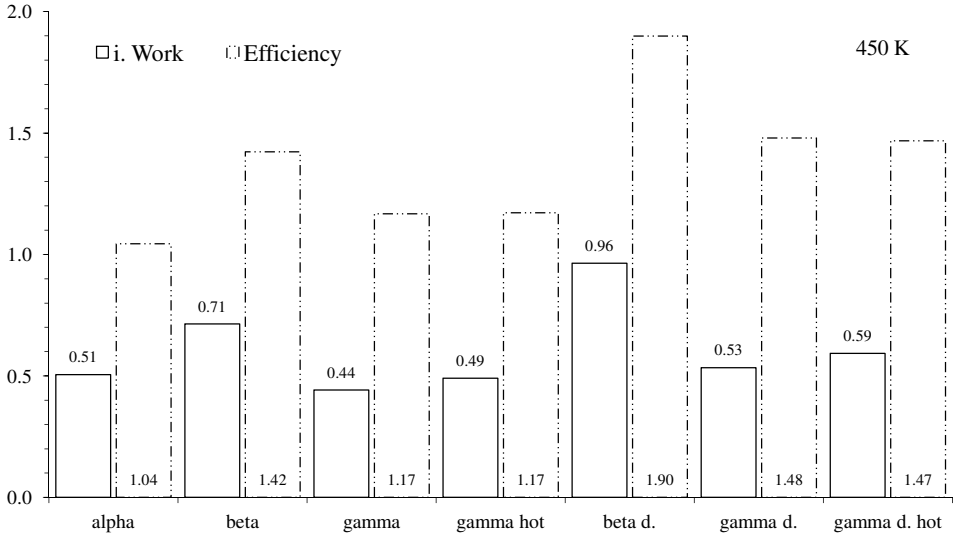

Figure 3.18: Indicated work and efficiency of single gas circuit engines (normalised to the indicated work and efficiency of a double-acting four cylinder Siemens configuration)

cated work and efficiency of a double-acting four cylinder Siemens configuration (which is basically twice the indicated work of a single-acting alpha engine; the set-up is explained in Section 3.2.1). Shown are the values for 450 K heat source temperature; the ranking does not change for 1000 K heat source temperature (except for the gamma engine with discontinuous displacer operation which performs relatively more poorly). It is interesting to note that the modified gamma configurations (hot piston, discontinuous operation and the combination of hot piston and discontinuous operation) show a similar or higher work output than the alpha engine, with higher efficiency (even without considering mechanical losses; see below). Therefore alpha engine designs should be avoided for single gas circuit engines. Nevertheless beta engines perform significantly better in terms of indicated work output independent of the type of displacer motion. Modified gamma engines can achieve similar efficiencies as standard beta engines.

Figure 3.19 illustrates the influence of dead volume on (a) the power output and (b) the efficiency of the three different basic configurations, each for the high and low temperature source. The need for minimising the dead volume

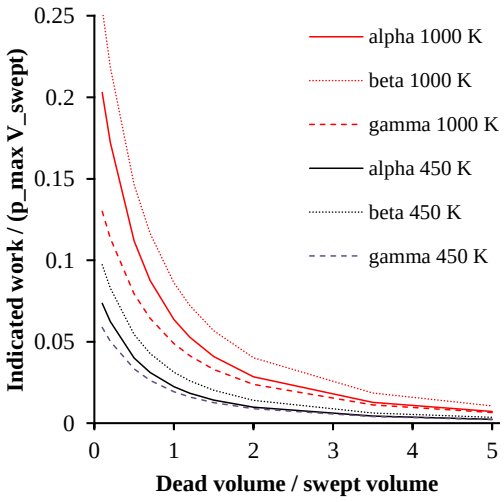

(a)

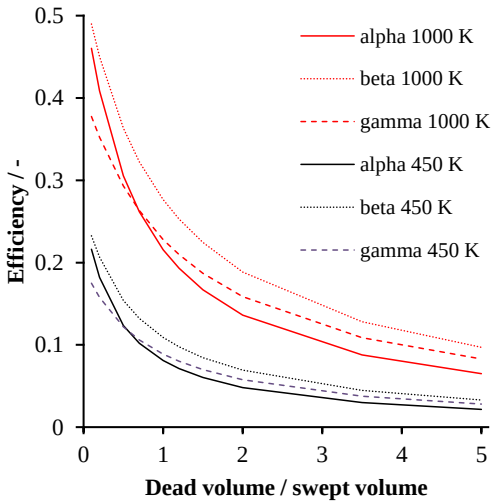

(b)

Figure 3.19: Indicated work and efficiency over dead volume, p_{max} constant

and balancing heat exchanger areas becomes obvious. This cannot be done by using the isothermal analysis but is exactly where the Sage modelling is needed. The reason why the efficiency for alpha engines is more susceptible to increased dead volume is due to the optimisation. As optimisation is done to maximise the indicated work, the effect of varying the dead volume on the efficiency is different than for displacer-type engines.

3.2 Double-acting multi-cylinder arrangements

In order to increase the power output of a single gas circuit engine the working pressure can be elevated and the swept volume can be increased. This is only reasonable to a limited extent as higher pressures require thicker cylinder and heat exchanger walls which adversely affect heat exchange and increase heat conduction losses. Larger swept volume implies larger piston diameter and/or stroke, which increases the mass forces and necessitates a larger flywheel and counterweights. The sealing of large piston diameters is also more difficult since the length of the leakage path increases with the diameter [22]. The simplest way to achieve a multi-cylinder arrangement is to combine a number of single cylinder engines on one crankshaft with an equally divided phase shift between the pistons, as was done by Philips and Thermomotor [23]. The demand for a large flywheel is reduced and a smoother running engine is achieved.

Using both sides of a piston is a very useful way to increase the power density of an engine of a given size. With the same engine size (swept volume) and unchanged number of moving parts, specific power output can be increased significantly, as well as the efficiency. Other benefits of the double-acting principle are, if applied appropriately, improved mechanical efficiency by reducing the net forces in the piston rods, reduced moving mass, and improved piston-ring sealing. Chapter 5 discusses these effects with respect to the cylinder space compounding.

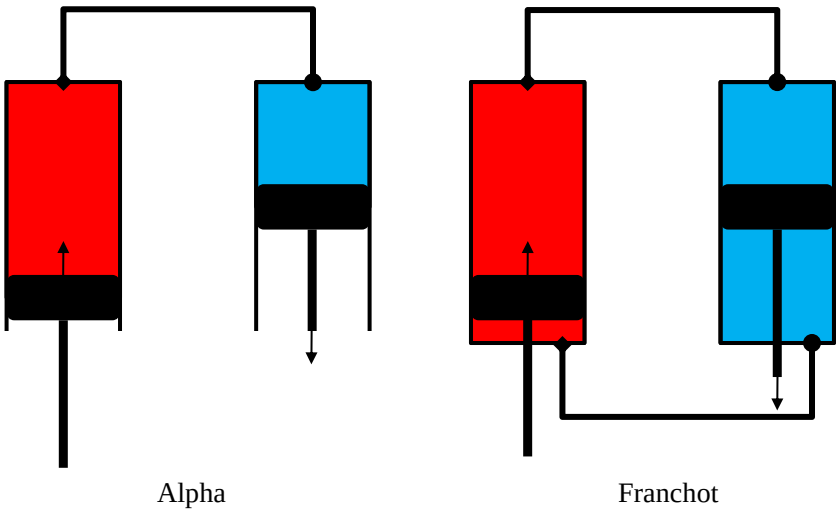

Figure 3.20: Single-acting alpha engine (a) and double-acting Franchot engine (b)

3.2.1 Alpha multi-cylinder engines

Possibly the simplest way to transform an alpha engine into a multi-cylinder or better multi-cycle engine is simply by sealing the piston rods against the crank case and connecting the resulting cylinder spaces by a set of heat exchangers and a second regenerator with each other as explained in Figure 3.20. Such a double-acting alpha engine is also known as Franchot arrangement.

The Franchot arrangement has a disadvantage in design for the piston seal in the hot cylinder. Usually for alpha engines operating at high temperatures this seal is located in a cooled area of the cylinder separated by an elongated piston dome. If both sides of the expansion piston are in contact with the hot gas cooling of the piston seal and the rod seal becomes more complicated. The practical advantage of the Franchot arrangement is the fact that a minimum of two pistons is sufficient to create a working engine with a freely adjustable phase angle. Another advantage is the symmetric thermal expansion on both sides of the pistons and cylinders as well as the omitted heat conduction. However, since the temperature difference is low for the proposed application these effects are

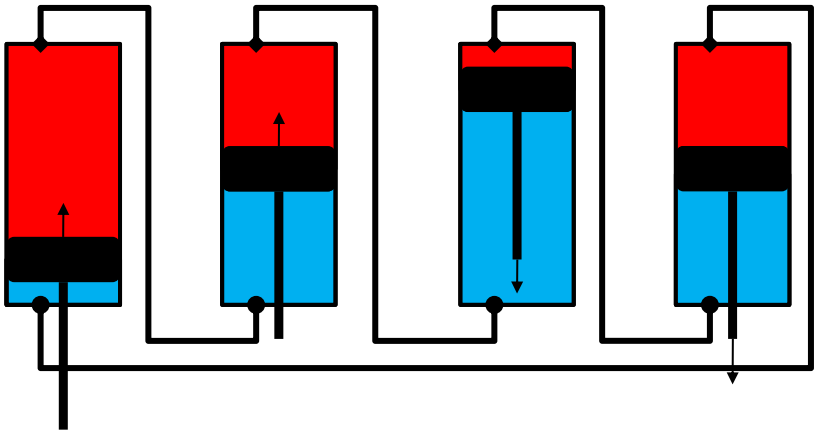

Figure 3.21: Siemens or Rinia configuration

much less pronounced than at high temperature differences.

The standard configuration used for alpha multi-cylinder engines is the so-called Rinia or Siemens configuration[5]. Here, four double-acting pistons are used to create four gas circuits operating at a phase difference of 90 degrees. In Figure 3.21 this becomes clear: Starting with a single set of compression and expansion pistons phased by 90 degrees (just as a regular alpha engine) and adding one after another gas circuit on the back of the compression piston, the forth is then formed by the backside of the first piston as compression piston. So it is possible to keep each piston seal in the cold part of the engine. Due to the equal phasing of the pistons a more uniform power development is achieved. As a positive side effect the work needed for compression can be partially provided by the adjacent expansion space, relieving the crank shaft and making the engine more efficient, as loads on bearings are reduced.

If the phasing is adjusted different cylinder numbers for double acting alpha engines are possible too. At least three pistons are required. The phase angle

[5]Different authors quote different inventors of this arrangement, who might have come to the same solution independently. Amongst them also the earlier mentioned Franchot. Nevertheless the first engine that is confirmed to be built on that principle is the one designed by Rinia and others at Philips [23]. Rinia and Siemens arrangements are both used synonymously.

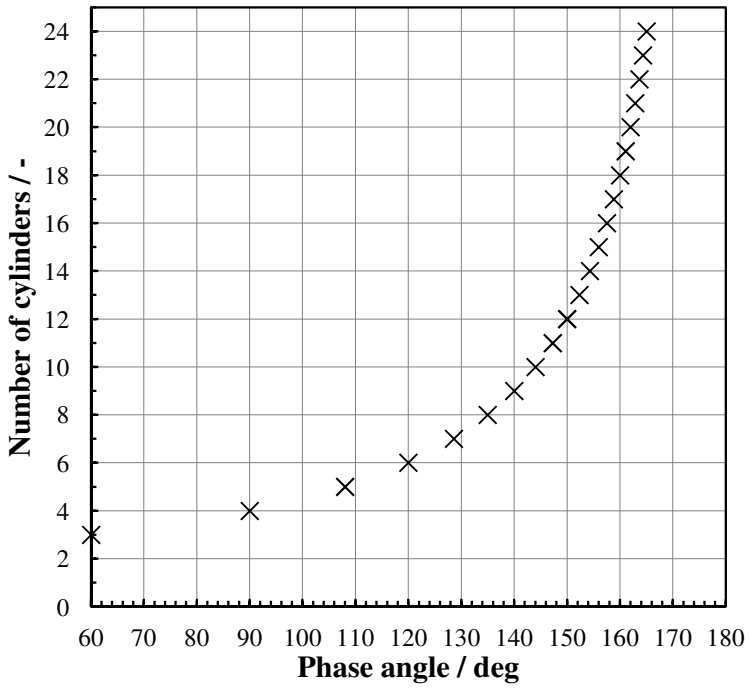

Figure 3.22: Number of cylinders (N_c) as a function of the phase angle (α) for the double-acting Siemens configuration. With more cylinders larger phase angles and smaller increments can be realised.

between the pistons then becomes

$$\alpha_p = \frac{2\pi}{N_c} = \frac{360^\circ}{N_c}, \tag{3.15}$$

where N_c is the number of cylinders or pistons. The thermodynamic phase angle (α) between interconnected hot and cold volumes becomes

$$\alpha = \pi - \frac{2\pi}{N_c} = 180^\circ - \frac{360^\circ}{N_c}. \tag{3.16}$$

Alternatively, the number of cylinders can be calculated as a function of the thermodynamic phase angle:

$$N_c = \frac{2\pi}{\pi - \alpha} = 360^\circ/(180^\circ - \alpha). \tag{3.17}$$

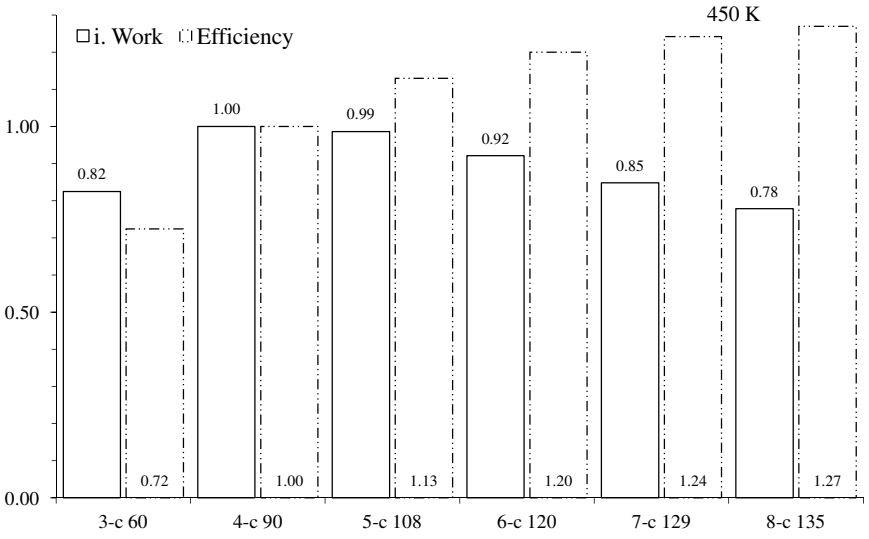

Figure 3.23: Indicated work and efficiency of alpha multi-cylinder engines. Normalised to the indicated work and efficiency of the four cylinder Siemens arrangement

In Figure 3.22 this correlation is visualized for whole-number values of N_c. It can be used to find the appropriate number of cylinders to approximate a desired thermodynamic phase angle. The larger the phase angle the smaller the incremental change resulting from adding or subtracting a cylinder.

Pressure-volume plots for double acting alpha engines can be found in Figure 3.2 if the corresponding thermodynamic phase angle is selected. Increasing the number of cylinders leads to more rounded $p - V$ plots with a decreasing pressure amplitude. The four-cylinder has the maximum power output due to its phase angle of 90 degrees ($\pi/2$). Higher cylinder numbers show a decrease in indicated work but an increase in efficiency, as shown in Figure 3.23. Figure 3.24 shows the influence on the brake power (mechanical losses neglected) for different numbers of cylinders. The smoothing effect of augmented cylinder numbers becomes obvious: Whereas the three cylinder engine partially consumes net power during one revolution and therefore still needs a substantial flywheel, this need

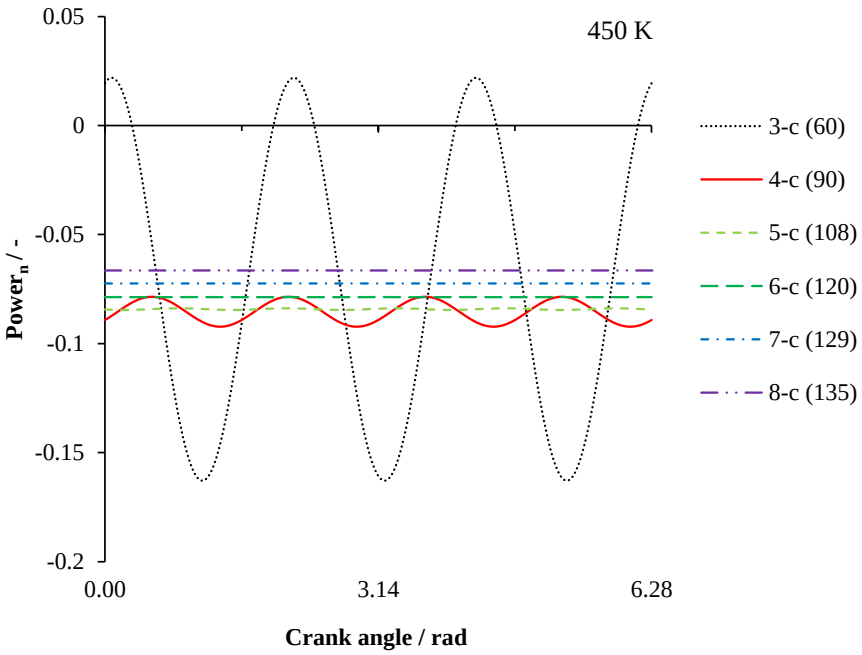

Figure 3.24: Power output of alpha multi cylinders vs. crank angle

is largely diminished in the four cylinder design. Engines with higher cylinder numbers show almost constant net power generation.

A third possibility for alpha multi-cylinder engines is the so-called Finkelstein arrangement [164]. Here the basic idea is to rearrange the Siemens configuration in such a way that two pistons are always rigidly coupled together. With an even number of pistons pairs can be found that are always moving in opposite directions (180° phase). If one of the pistons from each pair is turned upside down with its gas cycles unchanged, it will always be the case that two pistons move in phase and can be coupled without changing the thermodynamics. This is further clarified in Figure 3.25 for a four cylinder engine: Starting with the Siemens configuration from Figure 3.21 the two pistons on the right hand side are turned upside down (Figure 3.25 (a)) and then connected to the two pistons on the left hand side (Figure 3.25 (b)). Doing this, the number of moving parts is halved and the crankshaft becomes shorter. Unlike the claim in the original publication,

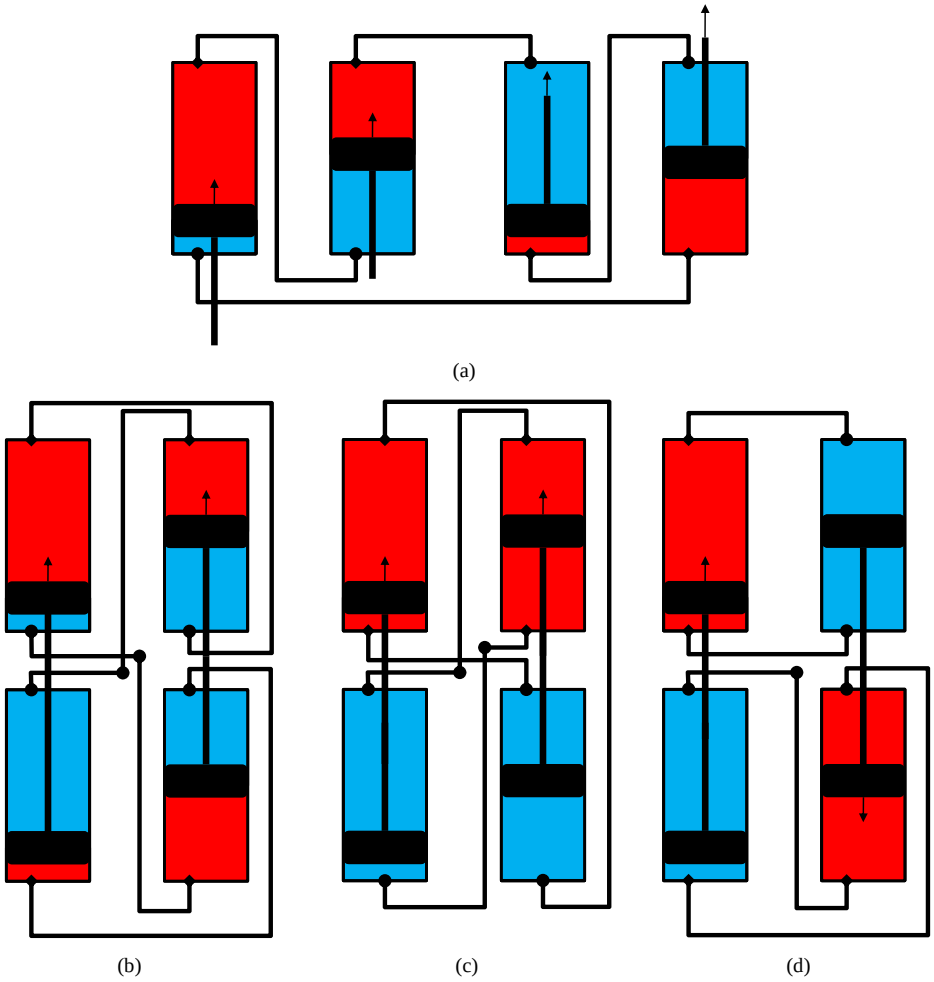

Figure 3.25: Finkelstein arrangement: Set-up and variations

internal balancing of compression with expansion forces is not possible to a higher extent than it is in the original Siemens arrangement, as will become clear below.

Another advantage of this configuration is that the hot and cold spaces can be rearranged to separate hot and cold areas more effectively in the machine (Figure 3.25 (c)). The thermal losses due to conduction and shuttle losses between the hot and the cold side can easily be minimised, omitting the bulky piston dome. This, of course, gives the same challenges regarding the hot cylinder seal as for the Franchot arrangement. Nevertheless, for a low temperature application the problem of keeping the seal at acceptable temperature levels is less severe and can be neglected completely by using a clearance seal. The piston connections formed by the heat exchangers are not very practical as they all have different lengths and several duct crossings are necessary. If the cylinders are rearranged as in Figure 3.25 (d) a simpler physical design can be found but using common parts for the heat exchanger manifolds as in other arrangements is not possible. The thermodynamics, however, remain unchanged.

Thermodynamically these three configurations are identical, as can be seen from Figure 3.26. In the case of the Franchot arrangement a four cylinder engine is calculated to be comparable with the Siemens and Finkelstein arrangements. The first set of plots ((a), (c), (e) in Figure 3.26) show the different pressures acting on the first reciprocating element (dashed lines), the resulting effective pressure and the movement of the element (continuous line). For the Franchot arrangement the movement of the compression piston is depicted by the dotted line. It can be seen that the effective pressure acting on the reciprocating element has a different characteristic for each case.

In the Siemens configuration the amplitude of the effective pressure is lowest due to the 90 degree phase difference of the involved cycles, and the maximum and the minimum are not spaced 180 degrees apart. This leads to a less symmetric power generation, plotted for all four cylinders in Figure 3.26 (b). The fact that

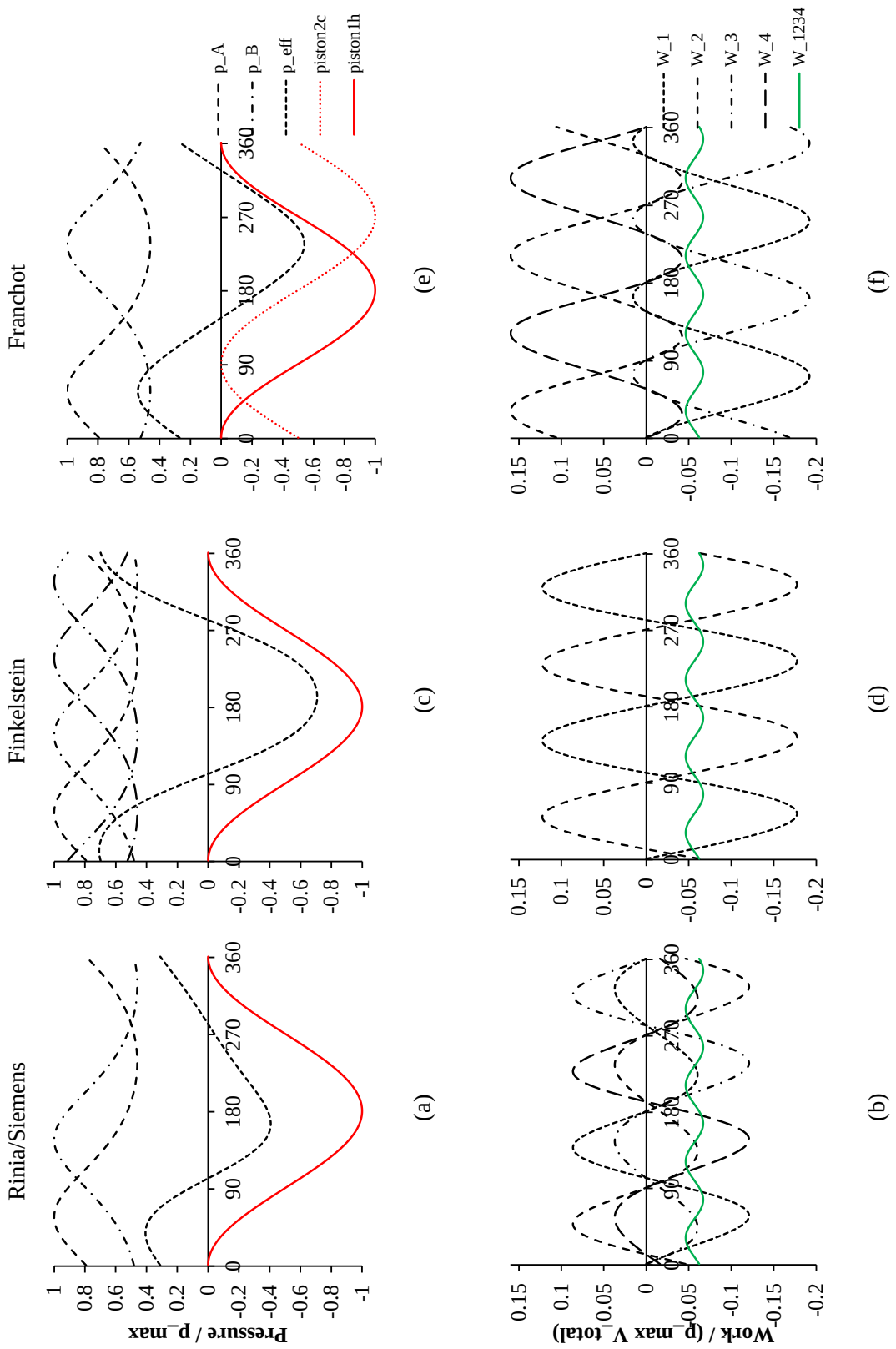

Figure 3.26: Effective pressure and work development of Siemens, Finkelstein, and Franchot arrangement

the second pressure peak is before the bottom dead point makes the upward motion less effective than the downward motion.

This is not the case for the Finkelstein arrangement (Figure 3.26 (c) and (d)); here, the effective pressure is symmetric as the pressures of all four cycles add together. The peaks of the effective pressure occur shortly after the top and bottom dead points resulting in symmetric power generation (which makes it also interesting for self-starting and free piston operation). Since always two sets of pistons are combined on one connecting rod the pressure amplitude has to be higher as a result. The work that has to be transferred from the power generating piston to the compression piston via the connecting rod is exactly the same as that which has to be transferred between the four pistons in the Siemens configuration. This is simply because the pistons that are combined on one rod are the pistons 1 and 3 (see Figure 3.26 (b)) for the first set and 2 and 4 for the second piston set, i.e. paired pistons that produce and consume power at the same time (even if the amplitude is different). As a result the forces are not balanced internally to a bigger extent on the rods than it is the case for the Siemens configuration; due to the same sign the forces are simply added.

For the case of the Franchot engine things are somewhat different. The resulting effective pressure is symmetric too and acts very efficiently on the expansion piston, because the peaks occur close to the point of largest volume change. As a result very little mechanical work has to be added to the expansion piston for compression. For the compression piston, this is not the case. With the pressure peaks occurring before the dead points, mechanical work has to be added during most parts of the cycle. Compared to the Siemens and Finkelstein arrangements: the mechanical work that is needed to be supplied externally for compression, and the work that is generated at the expansion pistons are both higher for Franchot engines; the gas forces are less well balanced; and more power for compression has to be transferred via the crank shaft. Engine components thus have to be built

stronger and friction in bearings and seals is higher, even though the indicated work is identical to the other arrangements. As was the case for single-acting alpha engines, Franchot engines have major drawbacks compared to the other designs.

3.2.2 Beta multi-cylinder engines

The simplest way to achieve a double-acting beta engine is to place a second piston-displacer pair parallel to the first set with a 180 degree phase offset. The previously unused space at the backside of one piston is now connected with the compression space of the other part engine. Figure 3.27 explains this set-up. The basic idea is that by using the additional compression space under the pistons the displacer amplitude can be increased too, so that swept volume and the pressure amplitude can be increased. Also the expanding gas volume of one cylinder partially compresses the gas enclosed in the second cycle and vice versa, without making the deviation over the crank drive so that engine components can be less massive.

A second option for creating a double-acting engine is to connect a second engine back-to-back. The power piston can be coupled rigidly with the second power piston, and so can the displacers. The power piston then can be made double-acting, completely avoiding the second piston. An example for a similar device is the heat-actuated free-piston heat pump ('Duplex') researched at Sunpower [165–167]. Figure 3.28 explains the basic set-up. The advantage of the overlapping stroke of the power piston and hence compact design is only achievable with a linear alternator for power conversion. An attempt to build a double-acting beta engine was made by Philips and can be found in Hargreaves' book[6]. In order to accommodate a crankshaft the power piston is divided into two rigidly connected pistons, so that the advantage of using a common seal and overlap of

[6]Hargreaves pp 257-258 [23]

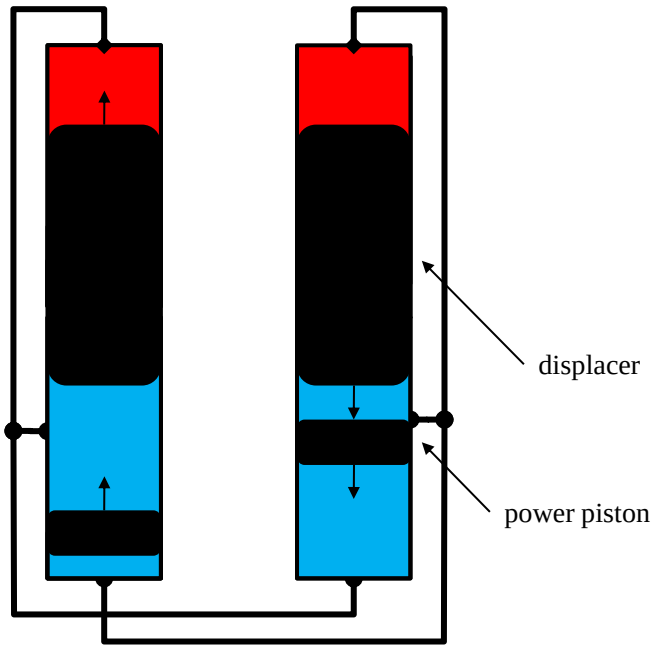

Figure 3.27: Double-acting beta engine using two parallel cylinders with opposed moving pistons and displacers

the compression volume is lost. Nevertheless the number of moving parts of the crankshaft is largely reduced as the two pistons and the two displacers each share the same crank mechanism. One drawback of this design is that now there are two hot ends, requiring a more complicated heating system. However, the specific output of this engine is identical with the performance of a single-acting engine.

Similar to the first beta double-acting concept of Figure 3.27 this set-up can be expanded to larger cylinder numbers. The phase angle then changes accordingly. Similar to the Siemens arrangement the space on top of one piston is connected to the space under the next piston, moving with a phase difference of $2\pi/N_c$. Figure 3.29 shows a four cylinder engine as an example; the pistons have a phase difference of 90°.

In Figure 3.30 the resulting piston amplitudes, pressure amplitudes, and the power development are given after optimisation for maximum power output. The

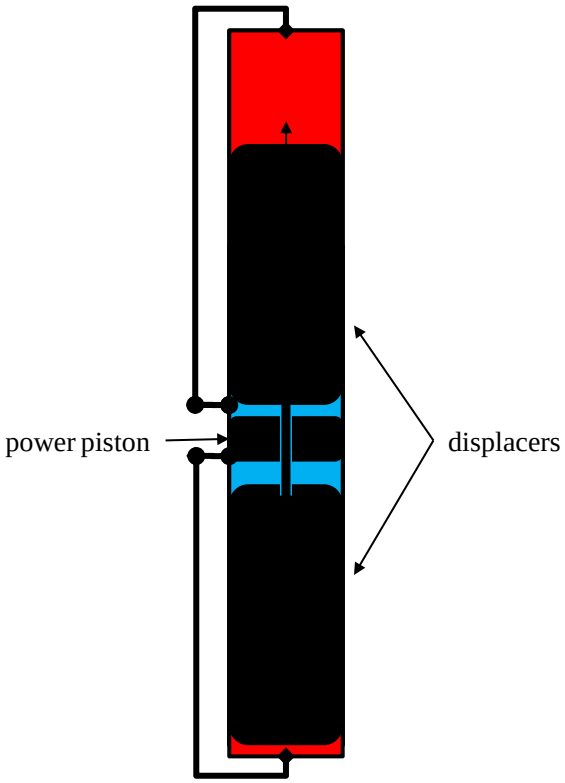

Figure 3.28: Set-up of the double-acting beta single-cylinder engine (duplex)

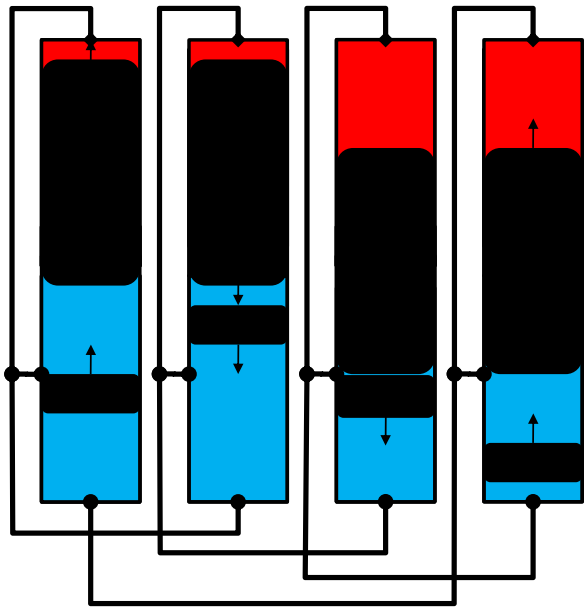

Figure 3.29: 4-cylinder double acting beta engine

two cylinder opposed (duplex) and the two cylinders parallel engine are each simulated with a second, identical engine phased in such a way that the power output is smoothed. Each of the simulated engines thus has four gas cycles for better comparability. It can be seen that the duplex engine (c) has the highest piston amplitude which is a result of it being a two piston rather than a four piston engine. Scaled to a four piston engine, and therefore with half the amplitude, it would be in-between the two parallel cylinder engines. The four cylinder version (Figure 3.30 (a)) manages to create a larger piston amplitude than the two cylinder version (e) due to the phasing of the pistons and displacers. The effective pressure of the duplex and the two cylinder engine is very similar due to the phase shift of 180° of the individual pressures. As the piston amplitude is higher for the duplex the power output is higher than for the two cylinder parallel engine (Figure 3.30 (d) and (f)). The power output for the four cylinder engine is slightly lower, despite the higher piston amplitude, because the shape of the effective pressure curve is less beneficial.

As the arrangements are somewhat similar to the alpha engines described so are the resulting pressure variations. Looking at Figure 3.30 and comparing it to Figure 3.26 this becomes obvious. Having the 90° phase difference between two interconnected pistons as a common factor, a similar pressure and work development can be found in the four cylinder beta and in the four cylinder Siemens configuration (Figure 3.26 and 3.30 (a), (b)). The beta back-to-back engine shows similar characteristics as the Finkelstein arrangement (Figure 3.26 and 3.30 (c), (d)). The parallel double cylinder engine from Figure 3.30 (e) and (f) shows similarities with the Franchot arrangement in that it shares the 180° phase difference between the pressure peaks. Since the second piston is not becoming a mere compression piston it is a partly balanced double-acting piston with much smaller power amplitudes at the individual pistons.

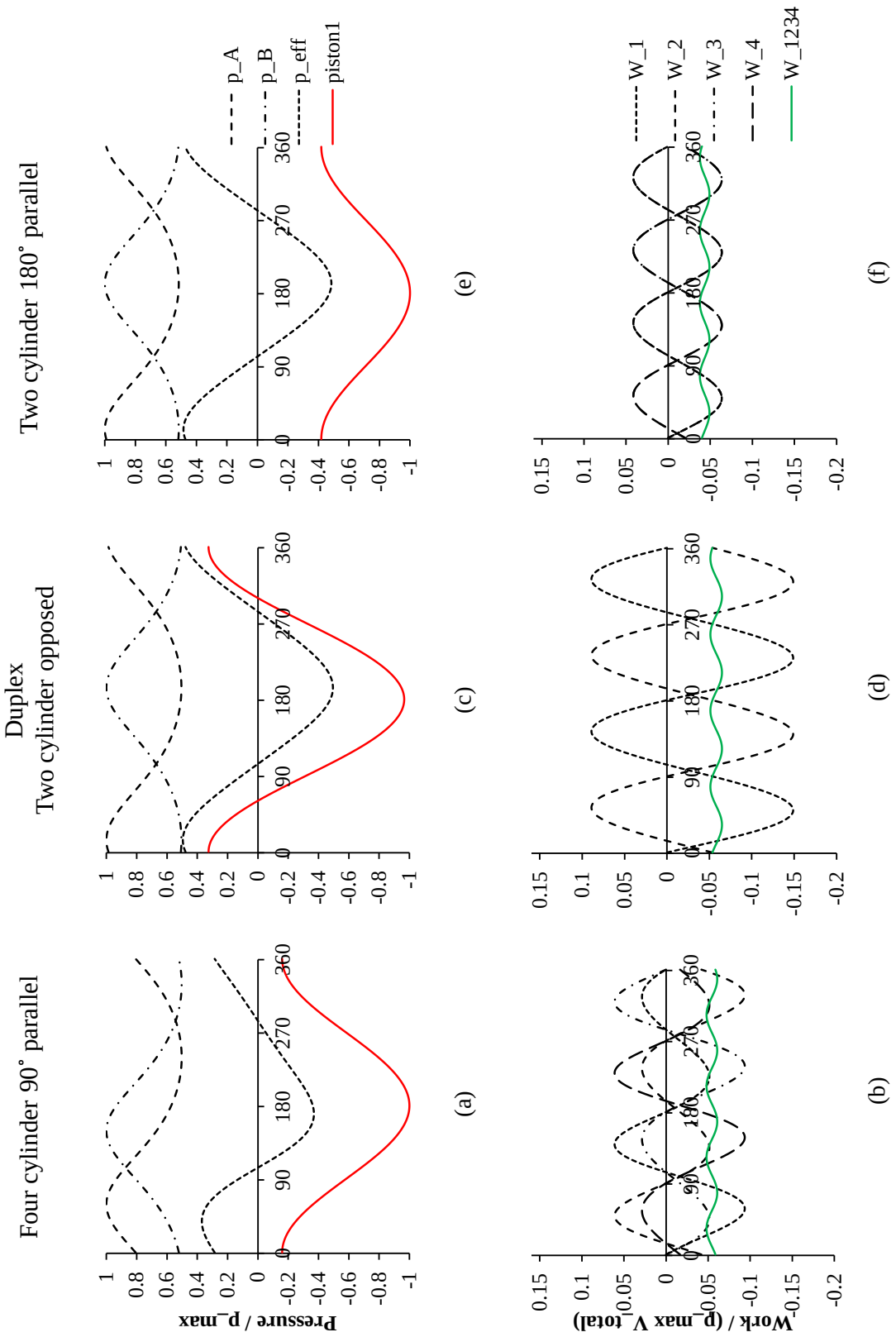

Figure 3.30: Effective pressure and work development of the beta-type double-acting engines

3.2.3 Gamma multi-cylinder engines

Double-acting gamma engines are relatively simple to realise as an early example of Stirling's work shows (see Figure 1.7 (a)). A similar design was proposed by Walker for large coal burning engines [168]. Due to the poor performance of single-cylinder gamma engines compared to alpha and beta engines no multi-cylinder arrangements were developed in greater detail. The shortcomings in terms of dead volume in the cylinders are inherent and cannot be overcome by the use of multiple cylinders. Performance can be improved but only marginally, as can be seen in the following section.

3.2.4 Comparison of double-acting multi-cylinder engines

Figure 3.31 shows the efficiency and the power output of the different double-acting multi-cylinder engines in comparison, all normalised to the power and efficiency of the Siemens four-cylinder engine. Among the sinusoidal moving engines the Siemens configuration performs very similarly to the four-cylinder beta, and the beta duplex. Double-acting gamma engines, be the piston hot or cold, show much poorer performance. Even discontinuous displacer motion does not improve performance enough to be competitive. Discontinuous displacer operation in the beta engines, however, allows the performance to be increased substantially. The two cylinder engine then performs similarly to the Siemens benchmark; the four-cylinder exceeds it by 25 %, and the duplex by more than 80 %. The large improvement of the latter is only of academic interest, as it cannot be incorporated in a physical design easily.

The comparison to single-cylinder engines in Figure 3.18 clearly shows the advantage in power density for double-acting designs. Only the beta single-cylinder engine with discontinuous displacer operation comes close to the power output of

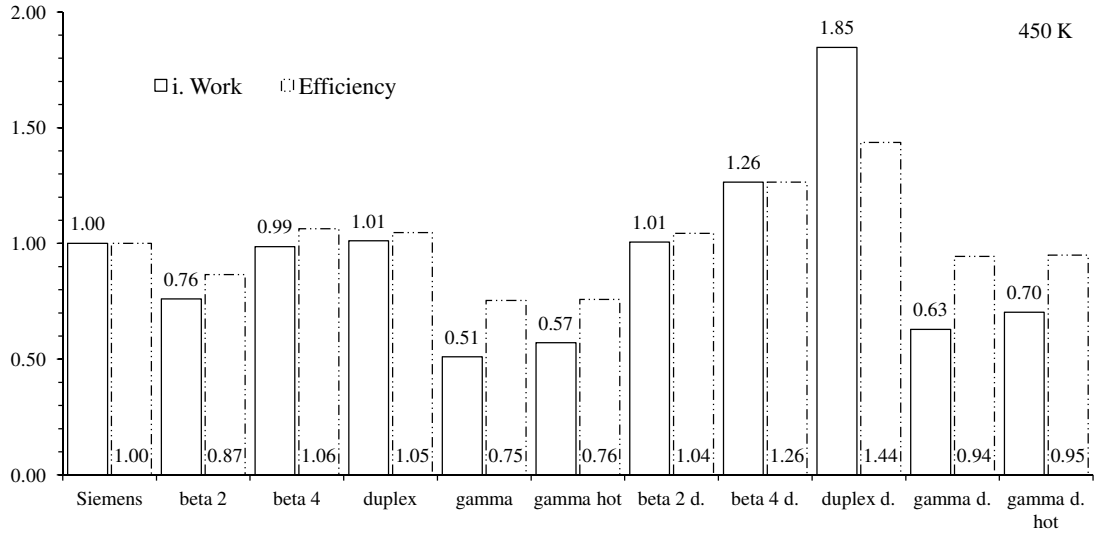

Figure 3.31: Indicated work and efficiency of double-acting multi-cylinder engines, normalized to the performance of the Siemens four cylinder engine

the Siemens arrangement. All other designs perform significantly more poorly. Interestingly, the beta single-cylinder engine performs at least as well as any gamma design, single- or double-acting, with much better efficiency.

Isothermal analysis makes a highly simplified assumption when the heat transfer is considered ideal and independent of the frequency. This is especially true for the low-temperature difference environment where heat transfer rates are inherently low. The simplicity of the Siemens arrangement combined with the good thermodynamic performance makes it a preferred choice from the analysis done. However, due to the shortcomings of the isothermal model the double-acting beta engine will also be considered for further investigation. A more detailed simulation of realistic heat transfer in the Sage environment is to be performed to identify the thermodynamically most favourable engine set-up.

3.3 Multi-cylinder comparison (Sage simulation)

Using Sage to perform the optimisation of the thermodynamically important part of the heat exchangers and the regenerator allows a realistic simulation of the performance of Stirling engines at these low temperature differences. In the isothermal analysis the heat transfer from the heat exchangers to the working fluid is assumed to be perfect; there is no temperature difference between the walls and the gas. The smaller the temperature difference between heat source and sink the worse the heat transfer and the less 'ideal'. The more realistic Sage simulation is able to include a realistic heat exchange and adiabatic effects into the calculations which is vital for accuracy, especially at the low temperature differences. From the isothermal modelling, interconnected double-acting multi-cylinders of the alpha- and beta-type were identified as the most promising set-ups. The following simulation of the two engine types is conducted in Sage using simplified models.

3.3.1 Alpha engines[7]

The set-up of the alpha engine is given in Figure 2.2 where the main model and the corresponding sub-models are shown. This set-up resembles the opposed piston configuration which is, since only the thermodynamic and fluid-dynamic processes in one gas circuit are simulated, identical in terms of indicated power output and thermal efficiency. Here, in the multi-cylinder layout the phase angle is defined by the number of pistons. For the engine of the given dimensions restrictions were made in the allowable regenerator diameter and in the maximum number of tubes to be used for the heat exchangers, according to Table 3.2.

Little is known about the exact influence of operating and design parameters on engine performance utilizing low temperature heat sources of 100-200 °C. In

[7]The work presented in this section was also published as a contribution to the International Stirling Engine Conference 2012 [169].

Table 3.2: Simulation parameters of the preliminary simulations in Sage

	value	unit
Bore	0.2	m
Stroke	0.2	m
Material	steel	-
Heat source temperature	150	°C
Heat sink temperature	40	°C
Mean pressure	5	MPa
Max. regenerator diameter	0.5	m
Max. number of tubes	1000	-
Wall thickness regenerator	7.5 E-10 p_{mean} d_{reg}	m
Gas model	Redlich-Kwong	-

Chapter 4 a more detailed discussion of the various parameters is given. Here, the focus is only on frequency and phase angle. For each combination of the two parameters the geometry of the heat exchangers and the regenerator is optimised in order to achieve the highest possible power output. The performance of each component is mapped in a separate model by varying its geometry with the geometry of the other two components unchanged. For the three components this can be done simultaneously in three parallel running simulations. Then the geometry that results in best performance is selected and implemented into the other two simulations. When all three models converge to the same power output the simulation can be stopped as each component is now mapped with the other two optimized. Usually two or three iterations are sufficient to find the best overall performance possible with a set of parameters.

The design parameters that define the performance of an alpha engine of the size and operating conditions given are frequency and phase angle. A detailed mapping of these parameters is given in Figure 3.32 for hydrogen (a, b), helium (c, d), and nitrogen (e, f) as the working gases at a heat source temperature of 150 °C and 5 MPa mean pressure. It can be seen that the maximum achievable power output is doubled if helium (12 kW) is used instead of nitrogen (6 kW), and doubled again if hydrogen (24 kW) is used instead of helium. This is partly due

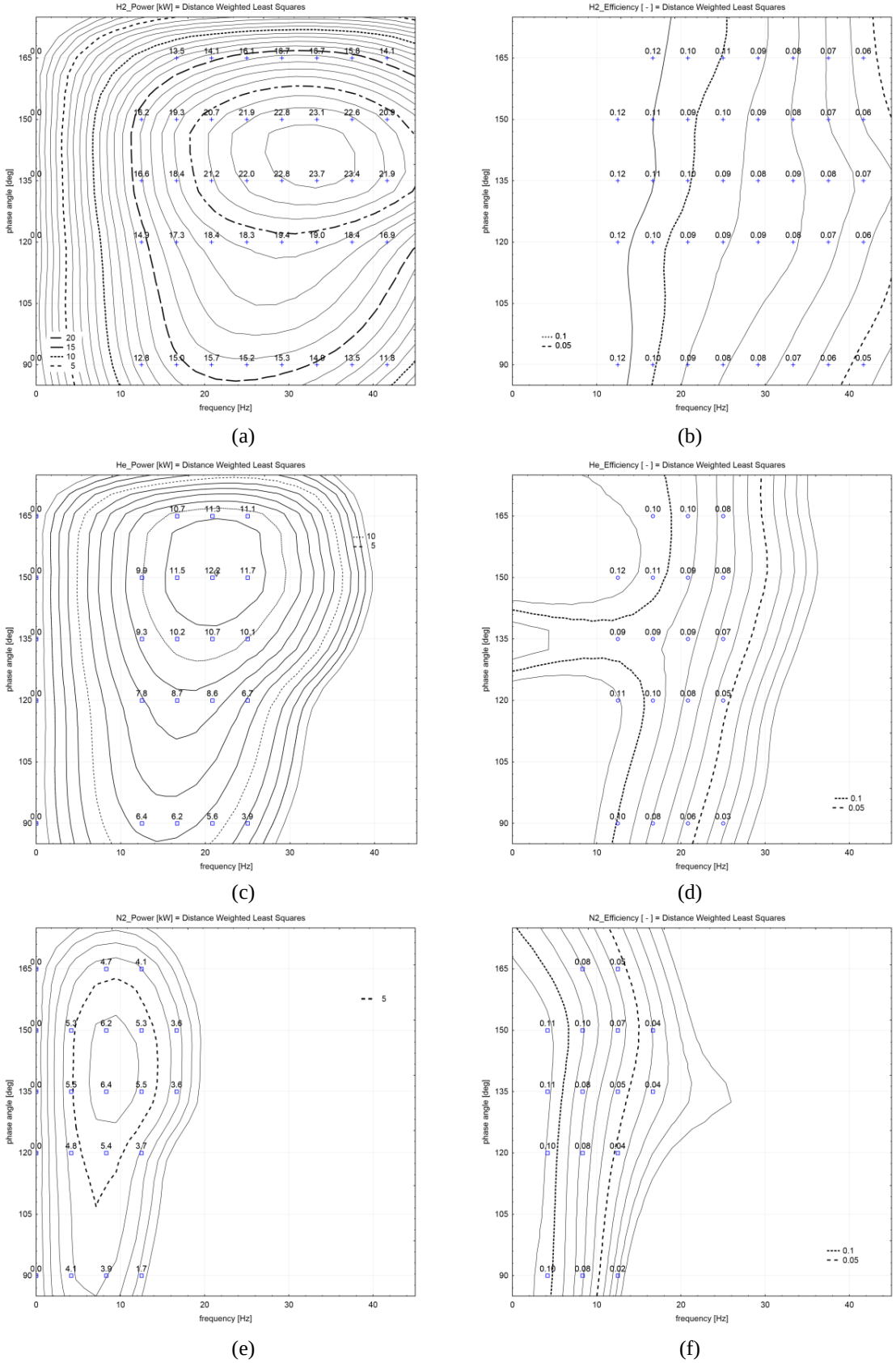

Figure 3.32: Power and efficiency for hydrogen (a,b), helium (c,d), and nitrogen (e,f) at $T_{hot} = 150\,°\mathrm{C}$, $T_{cold} = 40\,°\mathrm{C}$, and $p_{mean} = 5\,\mathrm{MPa}$

to the decreasing density (ρ (N_2) > ρ (He) > ρ (H_2)) which allows for higher frequency and thus more power, and partly due to the thermal properties of the different gases. The influence of the working gas is discussed in greater detail in Chapter 4.

In the range considered the efficiency drops as the frequency rises. The higher the frequency the higher the temperature difference between the working gas and the heat exchangers, and thus the smaller the temperature difference in the working gas and hence the efficiency is also lower. As the optimisation of the heat exchanger components was carried out in order to achieve the highest possible power output the efficiencies could be improved at the expense of power density. At the maximum power point the efficiency is independent of the working gas at around 8 %, which is 30 % of the Carnot efficiency.

3.3.2 Beta engines

A schematic set-up for a double-acting beta engine can be found in Figure 3.29; here the number of cylinders is not limited to four. For simulation purposes the existing Sage model of the alpha engine was modified and expanded to represent the double-acting beta configuration. Figure 3.33 shows the main model; the corresponding sub-models are identical. Comparing this model to the one in Figure 2.2 which represents the alpha configuration, it can be seen that one of the pistons has been converted into a displacer and that a second piston has been added to the model. The gas is moved from the right hand side of the displacer and the expansion space through the heat exchangers and the regenerator. After the cold heat exchanger the mass flow is split and parts of it ($\dot{m}_{Gt}$ 22) enter the compression space under the displacer, just as in a single-acting beta engine, and the other part ($\dot{m}_{Gt}$ 28) enters the compression space underneath the adjacent piston.

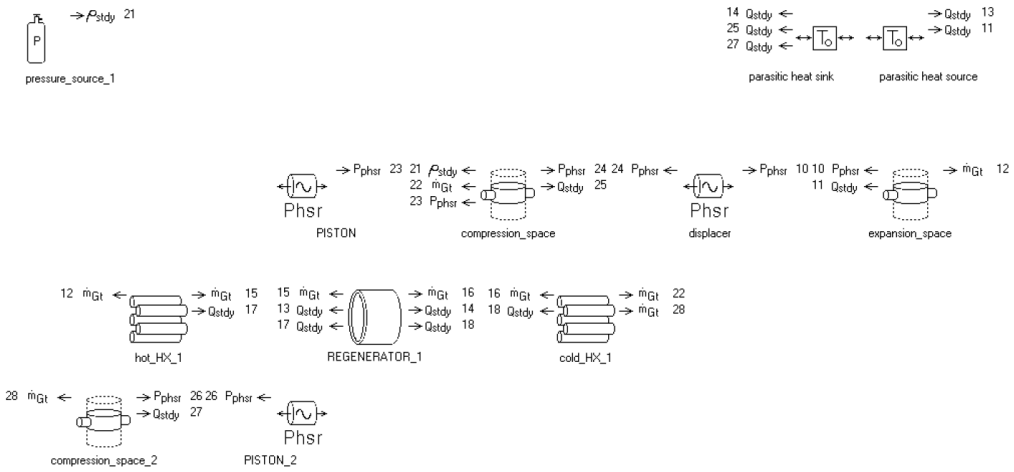

Figure 3.33: Sage model of the double-acting beta multi-cylinder

The introduction of the displacer brings two new degrees of freedom to the system: Firstly, the phase angle between the piston and the displacer which run in the same cylinder (α_d); and secondly, the ratio of the amplitudes or strokes of piston and displacer ($k = A_{piston}/A_{displacer}$). Together with the phase angle between the pistons (α_p), which is defined by the number of cylinders as for alpha engines, these three parameters define the volumetric changes within the engine. In order to simulate the identical cylinder size (swept volume) as for the alpha engine (total stroke of 0.2 m) the amplitudes of the pistons and the displacer as well as the mean volumes of the variable gas spaces have to be adjusted depending on the volume ratio and the phase angles. This can be achieved by solving the equations given in Section 3.1.2 and implementing the values found in Sage.

As only a comparison between the alpha and beta multi-cylinder arrangement is sought, and as the number of simulations required is large due to the newly introduced degrees of freedom, only helium is used as the working fluid and the frequency is set to 20.83 Hz (1250 rpm) - the optimum value for the alpha engine where maximum power output was achieved. The main parameters are identical to the ones used for simulation of the alpha engine, given in Table 3.2. The simulation and optimisation is performed using the same method as for the alpha

configuration. Figure 3.34 shows the influence of the two phase angles and the volume ratio on the power output. Six values for the phase angle between the pistons are chosen which correspond to: 2-cylinder ($\alpha_p = 180°$); 4-cylinder (90°); 6-cylinder (60°); 8-cylinder (45°); 12-cylinder(30°); and 24-cylinder (15°) engines.

Looking at the maximum achievable power for each of the multi-cylinder configurations in Figure 3.34 it is striking that the difference between them is quite small, especially for piston numbers between 4 and 12. In the alpha multi-cylinder the change from a 4-cylinder to an 8-cylinder engine roughly doubles the power output per cylinder (Figure 3.32). Here, in the double-acting beta configuration the power is increased only by 3 %, also between the 4-cylinder and the 12-cylinder. The optimum parameter combination of displacer phase angle and volume ratio changes with decreasing piston phase angle, starting at a small piston stroke and a large displacer phase angle which changes to a volume ratio of unity and a small displacer phase angle. In the case of the 12-cylinder engine the optimum power is found to be at a volume ratio of 1 and no phase shift between displacer and power piston (displacer phase angle of 0 degree). Such an engine corresponds exactly to an alpha engine with twelve interconnected cylinders in terms of the volumetric changes, as piston and displacer move as one part, thereby not creating any variable gas space between them.

Figure 3.35 illustrates the movement of the different components (pistons and displacer) as well as the resulting volumetric changes for each of the examined configurations. The parameter combination that yields the maximum power output was chosen to represent the corresponding engine. Looking at the lower part of Figure 3.35 (b) which is the plot of the 4-cylinder arrangement the stroke of the displacer and its corresponding piston (1) can be seen to fit into the defined stroke of 0.2 m. The phase shift of 0.2 π between displacer and piston 1 is clearly visible as is the phase shift of 0.5 π (90°) between the two pistons. In the upper

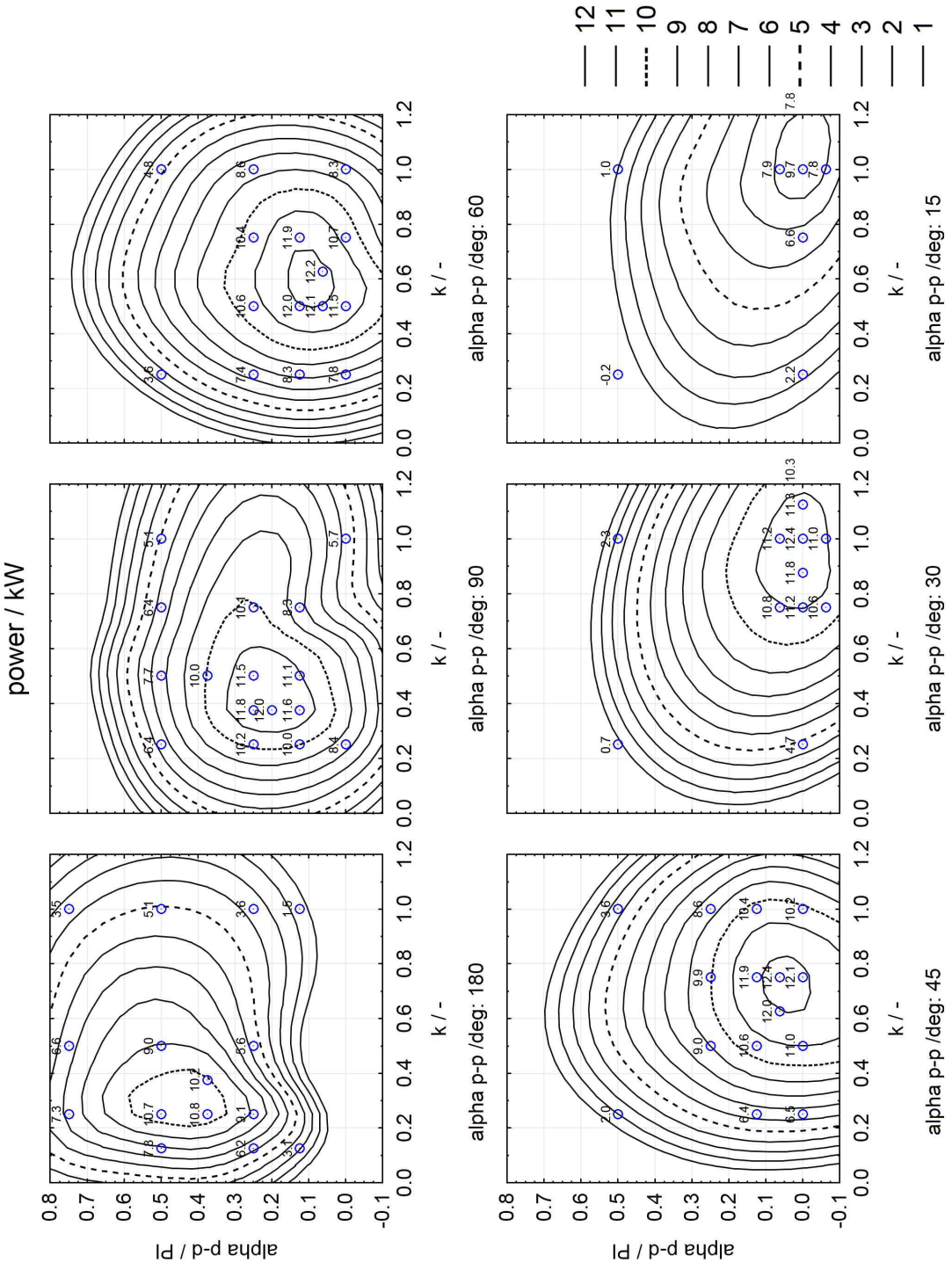

Figure 3.34: Power output versus displacer phase angle (α_d) and volume ratio (k) for double-acting beta engines with different numbers of pistons (phase angle between the pistons α_p); the circles represent the simulated parameter combination with the corresponding power output.

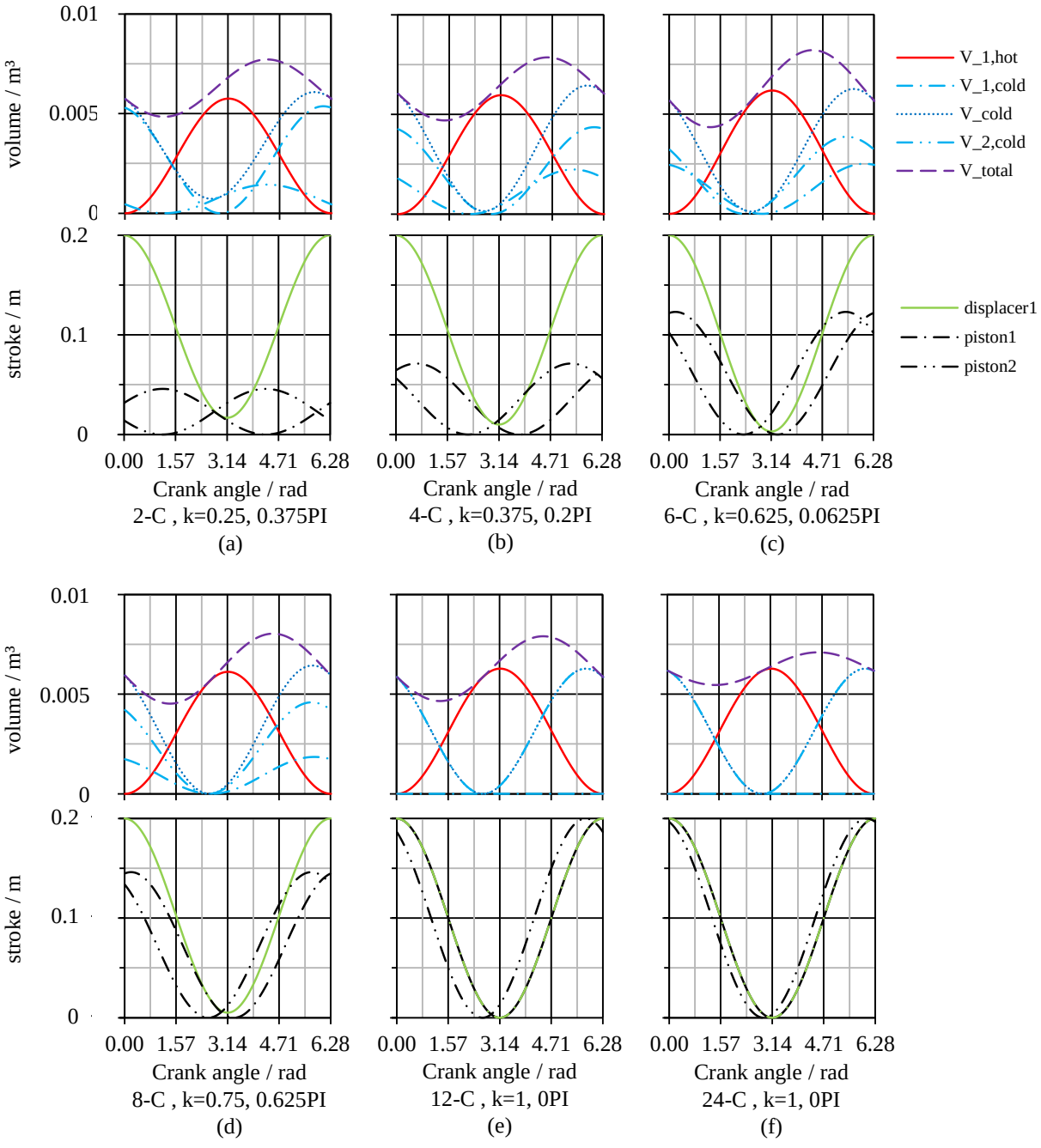

Figure 3.35: Displacer and piston positions for double-acting beta engines. The resulting volume variations for the hot and cold spaces are given above.

part of Figure 3.35 the resulting volumetric changes are given. The hot volume is defined by the space above the displacer, and the cold volume by the sum of the two separated cold volumes. The first of these cold volumes is determined by the space between the displacer and piston 1; the second by the space below piston 2. The sum of all three volumes gives the total volume. Observing Figures 3.35 (b) to (e) it can be seen that, despite the large difference in the input parameters (the two phase angles and the volume ratio), very similar volumetric changes of the total volume and the hot and cold volume can be observed - similar not only in terms of the amplitudes but also in terms of the phasing. Similar volumetric amplitudes together with similar phasing lead to very similar pressure changes. Consequently, the power outputs from the different engines are almost identical, as can be observed in Figure 3.34; from Figure (b) to (e) the power rises only very little and reaches the value of 12.4 kW per cylinder as the alpha 12-cylinder does. Optimum use of the pressure is achieved when the maximum of the hot volume is reached during the maximum rate of expansion while the cold volume is minimal, and vice versa during compression. Coinciding with the largest possible volume change the highest power output is reached. There is always a trade-off between these two counter-acting effects, so that the phasing shown here represents the optimum configuration for this temperature difference. In contrast to the alpha multi-cylinder engine, different numbers of cylinders can be used to create similar favourable volumetric changes and thus power output. However, these beta multi-cylinder engines cannot be used modularly as their kinematics and also the position of connectors for the cold volume underneath the displacer vary strongly with the piston phase angle.

A 12-cylinder beta configuration that essentially works like a 12-cylinder alpha engine and produces the identical power output per cylinder is definitely not an option because of the unnecessary complexity and the doubled number of parts. The identical number of moving parts can be realised with a beta engine having

6 cylinders and thus 12 reciprocating parts, as the 12-cylinder alpha engine. The power output per cylinder of the beta engine and the alpha engine would still be in a very similar region. However, while the total power output of the alpha engine would be twice that of the beta engine, twice the number of heat exchangers would be required. The same is true for the 4-cylinder engine. There is no advantage in power output but these engines offer the possibility of an efficient realisation of the Stirling cycle with a smaller number of gas circuits, and in the case of the 4-cylinder engine a classic square four cylinder arrangement. Considering the added complexity of the displacer linkage and sealing as well as the additional restrictions in terms of a feasible physical design, beta multi-cylinder engines are, compared to their simplistic piston-only counterpart, the less favourable choice.

3.4 Conclusion on suitable design

In this chapter a great number of possible engine configurations have been compared. Amongst these are single- and double acting set-ups of the alpha-, beta-, and gamma-type. Two different simulation tools were used to identify the most suitable engine configuration. First, isothermal analysis was used in order to reduce the number of possible candidates by means of a highly idealised simulation. Second, the two most promising candidates from the preliminary simulations, namely the alpha and the beta double-acting engine, were simulated in greater detail using the third-order simulation tool Sage. It was shown that the double-acting alpha multi-cylinder engine provides the highest power density together with the simplest engine design. The optimum thermodynamic phase angle varies strongly from the common 90° found in many designs and is more likely to be around 150°. This differs also from the results gained with the isothermal analysis which recommends the 90° offset. More in-detail simulation is necessary to understand the behaviour of alpha engines at low heat source temperatures and to find the most suitable working conditions.

Chapter 4

Thermodynamic optimisation of the LTD

In the previous chapter the achievable power density of alpha and beta multi-cylinder engines was examined and double-acting alpha engines were identified as being able to make better use of a swept volume given while providing a simpler mechanical set-up. In this chapter[1], the double-acting alpha engine is explored in greater detail. Firstly, design and operating parameters are optimised in order to achieve the highest power output from a given cylinder size; then the sensitivity of these parameters to changes from the optimum values is established; and implications on engine design are discussed. In addition a comparison between low-temperature difference engines and engines working at the upper end of the temperature scale is made.

[1]Parts of the work presented in this chapter have also been published in Proceedings of IMechE part C [170].

4.1 Simulation set-up

4.1.1 The Sage third-order simulation model

The basic set-up of the simulation model and its sub-models has not been changed, so that the structure is identical to the schematic given in Figure 2.2. Here, the main model is shown at the top, the spatial discretisation of the individual components in the middle (each component is composed of a number (N_C) of identical elements), and the corresponding sub-models for each component at the bottom. The model includes all the physical elements of a real engine. The two pistons (not shown in the figure) are set to the desired phase difference. Depending on the established frequency the gas is moved between the hot heat exchanger, the regenerator and the cold heat exchanger; the volume in the cylinder spaces is changed accordingly. All gas flow paths between the components are shown in the figure, as well as the heat flow paths through solid bodies and between working fluid and surfaces. For all parameter variations and optimisations the set-up of this model was not modified; only the values of different parameters within the components were changed. The unaltered key specifications of the model are listed in Table 4.1. The greatest differences from the geometry used in the previous model are: the reduced stroke, the fixed regenerator and the fixed heat exchanger tube diameter.

4.1.2 Heat exchanger type selection and design

An obvious consequence of the lower thermal efficiency that is achievable if utilising a low-temperature heat source is that the heat exchangers become a very critical component of the design and of the total cost of the engine. In comparison with high temperature heat source engines the heat exchangers have to be of larger size to achieve a particular engine power output. Thus the annular heat exchangers described in Section 1.2.7 seem less suited for the low-temperature application

Table 4.1: Specifications of the Sage model

Engine type	alpha
Material (heat conductors and regenerator)	steel
Bore (L)	0.2 m
Stroke (L/2)	0.1 m
Heat exchanger type	tube bundle
Maximum number of tubes	2000
Tube diameter	3 mm
Tube wall thickness	0.5 mm
Regenerator diameter (L)	0.2 m
Regenerator wall thickness	7.5 mm
Regenerator matrix	random fibre 0.05 mm
Heat source temperature	150 °C (LTD) 750 °C (HTD)
Heat rejection temperature	40 °C
Mean pressure	5×10^6 Pa
Working fluid	He (Redlich-Kwong)

since the surface area is smaller and the wall thickness is higher compared to a tubular heat exchanger packed in an external canister.

For the heat exchangers tube bundles, as opposed to a finned annulus, were selected. The low temperature heat source requires a large surface area to allow sufficient heat transfer from the source to the working gas and also when rejecting the heat. The pressure loss in a straight tube is also very small and shell-side heat transfer can be increased by using finned tubes. Shell and tube heat exchangers are a simple and proven design with many applications in different industries. Depending on the design they can also easily be dismantled and cleaned if fouling or scaling occurs, which is a necessary consideration when using geothermal brine. The maximum number of tubes is limited to 2000 for practical reasons, as it corresponds to a minimum centre-to-centre of around 4 mm for the given cross-sectional area of the cylinder and the regenerator. As the tube diameter is fixed to 3 mm this results in a minimum pitch ratio of 1.3, a typical value according to Gupta [171]. Section 6.1 provides further information on heat exchanger design and heat exchanger arrangements.

The regenerator is a key component for Stirling engine performance. For maximum power output the pressure loss has to be very low and the gas volume in the regenerator very small. This necessitates a compromise for the porosity (void volume in the regenerator divided by the volume of the regenerator canister) since low pressure losses are reached with a high porosity which then increases the gas volume in the regenerator. For the regenerator matrix random fibre with a wire diameter of 0.05 mm is used. A large regenerator shell diameter is beneficial as it reduces the pressure drop for a given porosity and length. However, here this diameter is set to the diameter of the piston in order to assure a uniform flow through the regenerator and to avoid sections in the matrix that do not contribute to regeneration. This would be the case for a regenerator with a very large cross-section and widely spaced heat exchanger tubes. In addition, such a regenerator would be much harder to accommodate in a multi-cylinder arrangement.

4.1.3 Parameter optimisation

The simulations performed with the described model are independent of the actual physical set-up; in single and double-acting engines of identical geometrical and operating parameters the pressure and volume variations in one gas cycle are identical. Only the resulting net power distribution on the reciprocating elements changes depending on the physical set-up. This can have influence on the mechanical efficiency and is discussed in detail in Chapter 5. The indicated power and efficiency per cycle, however, is identical. Parasitic heat losses, such as thermal conduction from the hot part of the cylinder to the heat sink which may vary for different set-ups, has been neglected in the model to allow better comparability. For the LTD such losses are inherently small and have only very little influence on the performance.

For the high temperature difference engine (750 °C heat source temperature, HTD) and the low temperature difference engine (150 °C, LTD) an identical model

is built and parametrized with the desired frequency (f), phase angle (α), and temperatures (T). For each temperature level copies of these models are made and are then used to optimize each of the heat exchanger components (hot and cold heat exchangers, regenerator) separately to achieve maximum power output for the given set of operating conditions. For the hot and cold heat exchangers the number of tubes (N_{HX}) and the tube length (L_{tube}) are mapped, and the best parameter combination is saved; for the regenerator the porosity (P_{reg}) and the length (L_{reg}) are mapped. In an iterative process the heat exchanger parameters are updated with the optimum values found from the parallel simulations. After two or three iterations the heat exchanger parameter configuration that yields the highest power output can be found. Doing so saves a large amount of computational time in comparison with a model in which all permutations of the parameters are calculated. Also the simulation runs tend to be more stable.

Experience in running the simulation models revealed that results were able to be obtained more quickly if a specific phase angle was chosen first to then map the frequency. The geometries of the heat exchangers can subsequently be optimized for rising or falling frequency levels, using the parameters gained from the previous optimization as the starting point. The inverse approach of keeping the frequency constant and then optimizing for different phase angles was much slower in comparison.

4.1.4 Efficiency considerations and non-dimensional parameters

The ideal thermodynamic cycle that describes SE performance is the Stirling cycle which consists of two isothermal and two isochoric changes of state, and which performs according to the Carnot efficiency. The Carnot efficiency (η_{Carnot}) is

defined as

$$\eta_{Carnot} = 1 - \frac{T_{sink}}{T_{source}} \tag{4.1}$$

and represents the theoretical limit of the efficiency for SEs. At low temperature differences the Carnot efficiency and therefore the theoretical maximum is inherently low. The ratio (r_{Carnot}) of indicated efficiency to Carnot efficiency reveals how closely ideal performance can be matched.

$$r_{Carnot} = \frac{\eta_{ind}}{\eta_{Carnot}} \tag{4.2}$$

Also comparing the efficiency of two engines with different heat source temperatures gives more insight when the comparison is made relative to the Carnot efficiency determined for each source temperature.

Further normalisation of parameters has been done. The dimensions of all heat exchanger components (L_x) are normalised to the diameter of the bore (L):

$$L_x^* = \frac{L_x}{L} \tag{4.3}$$

The normalised pressure (p^*) is defined as

$$p^* = \frac{p}{p_{mean}} \tag{4.4}$$

with p_{mean} being the mean cyclic pressure. The normalised volume (V^*) then becomes

$$V_x^* = \frac{V_x}{V_{swept}} \tag{4.5}$$

with V_{swept} being the volume swept in one cylinder of bore L and stroke 0.5 L.

4.2 Optimisation of a LTD alpha engine for maximum power output

In order to achieve the highest power density possible (which affects plant capital costs and hence economic viability) the heat exchanger and the regenerator geometries are optimised for highest power output rather than for highest efficiency. Since the energy cost for geothermal or waste-heat applications is low compared to fossil fuel sources the efficiency is somewhat secondary to the specific power output. By changing the geometries of the heat exchanger components it is therefore possible to increase the efficiency levels compared to the ones shown below, but at the expense of power. For each combination of phase angle (between the volume of expansion and compression space) and the operating frequency, this optimisation is done individually. Figure 4.1 shows the resulting power versus the phase angle for different frequencies; Figure 4.1 (a) for 150 °C and Figure 4.1 (b) for 750 °C heat source temperature. Each of the data points is generated by an individual optimisation of the heat exchanger parameters. The very large difference in absolute power output is clearly visible and comes as no surprise. The much higher sensitivity of the LTD system also becomes evident. In the following sections the influence of the phase angle and the frequency on the engine performance is discussed.

4.2.1 Influence of the phase angle

Effective volumetric change and heat transfer

The choice of the phase angle has three major effects on SEs: it influences the time-dependent distribution of the working fluid, its flow characteristics and thus the heat transfer, and the total volumetric change of the gas and thus also the pressure amplitude. Figure 4.2 illustrates the piston movement for three different

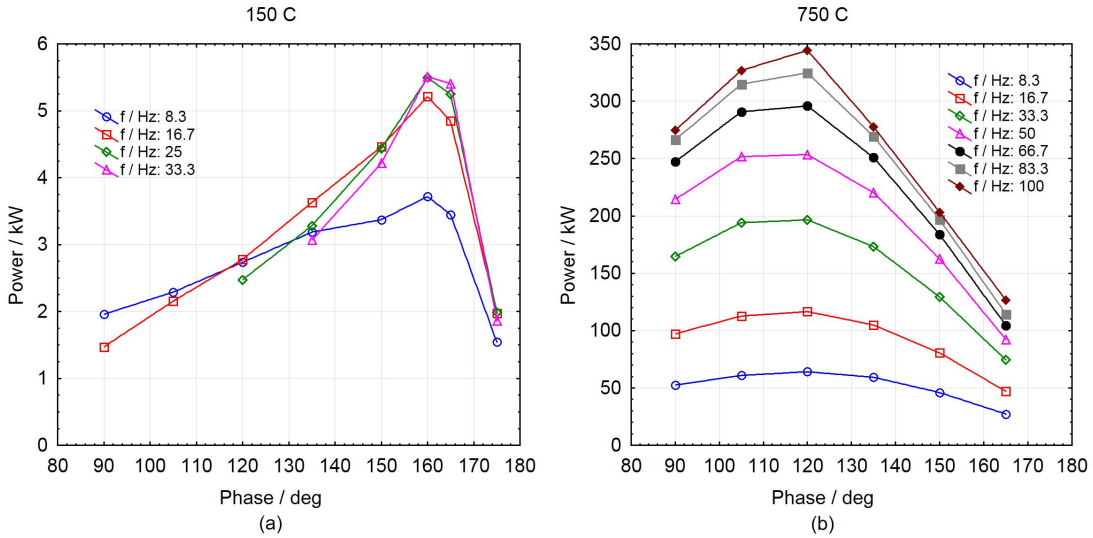

Figure 4.1: Indicated power output versus phase angle for 150 °C (a) and 750 °C (b) heat source temperature at different frequencies. The optimum for the LTD occurs at 16.7 Hz and higher and 160° phase angle; for the HTD at 100 Hz and 120°

cases and shows the resulting volumetric changes; the left piston acts as expansion piston, the right piston as compression piston. A phase angle of 0° would mean that both cylinder gas spaces were either expanding or compressing at the same time with no gas being moved from the hot side of the engine to the cold side. The volumetric change is at its maximum here and so is the pressure amplitude. For a phase angle of 180°, on the other hand, there is no volumetric change at all, as the increase on one side is the decrease on the other side and vice versa. The heat transfer to and from the gas in the latter case is best because the gas velocity is (for a given frequency and heat exchanger geometry) highest, which increases the heat transfer coefficient in the heat exchangers as well as in the regenerator matrix. All the gas from one cylinder is swept completely to the other side and all the gas volume from the two cylinders experiences a temperature change. Unfortunately, a larger phase angle means a smaller volumetric change. Therefore the pressure amplitude is comparatively small as it is solely generated by the temperature change and not by the compression of the gas. The case for 90° phase angle

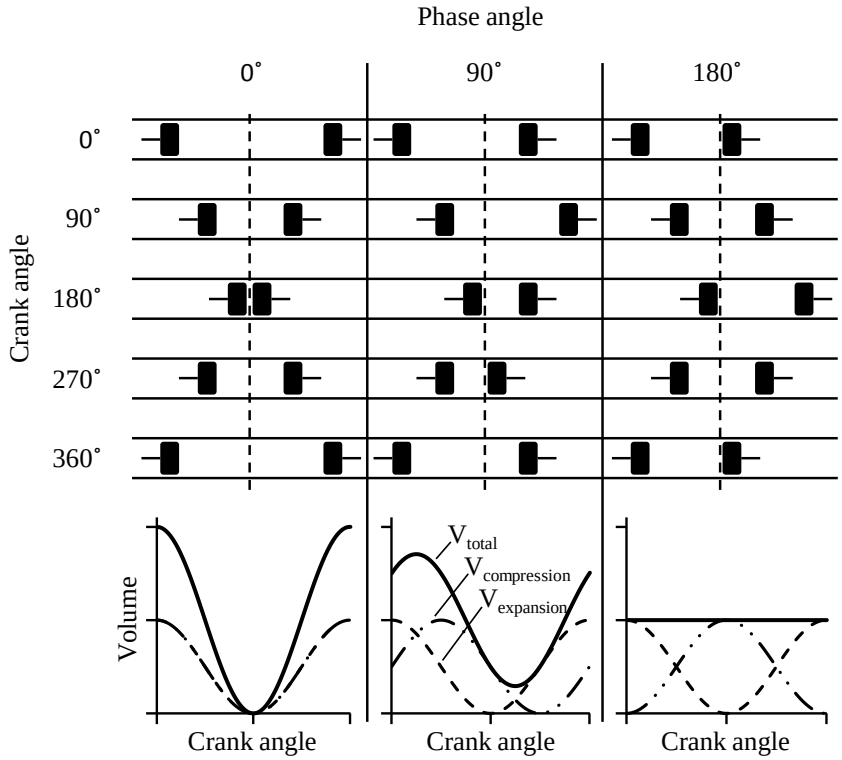

Figure 4.2: Piston movement and volumetric changes in an alpha SE for three different phase angles over one cycle. The left piston acts as expansion piston, the right piston as compression piston. Increasing the phase angle leads to decreasing total volume amplitude and more gas being swept from one side to the other.

is shown in the middle; it represents a compromise between a large volumetric change and a large gas exchange. Iwabuchi et al. showed experimentally that the heat transfer coefficient can be increased by 30 to 50 % if the phase angle is changed from 90 to 180° [141]. An improved heat transfer coefficient can partially offset the negative impact of the low temperature difference in order to achieve a better heat transfer.

It is interesting to note that the optimum phase angle found in Figure 4.1 is independent of the operating frequency and quite different at both ends of the usable temperature scale. At 150 °C the optimum phase angle is strongly pronounced at around 160° whereas at 750 °C the optimum phase angle is in the vicinity of 120°. For the HTD engine this peak is much less pronounced so that

a deviation off the optimum value has a much smaller effect. It is a common misunderstanding that a phase angle of 90° leads to maximum power output, which is only the case if heat transfer and regeneration are assumed to be ideal, as it is done in the isothermal analysis. The fact that most current alpha engines use a phase angle of 90° is mostly due to design reasons (common crank pin in the V-arrangement or square-four arrangement) and not because of the thermodynamic optimum.

Adiabatic compressive heating

Isothermal compression and expansion of the working fluid is a highly idealised assumption, which assumes linear behaviour is the relationship between the pressure-volume product (pV) and the product of mass (m), gas constant (R), and temperature (T).

$$pV = mRT = const \tag{4.6}$$

This is suitable for situations where machines are slow-operating and cycle times are very long, thereby permitting heat transfer between the working fluid and the walls. In historical engines that tended to be physically large and hence slow-moving and used a large temperature difference this assumption might have been a valid approximation and has dominated design considerations in the past. However, it is an unrealistic assumption in situations where low temperature differentials and high frequencies are found.

In the isothermal analysis the optimum phase angle can be found to be 90°, see Section 3.1.1. During compression the temperatures remain at their defined levels, as a result the power needed for compression remains minimal. This is not the case for adiabatic compression as can be seen in Figure 4.3. If the gas is compressed or expanded too fast, heat transfer is significantly reduced - especially in the cylinders - and the processes are closer to being adiabatic. For pure adiabatic

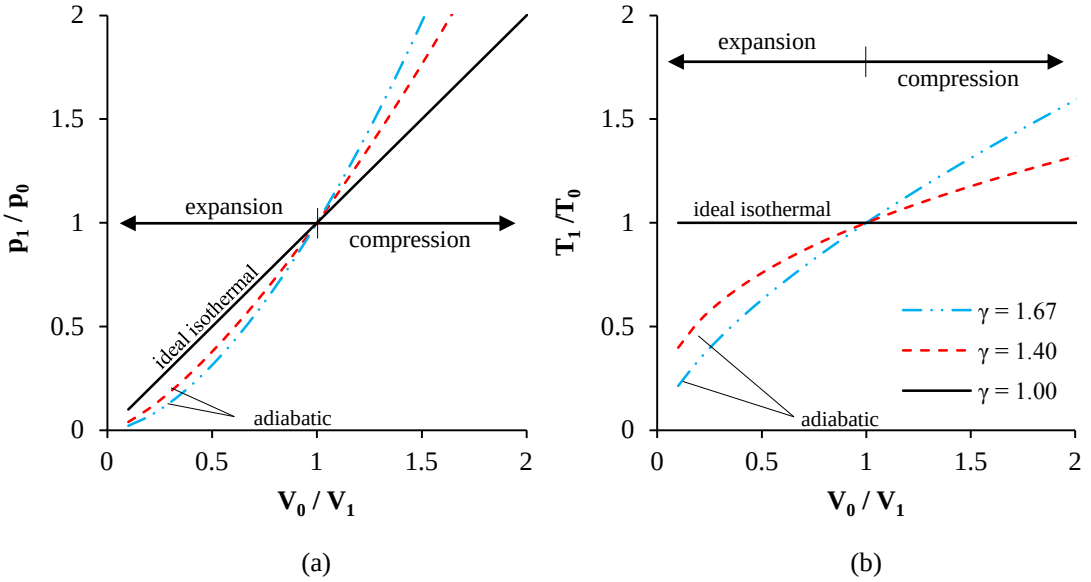

Figure 4.3: Pressure - volume (a) and temperature - volume (b) plots for an ideal gas of different adiabatic indices γ ($\gamma = 1$ isothermal expansion and compression, $\gamma = 1.4$ diatomic gas (e.g. N_2, H_2), $\gamma = 1.67$ monoatomic gas (e.g. He)); the gas is compressed if $V_0/V_1 > 1$ and expanded if $V_0/V_1 < 1$.

compression or expansion from V_0 to V_1 the resulting pressure can be calculated as

$$p_1 = p_0 \left(\frac{V_0}{V_1}\right)^{\gamma} \tag{4.7}$$

and the corresponding temperature of the gas as

$$T_1 = T_0 \left(\frac{V_0}{V_1}\right)^{\gamma-1}. \tag{4.8}$$

as demonstrated in standard thermodynamics textbooks. The higher the adiabatic index γ the more the pressure increases during compression and decreases during expansion, see Figure 4.3 (a). As a consequence the more the adiabatic index differs from the isothermal case ($\gamma = 1$) the more work has to be done during compression and the less can be extracted during expansion. The temperature also rises and decreases more strongly for higher values of γ as can be seen in

Figure 4.3 (b). Too high a temperature after compression reduces heat addition during expansion and makes a larger cooler necessary. Especially at low temperature differences this additional compression work and temperature can become crucial. In alpha-type Stirling engines the compression ratio V_{max}/V_{min} is defined by the swept volume of the cylinders, the phase angle, and the dead volume (gas volume in the heat exchangers, regenerator, and manifolds). Thus the larger the phase angle and the larger the dead volume the smaller the increase in pressure and the smaller the disadvantageous temperature rise during compression.

Figure 4.4 illustrates the influence of adiabatic temperature rise on the fluid temperatures in the expansion and compression space. In Figure 4.4 (a) the temperature profiles for the LTD and the corresponding volume variation is given. For a phase angle of 160° (solid lines), which corresponds to the optimum value, it can be seen that the temperature oscillates with the volume (cooling during expansion, heating during compression) but that the distinctive temperature levels can be kept. If the phase angle is lowered to 90° (dashed lines) with all other parameters unchanged the volume amplitude becomes larger (see also Appendix B). This directly influences the compression ratio of the engine and thus the adiabatic temperature rise of the working fluid. The temperature of the working fluid is now dominated by the compression and expansion of the gas and the two distinct temperature levels have vanished. Such an engine does of course not produce any power output at all. In order to transform a LTD having such a small phase angle to a power producing engine the dead volume in the engine has to be increased in order to reduce the pressure amplitude. The two distinct temperature levels can then be re-established. Figure 4.4 (b) shows why the effects of adiabatic temperature rise are less severe in high temperature differential engines. The HTD shown is equipped with the same heat exchanger set-up as the LTD above (not the optimum configuration for high temperature operation). It can be seen that reducing the phase angle from 160° to 90° has a similar effect on the compression space

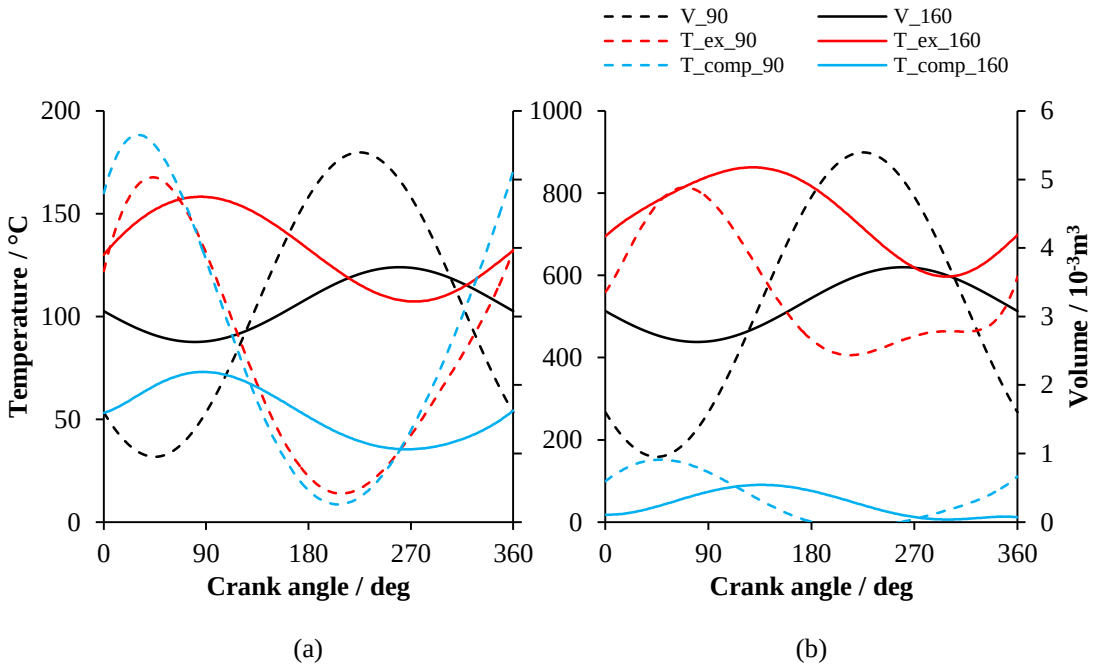

Figure 4.4: Temperatures of the gas in the expansion (T_ex) and compression (T_comp) space for 150 °C (a) and 750 °C (b) heat source temperature; frequency 16.7 Hz. The phase angle is 90° (- - -) and 160° (—). Heat exchangers and regenerator parameters are identical for all set-ups and correspond to the optimum values for the engine with $T_{hot} = 150\,°C$ and $\alpha = 160°$. The volume plots (V_90, V_160) represent the sum of compression and expansion volume.

temperature, i.e. the temperature rises up to 200 °C, but since the temperature in the expansion space is so much higher the temperature distribution in the engine does not vanish. The strong influence of adiabatic effects on low temperature differential operation of a Stirling engine makes the use of a third-order model including these effects very necessary for optimisation of such a system.

Optimum phase angle

The deviation from 90° phase angle found in the isothermal analysis can be explained as follows: for high temperature differences and therefore inherent good heat transfer the optimum phase angle lies in the vicinity of the popular 90°. Adiabatic effects are less pronounced than for low temperature differentials and

relatively large compression ratios are possible and hence relatively large volumetric changes. At low temperature differences the heat transferred to and from the gas under identical flow conditions is much less than at high temperature differences. The higher the compression ratio of the engine (lower phase angle), and thus the temperature increase of the working fluid during compression, the more difficult it is to add and reject heat. In fact a too high compression ratio can easily increase the gas temperature near the temperature of the heat source during compression in the LTD, as shown above. Therefore it is necessary to reduce the compression ratio and increase the convective heat transfer coefficient, heat more gas during expansion, and cool more gas during compression by increasing the phase angle closer to 180°; unfortunately this comes at the expense of volumetric change. In the end the optimum phase angle balances the heat transfer, the pressure amplitude, and the volumetric change. Another means to reduce the pressure amplitude is the introduction of additional dead volume which is explained in greater detail in Section 4.3.6 and Section 4.3.7. The independence of the optimum phase angle from the frequency then also becomes clear; since the frequency does not affect the compression ratio as strongly as the phase angle it also does not affect the location of the optimum phase angle.

4.2.2 Frequency limits

From Figure 4.1 it can be seen that optimum power for the LTD occurs at around 25 Hz whereas for the HTD it lies around 100 Hz. For the HTD the simulation was stopped here because the gain in performance due to increased frequency becomes very small and the focus of this study is on the LTD. The achievable frequency in the case of the LTD is much lower and, as a result, so is the indicated power output. The stronger dependence on frequency for the low temperature situation is explained as follows: At identical flow conditions (f, α) less heat can be transferred to the working fluid as the heat flow in and out of the SE is a function of the heat

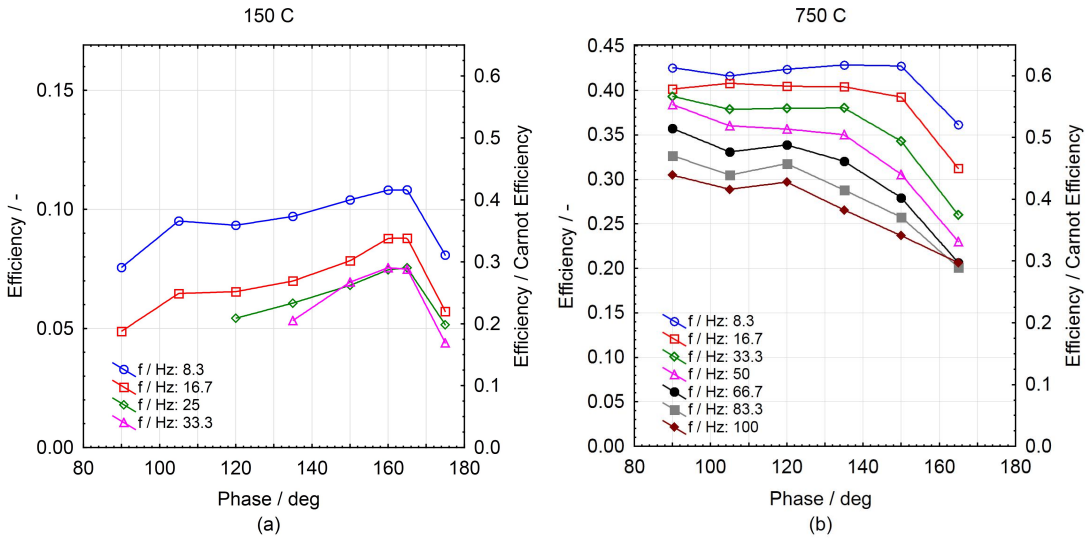

Figure 4.5: Indicated efficiency versus phase angle for 150 °C (a) and 750 °C (b) heat source temperature at different frequencies

transfer coefficient (h, identical for identical flow conditions), the area (A), and the temperature difference:

$$\dot{Q} = h\ \Delta T\ A \tag{4.9}$$

More heat can thus be added by increasing the heat transfer area and/or the frequency (to improve the convective heat transfer coefficient) for a given temperature difference. The latter is limited since as the frequency rises so do the pressure losses in the flow which outweigh the gain in power much sooner in the case of the LTD. In Section 4.3.2 these losses are quantified and illustrated.

4.2.3 Achievable efficiency

The operating frequency also has a very strong influence on the achievable efficiency. In Figure 4.5, it can be seen clearly that the lower the frequency, the higher the efficiency obtained. Reducing the frequency further reduces the efficiency until the engine stalls and the efficiency is zero. As for the power output, the influence of the phase angle on the efficiency is stronger for the LTD than for the HTD;

for the low temperature difference there is a clear efficiency peak located where the maximum power output also occurs. For high temperature differences the influence of the phase angle on efficiency is very low but the influence is increasing with the frequency. Reducing the frequency reduces the temperature difference between the heat exchanger surface and the working fluid which increases the overall temperature amplitude of the working gas. The higher this temperature difference the higher the efficiency. A lower frequency not only reduces the internal pressure losses, as the flow velocity drops. It also makes it possible to use a shorter regenerator of a lower porosity providing a larger thermal mass, which then increases the efficiency, as can be seen in Figure 4.6.

4.2.4 Optimum regenerator design

The efficiency and the regenerator design of a SE are closely linked. A low porosity regenerator increases the efficiency of a Stirling engine as it allows it to store and release more heat internally while having less dead volume. On the other hand a low porosity increases flow losses as it increases blockage of the fluid pathways. Looking at Figure 4.6 and comparing the plots for identical frequencies it can be seen that the optimum porosity for the LTD is much higher than for the HTD as only small flow losses can be tolerated before performance drops. At the optimum phase angle the optimum regenerator length is similar in both temperature scenarios. For phase angles lower than the optimum in the LTD the optimum regenerator length increases rapidly. As explained above smaller phase angles create higher pressure amplitudes for identical heat exchanger set-ups. To avoid the detrimental effect of a high pressure amplitude for the LTD the length of the regenerator and hence the 'dead' volume increases during the optimisation, so that a net power output is conserved.

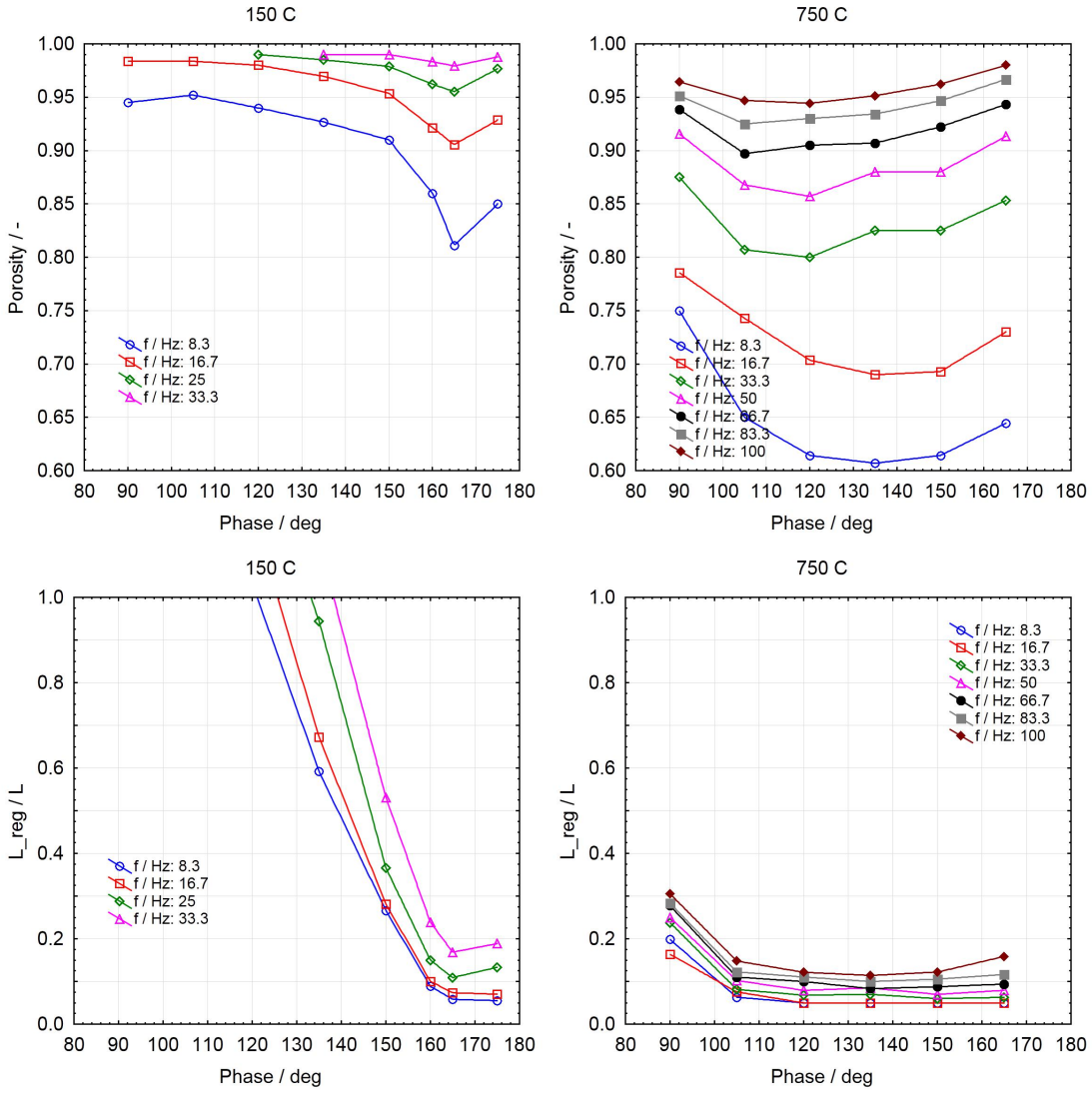

Figure 4.6: Optimised regenerator geometry - optimum porosity and optimum length vs. phase angle for 150 °C and 750 °C heat source temperature at different frequencies

4.2.5 Optimum heat exchanger design

As for the regenerator, the optimum heat exchanger geometry varies strongly for the two engines at both ends of the temperature scale. With the tube diameter fixed to 3 mm, the number of tubes (N_{HX}) and the tube length (L_{tube}) can be varied in order to gain the maximum power. At the low temperature difference the temperature of heat input and rejection are so close together that the characteristics of the working gas are very similar. With the achievable efficiencies being inherently low the amount of heat to be transferred at the hot and cold end is also

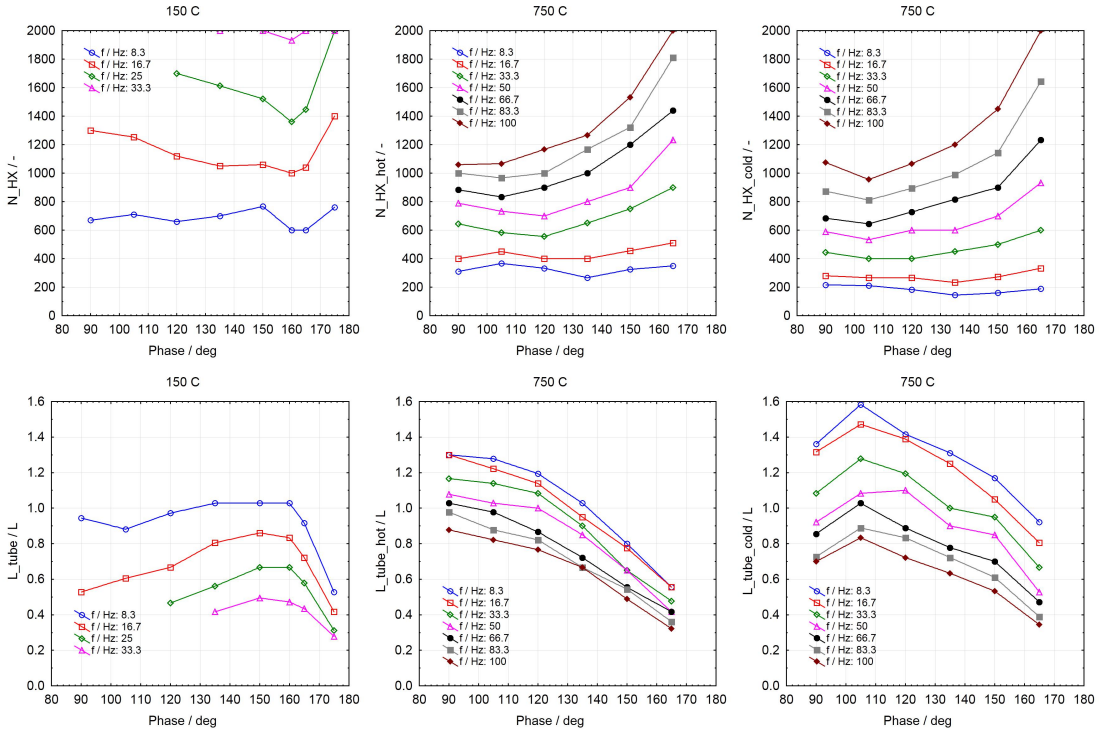

Figure 4.7: Optimised heat exchanger geometry - optimum number of tubes and optimum tube length vs. phase angle for 150 °C and 750 °C heat source temperature at different frequencies. For the LTD the hot and cold heat exchangers are identical, in the case of the HTD they are optimised separately.

of a similar magnitude. As a result a unique design for each of the components does not show an improvement in performance. Also, simulation time can be saved while computing identical heat exchangers on the hot and cold side. More important than simulation time, however, is the fact that identical hardware can be used for heating and cooling which facilitates production and can reduce costs.

High temperature engines usually use different means for heating (for example, combustion gases, solar radiation) and cooling (water, air) so that distinctive physical designs are necessary which then can also accommodate the different temperature regimes. The high thermal efficiency achievable with a high temperature heat source is also reflected in the amount of heat to be transferred so that the heat input can exceed the output by a factor of up to two. Figure 4.7 shows the optimum number of tubes (for maximum power output) and their correspond-

ing length versus the phase angle for different frequencies. It can be seen that, for example, at a frequency of 16.7 Hz the optimum number of tubes for the low temperature engine is significantly higher than the number of tubes in any of the heat exchangers of the high temperature difference engine. At the same time the tube length is significantly shorter. This is a result of the need for a much larger surface area compared to the HTD to get the heat in and out as well as for a low flow resistance. Increasing the frequency makes more and shorter tubes necessary to compensate for the flow losses. At the low frequencies reachable with the LTD (up to 33 Hz) the optimum number of tubes is minimal (or close to the minimum) for the phase angle where the highest power output can be found, for the LTD as well as for the HTD. The optimum tube length on the other hand is at the maximum or close to the maximum. A low number of tubes has the capacity to reduce costs, especially when a high power output can be reached at the same time. Another benefit of a low tube number is the lower pressure loss on the shell side of the heat exchanger (important when using the SE as a bottoming cycle for an ORC); cleaning of the shell side is also largely facilitated which is very important when dealing with heat sources, such as geothermal brine, for which regular maintenance is necessary .

4.2.6 Pressure amplitudes and power development

Observing the pressure amplitudes over one cycle for different phase angles and heat source temperatures (at 16.7 Hz) in Figure 4.8, two factors that strongly influence the power output are discernible. First, the amplitude of the pressure variation is much higher in the case of the HTD. Since the temperature difference is higher and the volume variation is identical, higher pressure amplitudes result according to the ideal gas law. Second, comparing the location of the pressure peaks for the same phase angle at the two different temperatures it can be seen that the peak pressure always occurs later in the case of the HTD. For an identical

volumetric change in the expansion space a maximum pressure which acts closer to the maximum volumetric change produces higher volumetric work ($\delta W = p\,dV$).

Looking at the $p - V$ plots for the expansion and the compression space in Figure 4.8, for the low-temperature case the benefits and the necessity of balancing compression and expansion spaces becomes evident. Even for the case closest to the optimum performance ($\alpha = 165°$) the compression work is much larger than the net work (the area enclosed by p^*_{total}) and close to the magnitude of the expansion work. A force-balancing design reduces the load on the crank arrangement significantly, allowing for lighter parts and smaller bearings. Friction and side loads can thus be reduced significantly and an increased mechanical efficiency makes sure that more of the hard-earned indicated power is transferred to a usable shaft power. Of course, the beneficial effect is not limited to LTDs but here the effect is much more pronounced. Chapter 5 explains force-balancing and the effects on the mechanical efficiency in greater detail.

The maximum allowable cycle pressure is defined by the wall thickness of the pressure vessel and the quality of the seals. If one engine set-up is to be compared under different working conditions, it is this maximum pressure that should be kept constant. Doing so would increase the power output for the LTD substantially since the mean pressure would rise by approximately 60 % and the power output by 40 % to about 7.2 kW (at 16.7 Hz); with this correction the HTD then produces about 16 times the indicated power of the LTD from an identical swept volume. Unfortunately the maximum pressure is not easily implemented into the Sage simulations which is why it has not been incorporated into this study in which it is the mean cyclic pressure (p_{mean}) that is held constant. In the case of the LTD the pressure ratio has a strong effect on the engine performance. It can be seen that the maximum pressure remains relatively constant for the different phase angles before it finally drops (due to the lack in compression for the largest phase angle plotted). The effect of the pressure ratio on LTD performance is

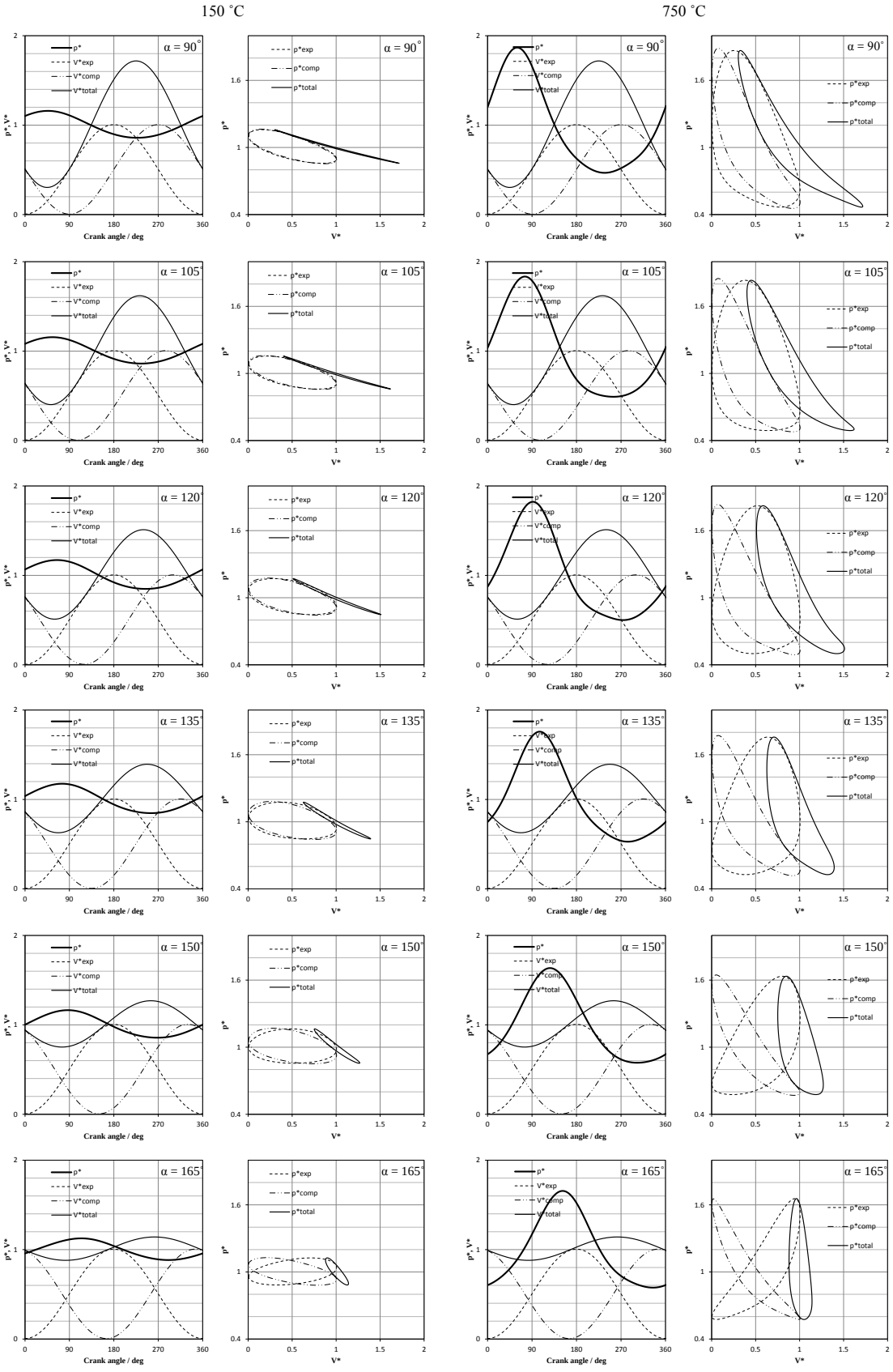

Figure 4.8: Pressure and volume variations for different phase angles and temperatures at 16.7 Hz. The position of the pressure peak relative to the volume variation and its amplitude is clearly visible.

discussed below in greater detail (see Section 4.3.6). However, since the optimum pressure amplitudes are very similar for the LTD, and thus the maximum pressure, optimisation of the phase angle gives viable and comparable results.

This section has identified specific design parameters and shown how they affect engine performance at low-temperature differences. The inclusion of fluid-dynamic and thermodynamic imperfections and inefficiencies permits more realistic design implications to be identified than the conventional practice of isothermal modelling. Importantly, the influence of the frequency on performance has been presented - a parameter dependence which is not included in more basic models.

4.3 Sensitivity analysis of a LTD alpha engine

In the previous section optimum operating and heat exchanger parameters were identified which were obtained from a third-order model described in detail. Now the effects of a deviation from these optimum parameters are presented and implications on LTD design are discussed. In the following the influence of variations of the operating parameters as well as of variations of the geometry of the heat transferring components on power output and efficiency will be shown.

As base cases for this investigation the optimized designs from the preceding analysis at 16.7 Hz (1000 rpm) are used. Two engines are compared, one operating at a high heat source temperature (HTD) and the other operating at a low heat source temperature (LTD). The identical frequency is chosen to represent two engines with identical piston speed and therefore an identical mechanical efficiency, so that indicated performance and brake performance of the two engines have the same ratio. Furthermore, this relatively moderate operating frequency is found in some stationary HTDs for mechanical reasons [155, 172]. Large reciprocating gas compressors having similar working conditions (oil-free operation, dry gas, high pressure) also do not exceed frequencies above 1000 rpm and piston speeds of

Table 4.2: Optimum design parameters for maximum indicated power of the low and high temperature engine at a frequency of 16.7 Hz

parameter	LTD	HTD
phase angle / °	160	120
hot heat exchanger:		
number of tubes / -	1000	400
tube length / L	0.83	1.14
cold heat exchanger:		
number of tubes / -	1000	270
tube length / L	0.83	1.39
regenerator:		
porosity / -	0.92	0.70
length / L	0.1	0.05
power / kW	5.2	116.6
efficiency / -	0.088	0.405

$5\,\mathrm{m\,s^{-1}}$ [173]. For the LTD the phase angle of 160° is chosen and 120° is chosen for the HTD which are the phase angles that allowed maximum performance in the corresponding engine. The optimum parameters from the previous study are summarised in Table 4.2. The simulation model is the same that has been used for the preceding study where it is described in detail.

To facilitate readability and comparability of the plots, power (W) and efficiency (E) are normalised by the corresponding values form the optimised configuration:

$$W^*_{150} = \frac{W}{5.2\,\mathrm{kW}} \tag{4.10}$$

$$E^*_{150} = \frac{E}{0.088} \tag{4.11}$$

$$W^*_{750} = \frac{W}{116.6\,\mathrm{kW}} \tag{4.12}$$

$$E^*_{750} = \frac{E}{0.405} \tag{4.13}$$

The dimensions of the heat exchangers and the regenerator are normalised by the characteristic length (L), the bore of the cylinder. No further optimisation for the heat exchangers and the regenerator is carried out in this study, so the only

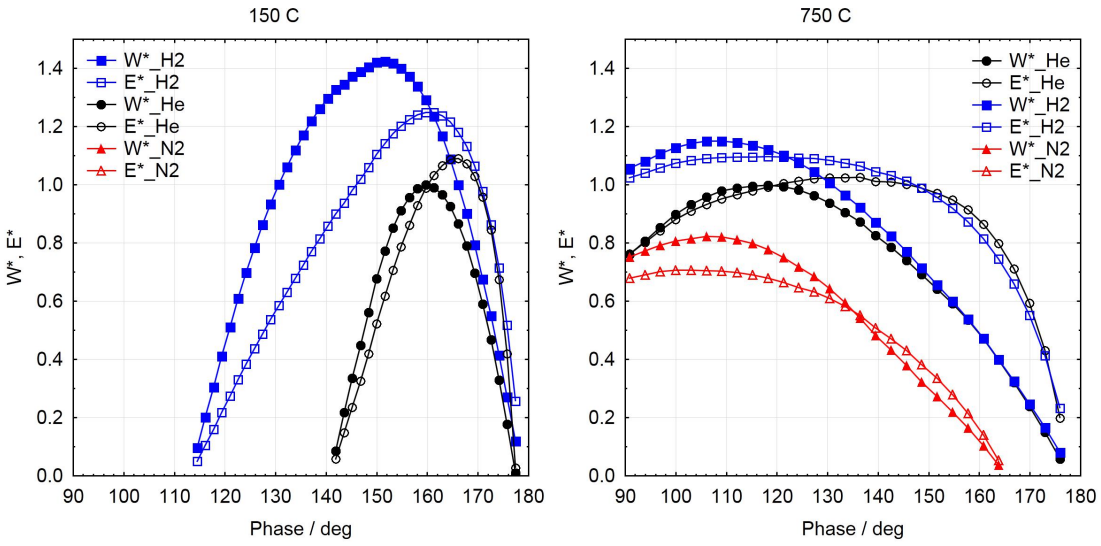

Figure 4.9: Power and efficiency versus phase angle at 16.7 Hz for different working fluids and heat source temperatures. The LTD is very sensitive to the phase angle. Hydrogen or nitrogen instead of helium reduces the optimum phase angle.

parameter changed from the optimum configuration are the ones mentioned in the corresponding plot.

4.3.1 Variation of the phase angle

In alpha-type engines the phase angle is a crucial design parameter which is, in the Siemens configuration (double-acting, interconnected multi-cylinder engines with one expansion and one compression space on opposite sides of a piston), directly coupled to the number of cylinders. Figure 3.22 illustrates this correlation. Here, the phase angle cannot be adjusted in the physical design and therefore has to be optimised during the design stage.

The LTD in Figure 4.9 is thermodynamically optimised for a phase angle of 160° using helium as the working fluid. Changing the phase angle to 150° which corresponds to a change from 18 to 12 interconnected cylinders in the Siemens arrangement results in a reduction of 30 % in power output per cylinder and 46 % drop in efficiency. This effect is less pronounced (14 % power and 11 % efficiency) if

the heat exchangers and the regenerator are adjusted to the changed phase angle, see Figure 4.1 and Figure 4.5. It is therefore important to redesign the heat transferring parts if, during the design process, the phase angle (or the number of cylinders) is changed. However, from a thermodynamic perspective it is not advisable to change the phase angle from its optimum point since the range of operation is very small - whether or not heat exchangers are optimised - due to the very steep slope of the performance curves. Especially at high phase angles in the vicinity of 160° the phase angle can be adjusted by increments between 1 and 2°, by addition or removal of a cylinder (and an adjusted drive mechanism in the case of a kinematic engine). This allows for a tuning of the engine in the desired range without compromising the phase angle if the large number of cylinders is allowable.

If hydrogen is used instead of helium, it can be seen that the optimum phase angle shifts to a smaller value of around 150° and that the range of operation is enlarged. This is a direct result of the different adiabatic index discussed in Section 4.2.1. The monoatomic gas helium has an adiabatic index γ of around 1.7 whereas the diatomic hydrogen has an adiabatic index of around 1.4 (see also Appendix C for fluid properties) which is also the case for nitrogen. As stated above the lower the adiabatic index the smaller the increase in temperature and pressure during compression and hence smaller phase angles (or compression ratios) are possible which provide a higher effective swept volume. The power output for hydrogen rises by 42 % and the efficiency by 14 % when the phase angle is changed. The necessary number of cylinders is reduced from 18 to 12; even an 8 cylinder engine (not optimised) would provide the same power output as the 18 cylinder helium-charged engine (power per cylinder). If the phase angle remains unchanged the power output still increases by 30 % and the efficiency by 25 %. Nitrogen as the working fluid does not produce a positive power output with the given heat exchanger configuration. In Section 3.3.1 it was shown that if the

heat exchangers are optimised for a specific working fluid then the performance can be increased even further using hydrogen and using nitrogen would result in a positive power output, too. Since the choice of working gas largely influences the heat exchanger design and the optimum phase angle which corresponds to the number of pistons, it is an important parameter in the overall engine design. If an engine thermodynamically designed for helium is run with hydrogen instead it will perform better but not as well as if it were designed specifically for hydrogen. If an engine is designed for hydrogen ($\alpha = 150°$) and runs with helium instead the result will be disappointing. Before deciding on a specific phase angle it is therefore important to make a decision on the working gas considering all the implications it has on the engine design (e.g. volatility, safety, availability, and costs) and then stay with it.

For the HTD the introduction of hydrogen makes a noticeable difference too but the effect is not as strong as for the LTD. On the other hand, nitrogen also produces a noticeable power output which is, of course, much lower. The phase shift of the optimum performance towards a lower phase angle can also be observed for hydrogen as well as for nitrogen. Generally the plots are much flatter indicating a much less pronounced sensitivity to the phase angle.

4.3.2 Variation of the frequency

A change of the operating frequency has a strong effect on the efficiency, especially for the LTD where the efficiency can be increased by up to 50 % by reducing the frequency (10 % for the HTD), which happens at the expense of power output as can be seen in Figure 4.10. Decreasing the frequency also decreases the temperature difference between the heat exchanger walls and the working gas which then increases the overall temperature difference in the engine and thus the efficiency. This increase in efficiency is much more pronounced for the LTD as even

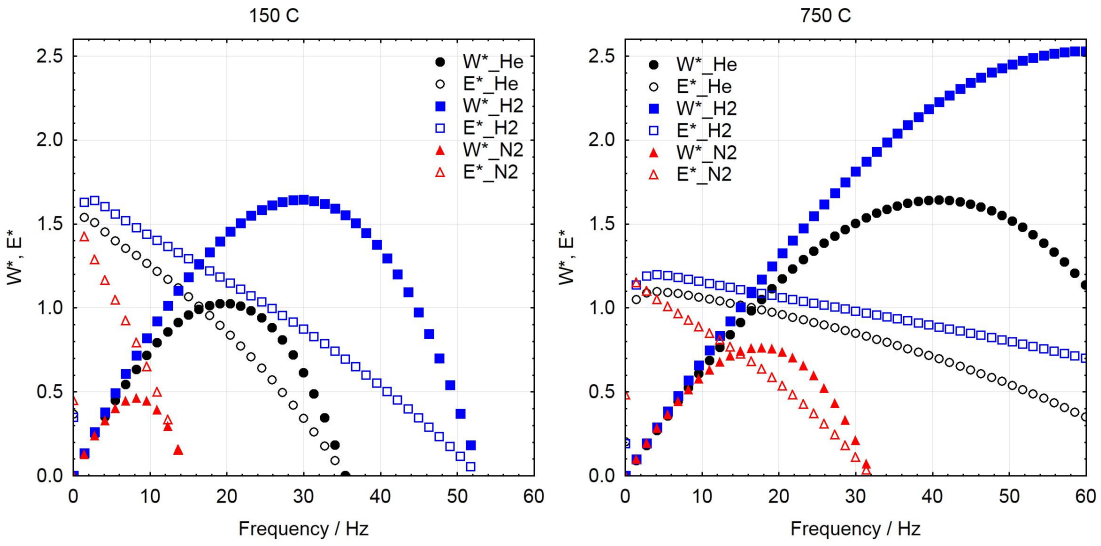

Figure 4.10: Normalised power and efficiency versus frequency for different working fluids and heat source temperatures. Hydrogen allows for much higher frequencies, nitrogen only for much lower frequencies. Higher frequencies reduce the efficiency due to the reduced internal temperature difference.

a small change in temperature is a relatively big fraction of the total temperature difference.

A lower frequency reduces the internal losses due to fluid friction in the engine and thus increases the efficiency. Figure 4.11 shows the pumping losses due to fluid friction for the two temperature regimes. The pumping losses are given for the different heat exchanger components (HXs and regenerator). It can be seen that total losses rise much faster for the LTD since fluid density and hence pumping losses are generally higher. In both cases the losses are approximately 40 % of the power at maximum power output but the frequency is doubled for the HTD. Due to the lower density of the working fluid the pressure losses in the hot heat exchangers are the smallest. With the heat exchangers being identical in the LTD the pressure loss for the cold heat exchanger is very similar, only slightly higher. The different geometries in the HTD make a direct comparison difficult here but the tendency is identical. According to the optimised geometry of the regenerator (see below) its share on the total losses differs.

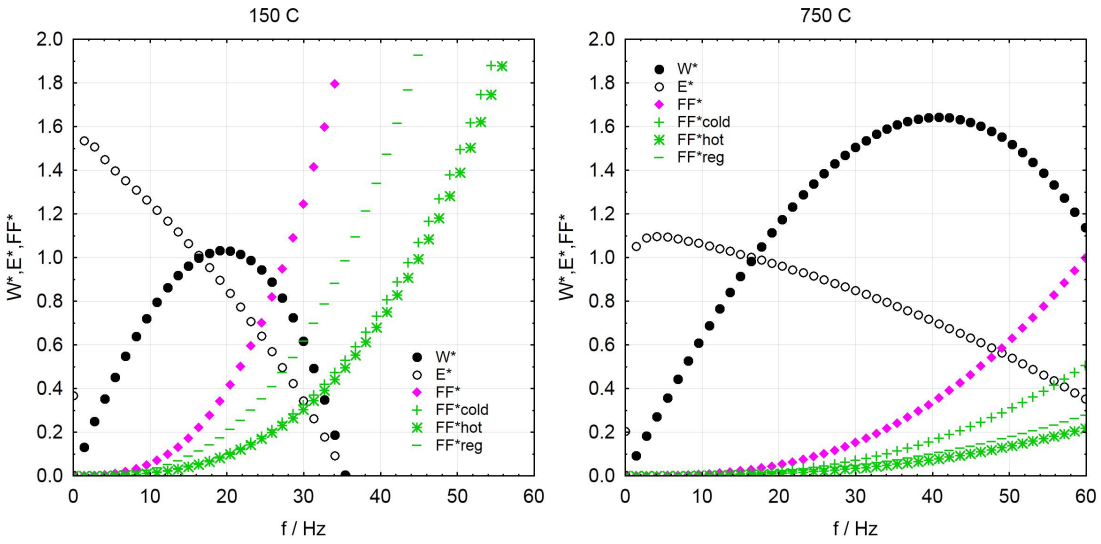

Figure 4.11: Power loss due to fluid friction (pumping losses) (FF) for the optimised LTD and HTD engines. Relative to the indicated power the losses rise faster with the frequency in the LTD.

Generally the frequency range in which the LTD can operate is smaller than for the HTD because of the relatively large pumping losses compared to the power output. This makes the LTD more suited for steady-state operation at a moderate frequency.

According to Equation 2.26 the pumping losses are proportional to the density (ρ) and the flow velocity (u) and thus also the frequency:

$$\Delta p \propto \rho u^2 \tag{4.14}$$

If the frequency is cut in half, nitrogen or air which have a much higher density (see Appendix C) can be used as the working fluid in the LTD as well, as can be seen in Figure 4.10. Specially designed heat exchangers and a regenerator can then increase the normalised power output to over 50 % for nitrogen or up to 200 % for hydrogen (see Section 3.3.1).

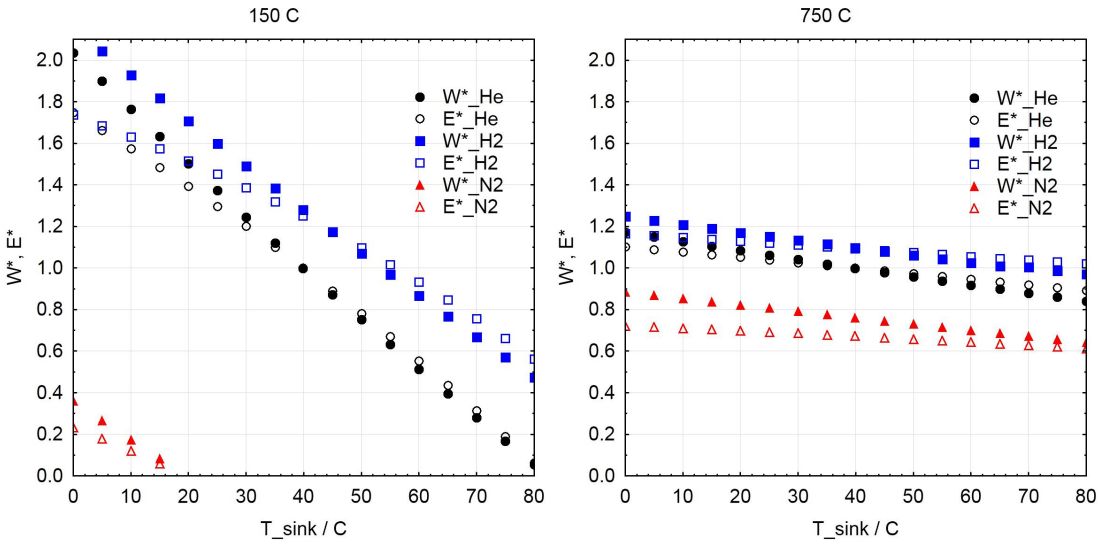

Figure 4.12: Normalised power and efficiency versus heat sink temperature for different working fluids and temperatures at 16.7 Hz. The LTD shows to be extremely sensitive to the sink temperature.

4.3.3 Variation of the heat sink and source temperature

Reducing the frequency increases the efficiency due to the increased internal temperature difference, as was shown above. This observation can be explained by the definition of the Carnot efficiency (η_{Carnot}) the theoretical limit for every heat engine which relates the heat sink (T_{sink}) and source temperature (T_{source}) to the efficiency:

$$\eta_{Carnot} = 1 - \frac{T_{sink}}{T_{source}} = \frac{T_{source} - T_{sink}}{T_{source}} \qquad \text{(4.1 repeated)}$$

The same principle explains the influence of a change in the heat source or sink temperature. From Equation 4.1 it can be seen that a change in the temperature difference between heat source and sink has a stronger effect on efficiency when the heat source temperature is smaller, as is the case for the LTD. Figure 4.12 shows the influence of a change in the surface temperature of the cold heat exchanger on engine performance. The difference between heat rejection to the ambient on a cold winter day (0 °C) to the reference hot summer day (40 °C) is 100 % in terms of power. For the HTD this change is much less pronounced with only 20 %

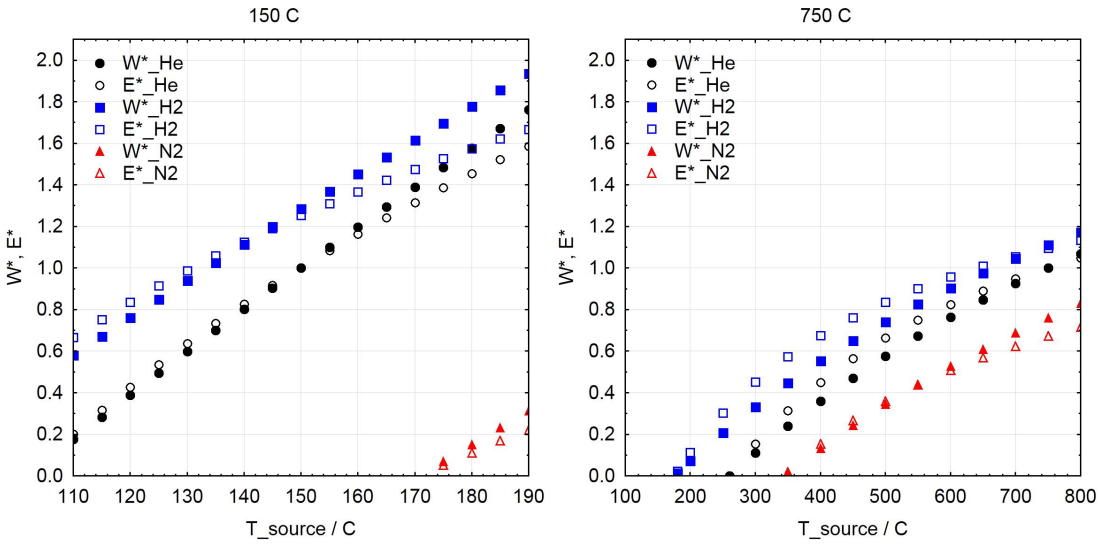

Figure 4.13: Normalised power and efficiency versus heat source temperature for different working fluids at 16.7 Hz, note the different temperature scales for LTD and HTD. Small changes show a large influence in the LTD.

increase. As is the case for power, the efficiency changes are smaller but still very large. Additionally, a relatively small temperature change of 5 K at the cold heat exchanger wall changes both power and efficiency by more than 10 % for the LTD and only around 1.5 % for the HTD. An effective and efficient cooling system is therefore mandatory, especially for the LTD.

Figure 4.13 shows the effect of a variation in the heat source temperature. From Equation 4.1 it can be seen that the effect has to be smaller than the effect of the sink temperature. However, for the LTD small changes in the heat source temperature do have a strong effect on performance. Good care should be taken to ensure that none of the exergy of the heat source is wasted during the transport of the heat carrier. For the HTD it can be seen that the effect is less pronounced. If an engine optimised for operation at 750 °C operates at reduced heat source temperature the range of operation (positive power output) ends significantly before the 150 °C heat source temperature of the LTD. Using a HTD design and converting it to a LTD simply by reducing the heat source temperature does not

result in an operational LTD design, not even at this relatively low frequency. Further measures such as adjusted heat exchangers and a corrected phase angle are necessary for a feasible design. Converting a LTD to a HTD by increasing the temperature, on the other hand, would result in a functional engine, although of mediocre performance.

Adding fins on the outside of the heat exchanger tubes of a LTD should be considered as it allows the surface temperature of the hot and cold tubes to match the temperature of the heat carrier more closely and therefore improve the performance for a given heat source and sink. Refer to Section 6.1 for further discussion of the heat exchanger design.

4.3.4 Variation of the mean gas pressure

Increasing the mean pressure increases the gas mass in the cycle and, up to a certain point, the power output of the engine but at the expense of efficiency, as shown in Figure 4.14. With increasing gas pressure the density of the working fluid rises and so do the pumping losses in the engine (power needed to move the working fluid within the engine), as they are directly proportional to the density and the square of the fluid velocity which does not change at a constant frequency [22]. Adjusting the heat exchangers and the regenerator can even extend the pressure range, but higher pressures do challenge not only the pressure vessels and joints between adjacent components mechanically but also seals to the ambient and therefore working fluid containment.

For the LTD the density of the working fluid is always higher than for the HTD at identical mean pressure (see also fluid properties in Appendix C). This fact also increases the inevitable and crucial pressure losses in the LTD. It is therefore also more sensitive to an increase of the mean pressure and the pressure cannot be increased as high as for the HTD without modification of the gas circuit.

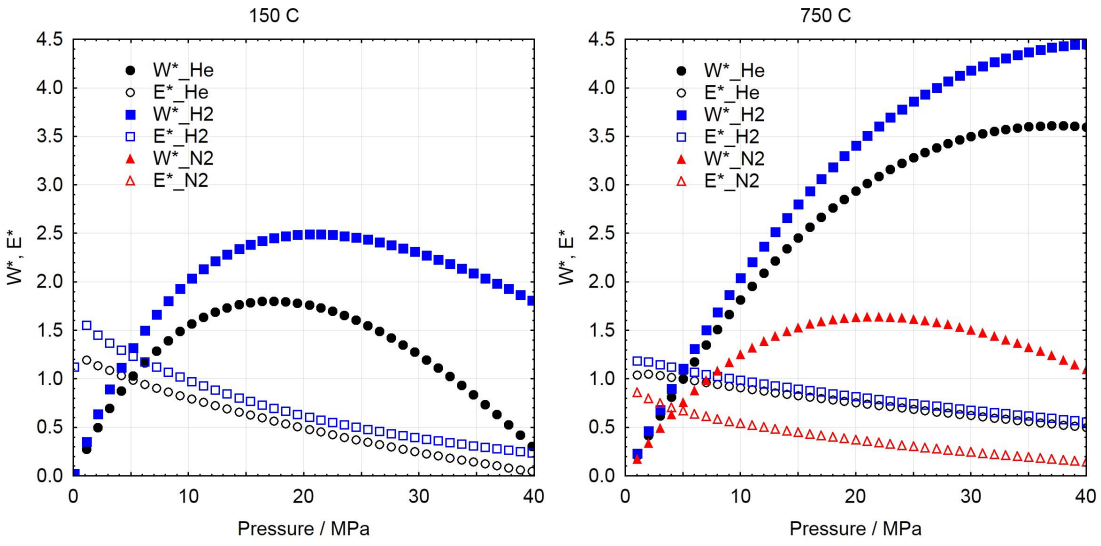

Figure 4.14: Power and efficiency versus mean pressure at 16.7 Hz for different working fluids. Increasing the pressure increases the power output to the point where the increased density of the gas and thus the pumping losses reduce the power output.

4.3.5 Heat exchanger and regenerator design

The heat exchangers are the most cost-intensive component in Stirling engines. This is especially true in LTDs, where a large surface area is needed to transfer heat in and out of the engine which translates directly into a larger number of tubes compared to the HTD. Together with the design of the regenerator, heat exchanger design influences engine costs and performance strongly. Looking at the engine's sensitivity to changes of the geometry in the heat transferring components allows cost reduction opportunities to be identified without compromising too much on the performance side.

Sensitivity of the regenerator

The most widely used regenerator design is the random fibre type. Other designs such as wire screens or the rolled or stacked foil type have been studied (see Section 1.2.7), with the latter not commonly found in existing engines. This study

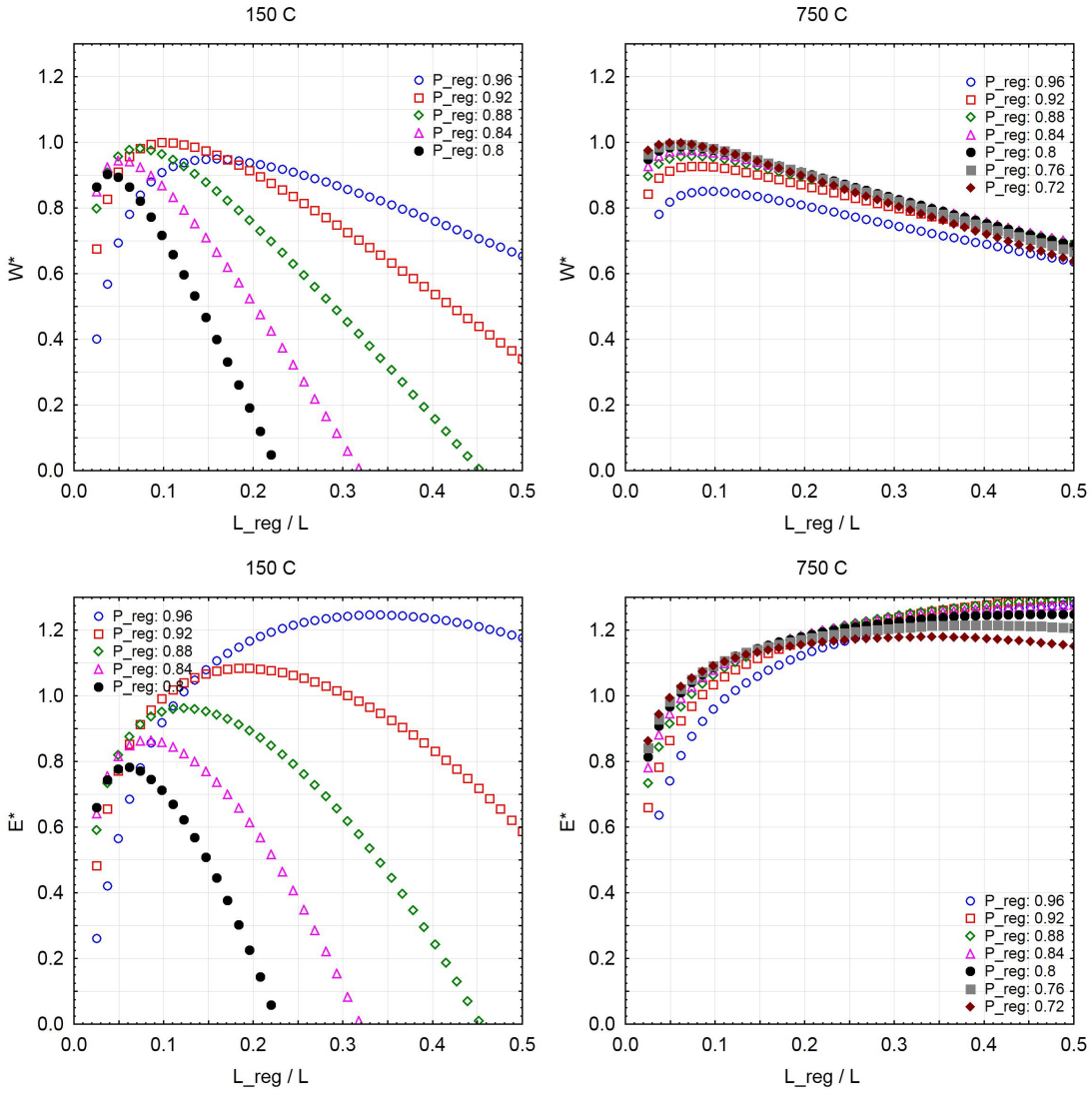

Figure 4.15: Influence of regenerator parameters porosity (P_{reg}) and matrix length (L_{reg}) on power and efficiency. It can be seen clearly that for the LTD the porosity of the regenerator is a very critical parameter much more than for the HTD.

thus focuses on the first type. With the regenerator diameter fixed to the diameter of the cylinders and the wire diameter fixed to 0.05 mm, only the porosity and the length of the regenerator can be modified in order to optimise performance or to satisfy geometrical design constraints.

Figure 4.15 shows the influence of the regenerator porosity (P_{reg}) and the regenerator length (L_{reg}) on power output as well as on efficiency. The parameters can quickly be identified as being much more sensitive in the LTD than in the HTD. For each porosity shown there is a relatively small range for the regenerator

length where the engine shows its highest power output. If the length is adjusted a small change in porosity can be tolerated without reducing the power significantly. The greater the amount of wire material installed in the regenerator (i.e. the lower the porosity) the shorter the regenerator has to be to function properly. Longer and more porous regenerators show the ability to increase the efficiency significantly and are less sensitive to changes in the length.

For the HTD the performance is much less dependent on the regenerator length as the optimum power occurs at very similar lengths relatively unaffected by the porosity. Also a change in porosity has a much smaller influence on performance in general.

Sensitivity of the heat exchangers

Shell and tube heat exchangers are used for many industrial applications of a wide variety of scales, from palm-sized laboratory devices to gigawatt-sized evaporators for power plants. A broad base of knowledge for manufacturing and operation is available as it is a very mature technology. Low pressure losses and a large surface area make shell and tube heat exchangers a favourable choice for LTDs. Specific heat sources such as geothermal brine make regular cleaning intervals necessary and, if shell and tube side are designed to be demountable, even mechanical cleaning in addition to chemical cleaning is possible.

A reduction of the number of tubes as well as of the tube length compared to the optimum configuration shown in Table 4.2 shows the ability to reduce materials and manufacturing costs. In doing this the change of performance has to be monitored and cost savings and thermodynamic performance have to be balanced. An economic analysis of this trade-off is out of the scope of this thesis but the sensitivity of the Stirling engine to changes of the geometry (i.e. the number of tubes and their length) is shown here.

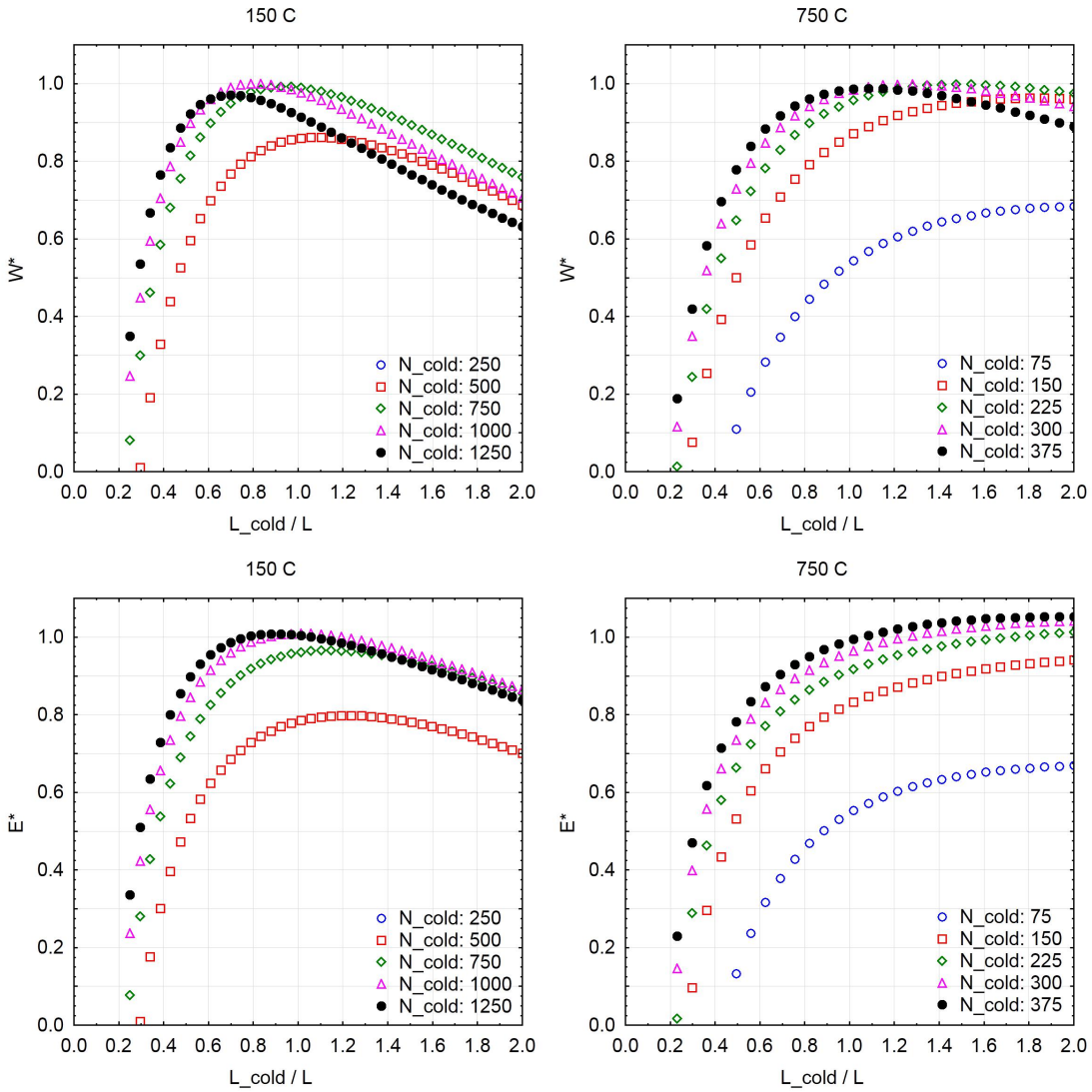

Figure 4.16: Influence of cold heat exchanger parameters number of tubes (N_{cold}) and tube length (L_{cold}) on power and efficiency, for a tube diameter of 3 mm. The LTD shows to be more sensitive to both parameters than the HTD but a relatively large deviation from the optimum is still allowable without compromising the performance too much.

Figure 4.16 shows the influence of a variation of tube number and tube length for the cold heat exchanger alone while the hot heat exchanger remains unaltered (also in the case of the LTD). The tube diameter is held constant at 3 mm as for the rest of this study. The number of tubes is changed in steps of 25 % of its optimum value. Increasing or decreasing the thermodynamically-optimal (highest power density) number of tubes ($N_{cold} = 1000$) of the LTD by 25 % has only a very small effect on the power output especially when the tube length is adjusted. In this case the efficiency drops by less than 5 %. A further reduction to only 50 % of the tubes shows to have a much stronger impact on the performance; more than 15 % power and 20 % efficiency are lost. A simulation with 250 tubes in the cold heat exchanger shows no positive power output at all.

Again, the HTD can be seen to be less sensitive to changes in the heat exchanger geometry. At 50 % tube number and adjusted heat exchanger length the power drops only by a few percent and the efficiency by less than 10 %. Even a reduction to 25 % of the tubes allows for a performance of around 70 % of the optimum value.

In contrast to the regenerator (for which a variation in the geometry has a strong influence on both power and efficiency, and efficiency can be increased at the expense of power), geometry variation of the heat exchangers does not have the ability to improve the efficiency any further.

For the optimum configuration of the heat exchangers in the LTD, identical geometries for the hot and cold tube bundle were used. Observing the optimum parameter configuration for the cold heat exchanger found in Figure 4.16 and comparing it to the values shown in Table 4.2 it can be seen that the optima for both cases are very close, so that an identical design is justified.

4.3.6 Influence of additional dead volume

So-called dead volume has always been perceived as the greatest enemy of Stirling engine performance, be it the volume in the heat exchangers, the regenerator, cylinder clearances or connecting ducts, and thus aspiring Stirling engine designers typically try to minimise it. It is suggested here that this is not necessarily appropriate, and a misconception generated by an over-reliance on the isothermal analysis. In fact most of these 'dead' volumes are very active as in the heat exchangers and the regenerator and may have a beneficial influence on the cyclic pressure variation in the heat exchangers and, thus, on the transferred heat.

Figure 4.17 shows the influence of the introduction of an additional dead volume located between the cold heat exchanger and the compression piston. In the Sage model it is included as a tubular heat exchanger component with a single tube of diameter D_{dead} and length L_{dead}. For the power output it can be seen, as expected, that every addition of 'real' dead volume diminishes the power output. For the LTD a certain diameter of the tube must be secured in order to generate a positive power output. From the plot it can be seen that a diameter of 0.25 L reduces the power output by 50 % and that a tube diameter of 0.125 L results in no positive power output at all. Small diameter ducts have a less severe effect on the HTD as can be seen on the right hand side. Here, even relatively small diameters allow for a positive power output close to the optimum value. For the design of an actual engine this implies that the diameter of connecting ducts has to be larger for the LTD than for the HTD and carefully designed or, even better, avoided as it can increase the crucial pumping losses. The efficiency can be increased by more than ten percent by the introduction of extra dead volume. This is an interesting effect, that should be explored further but which is beyond the scope of this thesis.

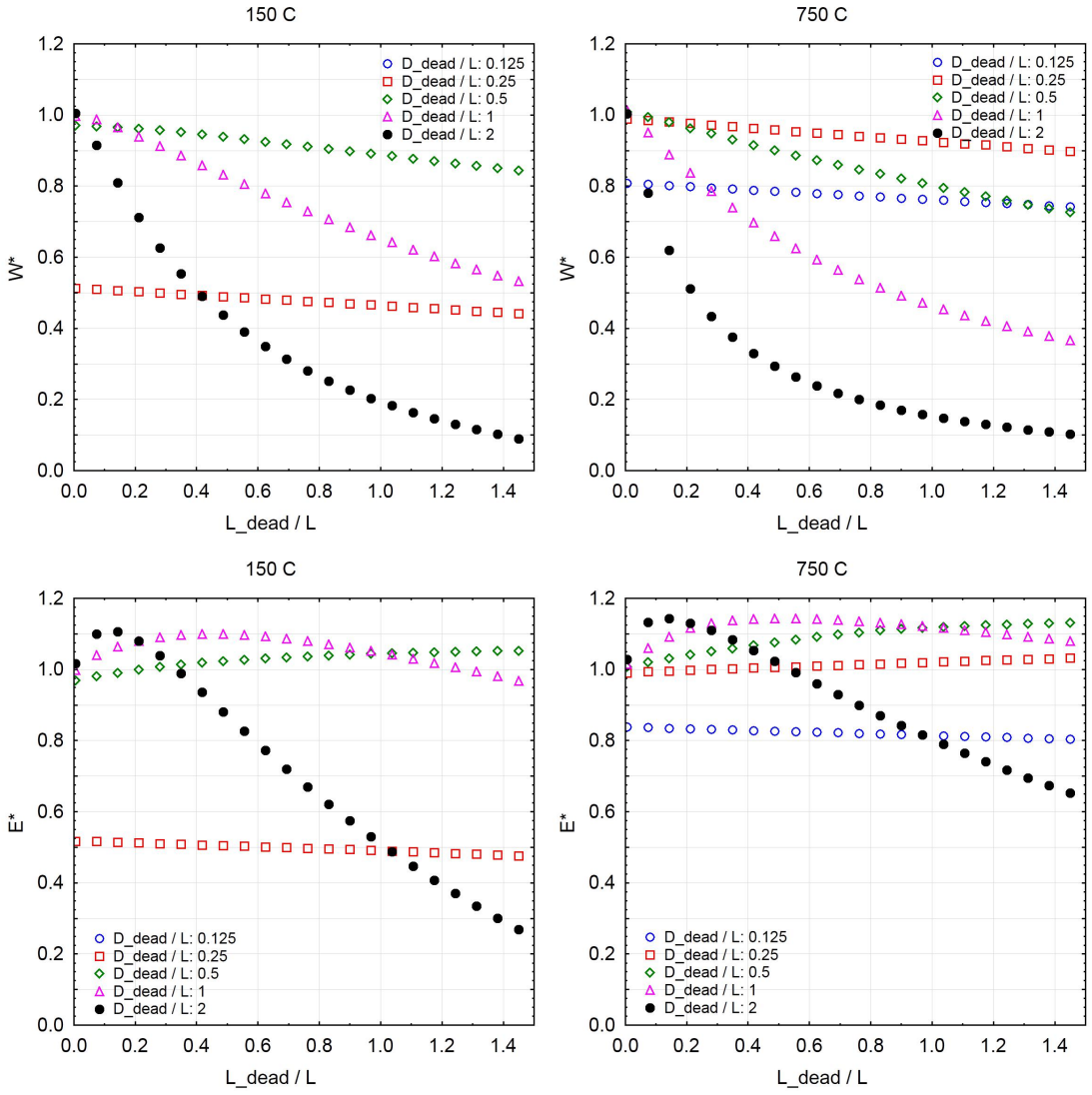

Figure 4.17: Influence of the geometry of a tubular dead volume introduced between the compression space and the cold heat exchanger on power and efficiency. Power output is always diminished, efficiency can rise depending on the geometry.

4.3.7 Optimised pressure amplitudes by introduction of additional dead volume

If, in an engine with a fixed heat exchanger and regenerator geometry, the phase angle is lowered from 180 to 90° the volume amplitude is increased and so is the pressure amplitude (see Figure 4.2). Looking at Figure 4.8 it can be observed that the pressure amplitude for the optimised LTD remains virtually identical for each of the phase angles shown. A large pressure amplitude in a low temperature engine leads to high gas temperatures during compression because compression in the cylinders is nearly adiabatic. If the gas temperature is too high before expansion almost no heat can be added during expansion. The power needed for compression then also exceeds the expansion power multiple times. During optimisation for the different phase angles as shown above it is mainly the regenerator which influences the pressure amplitude. Figure 4.6 shows a large increase in regenerator length and porosity and thus void volume for the LTD if the phase angle is lowered below its optimum value. So the regenerator acts as an artificial dead volume. It becomes a compromise between adapted pressure amplitude and good regenerator performance. Therefore the introduction of an additional dead volume is thought to be beneficial for non-optimum phase angles in order to reduce the pressure amplitude and allow for an optimised regenerator.

Figure 4.18 shows the effect of the introduction of an additional dead volume of diameter L (large diameter to avoid pumping losses) and length (L_{dead}) on power output and efficiency. As a reference the plots for optimised heat exchanger geometries from Figure 4.1 (a) and Figure 4.5 (a) with no additional dead volume are shown (optimised HX, no dv). The geometry of the heat exchangers and the regenerator is the optimum found for a phase angle of 160° and is not changed here (for the L_{dead} plots). In fact changing or optimising these parameters for different phase angles and dead volume length does not show a significant improvement. At 160°, where the pressure amplitude is already optimised due to the larger un-

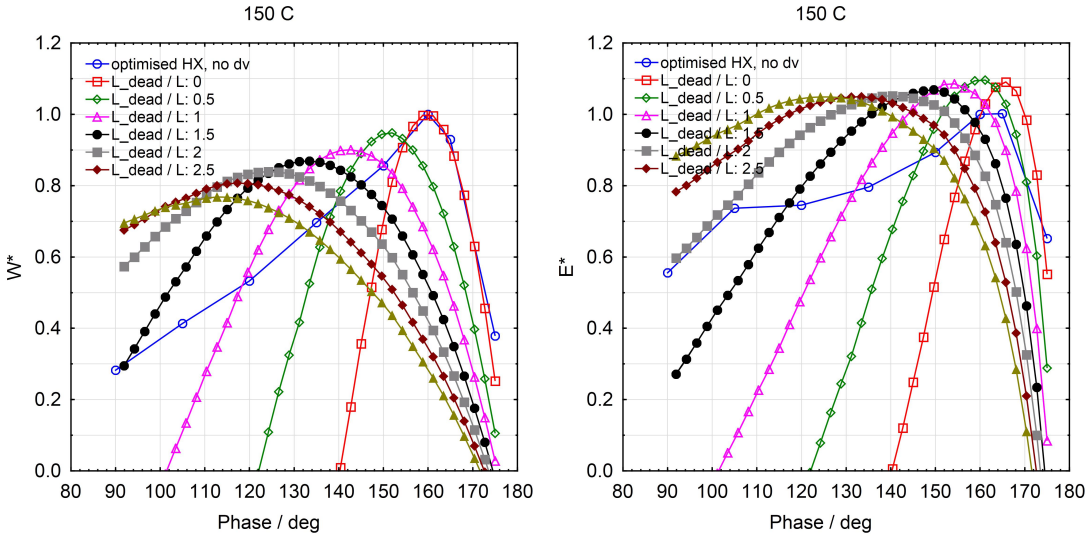

Figure 4.18: Power output and efficiency versus phase angle for different additional dead volumes. For comparison the optimised values for no dead volume are plotted. The addition of dead volume reduces the pressure amplitude and hence the power needed for compression as cooling is more effective

compressed volume in the cylinders, any additional dead volume cannot improve the performance. At lower phase angles, however, a significant improvement compared to the optimisation without extra dead volume (optimised HX, no dv) can be observed.

In real engines no dead volume is only possible in an opposed piston engine where the heat exchangers are mounted in-line between the facing cylinders (see Figure 1.3). A double-acting engine design makes connecting ducts and manifolds necessary in order to connect the heat exchangers with the cylinder spaces. This fact directly relates to the selection of the optimum phase angle. If for example a manifold equivalent to a dead volume of $L_{dead}/L = 0.5$ and diameter $D_{dead}/L = 1$ is necessary for practical reasons and the optimised phase angle for no dead volume of 160° is chosen the power is reduced by almost 20 %. An adjusted phase angle of 150° reduces the power only by 5 % as can be seen in Figure 4.18. The additional dead volume needed to achieve the maximum possible power output for a specific phase angle rises for smaller phase angle and even exceeds the cylinder volume.

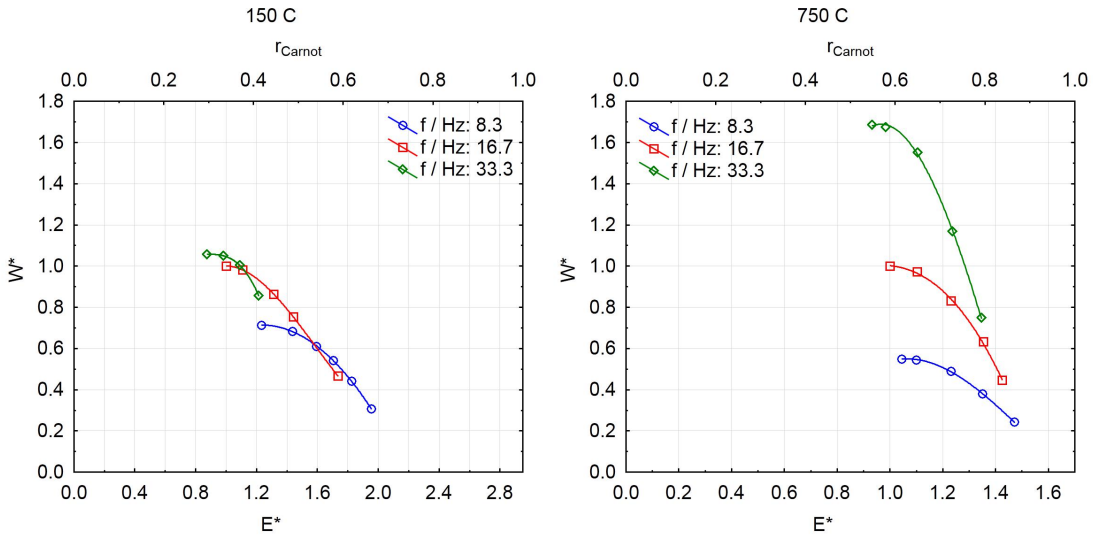

Figure 4.19: Pareto front for power and efficiency at different frequencies. The unavoidable compromise between power and efficiency is illustrated and the limits for both parameters at a certain frequency are given. Different combinations are generated by adjusted heat exchanger and regenerator layouts.

4.4 Power and efficiency limits

An ideal Stirling engine would provide highest power output and efficiency at the same time. However, as for most engines, this is not the case. Power and efficiency are both affected by operating parameters as well as heat exchanger and regenerator design. Between both values there is always a trade-off that has to be accepted in order to achieve the desired performance. Figure 4.19 illustrates this trade-off in the form of the Pareto front for different frequencies and source temperatures. No combination of operating or heat exchangers parameters can be found that exceeds the line of the Pareto front. All parameter combinations that lead to power - efficiency combinations with values smaller than the Pareto front can be optimised to improve either or both of the objectives [113].

For the two different heat source temperatures in Figure 4.19 the position of the Pareto fronts for the different frequencies are quite different. In the HTD the highest frequency shown of 33 Hz dominates the power as well as the effi-

ciency over most part of the efficiency range; LTDs running at lower frequencies become superior as higher efficiencies are demanded. Lower frequencies also allow larger engines to be built because of the reduced inertial forces of the pistons and crankshaft assemblies. Wear and friction is also reduced if the frequency is reduced. Thus a LTD design should not aim for too high a frequency as the gains in indicated work are relatively small compared to the increased friction (not quantified here) and the thus impaired longevity.

Comparing the efficiencies of the LTD and HTD relative to the Carnot efficiency (r_{Carnot}) it can be seen clearly that the HTD shows the ability to reach a much higher fraction of over 80 %, whereas the LTD reaches only up to 70 % for a lower frequency and 40 % for the higher frequency. Walker's observation that HTD designed for maximum power density achieve around 50 % (brake) efficiency seems to be reflected in these simulation results [22].

As discussed earlier, there are two major reasons for the lower relative efficiency of the LTD. First, the temperature difference between heat exchanger walls and working fluid reduces the internal temperature difference, which has a stronger effect as the frequency rises. With the temperature of the heat exchangers used to calculate the Carnot efficiency this reduces the relative efficiency drastically. For a large temperature difference this effect is much less pronounced because the temperature difference changes by a much smaller fraction. Second, pressure losses increase with frequency and diminish the net power output further, as well as the efficiency. In the case of the LTD pressure losses (or pumping losses) represent a relatively large fraction of the net power generated as opposed to the HTD were these losses are relatively small.

4.5 Discussion and Summary

The parameters discussed can be divided into two groups. First, parameters that are decided during the design phase of the engine which cannot be changed during the operation as they are expressed as hardware features, such as the phase angle and the geometry of the heat exchangers and the regenerator. Second, parameters which have to be decided during the design phase but can vary during operation of the engine: the frequency, the temperature of the heat sink and source, and the mean pressure of the working fluid.

Figure 4.20 shows the limits of parameter variation for parameters of the first type in order to stay within a range of 5 % and 10 % of the optimum power output. It can be seen that relatively small changes of a few percent of the phase angle and the regenerator porosity have a relatively large effect on the power output. Even though both phase angle and regenerator porosity can be controlled to be within the desired range during manufacture, before making a detailed engine design any experimental validation and optimisation should be focussed mainly on these two parameters. In addition the relation between dead volume (as a necessary evil for connecting ducts) and phase angle has to be explored experimentally. The heat exchanger geometry and especially the length of the regenerator have been shown to be less critical in terms of power output. Less sensitivity for these parameters is equivalent to an increased freedom in a physical design or possible cost savings especially for the heat exchangers.

As the design of the heat exchanger and the regenerator is highly dependent on the intended frequency, a decision on this has to be made during the design phase. If the designed SE is connected to a generator which is connected directly to the grid, fluctuations in the operating frequency are expected to be very small. However, unstable local grids or direct use of the mechanical power can result in a larger variation of the operating frequency. Figure 4.21 shows by how much

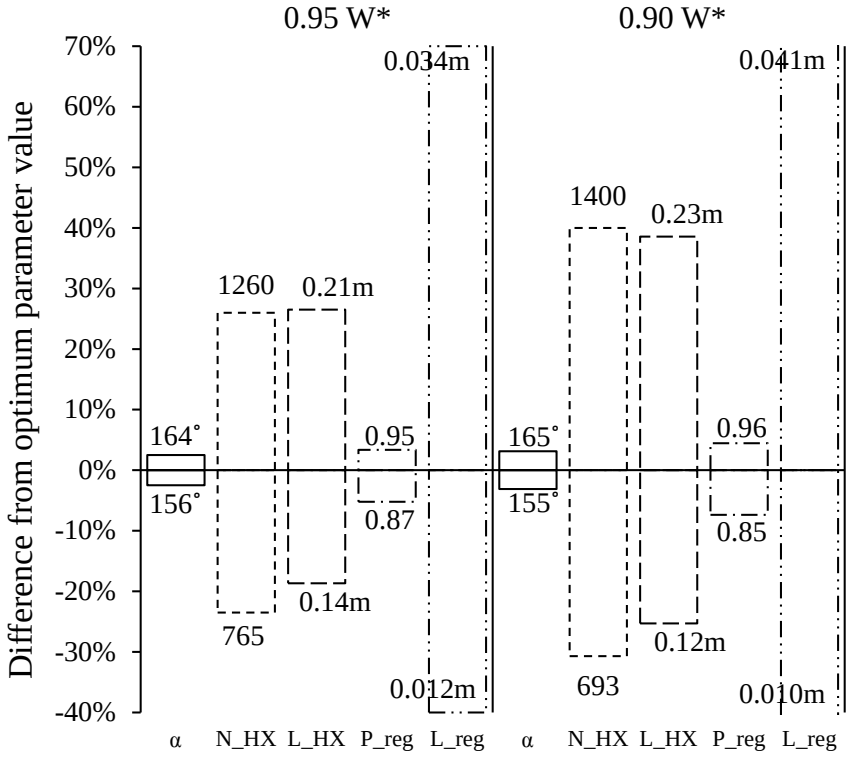

Figure 4.20: Allowable range of design parameters to perform at 95% and 90% of the maximum power output for the LTD. The most sensitive is the phase angle (α) closely followed by the regenerator porosity (P_{reg}); less sensitive are the length (L_{HX}) and the number of tubes (N_{HX}) of the heat exchanger. Least sensitive is the length of the regenerator.

the frequency can drop in order to keep the power output at 95 and 90 %. The frequency is the least sensitive of the operating parameters.

A gas leak from the SE would be more detrimental on power output. The power is reduced by 5 % when the pressure is reduced by 7 %, and by 10 % when the pressure is reduced by 13 %. It is therefore important to keep the mean pressure at its design point by a combination of adapted seal design and either an automated working fluid top-up from an external tank or regular servicing intervals where the desired gas pressure is restored.

The most sensitive operating parameter is the temperature difference of the two heat exchanger surfaces. A decrease in only 2 K due to a variation in the

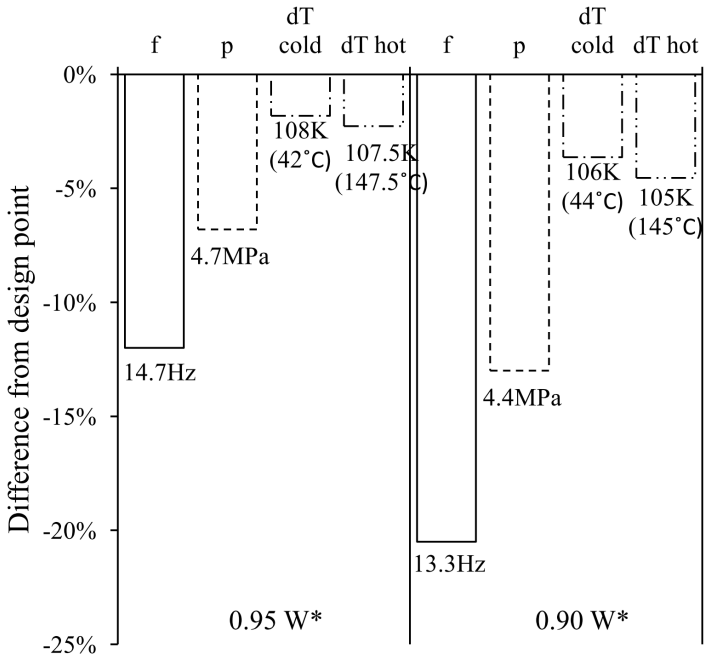

Figure 4.21: Lower limits for the operating parameters to produce 95% and 90% of the maximum power output for the LTD. The most critical is the heat sink temperature expressed by the temperature difference (ΔT_{cold}) closely followed by heat source temperature (as ΔT_{hot}); the least critical is the operating frequency (f) followed by the mean cyclic pressure (p).

sink temperature reduces the power output by 5 %, and a decrease of 4 K reduces the power output by 10 %. Reduction of the heat source temperature has a very similar effect if slightly less pronounced. Careful planning of heat sink and source usage pays out and even simple measures such as finned heat exchanger tubes or proper pipe insulation will make a noticeable difference.

Choosing the desired working fluid before starting with the thermodynamic design of the SE is crucial in order to make best use of the properties given. Each gas (H_2, He, N_2) has different advantages and disadvantages which directly influence the design.

4.6 Conclusion

This chapter provides a solid base for the design of an alpha-type LTD. Key parameters such as geometrical features as well as operating conditions that are crucial for the performance of the engine have been analysed and their impact has been compared. Not only constraints in design could be shown but also possibilities for variation. The thermodynamic design of LTDs imposes a number of challenges on engineers. Compared to the design of HTDs, most design and operating parameters are constrained by much narrower margins. Being aware of the sensitivity of these parameters allows for a faster start when actually designing a LTD, and chances of success are higher. The nature of low-temperature heat sources (cost and availability) makes SEs still an interesting option for power conversion, even if performance seems to be low compared to the potential of high-temperature SEs.

Thermodynamic performance has been discussed in great detail in this chapter as well as in the previous chapters. The next logical step is to investigate the influence of a specific engine set-up on the overall performance which is then given by the indicated power diminished by the mechanical efficiency of the system.

Chapter 5

Mechanical efficiency and force balancing in double-acting SEs

The previous chapters discussed the thermodynamic optimisation of the gas cycle in detail, largely independent of the actual physical set up. For alpha engines, for example, the optimisation is valid for single-acting engines as well as for double-acting engines of the Siemens and Franchot type. Here, in this chapter[1] the influence of the physical engine set-up on the mechanical efficiency, force balancing, and piston seal leakage are discussed. Contributions to describe mechanical losses due to the various friction forces have been made by various authors [174–177]. The scope of this chapter is not to provide a quantitative study of the different loss mechanisms but to provide insights into how the physical set-up and thus the forces acting on both sides of a piston in a specific set-up influence the mechanical efficiency quantitatively. Furthermore, the Franchot and the Siemens arrangement are discussed in greater detail regarding internal force balancing, seal leakage, costs, and longevity.

[1]This chapter contains material published earlier as a contribution to the 15th International Stirling Engine Conference in Dubrovnik [169]. Since then the model has been refined by incorporating data obtained from the Sage simulation described in the previous chapter.

5.1 The mechanical efficiency model

Depending on the physical set-up, some engines are more sensitive to the mechanical losses of the system than others. The two sides of each piston allow for a manipulation of the power development depending on the back pressure. If, for example, an expanding gas volume compresses the gas of an adjacent cycle in a multi-cylinder engine directly, the net power transferred to the crankshaft is reduced as part of the power is consumed for compression. The same principle applies to a single-acting engine with a buffer space on the backside of the piston which acts as a gas spring and stores mechanical energy during expansion so that it can be re-used for compression without taking the detour through the crank mechanism. All friction forces on the piston and the crankshaft directly relate to the net power transferred. The smaller the net power for an indicated power given and hence the forces in the piston rod, the smaller the friction from resulting side forces and thus the higher the mechanical efficiency. All the usable work that can be extracted from the cycle (negative sign, W^-) becomes diminished by the mechanical losses of the transmitting components ($\eta_{mechanism}$) which includes friction in bearings, cross-heads, and piston seals. It is defined by

$$\eta_{mechanism} = \frac{W_{out}}{W_{in}}, \tag{5.1}$$

so it is a measure how much energy is lost by friction in the mechanism (like a constant coefficient of friction). The remainder of that energy is partly needed to supply the mechanical work for compression (positive sign, W^+) where it is again subject to mechanical losses when it is transferred through the drive train. Combining the efficiency of the mechanism with the indicated work from Equation 2.18

the available work on the shaft can be calculated as

$$\begin{aligned} W_{shaft} &= \eta_{mechanism} \int_{-} p_{eff}(\theta) dV_{gas}(\theta) - {}^{1}/_{\eta_{mechanism}} \int_{+} p_{eff}(\theta) dV_{gas}(\theta) \\ &= \eta_{mechanism} W^{-} - {}^{1}/_{\eta_{mechanism}} W^{+}. \end{aligned} \tag{5.2}$$

The mechanical efficiency ($\eta_{mechanical}$) of the engine is then calculated as

$$\eta_{mechanical} = \frac{W_{shaft}}{W_{indicated}}. \tag{5.3}$$

A more detailed and very theoretical study on the influence of mechanical efficiency combined with isothermal analysis can be found in a book by Senft and associated publications (which lead to the conclusions summarized in the book) fully dedicated to this subject [177].

The mechanical losses in an engine are dependent on a number of parameters such as the friction of the seal between piston (or piston rod) and cylinder (depending on diameter, materials, side loads, speed), the friction in the bearings of the crank mechanism (depending on the load, speed, diameter, lubrication, number of bearings), and friction in the cross-head due to side-loads. Since these parameters vary for different engines the efficiency of the mechanism varies too. The exact value of this efficiency or loss coefficient is not known but Equation 5.2 can be used to determine the sensitivity of different engine types to inevitable mechanical losses.

5.2 Mechanical efficiency of displacer-type engines (Isothermal model)

This section applies the mechanical efficiency model to the displacer and piston engines described in Chapter 3. Although it could be shown that the displacer

engines are not an option for a simple engine of comparably high specific power, this analysis is shown here briefly for the sake of completeness. The pressure and volume variations used are those gained from the isothermal analysis in Chapter 3. Despite the fact that the pressure amplitudes calculated are very optimistic the general trend for the mechanical efficiency can be shown here. Figure 5.1 shows the influence of the mechanical effectiveness on the shaft power according to Equation 5.2. The engine set-up is optimised according to the losses. The plots show the performance at 450 K heat source temperature for the engines examined in the isothermal analysis (Chapter 3); at higher temperatures the tendencies are very similar and are not shown here. Discontinuous displacer operation is also not shown as no significant difference to their sinusoidally moved counterparts can be observed.

As shown in Chapter 3 above the single gas circuit engines (alpha, beta, gamma) in Figure 5.1 (a) show smaller power outputs than the multi-cylinder engines in Figure (b) in the loss-less case, as the swept volume is used less efficiently. All multi-cylinder alpha engines perform equally and double the power output of a single gas circuit engine for the case of loss-less mechanical transmission, due to their thermodynamic equality.

The slope of the plots in Figure 5.1 (a) and (b) indicate the sensitivity to the efficiency of the mechanism of a specific design. Independent of the heat source temperature, alpha engines seem most sensitive to mechanical losses, having much steeper gradients than the displacer engines. Looking at single-cylinder alpha engines the importance of sound mechanical design for low temperature engines becomes obvious. While at the high temperatures (1000 K, not shown here) a mechanism efficiency of at least 0.65 is needed to keep the engine running (without any usable power output), at the low heat source temperature this value is almost 0.8. Comparing the plots for Siemens/Rinia (Finkelstein) and Franchot arrangements the benefits of the partial balancing of expansion and compression

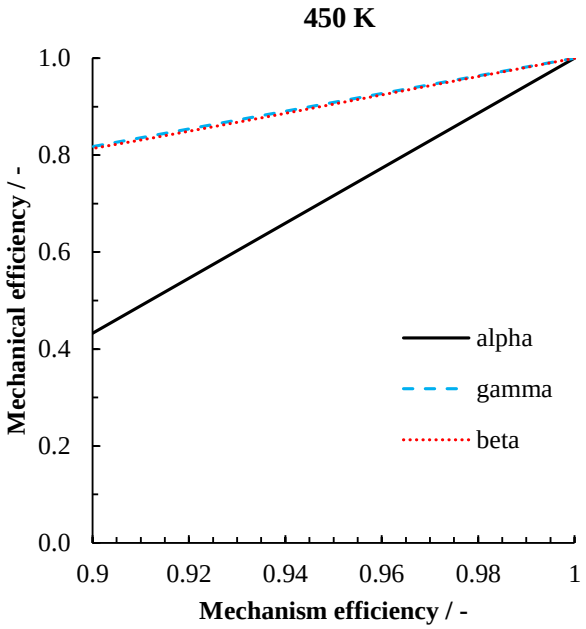

(a)

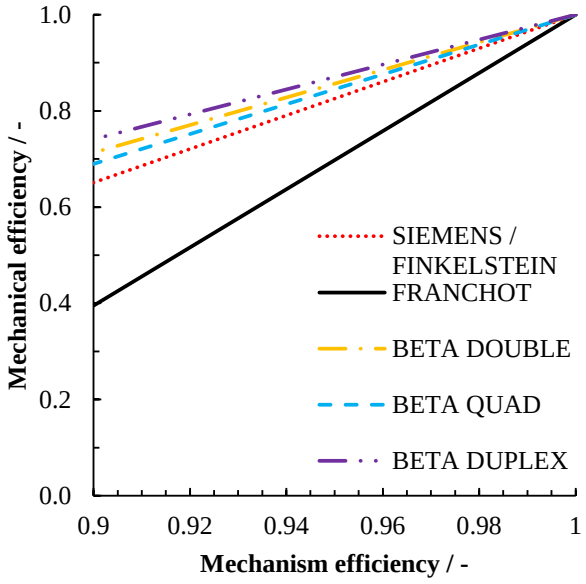

(b)

Figure 5.1: Influence of mechanism efficiency on the overall mechanical efficiency of the engine at 450 K heat source temperature. Single-acting engines are shown on top (a) and double-acting engines on the bottom (b). Displacer engines are generally better in terms of mechanical efficiency than piston-only engines are.

forces directly via the piston instead of taking the detour through the crankshaft becomes clear. Not only can components be built with less material since smaller forces act on them, the whole system also works more efficiently as the indicated work is diminished to a lesser extent. Since double-acting alpha engines have been shown to be the most promising candidate for low-temperature power generation they are discussed below in greater detail using the results from the Sage simulation.

Displacer engines are in general less sensitive to the effects of mechanical losses because the displacer itself consumes only very little power because the pressure difference is small and so are the forces needed to move it. As a result, the mechanical losses in the displacer drive are small too. As mechanism performance deteriorates, the volume ratio (piston to displacer volume) is lowered when optimising for the maximum power output. More gas is swept by the displacer and less is compressed and expanded by the piston. This leads to more upright $p-V$ plots and thus very little external work is needed to compress the gas (compare Figure 3.7 and 3.11, and note that the back pressure is the mean cyclic pressure). In this way the mechanical losses can be kept small, an option that is not applicable for alpha engines[2] (Figure 3.3). Just as for alpha engines, lower heat source temperatures demand sound mechanical design to conserve a reasonable power output. Due to the adjustable volume ratio it is much easier to create a LTD.

5.3 Mechanical efficiency of piston-type engines

Low temperature differences between heat source and sink in Stirling engines result in an unfavourable ratio of compression work to expansion work. Figure 5.2 shows this relationship clearly using $p-V$ plots for the expansion, compression, and total

[2]In fact this is one of the reasons why all ultra low-temperature difference engines that operate successfully are gamma engines, having a very large displacer volume compared to the swept volume of the power piston [177]

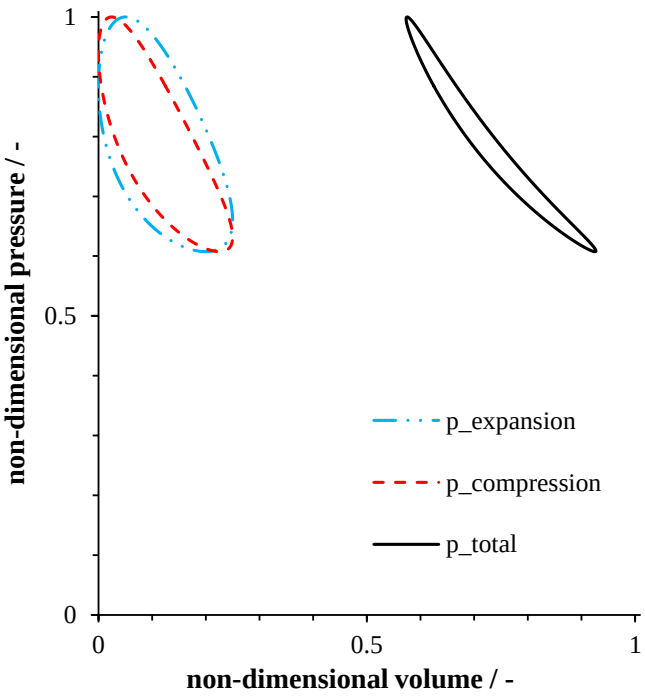

Figure 5.2: Pressure-volume variations for the expansion and compression space and the total gas volume. Isothermal model, phase angle 90°, 150-40 °C

gas volume for 150 °C heat source and 40 °C sink temperature. It can be seen that a large portion of the expansion work is consumed for compression. The net work (total) is largely diminished and the resulting $p-V$ plot is very narrow and relatively small compared to the work in the expansion and compression space. This effect is even more pronounced for the more realistic simulation as can be seen in the $p-V$ plots obtained from the optimised Sage model for different phase angles (Figure 4.8).

In a double-acting alpha arrangement two variable gas spaces are combined on the two sides of a piston. These can be a compression space and an expansion space in the case of the Siemens arrangement or two gas spaces of the same kind in the case of the Franchot arrangement (expansion-expansion, compression-compression). Figure 5.3 shows the non-dimensional power for each piston in a Four-cylinder engine obtained from the isothermal model. For each of the two

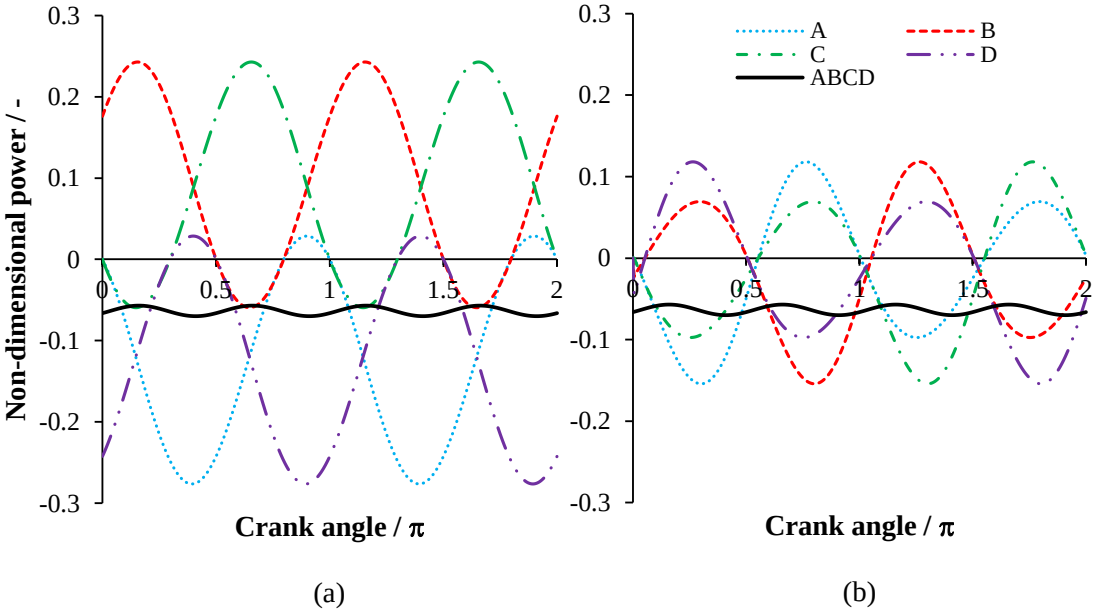

Figure 5.3: Non dimensional power for the Franchot (a) and Siemens (b) arrangement. Four-cylinder, 90° phase angle, isothermal model

different arrangements the power is given over one crankshaft revolution. In both cases the net indicated power of all four pistons ($ABCD$) is identical, which is not the case for the individual pistons. In the case of the Siemens arrangement (b) each piston shows the same characteristic. The combination of compression and expansion on one single piston leads to smaller power amplitudes and thus smaller loads on the piston rods as parts of the power is directly transferred between the two gas cycles. In the case of the Franchot arrangement (a), two pistons supply the crankshaft with power (A, D) and two pistons consume power (B, C) most of the time. This results in larger power amplitudes and loads on the crankshaft as the generated power has to be transferred from the expansion pistons to the crankshaft first and then back to the compression pistons.

The ratio of the magnitude of the load transferred from the pistons to the crankshaft and back has a direct influence on the mechanical efficiency of the engine. Applying the analysis of the mechanical efficiency explained above to the two arrangements, the benefits of internal balancing of expansion and compres-

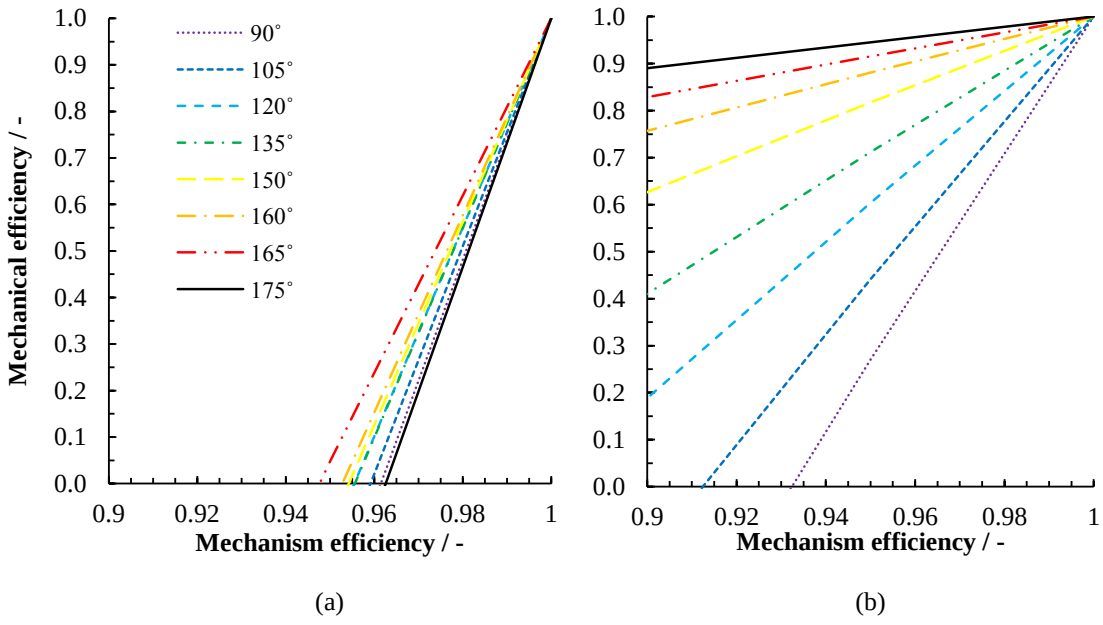

Figure 5.4: Overall mechanical efficiency as a function of the mechanism efficiency and the phase angle for Franchot (a) and Siemens (b) arrangement based on the Sage models from Figure 4.18 with optimised dead volume.

sion forces can be seen clearly. Figure 5.4 shows the overall mechanical efficiency as a function of the efficiency of the crankshaft mechanism. The data used to generate these plots was obtained from the more accurate Sage model, described in Chapter 4. As expected, the overall mechanical efficiency drops as the efficiency of the crank mechanism drops. A less efficient crank mechanism proves to have less serious consequences in the case of the Siemens arrangement. In fact, the performance of the Franchot arrangements deteriorates so fast that excellent mechanism efficiencies of over 99 % are required to achieve a satisfactory overall mechanical efficiency which is highly unlikely. For the Siemens arrangement, on the other hand, the mechanical efficiency improves with increasing phase angle (and thus number of cylinders) and is much higher, independent of the mechanism efficiency or the phase angle. Thus not only from a thermodynamic but also from a mechanical point of view multi-cylinder engines featuring large cylinder numbers in an Siemens arrangement are the preferred design option.

5.4 Gas leakage on the piston seals and net piston forces of double-acting piston engines

The type of compounding also has a strong influence on the pressure difference between the two gas spaces separated by the piston seal. A larger amplitude in pressure difference leads to increased leakage into the adjacent gas cycle. Grinnell [178] as well as Liu [179] showed that the mass flow rate ($\dot{m}$) of a compressible fluid through a thin passage of a specific geometry is proportional to the difference of the square of the pressures on each end:

$$\dot{m}_{leakage} \propto (p_1^2 - p_2^2) \tag{5.4}$$

Even though there is no net loss of the working gas as the direction of the pressure difference reverses, there is a loss in power. For the case of a tight clearance seal Walker and Senft correlate this power loss to the square of the pressure amplitude on the seal [165]:

$$P_{leakage} = \frac{\pi h^3 D}{24 \mu L} p_{amp}^2 \tag{5.5}$$

where h is the radial clearance of piston and cylinder, D is the cylinder diameter μ is the gas viscosity (for fluid properties see Appendix C). For an identical set-up the power loss is simply proportional to the square of the pressure amplitude:

$$P_{leakage} \propto p_{amp}^2 \tag{5.6}$$

Figure 5.5 shows the pressure difference acting on one piston, and hence its seal, for each of the two arrangements. Two phase angles are shown: 90 and 160°. For the Franchot arrangement the amplitude of this difference is almost 30 % higher at 90° and 400 % at 160°, with leakage and power loss increasing accordingly. At 160° phase angle the LTD optimised in Chapter 4 generates about 5.2 kW power. With helium as the working fluid, a radial clearance of 25 µm (typical value for a

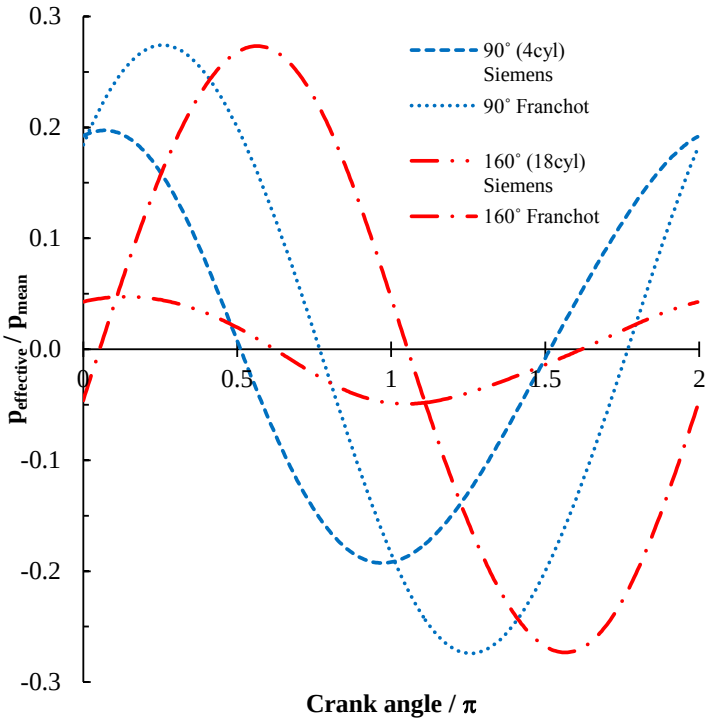

Figure 5.5: Effective pressure oscillation for the Siemens and the Franchot arrangement over one cycle for two different phase angles. Sage simulation, $T_{source} = 150\,°\mathrm{C}$

clearance seal according to White [180]), and a seal length of 0.02 m the power loss due to leakage can be calculated as 6 W for the Siemens arrangement and as 200 W for the Franchot arrangement. In this configuration the Siemens engine loses 0.1 % of the power generated and the Franchot engine 3.9 %; for an identical seal set-up this is 34 times as much which is a noticeable portion of the power generated (difference due to rounding). For the case of traditional piston ring seals a smaller pressure difference across the seal also allows fewer piston rings to be used, or a less 'tight' seal (less pre-tension). As a result, for a leakage rate provided, friction losses can be reduced significantly. Figure 5.6 shows a comparison of the effective pressure of a traditional 4 - cylinder engine (phase angle 90°) in Siemens configuration operating at a high temperature difference and the LTD engine with the phase angle optimised at 160°. In this configuration the power output of the HTD is about 95 kW at 16.7 Hz, about 18 times the value of the optimised LTD. As

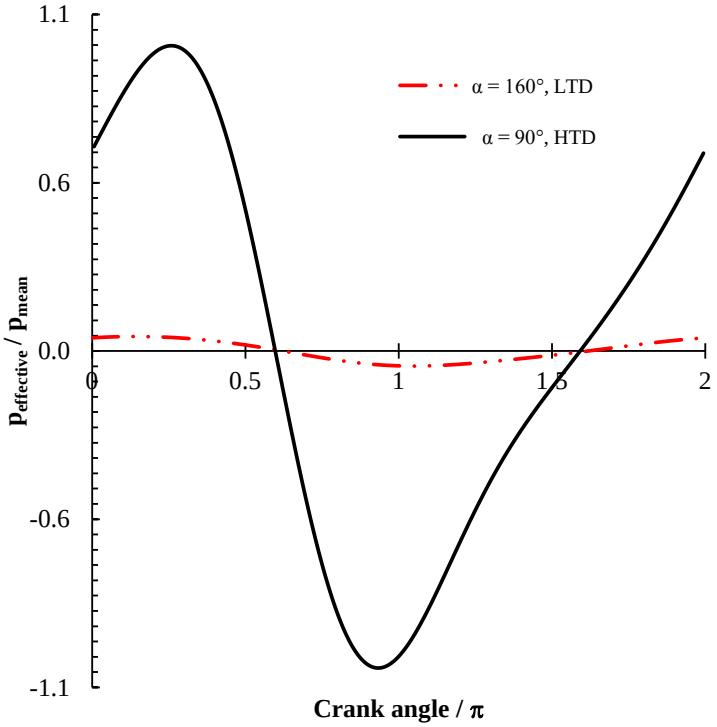

Figure 5.6: Effective pressure of an 18-cylinder LTD and a 4-cylinder HTD

can be seen from the Figure, the difference in the effective pressure amplitude is of similar magnitude, it is about 21 times higher. Applying Equation 5.4 results in a piston seal leakage 21 times higher for the HTD, for an identical seal set-up. The power losses according to Equation 5.5 is about two orders of magnitude smaller for the LTD. As a result the piston seal design for a low temperature engine can differ substantially from a high temperature design. Friction forces and power loss by seal leakage can thus be reduced more strongly than the power output is reduced due to the smaller temperature difference. This comes in addition to the better mechanical efficiency gained from better balancing of compression and expansion forces in the Siemens arrangement for the larger phase angles needed for the LTD (Figure 5.4).

For an identical piston diameter the effective pressure is also directly proportional to the force ($F = pA$) on the piston rod and the crankshaft. The large difference in the pressure amplitude for LTD and HTD engines and hence the

forces in the piston rods and crank mechanism allow for much lighter moving parts in the LTD. Reduced inertial forces and material savings are a welcome benefit for the low temperature design. Reducing the forces in the connecting rod by reducing the effective pressure amplitude for a given temperature level has several beneficial effects on the engine design and performance as discussed in the following section.

5.5 Conclusion - Implications for engine design

Although the indicated power is identical (identical phase angle) for the two alpha engine set-ups (Siemens and Franchot), and both arrangements effectively reduce the engine size by using the double-acting principle, the Siemens arrangement shows a number of advantages:

- The smaller pressure difference on the piston seals allows for better sealing between adjacent gas cycles, or allows for a seal with less friction.
- The reduced net power transferred between the pistons reduces the side-forces and other friction forces significantly and thus increases the mechanical efficiency. In addition, having to sustain lower loads, for a given material the piston rods and the whole crank assembly can be reduced in cross-section and bearings can be designed smaller. This reduction of mass also reduces the inertial and dynamic forces of the crank-assembly which have to be balanced and which also increase side-loads and piston ring friction (for slider crank assemblies) which is especially beneficial in the case of dry-running seals.
- A smaller rod diameter also decreases leakage to and from the crankcase as the sealed gap becomes smaller and thus the power output is increased slightly.

- Reduced load on the bearings and reciprocating seals also increases the longevity of the engine.
- In addition, all these factors show potential for savings in both capital and operating costs.

The Siemens arrangement can clearly be identified to be the superior choice as even for unfavourable phase angles the shaft power will always be higher than the shaft power of an optimised Franchot engine, with all the advantages listed above (identical mechanism provided). Despite its simplicity (with only two cylinders being required), the Franchot design is not suitable for power generation from low temperature sources.

The results of the two different analyses to optimise the shaft power by optimising the indicated power (see Chapter 4) as well as the mechanical efficiency (this Chapter) both indicate favourable working conditions in a similar region, namely large phase angles. Thus no compromise has to be found to reach maximum performance, which is an important outcome when dealing with low enthalpy heat sources. Compared to a high temperature design better mechanical efficiency and piston seal leakage rates are achievable if the engine is designed systematically for low temperature differentials.

With the analysis of the mechanical efficiency the engine selection could be narrowed down to a multi-cylinder alpha engine of the Siemens type. So far simulation work has given insights into optimum operating and design parameters. The next step (in Chapter 6 following) is to transfer these theoretical insights to physical design features and discuss the implications of the different options.

Chapter 6

Implications for LTD design

In the preceding chapters the main focus was on finding a suitable engine type (double-acting alpha-type, Chapter 3), suitable heat exchanger configurations and operating parameters (Chapter 4), and identifying the Siemens arrangement as the alpha-type engine which shows superior mechanical performance (Chapter 5). The quantitative findings from these thermodynamic and fluid-dynamic optimisation processes have to be translated to design features in order to preserve performance while creating a robust design. Insights gained will be extracted and put into the design context.

This chapter is considered as a starting point for the design of a future low-temperature SE rather than the draft for a detailed engine design. Implications for future designs are identified, and design ambiguities are reduced to only a few low-temperature differential specific options informed by the results from the analyses in the previous chapters. Each key component is discussed with regard to previous design solutions and the implications given by the low temperature operation. Two novel conceptual designs are developed specifically suited for the specific application.

6.1 Heat exchanger and regenerator assembly

The heat exchanger and regenerator assembly is the heart of every Stirling engine. It creates the foundation for a successful application of the SE technology. The demanding constraints found for the low temperature difference application make a sound thermodynamic and fluid-dynamic design necessary, as well as a consequent physical implementation.

6.1.1 Heat exchangers

In Sections 4.2.5 and 4.3.5 the optimum heat exchanger geometry has been discussed and its sensitivity to parameter variation shown. The main findings that influence the heat exchanger design for the LTD are summarised in the following:

- fluid friction (pumping loss) represents a dominant loss mechanism
- highly pressured engines provide more specific power
- large heat exchanger surface area is needed to add heat and reject heat
- low sensitivity to the number of tubes and the length of tubes
- high sensitivity to heat sink and source temperatures
- possibility of using identical HX for the hot and the cold sides in LTDs
- non-zero dead volume for optimum power output and efficiency

In addition the heat exchanger design should be

- easily demountable for cleaning
- of simple construction and proven design

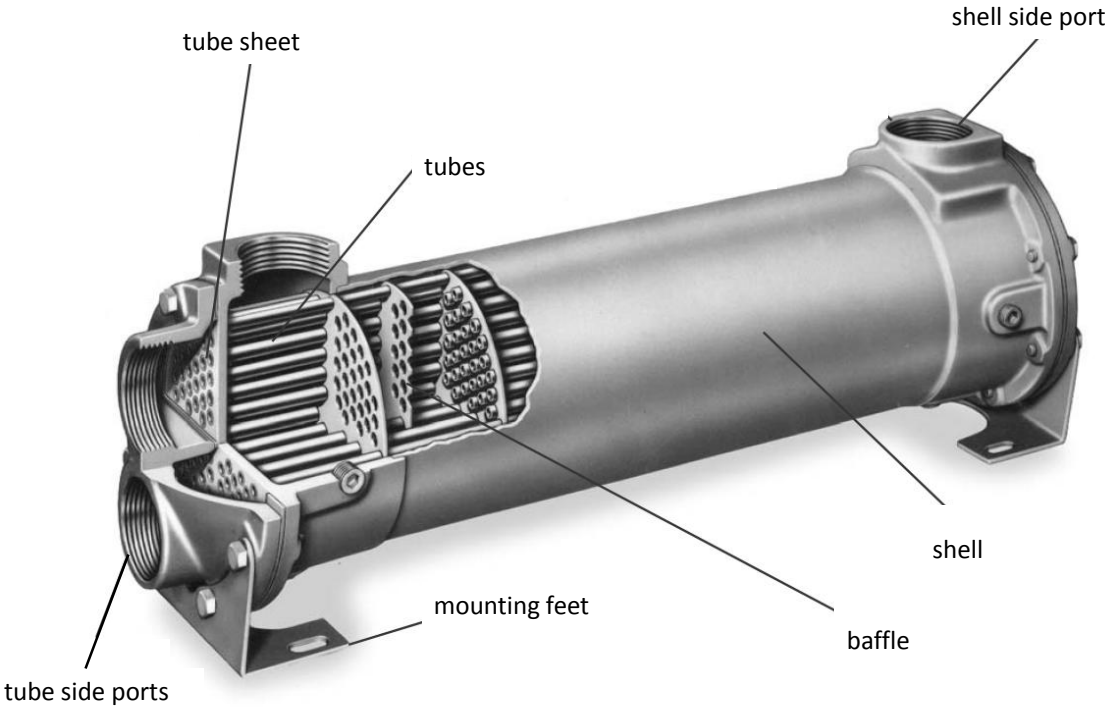

Figure 6.1: Shell and tube heat exchangers components [181]

In Section 1.2.7 common heat-exchanger designs for high temperature Stirling engines have been described. Hot combustion gases are used to supply the working fluid with heat. Each of the designs shows certain weaknesses regarding a low temperature application. The tubular designs shown feature large surface areas but rather complex designs of the tubes, especially in Figure 1.9 (a) where each tube has an individual shape. Also, a small diameter in the manifold as in Figure 1.9 (c) and (e) will increase the pumping losses significantly and make the operation with geothermal heat or waste-heat impossible. The designs with the finned annular gap, on the other hand, feature relatively large wall thickness since the wall of the heat exchanger has to resist the pressure at a diameter larger than the bore of the cylinder which reduces the heat transfer rate. In addition the heat transfer area for a hydraulic diameter given is smaller since only one side of the rectangular cut ducts is in direct contact with the heat source.

Heat exchangers come in all shapes and sizes; from the many possible solutions it is thought that only shell and tube heat exchangers combine all the characteristics needed, namely: large surface area; thin heat exchanger walls made from a material with high thermal conductivity; low pressure losses; high pressure resistance; simple to disassemble for cleaning (especially important if dealing with geothermal brine); a simple construction, and a proven design. The book by Gupta provides a good introduction to heat exchanger design, especially for the shell and tube type [171]. Figure 6.1 shows the general set-up of a shell and tube heat exchanger. In order to keep the pumping losses at a minimum it is necessary to have the working fluid on the tube side as opposed to the shell side of the heat exchanger. In addition the gas flow through the heat exchanger tubes should be of the single-pass type, i.e. parallel flow through all tubes. The mass flow of the geothermal brine or an alternative heat carrier in the case of waste-heat is guided by means of baffles through the shell on the outside of the tubes to ensure an even flow distribution. Figure 6.1 shows fixed tube sheets which means the tube assembly cannot be separated from the shell; for the geothermal application this is not an acceptable design as the heat exchanger has to be demountable for cleaning. The connection between the tubes and the tube sheet should be made by welding (or brazing if pressure and material compatibility allows) rather than expansion in order to create a stronger bond less prone to slackening due to the pressure oscillation of the working gas. The sensitivity analysis in Section 4.5 showed that the engine performance is not particularly sensitive to geometrical parameters such as the number of tubes and the tube length which increases the flexibility for the heat exchanger design.

Section 4.3.3 showed the importance of the level of the heat source and sink temperatures for the low-temperature scenario. In order to best utilise given heat source and sink temperatures, the heat transfer into and out of the SE should be optimised. The shell and tube design with thin wall thickness and

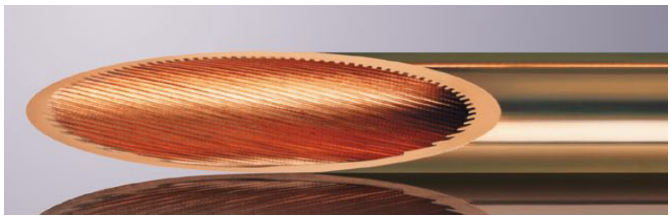

(a)

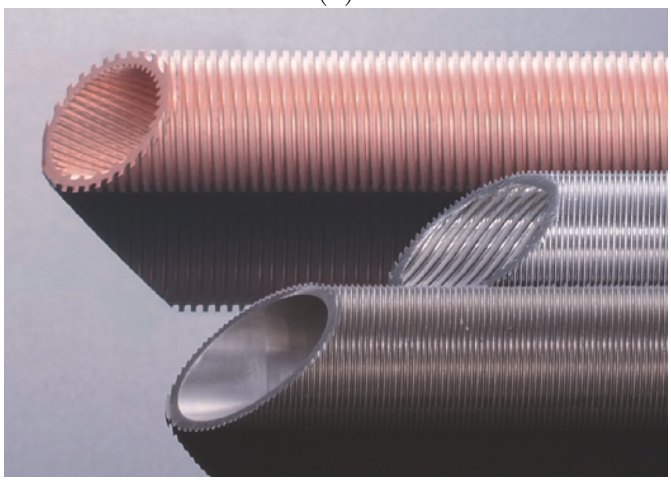

(b)

Figure 6.2: Internally grooved tube (a) and externally finned tubes (b); as can be seen combinations are available too [182].

large contact area of heat carrier and heat exchanger helps to provide a good heat transfer. In addition the heat transfer on the inside and the outside of the tubes should be increased. One possibility is the addition of fins on the outside and grooves on the inside. Figure 6.2 (a) shows an example for such an internally grooved tube; Figure 6.2 (b) shows externally finned tubes as well as externally and internally finned tubes. There is evidence that internal grooves can improve the heat transfer for steady state flow conditions significantly without increasing the pressure losses extensively (e.g. [183–185]). Kuosa et al. showed theoretically that improved performance can be expected in SE applications because the increase in heat transfer outweighs the additional pumping losses [186]. However, so far no experimental proof could be found that supports their reasoning. An experimental examination of the adaptability of such a heat exchanger design for reciprocating flow should be carried out in the future for clarification.

Another important outcome of the simulation was the possibility of using identical heat exchangers on the hot and on the cold side. Since the obtainable efficiency in a low-temperature difference device is inherently low the magnitude of the heat transferred to and from the gas is relatively similar. Fluid properties such as density, which largely influence pressure losses, vary less between the hot and cold heat exchangers of a LTD than between the heat exchangers of a HTD. Thus similar length and diameter of heat exchanger tubes can be found to be optimum. In addition to the similar geometrical layout it is possible to use the same material for both temperature levels since a special alloy on the hot side is no longer needed for the LTD. Potential cost savings can be identified by the use of identical components on both sides.

Figure 6.3 shows different design concepts for the heat exchanger and regenerator assembly. Figure 6.3 (a) features a design with a relatively small amount of dead volume which could be used in an arrangement with opposed pistons. One side would then be flanged onto the expansion cylinder space and the other to a duct and then the compression cylinder. In Section 4.3.7 it was shown that the introduction of additional dead volume has a positive effect on the power output for smaller, non-optimum phase angles. The smaller the phase angle the larger the permissible dead volume becomes, so that relatively long ducts (of a diameter large enough to keep pumping losses small) can be used. Having found a compromise between dead volume, phase angle (based on the number of cylinders), and mechanical efficiency, one can also choose from one of the designs shown in Figure 6.3 (b), (c), and (d). Here, the heat exchangers are designed for parallel pistons. A U-tube is used to reverse the flow. Each of the three designs allows for different layouts of the piston arrangement. Different mounting angles are possible, especially in design (d) where both heat exchangers can be mounted independently, at varying angles to the cylinder and between the two heat exchangers by rotating the flange connections accordingly.

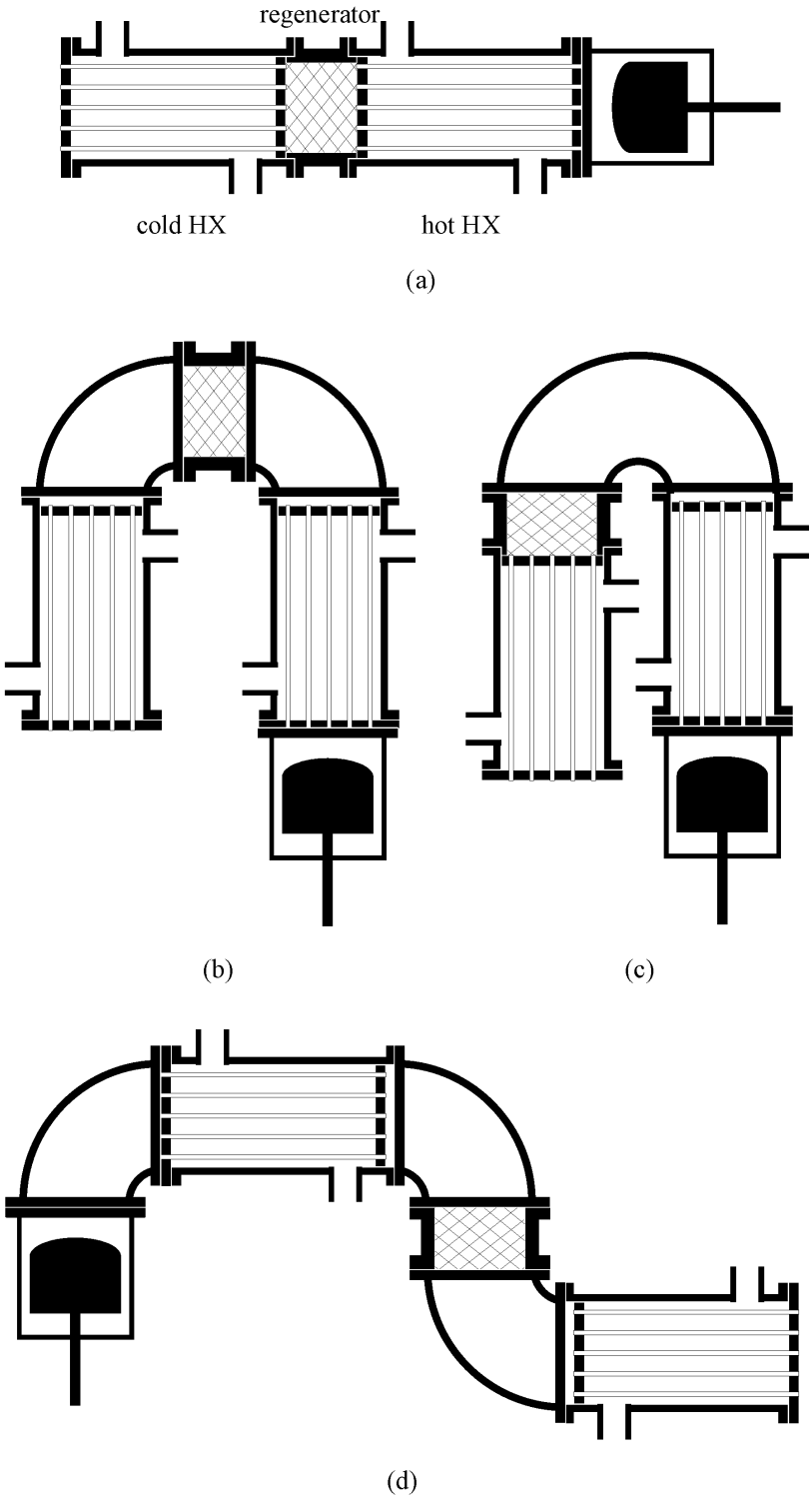

Figure 6.3: Tubular heat exchanger designs with identical heat exchanger on the cold and on the hot side. Variant (a) features a straight design; (b) features parallel heat exchangers and a symmetric set-up; in variant (c) the regenerator is used to bring the cold heat exchangers closer to the expansion side of the piston; in variant (d) the heat exchangers a mounted horizontally and can be rotated freely at the flanges; manifolds are not shown.

Another option or an addition to the design described above could be the use of a thermosiphon or heat pipe where an intermediate fluid is evaporated by the heat source and condensed at the hot heat exchangers of the Stirling engine. This design has a number of advantages: first of all conventional, proven, geothermal heat exchanger designs can be used. Usually the geothermal brine flows through the tube side of a shell and tube heat exchanger, where straight tubes are used and the heat exchanger can easily be cleaned mechanically by means of a water jet [187]. As the heat transfer by evaporation and condensation is very good, only a very small temperature gradient in the heat pipe is expected. By separating the heat exchangers on the SE side from the geothermal brine more material options are available since the aggressive brine is no longer in contact. Maintenance, cleaning, and de-scaling would then be necessary only for one part, and not every single, relatively fragile SE-heat exchanger. The downside of the heat pipe solution are the additional costs expected. For a waste heat application the heat pipe solution seems less appropriate since a heat carrier such as clean water or thermo-oil can be used directly. Philips successfully experimented with high temperature heat pipes as can be seen in Hargreaves book [23], which also inspired research at NASA [188–190] where different heat pipe fluids were investigated systematically. For the temperature range under consideration here, pressurised water is one of the most promising candidates due to low costs, non-toxicity, chemical stability, and material compatibility.

6.1.2 Regenerator

Different regenerator designs have been discussed in Section 1.2.7. For the LTD no major design changes have to be made. Both established designs - the random fibre mesh and the wire screen - seem equally suitable for the desired application. Care has to be taken to keep pumping losses in the regenerator matrix as low as possible, and to keep the flow through the matrix uniform (i.e. equal gas

velocity throughout the entire regenerator cross-section; see experimental studies by Hamaguchi [191]). Possible inclusions in the proposed heat exchanger set-up are given in Figure 6.3.

For the calculated case of a bore to stroke ratio of 2 a regenerator diameter of approximately the cylinder diameter seems appropriate. In the simulation larger regenerator diameters show the ability to increase the power output but show disadvantages in a physical design. A diameter larger than the diameter of the cylinder assembly is difficult to incorporate into the engine layout, longer connecting ducts are required, and a uniform flow becomes more difficult to achieve.

The sensitivity analysis in Section 4.5 showed that the porosity has a much stronger influence on the engine performance than the matrix length. Therefore experimental optimisation should primarily focus on the former. For an experimental set-up this could imply a fixed regenerator canister geometry filled with exchangeable matrices.

6.2 Power extraction, piston timing, and cylinder arrangement

Generally two ways of power extraction are possible for Stirling engines. The most common one is the use of an electrical alternator to produce electricity. Another option is the direct use of the mechanical energy to pump or compress[1] a fluid. If electric energy is to be produced there are two technological alternatives available: the conventional rotational electric generator and the linear alternator. Since the former device needs a rotating shaft as input, a kinematic mechanism is necessary

[1] A novel application for Stirling engine technology could be the direct compression of helium or hydrogen in large reciprocating compressors as they are used in the oil, gas, chemical and refining industries. The piston of the Stirling cycle on the one side would be rigidly connected to the process gas compression piston on the other side and powers the process. Both pistons can be made double-acting, with the Stirling side being of the proposed Siemens arrangement. Industrial waste heat or hydrogen combustion, where available, could be used as the heat source.

to transform the reciprocating motion of the pistons into rotating motion. The latter is directly connected to the piston rod without any additional linkage in between. In the following section the peculiarities of the two different systems are explained in greater detail.

Independent of the choice of a kinematic or a free-piston design it could be shown by simulation that:

- the double-acting alpha design provides the highest power density
- the Siemens arrangement, as opposed to the Franchot arrangement, is capable of reducing piston seal leakage, loads on the piston rod, and side-forces
- a high mechanical efficiency is necessary as LTD performance is generally low
- a large phase angle is necessary for optimum thermodynamic performance which results in a large number of interconnected cylinders

6.2.1 Kinematic engines

A very large number of kinematic linkages has been proposed in the past in order to transfer the reciprocating motion of the pistons into rotation. Side-loads generated by the mechanism have to be kept away from the (dry) sliding and sealing surfaces in the engine in order to assure the engine's longevity. The optimal mechanism for a Stirling engine would be simple and reliable, would generate only small side-forces and accommodate these and, in addition, a small space requirement is desirable. Side-forces not only threaten sealing surfaces, they also directly increase the friction and thus reduce the mechanical efficiency of the engine. Since a good mechanical efficiency is mandatory for the LTD (see Chapter 5), firstly side-forces have to be reduced, and then these reduced forces need to be kept away from the rods and pistons. Senft gives an overview of

possible kinematic linkages [192], and Clucas shows designs implemented in real engines [81]. Amongst these are, with some additions:

- slider-crank, the mechanism commonly found in internal combustion engines. In Stirling engines the use of cross-heads becomes mandatory in order to handle side-loads.

- scotch yoke, a mechanism providing pure sinusoidal motion. At first sight a simplistic and promising design; however, close tolerances are necessary for the translational moving part which also represents a challenging lubrication situation [104, 193–196].

- four-bar linkages (including the popular Ross-yoke) as found in the Philips 102 engine [22, 23], various engines from the University of Denmark [154], and various hobbyist engines [89]. A linkage is used to create a quasi-straight line motion and to transfer this motion into rotation. Side-forces can be kept away from pistons by the linkage. These advantages can disappear, however, particularly in the version with two pistons connected (Ross-yoke) which suffers from excessive lateral movement, resulting in a more complicated design if a reliable engine is to be built [172, 197].

- rhombic drive, developed at Philips originally for a beta-type engine [23, 198]. It uses two timed and counter-rotating crankshafts. Each reciprocating element is attached via two identical connecting rods to both camshafts. As a result no side-forces act on the piston and very good dynamical balance is achievable, even with a single cylinder. The geared crankshafts and the other parts of the mechanism make high precision in manufacturing and assembly necessary.

- radial drive, the predominant mechanism found in aeroplane IC engines during WWI. The cylinders are arranged around a central crankshaft, re-

sembling a star. The axes of all cylinders are in one plane, but multiple cylinder rows are possible [199].

- swash-plate and wobble-yoke, two drive mechanisms sharing some similarities. The centres of the cylinders are located on a circle, the parallel rods act on an inclined rotating disc. In the case of the wobble-yoke the sliding contact between disc and piston rod is turned into a rotation of additional yokes which limits the piston number to four. The square-four arrangement is also the most common application of this drive. [23, 81]

- Stiller-Smith and Parsons drive, two mechanisms which produce perfect straight line motion and which were proposed as a possible solution for the Finkelstein arrangement. Very tight tolerances are needed and side-forces are expected to be large, which then result in an expensive and inefficient mechanism [200–203].

- other 'custom' mechanisms, designed to improve the thermodynamic performance. Adding a highly complicated and cryptic mechanism to an engine which in most applications faces the challenge of economic viability is not thought to be a game-changer for Stirling technology. An illustrative example can be found in Kocsisek [204].

Especially for larger kinematic engines (>10 kW) the slider-crank mechanism in combination with cross-heads is the most popular choice. A large base of knowledge is available due to the large prevalence of the mechanism in reciprocating equipment. The high tolerance components, mainly the bearings, are off-the-shelf parts and readily available which help to save both time and costs. The rhombic drive as well as the radial drive are special forms of the slider-crank mechanism. The former has the advantage that no cross-heads are needed (at the expense of simplicity); the latter allows for a short and compact crankshaft with a largely reduced number of bearings. Of the other mechanisms mentioned, only the four-bar

linkages show potential. Despite the more complex mechanics the linear motion of the cross-heads can be converted to rotation so that a link with ordinary bearings can accommodate the side-forces. The remaining drive mechanisms proposed seem inappropriate for the use in large multi-cylinder engines because of the complexity and close tolerances involved.

In Chapter 3 it was shown that the double-acting alpha-type is able to provide the largest specific power while being of relatively simple design. The two possible mechanical arrangements of this design were compared in Chapter 5, and it was shown that only the Siemens arrangement, as opposed to the Franchot arrangement, has the ability to reduce loads on the crank mechanism while providing a satisfying mechanical efficiency. As a result, together with the large phase angle necessary (Chapter 4), a large number of cylinders has to be arranged in a way such that the cylinder spaces can be connected like a daisy chain. The expansion space of the last cylinder has to be connected with the compression space of the first cylinder. In addition identical parts should be used for the heat exchangers and manifolds to reduce costs and to keep the loads uniform.

The most obvious design for a multi-cylinder reciprocating engine is the in-line arrangement. All pistons are placed in one plane and connected to one crankshaft. Figure 6.4 (a) shows a sketch of such a design. For a double-acting SE the cylinders have to be connected in a circular way. Manifolds and heat exchangers should be designed identically for each cylinder to reduce costs and to provide identical thermodynamic conditions on each piston. Using a heat exchanger design as shown in Figure 6.3 (b), (c), or (d) allows for identical parts which can be modified during assembly to accommodate the different mounting angles necessary. One disadvantage of such a design is the restriction of geometry that some components impose on others. As an example the cylinder diameter and the heat exchanger diameter are competing for space which makes compromises necessary; other arrangements show more degrees of freedom for the heat exchanger geometry.

One kinematic design that allows the use of identical parts of the heat exchanger, and an arbitrary number of cylinders, is an arrangement where two parallel crankshafts are connected to two cylinder banks. The crankshafts are timed by means of gears. Amongst others, such a system is successfully used in the engines built by Kockums [53,54]. Recently the automotive company MAHLE started a solar Stirling project in which the kinematic design chosen also incorporates parallel crankshafts [205]. The main reason for this design mentioned at the ISEC 2012 conference in Dubrovnik was that, despite the more complex crank arrangement, costs can be reduced with the design of identical parts on the heat exchanger side. Figure 6.4 (d) shows a sketch of such a design. As the distances between the cylinders can be kept identical on either side, shell and tube heat exchanger designs using the concepts of Figure 6.3 (b), (c), and (d) are possible.

Another arrangement using two cranks, and having the same advantages for the heat exchangers as the one above, is a set-up where two opposed cylinder banks face each other on the hot end, as can be seen in Figure 6.4 (b). Cylinders are arranged in pairs which are mounted concentrically. The heat exchanger assembly can then be accommodated in parallel to the cylinders using the design described in Figure 6.3 (a). The two cranks have to be timed by means of a toothed belt or a chain to maintain the desired phasing. Since the distance between the opposing cylinder heads can be adjusted freely, the length of the heat exchanger assembly can be chosen to represent a thermodynamically-favourable geometry free of packaging constraints. This is the main advantage over the preceding design.

A fourth possible design option is an engine consisting of two part-engines, each having its pistons attached to a radial drive mechanism (see Figure 6.4 (c)). The expansion space of one part-engine is connected to a compression space on the other part-engine; the expansion space of this cylinder is then connected to the next compression space on the other cylinder bank and so forth until all

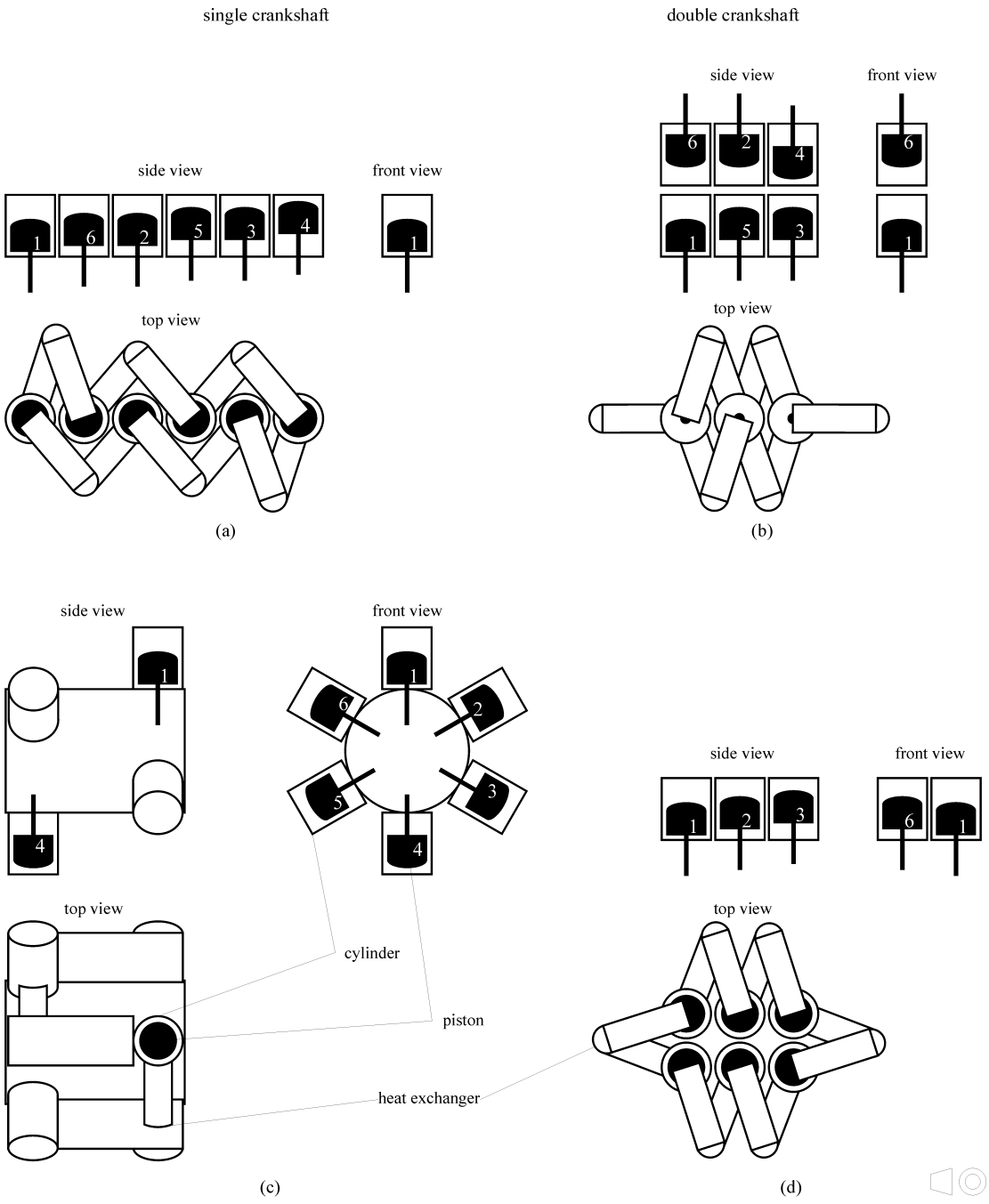

Figure 6.4: Kinematic arrangements for the double-acting LTD. A six cylinder solution is shown for each design, larger cylinder numbers can be generated accordingly. Option (a) features an in-line engine. In (b) the two cylinder banks are positioned facing each other. Design (c) shows a radial engine having two cylinder rows connected via the heat exchangers and the crankshaft, design (d) features two parallel crankshafts; cross-heads and crank-mechanism not shown, heat exchangers depicted only in top view.

working spaces are connected. All the heat exchangers are mounted parallel to the connecting crankshaft, and, as in the previous design, the distance between the two cylinder rows and hence heat exchanger length can be chosen freely. In order to make better use of the space available the generator can be placed between the two cylinder rows. Considering the large number of cylinders necessary for optimum phase angles the radial design allows the simplest possible crankshaft design. Only one crank web is necessary on each side and, as piston timing is a result of the cylinder position, no offset of the two webs is necessary if the two cylinder rows are placed accordingly.

Kinematic designs that feature the needs of large interconnected, double-acting engines are available, as discussed above. Generally every crank mechanism reduces the mechanical efficiency and introduces side loads. Using the Siemens arrangement is already one big step towards an efficient design. The only way to completely omit these, reduce wear, and enhance longevity is to directly use the linear motion of the pistons, as it is done with the free-piston engines.

6.2.2 Free-piston engines

The free-piston Stirling engine was invented by Beale in the 1960s [41]. Free-pistons, however, are not limited to SE [206]. In a free-piston arrangement no crank-mechanism is needed as the piston and, if applicable, the displacer are moved by gas and spring forces acting on the reciprocating members. Figure 6.5 shows a simplified set-up of such a system. A variation of having a kinematic piston and a free displacer also exists in the so-called Ringbom engine [207]. In order to achieve a resonant system the oscillating masses and the spring stiffness have to be tuned to the desired frequency. Free-piston engines operate only at this specific frequency which limits their application to power generation at a relatively constant power output [165, 208]. For the desired application of low-temperature power generation with a constant load this is no hindrance since tuning of the

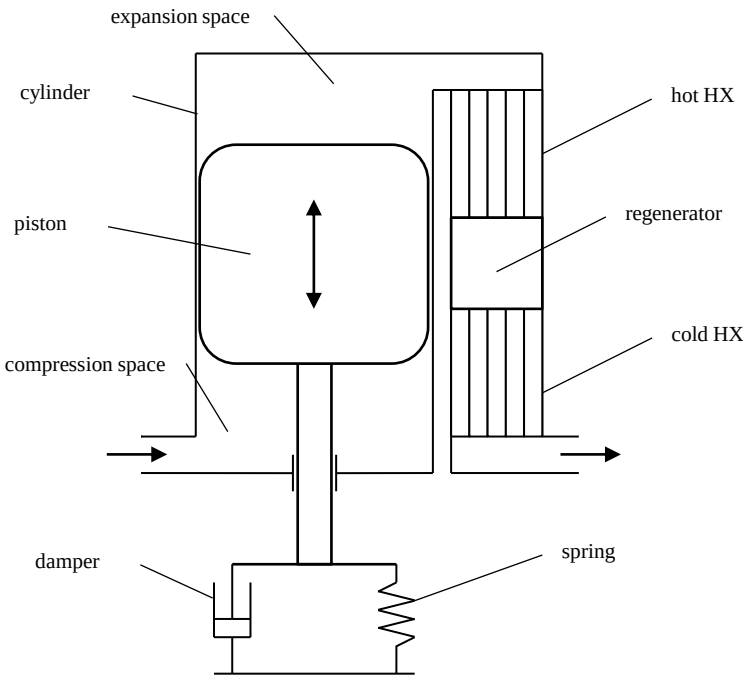

Figure 6.5: Set-up of a free-piston engine of the double-acting alpha-type. Gas forces, the spring force, inertia forces of the moving parts, and the force generated by a damper (i.e. friction, linear alternator) form an oscillating system

mass-spring system just needs to be made to match the low frequencies (<20 Hz) which result in optimum thermodynamic performance, see Section 4.3.2. Usually high temperature devices oscillate at 50 or 60 Hz if connected to the grid, or at even higher frequencies if operating independently (e.g. in space). Usually the reciprocating motion is converted directly into electricity by means of a linear alternator[2]. By omitting any sidewards motion of a crank mechanism no side-forces are generated in the system which can result in a virtually maintenance-free design. Typically the piston and the rod seals are designed to be a close tolerance clearance seal. Flexure bearings, a type of planar spring, are frequently used to centre the piston assembly and to avoid contact between the surfaces.

[2]Parallel with the evolution of the free-piston engines linear alternators have been customised and optimised for the application; efficiencies and reliability are now comparable to their rotating counterparts and can be found to be over 92 % [180, 209–213]

At NASA, free-piston Stirling systems have been investigated for many years and research is still ongoing. The most common design for use in a zero gravity environment is a two cylinder arrangement where the cylinders are mounted so that the expansion spaces are facing each other. The pistons are synchronised so that they always move in opposite directions and dynamic balance is achieved. So far the work has mainly focused on displacer engines; the largest engine built so far had a power output of 25 kW [39, 44, 51, 214–216].

Only recently it was proven experimentally that free-piston engines of the alpha-type show the potential for power generation [44, 45]. In their publications the authors emphasise the fact that interconnected engines of the alpha-type are less demanding when it comes to the tuning of the system, compared to the piston-displacer type. At Infinia large Siemens-type engines are under investigation for power ratings up to the megawatt range; the largest experimental engine has a capacity of 30 kW [110,217,218]. Kim and Berchowitz also investigated free-piston engines and showed possible arrangements for different engine sizes [46]. More recently experimental work on Siemens-type engines was carried out [47, 219].

In free-piston Stirling engines the reciprocating masses are relatively larger than in kinematic engines since parts of the linear alternators are rigidly attached to the pistons. In small single-cylinder engines no dynamic balance is achieved but the moving masses for small power outputs are relatively small. However, for large, multi-cylinder systems having massive pistons and alternators dynamic balancing has to be considered during the design. Figure 6.6 shows a concept for a large LTD which allows for a complete dynamic balance. The engine consists of a number of heat exchanger-piston-alternator assemblies (HEPA) as shown in Figure 6.6 (a). Each HEPA assembly is turned upside down relative to the previous one when connected, Figure 6.6 (b). All HEPA assemblies are located on a circle as shown in Figure 6.6 (c). If the number of cylinders is chosen to be the double of an odd number (i.e. 6, 10, 14, 18, 22, etc.) no rocking couple

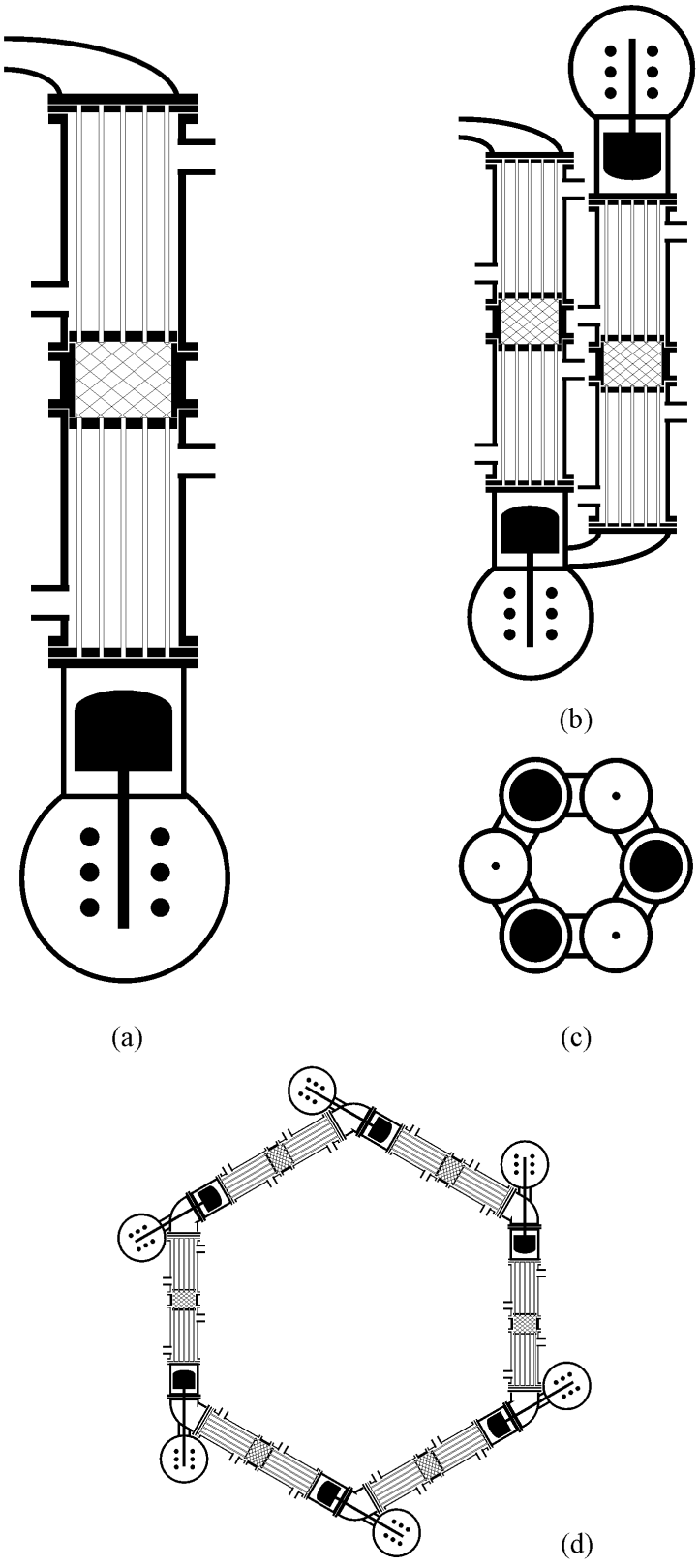

Figure 6.6: Possible free-piston arrangement for alpha-type LTDs. HEPA units (a) consisting of the heat exchangers, regenerator, pistons, cylinders, and alternators can be connected facing alternately up and down (b). All HEPA units are mounted on a circle (c). Alternatively units can be connected end to end (d).

is produced, since each pair of diagonally opposed pistons moves in parallel; the common centre of gravity then shows no net acceleration.

The arrangements with 18, 14, and 10 cylinder (thermodynamic phase angle 160°, 154°, and 144°) appear to be especially suited for the low-temperature application, as they provide the desired phasing. In the proposed configuration no extra dead volume is added on the hot end of the heat exchangers since the cylinder can be connected directly to the hot heat exchanger using a flange; the cold heat exchanger has to be connected to the compression space of the adjacent HEPA by means of a manifold. If designed for minimum pumping losses (smooth transitions, large diameter, short length) the resulting dead volume of the duct can be used to find the appropriate phase angle and hence number of cylinders (refer to Section 4.3.6). The thermodynamic phasing is a direct result of the number of interconnected cylinders and the resulting gas forces; White [45] reports evenly distributed phase angles for a four-cylinder free-piston arrangement. Additionally the alternators of opposed piston pairs (180° piston phase angle, e.g. piston one and four in a six cylinder engine) can be coupled electrically to stabilise operation. A duct between the alternator housings of these piston pairs could further stabilise the phasing and reduce hysteresis losses from gas compression in the alternator space.

An alternative arrangement using HEPA units is shown in Figure 6.6 (d). In contrast to the previous arrangement all units are mounted in one plane forming a polygon. The resulting engine is more accessible for maintenance but at the expense of a larger footprint. Dynamic balance cannot be achieved with a single engine due to the motion of the pistons.

Depending on the size of the alternator compared to that of the piston it could be possible to mount the alternator directly in the connecting manifold if it is small enough. In high temperature difference engines the alternator usually uses slightly more space than the swept volume; in the case a low temperature

engine it is hence very likely that the alternator is much smaller than the volume swept by the piston. By placing the alternator directly in the manifold the close tolerance seal for the piston rod can be saved. Only one reciprocating seal is then needed per cycle which also facilitates alignment.

Like some of the kinematic arrangements described above, the proposed free-piston design using HEPA units shows the advantage of having the length of the heat exchangers unconstrained. Only the diameter of the heat exchangers and the regenerator should not exceed the diameter of the alternator housing in order to keep the footprint of the engine small. By choosing suitable lengths for the cylinder and the connecting ducts, the hot heat exchangers can be located in one plane, thereby reducing piping. If using a thermosiphon a pressure vessel of simple design can be constructed to combine these heat exchangers in a condenser. Two dedicated cold ends are also formed where the working gas, the seals, and the alternators are cooled.

The most promising options found for a kinematic and a free-piston engine using a low-temperature heat source are thought to be the radial engine with two cylinder banks or the free-piston arrangement using parallel HEPA units. Both designs feature symmetric design of the heat exchangers and manifolds, small dead volumes, good dynamic balance, simple designs without complex parts, and a compact design. The kinematic design has the advantage that the electric alternator is an off-the-shelf product available in a large variety of sizes. The engine is also not limited to a specific frequency, which is not the case for the free-piston engine. Here, the frequency range is very limited which is not a problem for a grid-coupled device. The main advantage of this design is the further reduction of side-forces which increases efficiency and longevity of the system.

6.3 Crankcase design and working fluid containment

For the design of the crankcase two basic layouts are available: atmospheric and pressurised. The non-pressurised design is usually only combined with the kinematic engine; a pressurised housing is preferred for free-piston engines and can also be used with kinematic engines.

6.3.1 Non-pressurized crankcase

The greatest advantage of an atmospheric crankcase is the reduced weight because only the loads from the pistons have to be supported; high pressures are restricted to the cylinders and the heat exchangers. When SE were designed for automotive applications system weight and power density were important variables [23]. The components in the crankcase can be designed similar to internal combustion engines with oil sump and journal bearings. The greatest design challenge in this layout is the piston rod seal which has to seal over a large pressure difference ($p_{max} - p_{ambient}$) and which also has to prevent oil from entering the cylinder spaces. At Philips a solution in the form of the so-called 'roll-sock' seal was found and optimised; it consists of a rolling diaphragm which has the gas pressure acting on one side balanced with pressurised oil on the other [23].

A more common design can be found in reciprocating gas compressors (Figure 6.7): crankshaft and cross-heads are placed in the oil-lubricated crankcase. The piston rods are sealed using an oil-wiper packing. Since the oil film on the rod cannot be removed completely, an oil-slinger is placed on the rod to stop the advance of the oil film. An intermediate section of the length of the stroke makes sure that the oil-free zone and the lubricated parts do not overlap, so that the working fluid is not contaminated. Next to the piston a pressure packing,

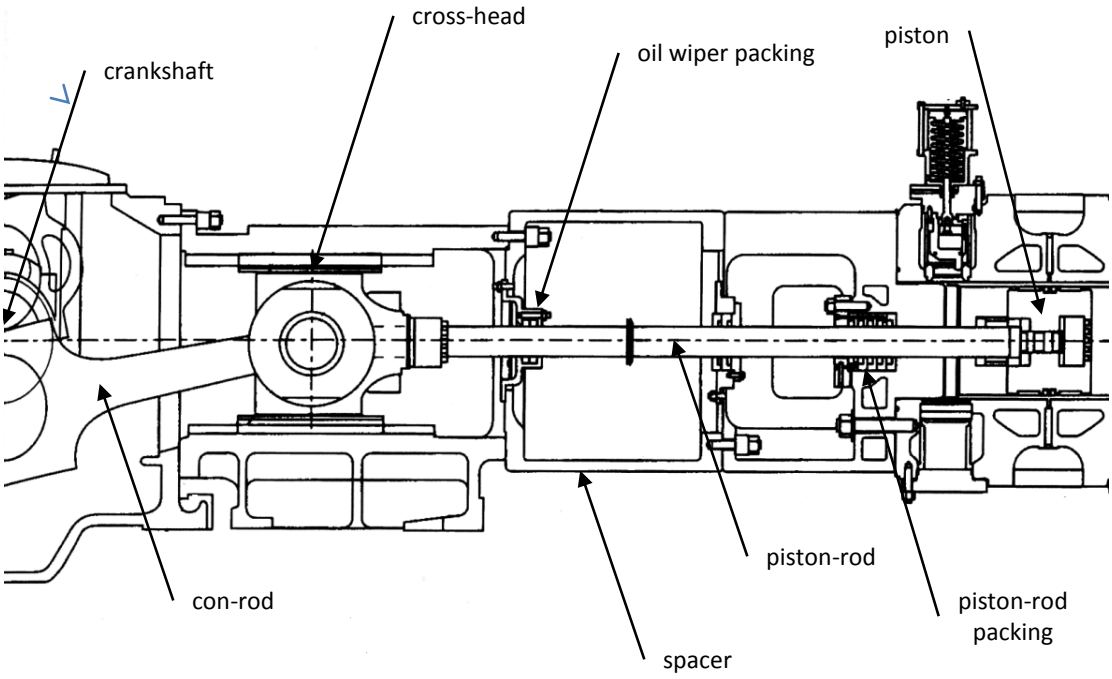

Figure 6.7: Typical set-up of an 'oil-free' gas compressor with the crankshaft and cross-head oil-lubricated on the left and the dry-running piston on the right. [173]

often water cooled, seals the compressed gas against the atmospheric pressure. Although this set-up represents a solid design solution its drawback is the bulky cross-head piston-rod assembly and the high pressure-difference piston-rod seal needed for each cylinder. Each of these seals generates friction which diminishes the usable power output.

It is thought by the author to be highly beneficial, especially for the low-temperature application, to omit a high pressure difference seal for every single piston and with it an additional parasitic loss mechanism by pressurising the crankcase. Depending on the design, only one rotating high pressure difference seal is needed if the shaft pierces the housing, or none at all if the energy is converted within the pressure vessel as it is explained in the following section.

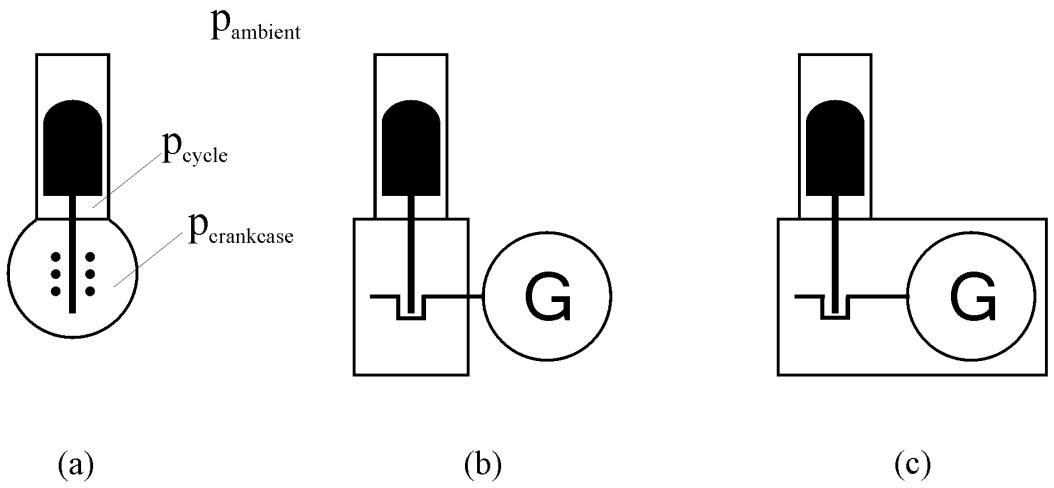

Figure 6.8: Variations of pressurised crankcase designs. Free-piston engine with linear alternator (a), kinematic engine with external (b) and internal (c) electrical generator. Designs (a) and (c) do not need the additional rotating seal at the crankshaft to seal against the high pressure difference against the ambient.

6.3.2 Pressurized crankcase

If the electrical generator is placed in the crankcase a sealed pressure vessel can be created (Figure 6.8 (c)). Doing so allows for a hermetically sealed engine, with a largely reduced need for working fluid top up as there are no reciprocating or rotating seals to the ambient pressure. Instead of a rotating shaft the engine's power output is an easily sealed cable. The crankcase is kept oil-free which eliminates the problem of working fluid contamination and regenerator blockage in the case of a seal failure; in addition oil-free engines become independent of the orientation, i.e. mounting the cylinders upside down becomes possible.

Hirata shows experimental results where an engine having a pressurised crankcase is transformed from having the electrical generator outside of the pressure vessel to a electrical generator in the pressurised shell [176] (from Figure 6.8 (b) to (c)). By omitting the rotating pressure seal the generated electrical power could

be increased significantly. Carlqvist proposed such a design for a kinematic design [220]; amongst others, the Whispergen engine [81,82] and all engines designed and built by the University of Denmark and StirlingDK (its spin-off company) feature this design and no evidence could be found that the greased bearings and specially designed cross-heads suffer from mechanical issues [50, 153, 154, 172, 197].

As opposed to internal combustion engines, where the loads from the explosive combustion show sharp, pronounced peaks, SEs deliver power rather smoothly which can increase bearing lifetime. Low-temperature engines provide power even more evenly than HTDs, as can be seen comparing the pressure plots in Figure 4.8. In free-piston devices no rotating bearings are needed since the motion is only linear. Gas bearings can be used to separate sliding surfaces.

If the gas volume of the crankcase remains constant, the pressure in the crankcase will stabilise to the mean cyclic pressure. The introduction of a check-valve between compression space and crankcase can reduce the pressure in the latter to the minimum cyclic pressure, the amount of gas needed to fill the crankcase, the stresses on the shell (material savings), and windage losses of the generator.

Optimisation of the thermodynamic side of the LTD showed that the pressure amplitude has to be kept relatively small in order to keep the working fluid temperature low during compression (see Sections 4.2.6 and 4.3.7). As a result the piston rod seal has to seal only a small pressure difference. Leaking gas is not lost but returns to the compression space when the direction of the pressure difference changes. Siemens arrangements having large cylinder numbers (or phase angles) reduce the net force on the piston rod to a minimum, as expansion and compression forces are balanced to a high extent (see Chapter 5). The rod can thus be reduced in diameter compared to other thermodynamically equal designs. The smaller the diameter and the smaller the pressure difference the less demanding the conditions for the seal.

For non-contact seals such as clearance seals, which are commonly found in

free-piston Stirling engines (for references see previous section) and also in some gas compressors [221, 222], losses due to friction are inherently lower than in contact seals where the seal is pressed against the reciprocating part. This is especially true if only a small pressure difference has to be sealed. A low friction rod-seal is one step closer to an efficient and reliable LTD; the pressurised crankcase is thus favoured for the low-temperature application. In combination with the internal electrical generator possible losses are reduced to a minimum.

6.4 Working fluid selection

Walker gives a good introduction to the different working fluids usable in SEs and their properties [22]. A summary of the properties of interest for the most commonly used working fluids is also given in Appendix C. Although exotic combinations, such as compounded or two-phase working fluids, have been proposed [22,223], the only working fluids actually found in SE are hydrogen, helium, and nitrogen/air.

Simulation and the literature indicate that the selection of the working fluid has a strong influence on engine performance. The current work shows, in Sections 3.3.1 and 4.3 that (provided frequency and heat exchanger geometries are adjusted):

- hydrogen has the ability to double the indicated power compared to helium
- helium has the ability to double the indicated power compared to nitrogen/air; thus the use of hydrogen can quadruple the indicated power output
- optimum phase angles (and thus number of cylinders in the Siemens arrangement) are smaller for hydrogen and nitrogen compared to helium due to their different adiabatic indices

- achievable frequencies are lowest for nitrogen/air, higher for helium, and highest for hydrogen which is directly reflected in the power output

The working fluid affects the performance and design of the SE through multiple ways, and is therefore a complex decision. The fluid affects the power, and hence the physical size engine and/or operating settings of the engine. It also affects the efficiency and hence the viability of harvesting low temperature difference heat sources. There are also cost, and in the case of hydrogen and air, safety issues to consider. These and other factors are reviewed below.

Specific power density and implications for engine layout

The higher the specific power of an engine for a specific mean pressure the lower the capital costs to install a certain capacity. If a superior working fluid is used for a desired capacity, the engine can either be designed to be smaller in size, run at a lower frequency or at a lower pressure, and savings can be made due to material costs or increased longevity of the system.

It was shown in Sections 3.3.1 and 4.3 that the phase angle for optimum power output in the proposed temperature range is smaller for hydrogen and nitrogen (around 150°) than for helium (around 160°). According to Figure 3.22 this corresponds to a reduction from 18 to 12 cylinders respectively in the Siemens configuration. This reduces the number of parts and the complexity of the engine significantly.

In Table 6.1 alternative engine layouts optimised for the different working fluids are proposed. The He-labelled engine layout represents the benchmark optimisation of the LTD discussed throughout Chapter 4 in detail. To achieve the desired phasing 18 cylinders are necessary. At a mean pressure of 5 MPa, a frequency of 1000 rpm, and the dimensions given, an indicated power output (P_{total}) of 94 kW is possible. With hydrogen (H_2) as the working fluid the necessary

number of cylinders (NoC) to achieve the optimum phase angle is reduced to 12. Having the identical cylinder size this 12-cylinder hydrogen-filled engine provides the same power output as its helium-filled 18-cylinder counterpart. In fact, in addition to the number of cylinders being reduced, fewer tubes are required for the heat exchangers (N_{HX}). The mean pressure ($H_2 - p_{mean}$) or the frequency ($H_2 - f$) can be reduced slightly, too. Another benefit of the use of hydrogen is the ability to increase the efficiency (E) by 15 %. A better efficiency for identical power output directly reduces the costs of cooling per kW installed. Hydrogen is thus capable of reducing capital costs significantly, not only by reducing engine size and complexity but also by reducing the size of the cooling system.

Table 6.1: Optimised engine layouts for different working fluids and identical power output

	He	$H_2 - p_{mean}$	$H_2 - f$	N_2
P_{total} / kW	94	94	94	**3 x 31**
E / -	0.088	0.101	0.102	0.088
α	160°	150°	150°	150°
NoC	18	**12**	**12**	**12**
$P_{cylinder}$ / kW	5.2	7.8	7.8	2.6
bore / m	0.2	0.2	0.2	0.2
stroke / m	0.1	0.1	0.1	0.1
N_{HX}/ -	1000	**700**	**650**	1000
L_{HX} / m	0.17	0.22	0.22	0.18
P_{reg} / -	0.92	0.86	0.85	0.93
L_{reg} / m	0.020	0.021	0.021	0.032
m_{gas} / kg	0.710	0.217	0.223	3.637
p_{mean} / MPa	5.0	**4.7**	5.0	5.0
f / rpm	1000	1000	**920**	**400**

For nitrogen as the working fluid the situation is somewhat different. Due to the large fluid friction the operating frequency has to be lowered significantly to achieve optimum performance. With the number of cylinders reduced to 12 in order to achieve the optimum phase angle, three engines of the size of the hydrogen engine are necessary to reach the desired power output of 94 kW. Alternatively larger cylinders could be employed, or a higher level of pressurisation could be

used, to reach the desired power output with two or only one engine. Since the efficiency and hence the heat to be rejected to the environment of the nitrogen filled engine is identical to the efficiency of the engine layout for helium, the external cooling system can be sized identical. Overall the amount of hardware needed for the nitrogen-filled engine is significantly higher than for the other two options - a fact which cannot be balanced by the use of a more 'user-friendly' working fluid. Compared to the hydrogen system the mechanical efficiency is worse since there are either more or heavier moving parts, another drawback of nitrogen as the working fluid.

The inherently low efficiencies at low temperature differences lead to relatively large engines compared to high temperature devices. It is thought that the use of nitrogen or air is not an appropriate option as the performance is low, meaning that engines become too large and therefore too expensive. The same argument could be applied to helium but possibly undesirable consequences of using hydrogen such as flammability, material embrittlement, and permeability make it necessary to have a closer look to evaluate the different options.

Hydrogen: safety issues

A commonly predominant thought associated with hydrogen is the fact that it burns quickly if mixed with oxygen and ignited. What makes for a spectacular school experiment does not apply directly to the SE. Of course care must be taken when handling hydrogen, and appropriate safety standards must be established; a broad base of knowledge and experience for handling hydrogen is available [224–226]. The high pressure in the SE prevents oxygen from entering the system so that an explosion of the pressure vessel is highly unlikely. In fact, no report of accidents caused by the use of hydrogen in SEs has been found in the literature; the only known accident reported happened with air as the working gas which

mixed with oil leaking from the crankcase and formed an explosive mixture inside the engine [23].

Hydrogen: material compatibility

Another issue with hydrogen is that it cannot be used in conjunction with certain materials as it can cause embrittlement in some metals. Even though reduced by this fact, the choice of materials is still large. Austenitic steels, brass, copper, aluminium, and their alloys are not subject to embrittlement in the proposed temperature range [227]. The Ni-steels (Inconel alloys) commonly used for the hot heat exchangers of high temperature engines cannot tolerate a hydrogen atmosphere, but are necessary to provide sufficient creep resistance at the elevated temperatures which is one reason for the exclusive use of helium or nitrogen in commercial high temperature applications. However, for low temperature differential engines such expensive alloys are not necessary which facilitates the use of hydrogen. The other working fluids helium and nitrogen are much less demanding when it comes to choosing suitable materials.

Hydrogen: volatility

Due to the small molecular size of hydrogen it is more difficult to contain in a pressure vessel than gases with larger molecules. The leakage rate through a solid increases with increasing pressure difference, decreasing wall thickness, and increasing temperature [228]; it is also dependent on the material of the solid. Typically the smallest wall thickness with the highest temperature and thus highest permeability found in SEs is located in the hot heat exchangers. To prevent loss of working gas through these components, high temperature engines using hydrogen as the working gas have their hot heat exchangers (at least the tubular type) covered with a thin silicon-based film [23]. Silicon has a much

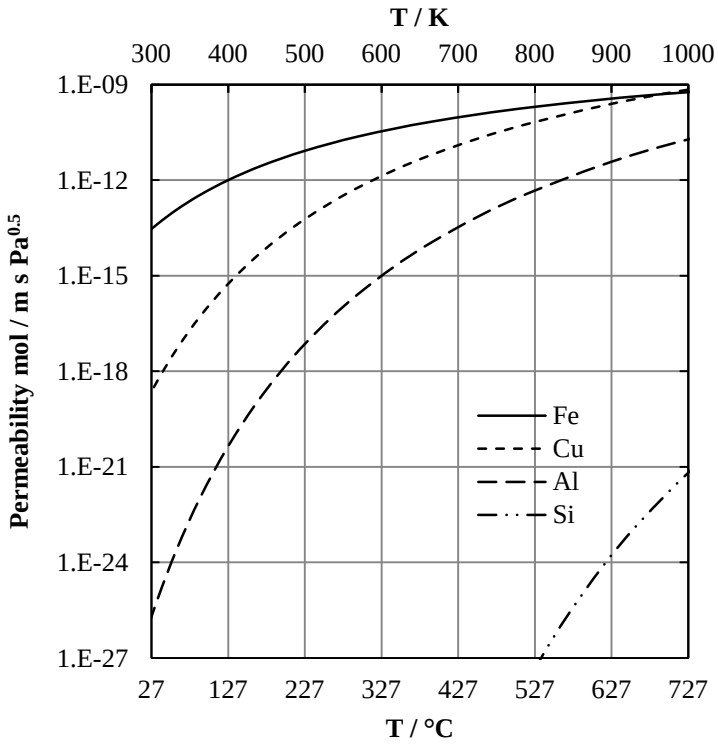

Figure 6.9: H_2 permeability vs. temperature modified after [228]

lower permeability for hydrogen than metals. Figure 6.9 shows the temperature-dependent permeability of different materials; it can be seen that pure silicon has a permeability many orders of magnitude smaller than iron. In iron the permeability for hydrogen is almost three orders of magnitude lower at 450 K compared to 1000 K. Aluminium and copper show even lower values and could be used as an internal tube liner or, if the external heat carrier fluid permits, as the heat exchanger material. The original approach of a silicon-based film would be another option to effectively reduce the leakage rate.

Piston seal leakage

In Section 5.4 it was shown that power losses due to piston seal leakage are also dependent on the viscosity of the working fluid (Equation 5.5). With the viscosity of hydrogen being approximately half the viscosity of helium, these losses double

if hydrogen is used instead of helium (see Appendix C for fluid properties). If, however, the Siemens configuration is chosen over the Franchot configuration (see Chapter 5.4) these losses still remain negligible.

Working fluid demand, costs, and availability

For one gas circuit of the LTD engine discussed in the previous chapters the amount of working fluid (m_{gas}), at 50 bar pressure and a phase angle of 160°, is 0.02 kg for hydrogen, 0.04 kg for helium, and 0.28 kg for nitrogen. Generally, the availability of the three gases is high. Since hydrogen and nitrogen are found in water and air, shortage or sudden increase in cost are highly unlikely. This is not quite the case for helium. Compared to hydrogen, helium, being a noble gas, is much more expensive since it is much more difficult to extract and world wide demand is high and growing for various applications [229]. Glowacki et al. quote the 2011 US market price for grade A helium (99.996 % purity) to be about USD 34 kg^{-1} [230]. The price for hydrogen generation is estimated to be between USD 0.4 and USD 3 kg^{-1} for fossil energy sources and up to USD 7.5 kg^{-1} for renewable energy sources [231]. Bonnici et al. estimate the price of hydrogen as USD 5.5 kg^{-1} and the price for low grade balloon helium (which has to be refined for use in SEs) as USD 14 kg^{-1} [232]. The cost for one single filling of the engine configurations proposed in Table 6.1 would add up to between USD 0.089 and USD 1.672 for the 12-cylinder engine using hydrogen; for helium one filling is estimated to be around USD 25. In any case the gas price is not a big cost contributor. Even if the hydrogen filling were to be renewed daily, annual costs would add up to a sum between USD 33 and USD 610; for helium the containability is much less of an issue and hence associated cost would be smaller. A positive side effect of hydrogen is that it can be generated easily from water by electrolysis on site and does not have to be carried in which is an advantage for remote operation or low availability of the fluid.

Conclusion

The purpose of this section was to evaluate the suitability of the different working fluids, with a particular focus on the situation of low temperature difference power generation (as opposed to the high temperatures more commonly used in SEs). Given the thermodynamic challenges of harvesting useful work at low temperature differences, power density and efficiency is an essential attribute of such a machine. Working fluids with low density and a small adiabatic index are preferred. A nitrogen engine will not deliver any useful work-output as the temperature difference drops to a certain value. Whereas a hydrogen engine will have a better work output for identical operating conditions, or be able to operate at even lower temperature differences thus accessing heat sources that are inaccessible to nitrogen. The geothermal and industrial world has more numerous and larger heat sources at low temperature difference than high, and consequently where work recovery is the objective then there is great advantage in having machines that can operate at lower temperature differences. This alone is a compelling reason to adopt hydrogen.

All things considered, hydrogen seems to show a higher potential at low temperatures than at high temperatures because it becomes easier to contain and the material choice is less limited. Compared to helium more care must be taken to fulfil the safety requirements associated with hydrogen, but a much higher power density of the engine becomes achievable. For engines of identical indicated power, the engine using hydrogen as the working fluid needs fewer cylinders to run optimally and can either reduce the frequency or the mean pressure (which increases the longevity of the engine and reduces material costs) compared to an engine running on helium. If the cost of meeting hydrogen safety requirements can be kept small compared to the benefits of the higher power density, hydrogen appears to be the most appropriate choice as the working fluid.

6.5 Cylinder, piston, and seal design

6.5.1 Reciprocating seals

Three types of seals can be distinguished: reciprocating seals to seal pistons and piston-rods; rotating seals to seal a shaft through a housing; and static seals to connect the various components. Static seals are not discussed any further here as the low temperature application does not have any specific implications on their design and standard solutions are available. Rotating seals are to be avoided, see Section 6.3; if external power conversion is necessary standard mechanical seals can be used to seal a pressurised crankcase to the ambient [233].

Finding an appropriate piston seal design, especially for high temperature differential engines, has been a challenge in the past and finding an appropriate balance between sealing effectiveness and seal life on the one hand, and mechanical friction on the other, was a major development time and cost consumer for the development of the WhisperGen[3]. Compared to the high temperature situation the low temperature difference operation has been shown to have some beneficial effects on the challenge of sealing the pistons and piston-rods, see Chapter 4 and Chapter 5:

- the Siemens configuration yields smaller pressure differences across the piston seal for identical phase angles compared to the Franchot arrangement
- the pressure amplitude acting on the piston seal in the Siemens configuration is much lower in the LTD than in the HTD, due to the lower total pressure amplitude and the higher optimum phase angle
- additionally, as the total pressure amplitude is much lower for the LTD, the pressure difference on the piston rod is much lower too

[3]John Raine (co-founder of WhisperTech), personal communication

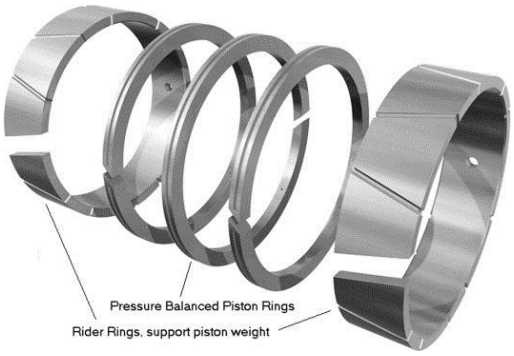

(a)

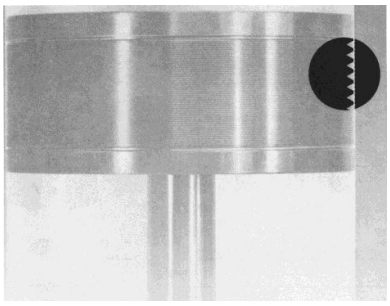

(b)

(c)

Figure 6.10: Reciprocating Seals: (a) contact seal, weight carrying rider rings on the outside - piston rings on the inside [234]; (b) non-contact labyrinth seal [173]; (c) gas supported rider rings for reduced wear [235]

- the piston rod diameter is smaller since the loads are much smaller; the resulting gap around the rod becomes shorter
- for the LTD thermal expansion is less so that tolerances change less during warm-up

Altogether the sealing of the reciprocating parts represents less of a challenge for the LTD. The smaller pressure difference on the piston seals allows for better sealing between adjacent gas cycles which is a welcome side-effect when dealing with low efficiencies.

The piston and rod seals used in Stirling engines and reciprocating, oil-free gas compressors (Figure 6.7 is a design example) have very similar design requirements due to the almost identical operating conditions. The absence of a liquid lubricant led to two basic designs which have evolved over the last decades. Figure 6.10 shows these basic designs.

The first design in Figure 6.10 (a) is a contact seal. On the ends of the piston are wide weight-carrying rings, the so-called 'rider'-rings. The sealing of the pressure difference is done by the pre-tensioned piston rings in between. Both ring types are made from PTFE combined with different filler materials providing a relatively low coefficient of friction ($\mu \approx 0.1$) and good wear resistance. Piston ring materials for oil-free operation are well researched and understood; filled PTFE show the highest wear resistance and lowest friction compared to other materials [234, 236–239]. However, due to the sliding contact between seal and cylinder wall the piston rings are subject to wear and have to be replaced regularly. At Stirling DK regular maintenance intervals including seal replacement are recommended every 4000 operating hours[4]. Due to the smaller loads and thus smaller resulting side-forces as well as the lower temperatures in the LTD it is anticipated that these intervals could be increased.

In the other design option this contact between piston seal and cylinder is eliminated and replaced by a narrow clearance. This very narrow gap of only a few microns is very demanding on the manufacturing process but reduces wear to an absolute minimum. It has been applied in Stirling engines for decades and has found its way into mass production with Infinia's solar power project [74]. Development for oil-free compressors in combination with a sealing labyrinth has been pioneered in the 1960s and could be established on the market despite the higher initial costs due to the lower down-times and mean times between overhauls [221, 222, 240–242].

[4]Jakob Falther (Stirling DK) - personal communication

A third design option which has emerged recently is a combination of the two principles described above: sliding piston rings seal the pressure difference and the rider rings have small nozzles and grooves to allow the process gas to support the piston's weight and to centre the piston in the cylinder. As for labyrinth seals the maintenance intervals can be extended due to the reduced friction [235].

All three options show the potential for solid piston seal and rod seal design in the LTD. The proven design in gas compressors and also the large scale production in Stirling engines made this crucial component more robust as well as sophisticated. If the available know-how is used instead of working on a custom-built solution no sealing problems are anticipated.

6.5.2 Piston and cylinders

Over the years different means for generating a volumetric change and to move the working fluid within the Stirling engine have been investigated: liquid pistons [243–246], diaphragms [42, 247–249], and standard pistons. Liquid pistons can be used to build simplistic water pumps but no effort has been made to generate power. Diaphragms and standard pistons, however, show the potential for power generation. In previous chapters it has been shown that:

- a relatively large swept volume is needed due to small specific power
- the pressure losses are crucial in LTD thus a larger bore is favoured
- a pressurised crankcase is favoured
- the temperature difference between hot and cold side is small for the LTD

Diaphragms used as power pistons have the advantage that a hermetic seal of the working space is achievable. No working fluid can leak past the piston, in this case the diaphragm, which is inevitable if conventional pistons are used.

Typically a combination of a large bore and a very small stroke is used, so that the deformation of the diaphragm material remains in the elastic region. For a pressurised low-temperature engine this results in very large diameters for the cylinders with very thick cylinder-walls. For a given pressure and swept volume this results in higher heat conduction in the cylinder wall and, for the case of a kinematic multi-cylinder engine unfavourable long crankshafts. Also not in favour of the diaphragm solution is the fact that the base of knowledge is relatively limited compared to more established and mature technologies such as conventional pistons. The inherently small pressure amplitudes found in low-temperature engines of the Siemens-type effectively reduce leakage past piston seals so that a hermetic seal can provide only a very small improvement (see Section 5.4).

The ratio of bore and stroke typically found in SEs of the alpha-type is about 2:1, a value suggested by Walker [22]. The idea behind it is to balance various effects since a larger diameter increases the leakage of the piston seal, its friction, and the heat conduction from the hot to the cold side (higher wall thickness - larger cross-section, shorter conduction path); a smaller diameter on the other hand increases the rubbing velocity and thus wear in a contact seal, and it also increases the size of the crankcase which, especially in the case of a pressurised crankcase, increases costs. For the special case of the LTD it is thought that a higher ratio, available space permitting, can be beneficial as the pressurised crankcase can be built smaller and material costs can be saved here. The large diameter of the bore, if also chosen for the regenerator diameter, can help to reduce thermodynamic losses by fluid friction (pumping losses). Care must be taken not to increase leakage and friction on the pistons excessively. The 2:1 ratio should serve as a good starting point for experimentation.

For high temperature difference operation, the displacer pistons in beta- and gamma-type engines, as well as the power pistons in double-acting alpha engines, are easily recognised by their unusual shape. Unlike the pistons in air compressors

or internal combustion engines where the diameter usually exceeds the height, the height of SE pistons or displacers is usually two to three times the diameter. This elongated shape is necessary to separate the hot and cold zone efficiently, reduce the heat flow between the two, and to keep the seal temperatures at a reasonable level. For the low temperature application the need for such an excessive piston dome is highly reduced. Shorter pistons and thus cylinders help to reduce reciprocating masses (reduced inertial forces and friction) and materials at the same time, which is another step towards an economical and efficient low-temperature difference engine.

Chapter 7

Comparison of Organic Rankine Cycle and Stirling machinery

In Chapter 1.1 Organic Rankine Cycle equipment (ORC) has been introduced as the standard solution for low temperature differential power generation. Not only geothermal power but also waste-heat from industrial processes and combined heat and power production (CHP) are growing markets. With the advance of technology nowadays, very low temperature differences can be used to produce electrical power, and small-scale power generation becomes more viable and economically feasible [250–252]. Nordquist gives an interesting overview on low-temperature ORC power generation in plants smaller than 1 MW_e over the last three decades [253]. Two companies currently dominate the ORC market worldwide: Italy-based Turboden [254] and the USA-based company Ormat [255]. Their smallest off-the-shelf turbine-based ORC systems start at 200 kW, and large units can produce 10 MW and more of electrical power. Units with smaller power capacities are available from other suppliers usually using screw or scroll expanders [256]. Even micro-scale (1 kW) ORC systems for domestic CHP are currently under investigation [257, 258].

Not only rotary expanders are used for the expansion of the organic vapour; the German company DeVeTec GmbH, aided by government funding, is developing a reciprocating piston engine with a power output between 100 and 200 kW_e [259, 260]. The engine is based on an internal combustion engine and comes in modular variable sizes with eight to twelve cylinders; a 20-cylinder engine is also planned. This ongoing project represents a positive indicator that large multi-cylinder reciprocating engines can be a viable solution for small power outputs in the hundred-kilowatt range.

A direct comparison of ORC and SE equipment for low-temperature power generation has not been available yet. An attempt for such a study has been performed by Bianchi [261] who compared different means to generate electrical power from waste-heat. Due to the lack of data and designs for SEs powered by low temperature heat sources, efficiency and specific power were extrapolated from a high temperature engine design. This chapter aims at giving a comparative study of a small scale ORC power plant and a SE of comparable capacity using representative data for the ORC and a suitable LTD design as proposed in this thesis. Providing information on the estimated size and efficiency of such systems will help to estimate the potential of the SE on the low-temperature, small-scale power generation market.

7.1 Hardware comparison

In Figure 1.1 the basic layout of an ORC plant is given which shows all the necessary components. The technical drawing in Figure 7.1 shows the layout of an actual, commercially available ORC plant. In the evaporator (1) the organic working fluid is heated and evaporated using an external energy source such as geothermal brine, exhaust gases, or any other form of low-grade heat. The hot vapour expands and transfers parts of its energy to a shaft via a screw-, scroll-,

vane-expander, a reciprocating device, or a turbine (2) as in this case. A generator (3) transforms the kinetic energy into an electric power output. In order to bring the working fluid back to its initial state it is condensed in the cooler (4). A feed pump (5) then pressurises the condensate back to the pressure in the evaporator and forces it back to the heater where it is evaporated again. Each of the components is needed only once per cycle in an ORC plant.

For a SE plant this set-up looks somewhat different. Basically all the components needed in the ORC can be found equivalently in the SE plant too but their numbers and size vary. As has been shown in the previous chapters, a double-acting multi-cylinder engine of the alpha-type shows various benefits regarding power output, efficiency, and longevity. The turbine and the feed pump of the ORC are replaced by the multi-cylinder engine. In the double-acting SE the expansion and compression processes both take place inside the engine at different times so no extra device for compression is needed here. Instead of one hot and one cold heat exchanger for the whole plant a much smaller heat exchanger pair is needed for each individual cycle.

The electrical generator component can be more or less identical for the two systems if a kinematic design is selected for the SE. Generally rotary machinery is operating at a higher frequency than the LTD which cannot exceed 2000 rpm due to the increasing influence of pumping losses (see Section 4.3.2). If the operating frequency exceeds the grid frequency, which can be the case for ORC expanders, either a gear box or an electrical inverter have to be used to adjust the frequency; both options reduce the overall efficiency of the plant. For a frequency lower than the grid frequency the pole number of the generator can be adjusted to synchronise the device with the grid ($N_{pole} = f_{grid}/f \times 2$). If, however, a free-piston design is employed one linear alternator is needed per cylinder.

Generally speaking, the SE provides a more compact and integrated solution of the various components needed which makes the engine less adaptable to con-

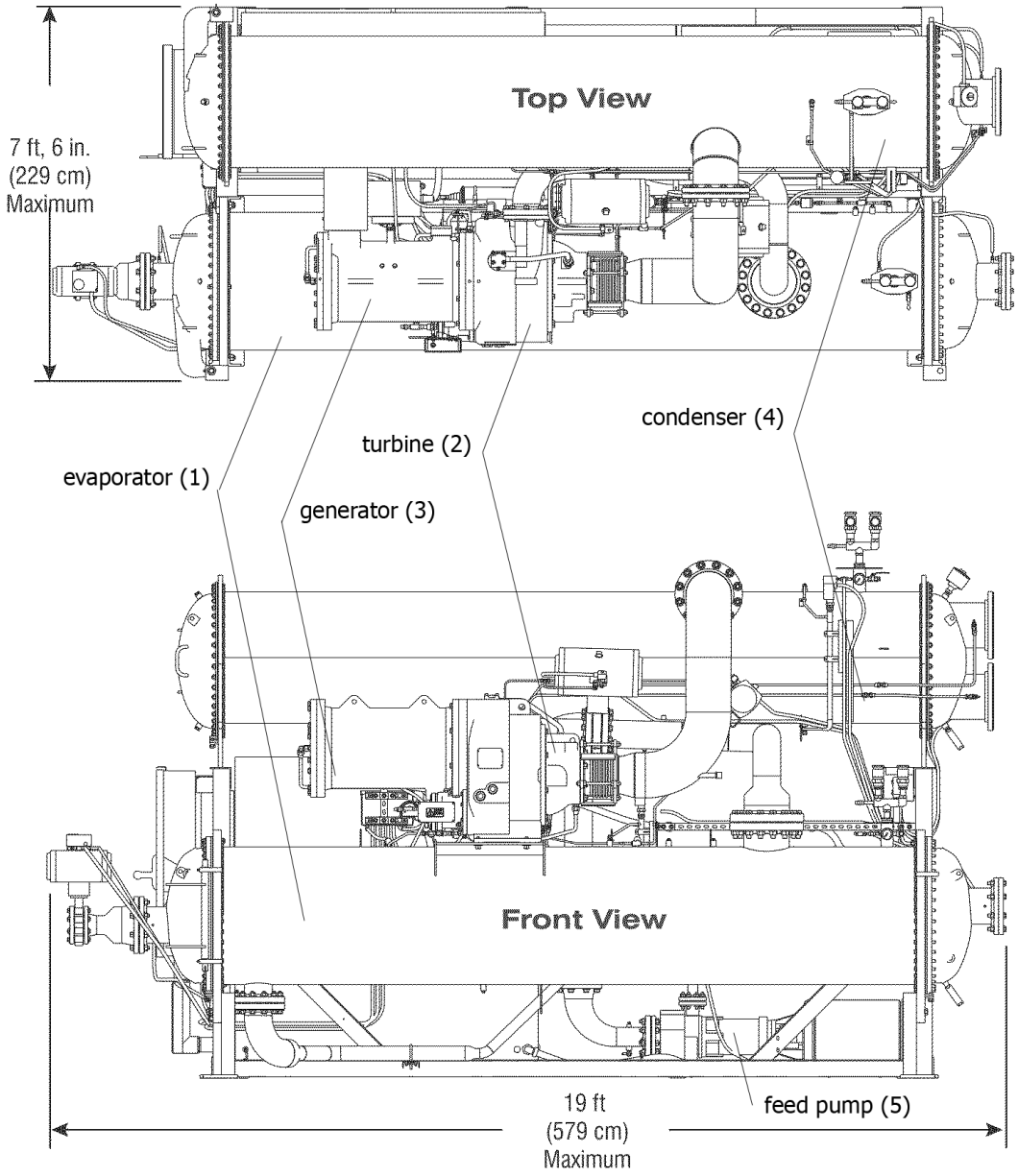

Figure 7.1: Layout of the 280 kW PureCycle plant [262]

ditions and sizes that differ from those on which the design was based. ORC systems are usually set-up using a modular system where components can be changed individually and adjusted to different operating conditions easily.

7.2 Working fluids

In Section 6.4 the three most common working fluids used in Stirling engines were discussed. As elaborated there, hydrogen shows the highest potential for low temperature applications followed by helium and then nitrogen. The three gases are all non-toxic; they are found naturally in the atmosphere and show no ozone depletion (ODP) or global warming potential (GWP). For the ORC the working fluids used are often hydrocarbons (e.g. pentane), other refrigerants (e.g. R134a), alcohols (e.g. ethanol), or other more exotic substances [252, 263]. In most cases these fluids exhibit a higher ODP and GWP, higher toxicity, and some are highly flammable. Despite the risks involved they are widely used for refrigeration and power generation purposes.

Since SE engines use a gas which is not subject to phase change, the amount of working fluid per unit is relatively small, as has been shown in Section 6.4. In an ORC plant the working fluid is found in its liquid phase and as a vapour. The density of the working fluids used (as a liquid) is typically three orders of magnitude higher than the density of the gases used in the SE and the evaporator is partially flooded. The total amount of working fluid necessary to fill the ORC plant is thus substantially higher and becomes a larger contributor to the capital costs. However, as Astolfi et al. report, typically the cost for ORC equipment are at least one order of magnitude higher than the cost for the working fluid itself [264].

7.3 Auxiliary power consumption

Independent of the power generating cycle, the working fluid has to be compressed after expansion to repeat the cycle. In the SE this is done by the reciprocating engine itself. In ORC plants an external, usually electrically powered, feed pump compresses the liquid fluid and transports it back to the evaporator. The amount of power consumed by this pump depends on the fluid used and the heat source temperature. Generally the lower this temperature the higher the power consumption of the pump. Borsukiewicz estimates the power consumption to up to 17 % of the electrical power output of the generator [265]. This is in accordance with Dickson who estimates this to be 9.5 to 17 % of the gross power of geothermal plants [266] and Velez (> 10 %) [251]. Pratt & Whitney's data sheets for the PureCycle give values over 7 %; Turboden data sheets for their smallest plants (200 and 300 kW) give values between 6 to 11 % at a heat source temperature of at least 200 °C, see Appendix D.

7.4 System pressure

The pressure of the working fluid in the SE is, if the engine is designed for minimum pressure losses, which is essential for the LTD, almost identical in the different parts of the engine. Over one cycle the pressure oscillates between the maximum and the minimum cycle pressure. The maximum cycle pressure is limited by the size of the engine and the material properties of the pressure vessel and the seal design. Between atmospheric pressure and this upper limit the pressure level can be selected freely, but care should be given to adjust (design) the heat exchangers for the expected density of the working fluid to avoid high pumping losses; generally the specific power output rises with the pressure (refer to Section 4.3.4). The highest pressure found in available experimental data (see Appendix A) is 220 bar

for a rather small swept volume. Hoeg et al. present a design for a maximum pressure of 135 bar in a LTD with a swept volume of 10 l per cylinder [107][1].

For the continuous thermodynamic process in the ORC the pressure depends on the state and the location in the plant. The pressure is highest in the evaporator, decreases during expansion, is lowest in the condenser, and the feed pump pressurises the fluid back to the evaporation pressure. Maximum and minimum pressures are thus dependant on the temperature of the heat source and sink and of the working fluid used; the lower the heat source temperature the lower the maximum pressure. As a result, for low temperature operation the maximum pressures are below 25 to 30 bar [251, 268]. Lower operating pressures reduce the material required for pressure vessels construction which is an advantage. On the other hand, power density cannot be increased simply by increasing the system pressure, as is possible in the SE.

7.5 Case studies

For high power outputs in the multi-megawatt range ORC plants using turbines are the established technology for low temperature power generation. However, for small power outputs in the range between 50 and 200 kW it is thought that a SE could provide a suitable alternative. In the preceding sections general differences between the two technologies have been highlighted. This section aims to compare a possible LTD design with commercially available ORC equipment. Two plants using different heat sources and temperature levels are investigated and compared to the SE solution. Since the likely manufacturing costs for a SE are not known this comparison is necessarily superficial as an economic evaluation. Instead of trying to give a cost analysis this section focuses on two aspects that can be quantified reasonably well: the amount and the cost of the working fluids, and the

[1] For comparison: modern Diesel engines reach maximum cylinder pressures of up to 250 bar in small fast running engines and up to 180 bar in large slow running engines [267]

dimensions required to accommodate the plant which allow to draw conclusions on material expenses.

7.5.1 PureCycle 250 kW - 150 °C

In Chapter 1 an ORC plant operating at a very low temperature difference was mentioned briefly. This plant uses two ORC units each providing about 200 kW_e. Figure 7.1 shows the layout of the plant including the overall dimensions. The design is originally based on refrigeration equipment from the American company Carrier [21] and was first marketed as PureCycle under the Pratt & Whitney brand, later by Turboden which are both part of United Technologies. At the moment the PureCycle plant is no longer available.

According to the data sheet the latest model, the PureCycle280, produces 272 kW gross power and 252 kW net power. It is designed to work with heat sources ranging from 91 to 149 °C. Detailed information about plant efficiency is not available; however, for the installation in Chena, Alaska, 8 % are reported which corresponds to 40 % of the Carnot efficiency [13, 14, 21].

In a 2009 study White cites a price of USD 484,220 per unit [269]. The overall dimensions of the plant are 5790 x 2290 x 3430 mm (L x W x H). A total weight of the operational plant is approximately 15 t of which 12.5 t account for the hardware and 2.5 t account for the fluids in the system. If identical volumes for the cooling water and the organic working fluid are assumed, approximately 1.5 t working fluid are used. The cost for the working fluid alone is estimated to be between USD 8,250 and USD 16,500 depending on the price for R-245fa, the refrigerant used. This corresponds to a price of USD 5.5 to USD 11 kg^{-1} [270, 271]. Since R-245fa has a relatively high GWP of over 1000, prices are expected to rise significantly if carbon taxing is applied; currently alternatives to replace it with a lower GWP fluid are being sought [272].

Table 7.1: Operating and design parameters PureCycle - LTD

	PureCycle	Stirling engine
prime mover	single stage turbine	12-cylinder
T_{hot} / °C	150	150
T_{cold} / °C	?	40
E_{ind}	?	0.087
E_{mech}	?	0.90
E_{gen}	0.96	0.96
P_{total} / kW	250	250
$E_{el} = E_{ind} \times E_{mech} \times E_{gen}$ / -	?	0.075
α	n/a	160°
$P_{ind,cylinder}$ / kW	n/a	24.4
bore / m	n/a	0.30
stroke / m	n/a	0.15
N_{HX}/ -	n/a	2300
L_{HX} / m	n/a	0.21
P_{reg} / -	n/a	0.90
L_{reg} / m	n/a	0.025
p_{mean} / MPa	< 2.0	5.0
f / rpm	?	1000
working fluid	R-245fa	H_2
m_{fluid} / kg	1500	0.753
overall dimensions (L x W x H) / m	5.8 x 2.3 x 3.4	2.3 x 1.2 x 1.2

The upper end of the usable source temperature of the PureCycle is 150 °C which is the same temperature as it has been used as the reference in the previous chapters. The temperature of the heat sink is not accessible from the data sheet. However, in order to create a comparable SE the same heat sink temperature (40 °C) as earlier is assumed. Other assumed parameters such as the various losses can be found in Table 7.1. In addition, the geometric and operating parameters necessary to produce a net power output (P_{el}) of 250 kW are listed. For such a low temperature and temperature difference a large number of interconnected cylinders are required. In this study a 12-cylinder engine using hydrogen as the working fluid was selected. However, other working fluids could be used with the consequences on design and performance highlighted in Section 6.4.

Figure 7.2 gives a comparison of the footprint of the PureCycle ORC plant and a SE optimised to reach an identical power output from twelve cylinders,

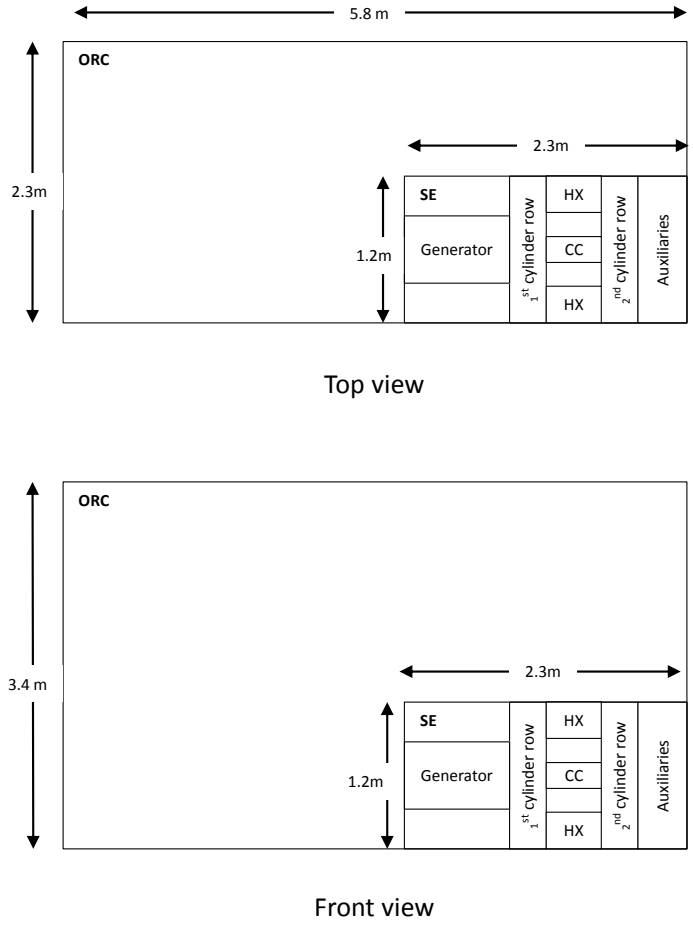

Figure 7.2: Footprint of the PureCycle ORC vs. a SE

according to the specifications in Table 7.1. The design employed for the SE engine is the radial engine design presented in Figure 6.4 (c). Two cylinder rows having six cylinders each are connected via a common crankshaft to the generator. The crankcase (CC) connects the two cylinder rows. Each expansion space is connected via a heat exchanger assembly (HX) with an expansion space on the other row. The dimension of the SE is based on the geometry of the individual components (bore, stroke, heat exchanger assembly length) as listed in Table 7.1 and appropriate dimensions for the radial crank drive, the size of the electrical generator is adopted from the PureCycle unit. Space for auxiliaries such as control electronics and a working fluid top-up device is allowed for too. Even if the footprint of the SE increases due to a necessary engine mount and piping, the size

of the whole structure is still significantly smaller than the size of the ORC, and it is expected that the material usage of the SE is lower.

7.5.2 **Turboden** 200 kW **-** 200 °C

Italian company Turboden who marketed the PureCycle plant until recently has terminated its commercial low temperature activities. The product portfolio does however still include a small scale solution for biomass or waste-heat applications; the data sheet can be found in Appendix D. The smallest unit produces an electrical net power output of 188 kW (200 kW gross, i.e. not considering the feed pump) with a net electrical efficiency of 15.2 % (16.2 % gross) from a 200 °C heat source and a 35 °C heat sink. Specific information about the plant size could not be found. Enquiries with Turboden have shown that the unit 'is containerised'; most probably a 20 foot container (approximately 6 m x 2.5 m x 2.5 m) is sufficient to hold the plant since a footprint similar to the PureCycle plant is assumed.

The elevated heat source temperature of 200 °C and the higher temperature difference is not only highly beneficial for the operation of the SE but also for its design. A smaller phase angle, which is about 130°, provides optimum performance at the higher temperature difference given. According to Figure 3.22 this can be closely matched with a 7-cylinder engine, or, if an even number of cylinders is preferred, with an 8-cylinder engine and, not as close, with a 6-cylinder engine. Compared to the 12-cylinder engine suitable for the lower temperature difference discussed above, the complexity of the engine design is reduced. In the case of a 6-cylinder engine it is thought that the HEPA free-piston design discussed in Section 6.2.2 and shown in Figure 6.6 is a viable choice, but a kinematic engine is possible too. Thus two concepts - a 6-cylinder free-piston engine and an 8-cylinder radial engine - are discussed in the following as alternatives to the ORC plant. In Table 7.2 data for the Turboden plant and the SE alternatives is presented. It can be seen that the available data for the ORC plant is relatively sparse but at

Table 7.2: Operating and design parameters Turboden-2 - LTD

	Turboden 2	SE max power	SE max power	SE max eff
prime mover	turbine	6-cylinder	8-cylinder	8-cylinder
T_{hot} / °C	200	200	200	200
T_{cold} / °C	40	40	40	40
P_{total} / kW	188	188	188	188
E_{ind}	?	0.141	0.155	0.176
E_{mech}	?	0.90	0.90	0.90
E_{gen}	?	0.96	0.96	0.96
E_{el} / -	**0.152**	**0.122**	**0.134**	**0.152**
α	n/a	120°	135°	135°
$P_{ind,cylinder}$ / kW	n/a	**36.3**	**27.2**	**27.3**
bore / m	n/a	**0.260**	**0.235**	**0.240**
stroke / m	n/a	0.13	0.12	0.12
N_{HX}/ -	n/a	1100	800	1100
L_{HX} / m	n/a	0.26	0.25	0.22
P_{reg} / -	n/a	0.89	0.85	0.91
L_{reg} / m	n/a	0.055	0.052	0.070
p_{mean} / MPa	?	5.0	5.0	5.0
f / rpm	?	1000	1000	1000
working fluid	?	H_2	H_2	H_2
m_{fluid} / kg	?	0.246	0.255	0.289
L x W x H / m	6 x 2.5 x 2.5	1 x 1.4 x 1.4	2.3 x 1 x 1	2.3 x 1 x 1

least information about the net efficiency (E_{el}) is available. The Stirling engines' layouts shown are a 6-cylinder engine optimised for maximum power density, an 8-cylinder engine optimised for maximum power density, and an 8-cylinder engine optimised to provide the identical efficiency as the ORC. Having fewer cylinders the 6-cylinder engine needs more swept volume per cylinder than the 8-cylinders to achieve an identical net power output (P_{el}). The engine optimised for efficiency needs a slightly larger swept volume than its power-optimised counterpart since efficiency is always increased at the expense of power density. A 6-cylinder engine with a higher efficiency could be designed just as for the 8-cylinder but is not shown here. Good efficiencies can thus be reached with both technologies - SE and ORC. The greatest advantage of the 6-cylinder over the 8-cylinder engine, be it a free-piston or a kinematic design, is the reduced number of complex parts (cylinder, HX) which has the potential to save costs without compromising much

on the thermodynamic side. The footprint is reduced slightly compared to the 12-cylinder design for lower temperature differences and could be reduced further by increasing either the frequency or the cycle mean pressure which are both assumed to have conservative values.

7.6 Conclusion

For the two temperature levels discussed it has been shown that the footprint of a SE of identical electrical power output is significantly smaller than that of a corresponding ORC unit. Pushing for higher frequencies and pressures, this footprint can be reduced even further. A highly reduced footprint indicates the ability to reduce costs because of the lower material usage anticipated. The number of parts in the SE is definitely higher but many parts such as cylinder, pistons, and heat exchangers are used repetitively which diminishes the negative impact.

The heat exchangers, piping, pump, and other parts used in the ORC plant are typically of larger dimensions, and a customised solution (e.g. modified heat exchangers, pumps, or turbines) can be implemented easily. The design of the SE is less flexible since the engine shows a high level of integration which also leads to the very compact design compared to the ORC where the single components can be installed rather remotely. It appears that both technologies can reach similar levels of efficiency which keeps the capital costs for cooling equipment comparable. An ecological advantage of the SE is that the working fluids used do not harm the environment neither by its ODP or GWP; for ORC working fluids this is not always the case. Table 7.3 summarises the major differences of the two systems.

Especially for the higher heat source temperature of 200 °C the Stirling engine appears to be a more promising solution than at the lower temperature since the number of cylinders, pistons, and heat exchangers can be halved while maintaining a desirable phase angle. Even the proposed free-piston arrangement seems to

Table 7.3: General differences in ORC and SE units

	ORC	SE
f / rpm	> 3000	< 2000
number of HX / -	2 / plant	2 / cylinder
number of expanders / -	1	> 6
type of expander	rotatory	reciprocating
p_{max}/ bar	< 30	< 200
$m_{workingfluid}/P_{el}$ / kg/kW$_e$	> 1	> 0.001
GWP	high	low
plant complexity	low	high
unit layout	modular	integrated

become a more feasible solution. Overall it seems that, especially for higher heat source temperatures, a SE design can be found which features simplicity and a compact footprint. Such a design shows the potential to replace ORC technology and appears to be worth pursuing. Given the nature of this study, a final statement for the low temperature 12-cylinder design cannot be made, but given the compactness of the plant and the potential for increased power density, further development does also not seem completely inappropriate.

Chapter 8

Summary and discussion

8.1 Outcomes

This thesis makes several novel contributions in three major areas to the field of power generation using SEs with the focus on low temperature differences: methodology, optimisation of the engine and the operating conditions, and conceptual engine design based on this thermodynamic optimisation. In detail these contributions are:

- This work provides a validation for the simulation of SEs using the simulation environment Sage. It proposes a model for a beta engine set-up and shows that calculated power output and efficiency are in good agreement with experimental data over a wide range of parameters. As a reference this allows for a more confident use of Sage and is an important addition for practitioners as well as academics.

- A side by side comparison of the performance of a large number of different engine layouts has been made, including discontinuous operating engines and more exotic configurations. It has been shown that engines using the

double-acting principle show the potential to outperform all single-acting designs. A novel configuration, the double-acting beta engine, has been investigated but has been shown to not be superior to the double-acting alpha design, neither thermodynamically nor mechanically.

- Suitable operating parameters such as phase angle and frequency have been identified using the established third-order engine model. These are quite different from the optimum parameters found in high temperature engines. Generally suitable phase angles are much higher and achievable frequencies much lower for the LTD. Conversions from HTD to LTD are therefore not easily possible.

- For the heat exchangers it has been shown that the hot and cold heat exchangers can be identical in their design without any negative impact on performance for the low-temperature difference situation. In comparison with HTDs, which require different materials and designs for the two heat exchangers, cost savings can be achieved.

- A sensitivity analysis of the optimised parameter set made it possible to identify freedoms and restrictions in the design of individual components as well as in the operating parameters. The phase angle, the regenerator porosity, and the temperature levels have been identified to be the most sensitive parameters.

- The adiabatic compressive heating has been identified to influence engine design strongly for low temperature applications. The negative effect on LTD performance can be mitigated by using large phase angles and hence number of cylinders. It has been shown also that the role of additional dead volume, such as in manifolds or ducts, plays a crucial and not necessary detrimental role in the operation of a LTD. Just as a large phase angle it can reduce the adiabatic compressive heating of the working fluid to a

level low enough to allow for low temperature difference operation. For optimized phase angles, however, engines without additional dead volume will still provide maximum power.

- Optimisation of power and efficiency is always a trade-off between the two parameters. The optimum combinations of the two performance indicators have been identified, so that it was possible to visualise the Pareto front of optimum solutions for this specific operating conditions.

- Double-acting alpha-engines can be built in two basic set-ups: the Siemens and the Franchot arrangements. It has been shown that the former provides a number of advantages over the latter: i.e. smaller forces in the piston rods; as a result side-forces which generate friction and thus directly influence the mechanical efficiency of the engine can be reduced significantly. This has a positive influence on the longevity of the system and also the weight. In addition piston seal leakage can also be reduced largely. Especially at the achievable low power levels the selection of the more efficient set-up is mandatory.

- The various insights gained from the thermodynamic analysis have been used to create conceptual designs of key components as well as of the system as a whole. Two novel engine set-ups are presented which are especially suited for the low-temperature difference case: one is a kinematic engine having two banks of radially connected pistons; the other is a free-piston device consisting of individual HEPA units which consist of the heat exchangers, the cylinder with piston, and the alternator mounted consecutively on a common axis. Both proposed set-ups feature simple design and identical parts for the heat exchanger components which is important for a cost-efficient design.

- A comparison between commercially available ORC plants and SEs with a

comparable net power output has been made. It has been shown that a SE plant provides a much reduced footprint compared to the ORC. For a slightly increased heat source temperature of 200 °C the possibility of using a simpler SE design has been identified which increases the likelihood of the adoption of SE technology for low temperature power generation.

8.2 Limitations and opportunities for future research

In this work the thermodynamic and conceptual foundation for a SE running on geothermal or waste-heat has been provided. The final goal of all future work is intended to be a fully-functional prototype ready for industrial production. A few necessary steps in between this work and the long term target are still to be accomplished; shortcuts can be expected to result in unsatisfactory outcomes as previous attempts to build a LTD showed.

Although the simulation model used for this study has proven itself through validation and is widely used, it is understood that modelling will always have its limitations. The confidence in the simulations is high due to the performed validation and the shared experience with other users; however, it is thought that as a first step some of the findings should be verified on a test rig, which also has the benefit that the model can then be fine-tuned for this specific application.

The most important finding that should be verified on a test rig is the correlation of optimum phase angle and dead volume for a specific temperature difference. An experimental set-up using liquid pistons is thought to be cost-efficient solution to gain the insights needed. Knowing the exact values for optimum performance will allow designers to find the best combination of the number of cylinders and volume in the manifolds necessary to connect them. With the simulation model

refined, other optimisation tasks can be performed virtually with much better accuracy.

Since the heat transfer between heat exchangers and working fluid is one of the key functional constraints in low temperature engines it has been proposed that it be improved by adding fins and grooves to enlarge the heat transfer area. The trade-off between increased heat transfer and pumping losses should be explored experimentally since the possibilities to do so in Sage are limited. This could be done on the same test-rig used for the study of the dead volume and phase angle correlation.

For a free-piston engine having a large number of inter-connected cylinders the ability of such a device to establish and maintain the desired phase angle should be studied in detail. So far, this has been done for 4-cylinder engines only; for engines having more than 10 cylinders, as needed for low-temperature operation, there is a place for further study to determine if additional means are necessary to operate the pistons at identical phase angles, or if the same measures as for the 4-cylinder engines are sufficient.

Finally, with the additional insights gained from such experiments, the design-and-built of a prototype engine could commence; the performance of the system as a whole could then be evaluated and the full benefit of the Siemens arrangement in a LTD could be shown.

8.3 Conclusion

This work represents a comprehensive study of SEs designed for low-temperature heat sources. Simulation models having different degrees of sophistication have been used to select a suitable engine type and layout for this particular and demanding application. It has been shown how particular engine and operating parameters influence engine performance and how they should be selected in order to accomplish a design which achieves the most out of the low efficiencies achievable. The thermodynamic insights gained have been used to created feasible conceptual designs with the focus on a simple engine layout with a maximum of common parts.

It has been shown that if certain design elements are incorporated into the design of low-temperature SEs the chances of an efficient, simple, and durable engine are higher than in previous designs. It must be acknowledged that, in order to have confidence in a final prototype engine design based on the insights derived from the simulation modelling of this research, further experimental verification of these findings is still necessary. Nevertheless, the evidence presented here is that, provided the design approach properly reflects and acknowledges the frequently non-intuitive insights from this research, SEs should be able to be used as prime movers to convert low grade heat to useful power output at reasonable efficiencies and power densities.

With the increasing costs of fossil fuels, and the thus increasing interest in energy saving, alternative fuels, and renewable energy, there will be a market for a prime mover which can tap into the widely available energy resource of low-grade heat. This could be one of the few applications where the heat source is exotic enough and the alternatives are sufficiently scarce, that Stirling engines could provide a suitable means of power conversion.

References

[1] L. Sinclair, S. Langdon-Arms, D. Smith, and G. McElroy, "Geothermal system engineering," final year project, Department of Mechanical Engineering, University of Canterbury, 2009.

[2] E. Huenges and P. Ledru, *Geothermal Energy Systems: Exploration, Development, and Utilization*. Wiley-VCH, 2010.

[3] R. DiPippo, *Geothermal Power Plants: Principles, Applications, Case Studies and Environmental Impact*. Elsevier, 2007.

[4] J. H. Horlock, *Combined power plants: including combined cycle gas turbine (CCGT) plants*. Pergamon Press, 1992.

[5] M. Mirolli, "Ammonia-water based thermal conversion technology: Applications in waste heat recovery for the cement industry," in *Cement Industry Technical Conference Record, 2007. IEEE*, pp. 234–241, 2007.

[6] Kalynacycle.net. http://kalinacycle.net/, last visited 15.05.2013.

[7] P. Valdimarsson and L. Eliasson, "Factors influencing the economics of the Kalina power cycle and situations of superior performance," in *Proceedings of International Geothermal Conference, Reykjavik*, pp. 31–39, 2003.

[8] S. Ogriseck, "Integration of Kalina cycle in a combined heat and power plant, a case study," *Applied Thermal Engineering*, vol. 29, no. 14, pp. 2843–2848, 2009.

[9] R. DiPippo, "Second law assessment of binary plants generating power from low-temperature geothermal fluids," *Geothermics*, vol. 33, no. 5, pp. 565–586, 2004.

[10] D. Chandrasekharam and J. Bundschuh, *Low-Enthalpy Geothermal Resources for Power Generation*. Taylor & Francis, 2008.

[11] J. W. Lund and T. Boyd, "Small geothermal power project examples," *Geo-Heat Centre Quarterly Bulletin (Klamath Falls, Oregon: Oregon Institute of Technology)*, vol. 20, no. 2, pp. 9–26, 1999.

[12] R. Bertani, "World geothermal generation in 2007," in *Proceedings European Geothermal Congress, Unterhaching, Germany, 30 May -1 June*, 2007.

[13] M. Aneke, B. Agnew, and C. Underwood, "Performance analysis of the Chena binary geothermal power plant," *Applied Thermal Engineering*, vol. 31, no. 10, pp. 1825 – 1832, 2011.

[14] G. Holdmann, "The Chena Hot Springs 400 kW geothermal power plant: experience gained during the first year of operation," *Chena Geothermal Power Plant Report, Chena Power Plant, Alaska*, pp. 1–9, 2007.

[15] G. Holdmann, "400 kW geothermal power plant at Chena Hot Springs, Alaska," final report prepared for Alaska Energy Authority, Chena Power, LLC, 2007.

[16] A. Franco and M. Villani, "Optimal design of binary cycle power plants for water-dominated, medium-temperature geothermal fields," *Geothermics*, vol. 38, pp. 379–391, 2009.

[17] H. Rothbaum, B. Anderton, R. Harrison, A. Rohde, and A. Slatter, "Effect of silica polymerisation and pH on geothermal scaling," *Geothermics*, vol. 8, no. 1, pp. 1 – 20, 1979.

[18] D. L. Gallup, "Investigations of organic inhibitors for silica scale control in geothermal brines," *Geothermics*, vol. 31, no. 4, pp. 415 – 430, 2002.

[19] I. Gunnarsson and S. Arnorsson, "Impact of silica scaling on the efficiency of heat extraction from high-temperature geothermal fluids," *Geothermics*, vol. 34, no. 3, pp. 320 – 329, 2005.

[20] S. Quoilin, R. Aumann, A. Grill, A. Schuster, V. Lemort, and H. Spliethoff, "Dynamic modeling and optimal control strategy of waste heat recovery Organic Rankine Cycles," *Applied Energy*, vol. 88, no. 6, pp. 2183–2190, 2011.

[21] J. J. Brasz, B. P. Biederman, and G. Holdmann, "Power production from a moderate-temperature geothermal resource," in *GRC annual meeting, Reno, Nevada*, 2005.

[22] G. Walker, *Stirling Engines*. Clarendon Press, 1980.

[23] C. M. Hargreaves, *The Philips Stirling Engine*. Elsevier, 1991.

[24] C. West, *Principles and Applications of Stirling Engines*. Van Nostrand Reinhold Company, 1986.

[25] I. Kolin, *The Evolution of the Heat Engine, Thermodynamics Atlas 2*. Longman Group Limited London, 1972.

[26] A. Bejan, "Models of power plants that generate minimum entropy while operating at maximum power," *American Journal of Physics*, vol. 64, no. 8, pp. 1054–1059, 1996.

[27] F. Curzon and B. Ahlborn, "Efficiency of a Carnot engine at maximum power output," *American Journal of Physics*, vol. 43, pp. 22–24, 1975.

[28] C. West, "Theoretical basis for the Beale number," in *Intersociety Energy Conversion Engineering Conference, 16th, Atlanta, GA, August 9-14*, vol. 2, p. 1886, American Society of Mechanical Engineers, 1981.

[29] J. R. Senft, "A simple derivation of the generalized Beale number," in *Energy - the spark and lifeline of civilisation, Proceedings of the 17th Intersociety Energy Conversion Engineering Conference ISECEC*, vol. 4, pp. 1652–1655, 1982.

[30] S. Iwamoto, K. Hirata, and F. Toda, "Performance of Stirling engines (arranging method of experimental results and performance prediction)," *JSME International Journal*, vol. 44, no. 1, pp. 140–147, 2001.

[31] J. Prieto, J. Fano, C. González, M. González, and R. Diaz, "Preliminary design of the kinematic Stirling engine using dynamic similarity and quasi-static simulation," *Proceedings of the Institution of Mechanical Engineers, Part C: Journal of Mechanical Engineering Science*, vol. 211, no. 3, pp. 229–238, 1997.

[32] J. Prieto, M. González, C. González, and J. Fano, "A new equation representing the performance of kinematic Stirling engines," *Proceedings of the Institution of Mechanical Engineers, Part C: Journal of Mechanical Engineering Science*, vol. 214, no. 3, pp. 449–464, 2000.

[33] H. Karabulut *et al.*, "An experimental study on the development of a beta-type Stirling engine for low and moderate temperature heat sources," *Applied Energy*, vol. 86, pp. 68–73, 2009.

[34] I. Iwamoto *et al.*, "Comparison of low- and high temperature differential Stirling engines," in *Proceedings of the 8th International Stirling Engine Conference*, pp. 29–38, 1997.

[35] M. Takeuchi and S. Suzuki, "Studie zur Konstruktion einer Niedertemperatur-Stirling-Maschine mit hoher Drehzahl - a study of designing high speed low temperature difference Stirling engine," in *Proceedings of European Stirling Forum 2000*, (Osnabrueck, Germany), pp. 347–354, 2000.

[36] M. Takeuchi, S. Suzuki, Y. Abe, and A. Kitahara, "Development of 1 kW class low temperature difference indirect heating Stirling engine unsing alpha+ type mechanism," in *Proceedings of the 13th International Stirling Engine Conference ISEC*, 2007.

[37] M. Takeuchi, Y. Abe, S. Suzuki, Z. Nakaya, and A. Kitahara, "Development of 10 kW class low temperature difference indirect heating Stirling engine using alpha+ type mechanism," in *Proceedings of the 13th International Stirling Engine Conference ISEC*, 2007.

[38] T. Finkelstein and A. J. Organ, *Air Engines*. Professional Engineering Publishing Limited, 2001.

[39] J. G. Schreiber, "Developmental considerations on the free-piston Stirling power convertor for use in space," Tech. Rep. NASA/TM-2007-214805, AIAA-2006-4015, NASA, 2007.

[40] R. Bauer, *Gescheiterte Innovationen: Fehlschlaege und technologischer Wandel*, vol. 893. Campus, 2006.

[41] W. Beale, "Free piston Stirling engines - some model tests and simulations," in *SAE International Automotive Engineering Congress Detroit, Mich. January 13-17*, 1969.

[42] E. Cooke-Yarborough, E. Franklin, J. Geisow, R. Howlett, and C. West, "Thermomechanical generator: an efficient means of converting heat to electricity at low power levels," *Proceedings of the Institution of Electrical Engineers*, vol. 121, no. 7, pp. 749–751, 1974.

[43] M. Dhar, "Stirling space engine program," Tech. Rep. NASA/CR-1999-209164/VOL1, NASA Glenn Research Center, 1999.

[44] S. M. Oriti and N. A. Schifer, "Recent Stirling conversion technology developments and operational measurements at NASA Glenn Research Center," Tech. Rep. NASA/TM-2010-216245 , AIAA-2009-4556, NASA Glenn Research Center, 2010.

[45] M. White, "The multi-cylinder free-piston Stirling engine - taking performance to a new level," in *Proceedings of the 3rd International Energy Conversion Engineering Conference (IECEC), San Francisco, CA*, AIAA 2005-5537, 2005.

[46] S.-Y. Kim and D. M. Berchowitz, "Specific power estimations for free-piston Stirling engines," in *Proceedings of the 4th International Energy Conversion Engineering Conference, IECEC*, AIAA, 2006.

[47] D. M. Berchowitz and Y.-R. Kwon, "Multiple cylinder free-piston Stirling machinery," *Journal of Power and Energy Systems*, vol. 2, no. 5, pp. 1209–1220, 2008.

[48] J. A. Duffie and W. A. Beckman, *Solar Engineering of Thermal Processes*. Hoboken, N.J. : Wiley, 2006.

[49] Cleanergy. http://www.cleanergy.com/, last visited 23.01.2013.

[50] H. Carlsen and J. Bovin, *9 kW Stirling engine for biogas and natural gas: final report*. Danish Energy Agency, 2001.

[51] S. M. Geng, L. S. Mason, R. W. Dyson, and L. B. Penswick, "Overview of multi-kilowatt free-piston Stirling power conversion research at Glenn Research Center," Tech. Rep. NASA/TM–2008-215061, NASA Glenn Research Center, 2008.

[52] Stirling DK. http://stirling.dk/, last visited 23.05.2013.

[53] H. Nilsson, "Submarine power systems using the V4-275R Stirling engine," *Proceedings of the Institution of Mechanical Engineers, Part A: Journal of Power and Energy*, vol. 202, no. 4, pp. 257–267, 1988.

[54] Kockums. http://www.kockums.se/en/products-services/submarines/stirling-aip-system/, last visited 10.12.2010.

[55] Infinia. http://www.infiniacorp.com/solutions/fueled-products/, last visited 21.05.2013.

[56] EHE-Whispergen. http://www.whispergen-europe.com/, last visited 07.12.2010.

[57] BIOS Bioenergy. http://www.bios-bioenergy.at/en/electricity-from-biomass/stirling-engine.html, last visited 07.12.2010.

[58] A. Gaun and E. Schmautzer, "Biomass-fuelled Stirling micro combined heat and power plants," in *International Conference on Clean Electrical Power, 2007. ICCEP '07*, 2007.

[59] F. Biedermann, "Small-scale CHP plant based on a 75kW hermetic eight cylinder Stirling engine for development, technology and operating experiences," in *2nd World Conference and Exhibition on Biomass for Energy, Industry and Climate Protection, 10-14 May 2004, Rome, Italy*, 2004.

[60] D. Berchowitz and Y. Kwon, "Environmental profiles of Stirling-cooled and cascade-cooled ultra-low temperature freezers," *Sustainability*, vol. 4, no. 11, pp. 2838–2851, 2012.

[61] Stirling Ultracold. http://stirlingultracold.com/, last visited 21.05.2013.

[62] Twinbird. http://fpsc.twinbird.jp/legacy/en/index.html, last visited 21.05.2013.

[63] Stirling Cryogenics. http://www.stirlingcryogenics.com/home/, last visited 21.05.2013.

[64] D. Veitch and K. Mahkamov, "Assessment of economical and ecological benefits from deployment of a domestic combined heat and power unit based on its experimental performance," *Proceedings of the Institution of Mechanical Engineers, Part A: Journal of Power and Energy*, vol. 223, no. 7, pp. 783–798, 2009.

[65] Microgen homepage. http://www.microgen-engine.com/, last visited 23.01.2013.

[66] bhkw-infothek.de. http://www.bhkw-infothek.de/nachrichten/10236/2012-12-03-hersteller-des-whispergen-muss-insolvenz-anmelden/, last visited 4.2.2014 (in german).

[67] pressebox.de. http://www.pressebox.de/pressemitteilung/bhkw-infozentrum-gbr/Verkauf-von-Whispergen-Stirlingmotoren-wegen-Insolvenz-vorlaeufig-eingestellt/boxid/559712, last visited 4.2.2014 (in german).

[68] Baxi. http://www.baxi.co.uk/renewables/combined-heat-and-power/ecogen.htm, last visited 2.4.2014.

[69] Navien. http://en.kdnavien.com/product/product_detail.aspx?skin=product&num=24, last visited 4.2.2014.

[70] Remeha. http://www.remeha.de/191/%3Cb%3EKraft-W%C3%A4rme-Kopplung%3C_b%3E, last visited 4.2.2014 (in german).

[71] Broetje. https://www.broetje.de/de/1265.htm, last visited 4.2.2014 (in german).

[72] Senertec. http://senertec.de/de/derdachs/dachs-stirling.html, last visited 4.2.2014 (in german).

[73] Viessmann. http://www.viessmann.de/de/ein-_zweifamilienhaus/produkte/mikro-kwk.html, last visited 4.2.2014 (in german).

[74] Infinia. http://www.infiniacorp.com, last visited 18.04.2013.

[75] solarserver. http://www.solarserver.com/solar-magazine/solar-news/current/2013/kw39/dish-stirling-csp-technology-provider-infinia-files-chapter-11-petition-to-continue-limited-business-operations.html, last visited 5.2.2014.

[76] Qnergy. http://www.qnergy.com/qnergy-has-acquired-the-assets-of-infinia-corporation-inc, last visited 5.2.2014.

[77] Ripasso. http://www.ripassoenergy.com/, last visited 18.04.2013.

[78] S. Simmonds, R. Corbishley, J. Hughes, G. Taylor, H. Hoffmann, P. Wieske, I. Reynolds, and D. Wise, "The development of the MAHLE 25kWe solar heated Stirling engine," in *Proceedings of the 15th International Stirling Engine Conference (ISEC)*, 2012.

[79] H. Carlsen and J. K. Bovin, "Progress report - 35 kW Stirling engines for biomass," in *European Stirling Forum, Osnabrueck*, 2000.

[80] Stirling Power. http://www.sp-usa.com/, last visited 5.2.2014.

[81] D. M. Clucas and J. K. Raine, "A new wobble drive with particular application in a Stirling engine," *Proc IMechE Part C: Journal of Mechanical Engineering Science*, vol. 208, pp. 337–346, 1994.

[82] D. M. Clucas and J. K. Raine, "Development of a hermetically sealed Stirling engine batterie charger," *Proc IMechE Part C: Journal of Mechanical Engineering Science*, vol. 208, pp. 357–366, 1994.

[83] N. W. Lane, "Commercialization status of free-piston Stirling machines," in *Proceedings of the 12th International Stirling Engine Conference, Durham, UK*, 2005.

[84] Cool Energy. http://www.coolenergyinc.com, last visited 18.04.2013.

[85] Sunpower. http://www.sunpowerinc.com, last visited 18.04.2013.

[86] M. B. Ibrahim and R. C. Tew, *Stirling Convertor Regenerators*. CRC Press, 2011.

[87] T. Takeuchi *et al.*, "Performance of new mesh sheet for Stirling engine regenerator," in *Proceedings of the 2nd International Energy Conversion Engineering Conference*, 2004.

[88] M. P. Mitchell, D. Gedeon, G. Wood, and M. Ibrahim, "Results of tests of etched foil regenerator material," in *Cryocoolers 14: proceedings of the 14th cryocooler conference*, 2007.

[89] A. Ross, *Making Stirling engines*. Ross experimental, 2011.

[90] G. W. Swift, *Thermoacoustics: A unifying perspective for some engines and refrigerators*. Acoustical society of America, 2002.

[91] R. Tew, M. Ibrahim, D. Danila, T. Simon, S. Mantell, L. Sun, D. Gedeon, K. Kelly, J. McLean, G. Wood, *et al.*, "A microfabricated involute-foil regenerator for Stirling engines," *NASA/TM-2007-214973*, pp. 1–37, 2007.

[92] M. B. Ibrahim, D. Gedeon, G. Wood, and J. McLean, "A microfabricated segmented-involute-foil regenerator for enhancing reliability and performance of Stirling engines. phase III final report for the radioisotope power conversion technology NRA," *NASA/CR-2009-215516*, 2009.

[93] M. B. Ibrahim, R. Tew, D. Gedeon, G. Wood, and J. McLean, "Microfabrication of a segmented-involute-foil regenerator, testing in a Sunpower Stirling convertor, and supporting modeling and analysis," in *Proceedings of the 6th International Energy Conversion Engineering Conference (IECEC)*, 2008.

[94] H. Takizawa, N. Kagawa, A. Matsuguchi, and S. Tsuruno, "Performance of new matrix for Stirling engine regenerator," in *Proceedings of the 37th Intersociety Energy Conversion Engineering Conference (IECEC)*, 2002.

[95] N. Kagawa, D. Kitahama, H. Takizawa, T. Takeuchi, A. Matsuguchi, and S. Tsuruno, "Performance of new matrix for Stirling engine regenerator," in *Proceedings of the 11th Stirling engine conference*, 2003.

[96] A. Matsuguchi, N. Kagawa, and S. Koyama, "Improvement of a compact 3-kW Stirling engine with mesh sheet," in *Proceedings of the 14th International Stirling Engine Conference (ISEC)*, 2009.

[97] Fondazione Bruno Kessler (FBK). Reneweable energy and environmental technologies unit, http://reet.fbk.eu/, last visited 23.05.2013.

[98] A. Organ, *Thermodynamics and Gas Dynamics of the Stirling Cycle Machine*. Cambrige University Press, 1992.

[99] L. Crema, F. Alberti, A. Bertaso, and A. Bozzoli, "Development of a pellet boiler with Stirling engine for m-CHP domestic application," *Energy, Sustainability and Society*, vol. 1, no. 5, pp. 1–11, 2011.

[100] J. R. Senft, *An Introduction to Low Temperature Differential Stirling Engines*. Moriya Press, 2004.

[101] I. Kolin, S. Koscak-Kolin, and M. Golub, "Geothermal electricity production by means of the low temperature difference Stirling engine," in *Proceedings World Geothermal Congress 2000, Kyushu - Tohoku, Japan, May 28 - June 10*, 2000.

[102] University of Saitama. http://www.nmri.go.jp/eng/khirata/stirling/kiriki/home.html, last visited 04.10.2013.

[103] F. Toda *et al.*, "Development of 300 W class low temperature differential Stirling engine," in *Proceedings of the 7th ICSC, Tokyo, JSME*, 1995.

[104] N. Kagawa *et al.*, "Design of a 100 W Stirling engine," in *Proceedings of the 7th ISEC, Tokyo, JSME*, 1995.

[105] Suction Gas Engine Ltd. http://www.suction.co.jp/, last visited 04.10.2013.

[106] B. Kongtragool and S. Wongwises, "A four power-piston low-temperature differential Stirling engine using simulated solar energy as a heat source," *Solar Energy*, vol. 82, pp. 493–500, 2008.

[107] A. Hoeg, T.-M. Tveit, and T.-A. Asphjell, "The development of a double-acting Stirling lab engine for low temperature heat utilisation," in *ISEC2009 - The 14th International Stirling Engine Conference, Groningen, the Netherlands*, 2009.

[108] C. C. Lloyd, "A low temperature differential Stirling engine for power generation," Master's thesis, Department of Electrical Engineering University of Canterbury, 2009.

[109] P. Gaynor, R. Webb, and C. Lloyd, "Power generation using low temperature differential Stirling engine technology," in *Proceedings of the World Geothermal Congress, Bali, Indonesia, 25 - 29 April*, 2010.

[110] M. A. White, S. Qiu, J. Wacknov, R. J. Wehrer, R. G. Mahorter, and M. F. Dufalla, "The multi-cylinder free-piston Stirling engine scaled to a megawatt-class conceptual design," in *Proceedings of the 13th International Stirling Engine Conference (ISEC)*, 2007.

[111] T.-M. Tveit, A. Hoeg, and T.-A. Asphjell, "A prototype alpha Stirling engine for low temperature heat recovery power generation," in *Proceedings of the 13th International Stirling Engine Conference ISEC*, 2007.

[112] Single Phase Power. http://www.sppower.no/, last visited 04.10.2013.

[113] T.-M. Tveit, A. Hoeg, and T.-A. Asphjell, "A simulation based interactive multi-criterion strategy for optimising Stirling-engine designs," in *ISEC2009 - The 14th International Stirling Engine Conference, Groningen, the Netherlands*, 2009.

[114] W. R. Martini, "Stirling engine design manual," tech. rep., Washington Univ., Richland (USA). Joint Center for Graduate Study, 1978.

[115] G. Schmidt, "Theorie der Lehmannschen calorischen Maschine," *Zeitung des Vereines deutscher Ingenieure*, vol. 15, no. 1-12, pp. 97–112, 1871.

[116] T. Finkelstein, "Generalized thermodynamic analysis of Stirling engines," vol. SAE paper 118B, 1960.

[117] A. Altman, "SNAPpro Stirling Numerical Analysis Program," in *Proceedings of the 11th International Stirling Engine Conference, Rome*, pp. 166–172, 2003.

[118] SNAP homepage. https://sites.google.com/site/snapburner/home, last visited 03.05.2013.

[119] B. Thomas, "PROSA - software for evaluation of Stirling cycle machines," in *Proceedings of the 10th International Stirling Engine Conference, Osnabrueck Germany*, pp. 67–74, 2001.

[120] B. Thomas, "Calibration routine for Stirling engine simulation program PROSA and comparison of results to experimental data," in *Proceedings of the 11th International Stirling Engine Conference, Rome, University of Rome*, pp. 29–37, 2003.

[121] PROSA homepage. http://userserv.hochschule-reutlingen.de/~thomas/prosa_english.php, last visited 03.05.2013.

[122] D. M. Berchowitz, I. Urieli, and C. J. Rallis, "A numerical model for Stirling cycle machines," *Journal of Engineering for Power*, vol. 102, no. 4, pp. 756–761, 1980.

[123] I. Urieli and D. M. Berchowitz, *Stirling Cycle Engine Analysis*. Adam Hilger Ltd, Bristol, 1984.

[124] N. Chen and F. Griffin, "Review of Stirling engine mathematical models," Tech. Rep. ORNL/CON-135, ORNL, 1983.

[125] D. Gedeon, "The optimization of Stirling cycle machines," in *Proceedings of the 13th IECEC*, no. Paper No. 789193, pp. 1784–90, 1978.

[126] D. Gedeon, "Sage - Object-oriented software for Stirling machine design," vol. AIAA Paper 94-4106, pp. 1902–1907, 1994.

[127] D. Gedeon, *Sage User's Guide*. Gedeon Associates, 2010. http://sageofathens.com/.

[128] F. J. Garcia-Granados, M. A. Silva-Perez, J.-I. Prieto, and D. Garcia, "Validation of a Stirling engine thermodynamic simulation program," in *Proceedings of the 14th International Stirling Engine Conference*, 2009.

[129] S. K. Andersen, H. Carlsen, and P. G. Thomsen, "Preliminary results from simulations of temperature oscillations in Stirling engine regenerator matrices," *Energy*, vol. 31, no. 10, pp. 1371–1383, 2006.

[130] K. Mahkamov and D. Djumanov, "Three-dimensional CFD modeling of a Stirling engine," in *Proceedings of the 11th International Stirling Engine Conference, Rome*, pp. 97–107, 2003.

[131] K. Mahkamov, "An axisymmetric computational fluid dynamics approach to the analysis of the working process of a solar Stirling engine," *Journal of Solar Energy Engineering*, vol. 128, pp. 45–53, 2006.

[132] R. W. Dyson, S. D. Wilson, R. C. Tew, and R. Demko, "On the need for multidimensional Stirling simulations," Tech. Rep. NASA/TM-2005-213975, NASA, 2005.

[133] R. W. Dyson, S. D. Wilson, R. C. Tew, and R. Demko, "Fast whole-engine Stirling analysis," Tech. Rep. NASA/TM-2005-213960, National Aeronautics and Space Administration, Glenn Research Center, 2005.

[134] R. W. Dyson, S. M. Geng, R. C. Tew, and M. Adelino, "Towards fully three-dimensional virtual Stirling convertors for multi-physics analysis and optimization," *Engineering Applications of Computational Fluid Mechanics*, vol. 2, no. 1, pp. 95–118, 2008.

[135] H. Rinia and F. du Pre, "Air engines," *Philips Technical Review*, vol. 8, pp. 129–160, May 1946.

[136] T. Finkelstein, "Optimization of phase angle and volume ratio for Stirling engines," in *Proc. SAE Winter Annual Meeting, Detroit, Michigan, Jan. 11-15*, no. 118C, 1960.

[137] D. Kirkley, "Determination of the optimum configuration for a Stirling engine," *Proc IMechE Part C: Journal of Mechanical Engineering Science*, vol. 4, no. 3, pp. 204–212, 1962.

[138] G. Walker, "An optimization of the principal design parameters of Stirling cycle machines," *Proc IMechE Part C: Journal of Mechanical Engineering Science*, vol. 4, pp. 226–240, September 1962.

[139] C.-H. Cheng and H.-S. Yang, "Optimization of geometrical parameters for Stirling engines based on theoretical analysis," *Applied Energy*, vol. 92, no. 4, pp. 395–405, 2012.

[140] I. Batmaz and S. Üstün, "Design and manufacturing of a V-type Stirling engine with double heaters," *Applied Energy*, vol. 85, no. 11, pp. 1041–1049, 2008.

[141] M. Iwabuchi and M. Kanzaka, "Experimental investigation into heat transfer under the periodically reversing flow condition in heat tube," in *Stirling engines - Progress towards reality*, pp. 77–85, I Mech E, Mechanical engineering publications, 1982.

[142] R. Demko and B. L. Penswick, "Sage simulation model for technology demonstration convertor by a step-by-step approach," in *Proceedings of the International Energy Conversion Engineering Conference (IECEC 2005)*, vol. 1, (San Francisco, CA, United states), pp. 270–289, August 15-18 2005.

[143] R. Tew, T. Simon, D. Gedeon, M. Ibrahim, and W. Rong, "An initial non-equilibrium porous-media model for CFD simulation of Stirling regenerators," in *Proceedings of the 4th International Energy Conversion Engineering Conference*, vol. 1, (San Diego, CA, United states), pp. 65–77, 2006.

[144] R. Tew, M. Ibrahim, D. Danila, T. Simon, S. Mantell, L. Sun, D. Gedeon, K. Kelly, J. McLean, G. Wood, and S. Qiu, "A microfabricated involute-foil regenerator for Stirling engines," in *Proceedings of the 5th International Energy Conversion Engineering Conference*, vol. 1, (St. Louis, MO, United states), pp. 326–350, 2007.

[145] G. A. Landis and K. C. Mellott, "Venus surface power and cooling systems," *Acta Astronautica*, vol. 61, no. 11-12, pp. 995 – 1001, 2007.

[146] S. Yagyu, I. Fujishima, J. Corey, N. Isshiki, and I. Satoh, "Design, simulation, and test results of a heat-assisted three-cylinder Stirling heat pump (C-3)," in *Proceedings of the 32nd Intersociety Energy Conversion Engineering Conference, IECEC*, vol. 2, pp. 1033 –1038, 1997.

[147] D. J. Haywood, *Investigation of Stirling-type heat-pump and refrigerator systems using air as the refrigerant.* PhD thesis, University of Canterbury, 2004.

[148] M. Gschwendtner, "The development of a Vuilleumier cryocooler for New Zealand′s high temperature superconductor industry," in *Proceedings of the 10th International Cryogenics Conference, Prague, Czech Republic*, pp. 89 – 96, 2008.

[149] V. K. Gopal, *Active Stirling Engine.* PhD thesis, University of Canterbury, 2012.

[150] J. Wendt, *Computational fluid dynamics: an introduction.* Springer, 2008.

[151] O. Zikanov, *Essential computational fluid dynamics*. John Wiley & Sons, 2010.

[152] B. Andersson, *Computational fluid dynamics for engineers*. Cambridge University Press, 2012.

[153] H. Carlsen and J. K. Bovin, "Test of 9 kW Stirling engine using biogas as fuel," in *Proceedings of 10th International Stirling Engine Conference*, pp. pp. 278–285, 2001.

[154] H. Carlsen and J. K. Bovin, "Analytical expression for an optimised link bar mechanism for a beta type Stirling engine," in *Proceedings of the 13th International Stirling Engine Conference ISEC*, 2007.

[155] S. K. Andersen, H. Carlsen, and P. G. Thomsen, "Numerical study on optimal Stirling engine regenerator matrix designs taking into account the effects of matrix temperature oscillations," *Energy Conversion and Management*, vol. 47, pp. 894–908, 2006.

[156] S. K. Andersen, *Numerical Simulation of Cyclic Thermodynamic Processes*. PhD thesis, Technical University of Denmark, 2006.

[157] J. Kentfield, "The thermodynamics of Stirling engines revisited-the relative merits of hot zone or cold zone work extraction," in *Proceedings of the 27th Intersociety Energy Conversion Engineering Conference, IECEC*, vol. 5, pp. 33–40, 1992.

[158] J. Kentfield, "A detailed study of the operation of the regenerators in both cold-end and hot-end connected gamma type Stirling engines," in *Proceedings of the 28th Intersociety Energy Conversion Engineering Conference, IECEC*, vol. 2, pp. 651–656, 1993.

[159] J. Kentfield and G. Walker, "Simple coal-fired Stirling engine for use as a village power unit," in *Proceedings of the 29th Intersociety Energy Conversion Engineering Conference, IECEC*, vol. 4, pp. 1954–1954, 1994.

[160] B. Thomas, H.-D. Kuehl, S. Schulz, and J. Kentfield, "Optimization of the swept volume ratio for cold-end and hot-end connected gamma type Stirling engines," in *Proceedings of the 29th Intersociety Energy Conversion Engineering Conference, IECEC*, vol. 4, pp. 1835–1840, 1994.

[161] N. Isshiki, S. Tsukahara, and M. Ohtomo, "Experimental and vector analysis on gamma type Stirling engine with hot power piston," in *Proceedings of the 30th Intersociety Energy Conversion Engineering Conference, IECEC*, 1995.

[162] V. Gopal, R. Duke, and D. Clucas, "Active Stirling engine," in *TENCON 2009 - 2009 IEEE Region 10 Conference*, 2009.

[163] V. K. Gopal, "Design and development of a test rig to validate the concept of an active Stirling engine," in *AUPEC 2010, Christchurch*, 2010.

[164] T. Finkelstein, "Balanced compounding of Stirling machines," in *Intersociety Energy Conversion Engineering Conference, 13th, San Diego, Calif., August 20-25*, vol. 3, pp. 1791–1797, Society of Automotive Engineers Inc., 1978.

[165] G. Walker and J. Senft, *Free Piston Stirling Engines*. Springer Verlag Berlin, 1985.

[166] D. M. Berchowitz and J. Shonder, "Estimated size and performance of a natural gas fired duplex Stirling for domestic refrigeration applications," in *Proceedings of the 18th International congress on refrigeration: new challenges in refrigeration*, pp. 1350–1354, 1991.

[167] G. Chen and W. Beale, "Thermally actuated duplex free-piston Stirling system for domestic cooling and heating applications," in *Int Conf on CFC's and Halon Alternatives, Beijing, China*, 1993.

[168] G. Walker, J. Kentfield, R. Fauvel, V. Srinivasan, and E. Johnson, "Coal-fired Stirling engines for railway locomotive and stationary power applications," in *Proceedings of the Institution of Mechanical Engineers, Part A: Journal of Power and Energy*, 1983.

[169] B. Hoegel, D. Pons, M. Gschwendtner, A. Tucker, and M. Sellier, "Theoretical investigation of the performance of an Alpha Stirling engine for low temperature applications," in *Proceedings of the 15th International Stirling Engine Conference (ISEC)*, 2012.

[170] B. Hoegel, D. Pons, M. Gschwendtner, A. Tucker, and M. Sellier, "Thermodynamic peculiarities of alpha-type Stirling engines for low-temperature difference power generation: optimisation of operating parameters and heat exchangers using a third-order model," *Proc IMechE Part C: Journal of Mechanical Engineering Science*, vol. Published online before print, November 20, 2013.

[171] J. P. Gupta, *Fundamentals of heat exchanger and pressure vessel technology*. Hemisphere Publishing, New York, NY, 1986.

[172] H. Carlsen, N. Ammundsen, and J. Traerup, "40 kW Stirling engine for solid fuel," in *Proceedings of the 31st Intersociety Energy Conversion Engineering Conference, IECEC*, vol. 2, pp. 1301–1306, 1996.

[173] H. P. Bloch, *Compressors and modern process applications*. Wiley-Interscience, 2006.

[174] K. K. Makhkamov and D. Ingham, "Analysis of the working process and mechanical losses in a Stirling engine for a solar power unit," *Journal of solar energy engineering*, vol. 121, no. 2, pp. 121–127, 1999.

[175] J. Prieto and A. Stefanovskiy, "Dimensional analysis of leakage and mechanical power losses of kinematic Stirling engines," *Proceedings of the Institution of Mechanical Engineers, Part C: Journal of Mechanical Engineering Science*, vol. 217, no. 8, pp. 917–934, 2003.

[176] K. Hirata, "Mechanical loss reduction of a 100 W class Stirling engine," in *Proceedings of the 11th International Stirling Engine Conference (ISEC)*, 2003.

[177] J. Senft, *Mechanical Efficiency of Heat Engines*. Cambridge University Press, 2007.

[178] S. Grinnell, "Flow of a compressible fluid in a thin passage," in *ASME Diamond Jubilee Semi-Annual Meeting, Boston, Mass. - June 19-23*, 1955. paper no. 55-SA-13.

[179] Y. Liu and Y. Yongzhang, "Prediction for the sealing characteristics of piston rings of a reciprocating compressor," in *Proceedings of the International Compressor Engineering Conference*, 1986. Paper 583.

[180] M. White, K. Colenbrander, R. Olan, and L. Penswick, "Generators that won't wear out," *Mechanical Engineering*, vol. 118, no. 2, pp. 92–96, 1996.

[181] API heat transfer, "Basco Whitlock hub-design heat exchangers." online data sheet, http://www.apiheattransfer.com/, last visited 01.07.2013.

[182] Wieland, "Cuprofin - standard pattern, inner-grooved seamless drawn copper tubes." online, http://www.wieland-thermalsolutions.com, last visited 02.07.2013.

[183] D. Gee and R. Webb, "Forced convection heat transfer in helically rib-roughened tubes," *International Journal of Heat and Mass Transfer*, vol. 23, no. 8, pp. 1127 – 1136, 1980.

[184] S. Al-Fahed, L. Chamra, and W. Chakroun, "Pressure drop and heat transfer comparison for both microfin tube and twisted-tape inserts in laminar flow," *Experimental Thermal and Fluid Science*, vol. 18, no. 4, pp. 323 – 333, 1998.

[185] S. Pethkool, S. Eiamsa-ard, S. Kwankaomeng, and P. Promvonge, "Turbulent heat transfer enhancement in a heat exchanger using helically corrugated tube," *International Communications in Heat and Mass Transfer*, vol. 38, no. 3, pp. 340 – 347, 2011.

[186] M. Kuosa, K. Saari, A. Kankkunen, and T.-M. Tveit, "Oscillating flow in a Stirling engine heat exchanger," *Applied Thermal Engineering*, vol. 45-46, pp. 15 – 23, 2012.

[187] M. Rock, "Mighty River Power Ltd," 2010. Personal comunication.

[188] A. Devarakonda and W. G. Anderson, "Thermo-physical properties of intermediate temperature heat pipe fluids," Tech. Rep. NASA/CR-2005-213582, NASA, 2005.

[189] A. Devarakonda, D. Xiong, and D. E. Beach, "Intermediate temperature water heat pipe tests," Tech. Rep. NASA/TM-2005-213581, NASA, 2005.

[190] W. G. Anderson, J. R. Hartenstine, D. B. Sarraf, and C. Tarau, "Intermediate temperature fluids for heat pipes and loop heat pipes," in *Proceedings of the International Energy Conversion Engineering Conference, St. Louis, MO*, 2007.

[191] K. Hamaguchi and I. Yamashita, "Effects of gap between housing ends and matrix on a uniform flow in regenerator," in *Proceedings of the 11th International Stirling Engine Conference (ISEC)*, 2003.

[192] J. Senft, "Small stationary Stirling engine designs," in *Stirling engines - Progress towards reality*, pp. 77–85, I Mech E, Mechanical engineering publications, 1982.

[193] X. Wang, A. Subic, and H. Watson, "Two-dimensional lubrication analysis and design optimization of a Scotch Yoke engine linear bearing," *Proceedings of the Institution of Mechanical Engineers, Part C: Journal of Mechanical Engineering Science*, vol. 220, no. 10, pp. 1575–1587, 2006.

[194] W. G. Sawyer, K. I. Diaz, M. A. Hamilton, and B. Micklos, "Evaluation of a model for the evolution of wear in a Scotch-Yoke mechanism," *Journal of Tribology*, vol. 125, pp. 678–681, 2003.

[195] K. Hirata, N. Kagawa, M. Takeuchi, I. Yamashita, N. Isshiki, and K. Hamaguchi, "Test results of applicative 100 W Stirling engine," in *Proceedings of the 31st Intersociety Energy Conversion Engineering Conference(IECEC)*, vol. 2, pp. 1259–1264, IEEE, 1996.

[196] K. Hirata, S. Iwamoto, F. Toda, and K. Hamaguchi, "Performance evaluation for a 100 W Stirling engine," in *Proceedings of the 8th International Stirling Engine Conference (ISEC)*, pp. 19–28, 1997.

[197] H. Carlsen and J. K. Bovin, "Field test of 40 kW Stirling engine for wood chips," in *Proceedings of the 8th International Stirling Engine Conference (ISEC)*, 1997.

[198] R. J. Meijer, *The Philips Stirling thermal engine - analysis of the rhombic drive mechanism and efficiency measurements.* PhD thesis, Technische Hogeschool Delft (now: Delft University of Technology), 1960.

[199] D. R. Greatrix, *Powered Flight: The Engineering of Aerospace Propulsion.* Springer, 2012.

[200] J. Smith and A. McKisic, "Stiller-Smith versus conventional V-8 bearing load and friction comparisons," *Proceedings of the Institution of Mechanical Engineers, Part D: Journal of Automobile Engineering*, vol. 203, no. 4, pp. 231–245, 1989.

[201] J. E. Smith, J. C. Smith, and A. D. McKisic, "A comparative study of the Stiller-Smith and slider-crank mechanisms for eight-cylinder internal combustion engine use," *Journal of Engineering for Gas Turbines and Power*, vol. 113, no. 3, pp. 350–358, 1991.

[202] P. Feulner, "Crank mechanisms for balance compounded Stirling engines," in *Proceedings of the International Stirling Forum*, 2004.

[203] K. W. Stanzel, "Stirling engine (1kWe) integrated into a pellet stove," in *Proceedings of the 13th International Stirling Engine Conference (ISEC)*, 2007.

[204] K. Kocsisek and B. Thomas, "A novel crank mechanism for enhanced power output and improved part load efficiency," in *Proceedings of the 11th International Stirling Engine Conference (ISEC)*, 2003.

[205] I. Reynolds, O. Fritz, H. Hoffmann, P. Wieske, S. Simmonds, and D. Wise, "The design of the MAHLE 25kWe solar heated Stirling engine," in *Proceedings of the 15th International Stirling Engine Conference (ISEC)*, (Dubrovnik), 2012.

[206] R. Mikalsen and A. Roskilly, "A review of free-piston engine history and applications," *Applied Thermal Engineering*, vol. 27, no. 14, pp. 2339–2352, 2007.

[207] J. Senft, *Ringbom Stirling Engines*. Oxford University Press, 1993.

[208] R. Redlich and D. Berchowitz, "Linear dynamics of free-piston Stirling engines," *Proceedings of the Institution of Mechanical Engineers, Part A: Journal of Power and Energy*, vol. 199, no. 3, pp. 203–213, 1985.

[209] M. Dhar, J. Rauch, S. Huang, and R. Bolton, "Space power demonstration engine linear alternator dynamometer test results," in *Proceedings of the 24th Intersociety Energy Conversion Engineering Conference (IECEC-89)*, pp. 1103–1107, IEEE, 1989.

[210] D. Berchowitz, M. Richter, and D. Shade, "Development and performance of a 3 kW (e) air charged free-piston Stirling engine with linear alternator," in *Proceedings of the 22nd Intersociety Energy Conversion Engineering Conference (IECEC)*, 1987.

[211] R. W. Redlich, "A summary of twenty years experience with linear motors and alternators," in *Linear Drives for Industry Applications, Nagasaki, Japan*, Sunpower, 1995.

[212] N. W. Lane and W. T. Beale, "Free-piston Stirling design features," in *Proceedings of the 8th International Stirling Engine Conference (ISEC)*, 1997.

[213] S. M. Geng, J. M. Niedra, and G. E. Schwarze, "Overview of NASA magnet and linear alternator research efforts," Tech. Rep. NASA/TM-2005-213411, NASA, 2005.

[214] H. W. Brandhorst and P. A. Chapman, "New 5 kW free-piston Stirling space convertor developments," *Acta Astronautica*, vol. 63, no. 1, pp. 342–347, 2008.

[215] J. Chan, J. G. Wood, and J. G. Schreiber, "Development of advanced Stirling radioisotope generator for space exploration," Tech. Rep. NASA/TM-2007-214806, 2007.

[216] N. W. Lane and W. T. Beale, "A 5 kW electric free-piston Stirling engine," in *Proceedings of the 7th International Conference on Stirling Cycle Machines*, pp. 62–67, 1995.

[217] M. A. White, S. Qiu, J. Wacknov, R. J. Wehrer, R. G. Mahorter, and M. F. Dufalla, "Conceptual design assessment of megawatt-class multi-cylinder free-piston Stirling engine," in *Proceedings of the 5th International Energy Conversion Engineering Conference (IECEC)*, vol. 1, pp. 31–42, 2007.

[218] US Department of Energy. http://www1.eere.energy.gov/solar/sunshot/csp_rnd_infinia.html, U.S. department of energy grant no. DE-AC11-98PN-38206, last visited 22.07.2013.

[219] S.-Y. Kim, N. Lane, and D. M. Berchowitz, "Multi-cylinder alpha free-piston Stirling engine for vehicle exhaust system," in *Proceedings of the 13th International Stirling Engine Conference (ISEC)*, 2007.

[220] S. Carlqvist and Y. Gothberg, "New concept, hermetically sealed 4-cylinder, double-acting Stirling engine," in *Proceedings of the 24th Intersociety Energy Conversion Engineering Conference, IECEC*, vol. 5, pp. 2265–2270, 1989.

[221] H. Kläy, "Reciprocating compressors with labyrinth pistons for helium," *Cryogenics*, vol. 15, no. 10, pp. 569–571, 1975.

[222] H. Vetter, "The Sulzer oil-free labyrinth piston compressor," in *International Compressor Engineering Conference*, 1972.

[223] C. M. Invernizzi, "Stirling engines using working fluids with strong real gas effects," *Applied Thermal Engineering*, vol. 30, no. 13, pp. 1703–1710, 2010.

[224] American Institute of Aeronautics and Astronautics, "Guide to safety of hydrogen and hydrogen systems," Tech. Rep. AIAA G-095, ANSI - American National Standard, 2005.

[225] NASA. http://www.nasa.gov/topics/technology/hydrogen/index.html, last visited 18.092013.

[226] Fuelcells.org. http://www.fuelcells.org/base.cgim?template=hydrogen_basics, last visited 18.09.2013.

[227] A. Godula-Jopek, W. Jehle, and J. Wellnitz, *Hydrogen Storage Technologies: New Materials, Transport, and Infrastructure*. John Wiley & Sons, 2012.

[228] F. Gallucci, E. Fernandez, P. Corengia, and M. van Sint Annaland, "Recent advances on membranes and membrane reactors for hydrogen production," *Chemical Engineering Science*, vol. 92, no. 0, pp. 40 – 66, 2013.

[229] W. J. Nuttall, R. H. Clarke, and B. A. Glowacki, "Resources: Stop squandering helium," *Nature*, vol. 485, no. 7400, pp. 573–575, 2012.

[230] B. Glowacki, W. Nuttall, and R. Clarke, "Beyond the helium conundrum," *IEEE transactions on applied superconductivity*, vol. 23, june 2013.

[231] J. R. Bartels, M. B. Pate, and N. K. Olson, "An economic survey of hydrogen production from conventional and alternative energy sources," *International journal of hydrogen energy*, vol. 35, no. 16, pp. 8371–8384, 2010.

[232] M. Bonnici, A. Tacchini, and D. Vucinic, "Long permanence high altitude airships: the opportunity of hydrogen," *European Transport Research Review*, 2013. DOI 10.1007/s12544-013-0123-z.

[233] Eagle Burgmann. http://www.eagleburgmann.com/products/mechanical-seals?set_language=en, last visited 23.09.2013.

[234] C. Radcliffe, "Sealing material developments for reciprocating gas compressors," *Sealing Technology*, pp. 7–11, 2005.

[235] Howden Thomassen Compressors BV, "The Howden Thomassen FFP, oil-free and virtually friction-free: the piston that flows on a film of process gas," product information, Howden Group Limited, 2012. www.thomassen.com.

[236] R. Hart, "Performance of PTFE based piston rings in an unlubricated reciprocating compressor," *Proceedings of the Institution of Mechanical Engineers*, vol. 181, no. 1, pp. 13–22, 1966.

[237] K. Graunke, "Developments in dry running seals for reciprocating compressors," in *International Compressor Engineering Conference*, 1996. Paper 1115.

[238] X.-B. Yang, X.-Q. Jin, Z.-M. Du, T.-S. Cui, and S.-K. Yang, "Frictional behavior investigation on three types of PTFE composites under oil-free sliding conditions," *Industrial Lubrication and Tribology*, vol. 61, no. 5, pp. 254–260, 2009.

[239] S. M. Yeo and A. A. Polycarpou, "Tribological performance of PTFE-and PEEK-based coatings under oil-less compressor conditions," *Wear*, vol. 296, no. 1-2, pp. 638–647, 2012.

[240] H. Meier, "Paper 8: Problems associated with modern designs of oil-free labyrinth piston compressors," in *Proceedings of the Institution of Mechanical Engineers, Conference Proceedings*, vol. 184, pp. 77–85, SAGE Publications, 1969.

[241] K. Graunke and J. Ronnert, "Dynamic behavior of labyrinth seals in oil-free labyrinth-piston compressors," in *International Compressor Engineering Conference*, 1984. Paper 425.

[242] Burckhardt Compression AG, "Laby - labyrinth piston compressors." http://www.burckhardtcompression.com/, last visited 21.09.2013.

[243] C. West, "Dynamic analysis of the fluidyne," in *Intersociety Energy Conversion Engineering Conference*, vol. 2, Oak Ridge National Laboratory, Oak Ridge, Tennessee, 1983.

[244] C. West, "Liquid-piston Stirling machines," tech. rep., Oak Ridge National Lab., TN (USA), 1984.

[245] O. Fauvel and L. Yu, "Displacer design and testing for a barrel fluidyne," in *Intersociety Energy Conversion Engineering Conference*, vol. 4, pp. 1950–1950, American Nuclear Society, 1994.

[246] J. D. Van de Ven and P. Y. Li, "Liquid piston gas compression," *Applied Energy*, vol. 86, no. 10, pp. 2183–2191, 2009.

[247] M. White, S. Emigh, D. Gray, J. Krogness, J. Noble, R. Olan, J. Oster, and P. Riggle, "Hermetic metal seals for Stirling engines," in *Proceedings of the Intersociety Energy Conversion Engineering Conference, IECEC*, (San Francisco, CA, USA), pp. 1982 – 1987, 1984.

[248] R. Ackermann and G. Privon, "Performance measurements for a diaphragm-coupled, free-piston Stirling engine heat pump module," in *Proceedings of the 23rd Intersociety Energy Conversion Engineering Conference*, (New York, NY, USA), pp. 27 – 32, 1988.

[249] O. Fauvel, G. Walker, and G. Reader, "Flat elastomeric diaphragm as Stirling engine piston," in *Proceedings of the Intersociety Energy Conversion Engineering Conference, IECEC*, vol. 2, (Atlanta, GA, USA), pp. 927–932, 1993.

[250] B. F. Tchanche, G. Lambrinos, A. Frangoudakis, and G. Papadakis, "Low-grade heat conversion into power using Organic Rankine Cycles–a review of various applications," *Renewable and Sustainable Energy Reviews*, vol. 15, no. 8, pp. 3963–3979, 2011.

[251] F. Vélez, J. J. Segovia, M. C. Martín, G. Antolín, F. Chejne, and A. Quijano, "A technical, economical and market review of organic Rankine cycles for the conversion of low-grade heat for power generation," *Renewable and Sustainable Energy Reviews*, vol. 16, no. 6, pp. 4175–4189, 2012.

[252] S. Quoilin, M. Broek, S. Declaye, P. Dewallef, and V. Lemort, "Techno-economic survey of organic rankine cycle (ORC) systems," *Renewable and Sustainable Energy Reviews*, vol. 22, pp. 168–186, 2013.

[253] J. Nordquist, "Use of small, sub 1 MW organic rankine cycle power systems and low temperature resources," in *Geothermal Resources Council (GRC) Transactions*, vol. 33, pp. 753–758, 2009.

[254] Turboden srl. http://www.turboden.eu/, last visited 09.04.2014.

[255] Ormat Technologies, Inc. http://www.ormat.com/, last visited 09.04.2014.

[256] A. Schuster, S. Karellas, E. Kakaras, and H. Spliethoff, "Energetic and economic investigation of Organic Rankine Cycle applications," *Applied thermal engineering*, vol. 29, no. 8, pp. 1809–1817, 2009.

[257] G. Qiu, H. Liu, and S. Riffat, "Expanders for micro-CHP systems with organic Rankine cycle," *Applied Thermal Engineering*, vol. 31, no. 16, pp. 3301–3307, 2011.

[258] R. Bracco, S. Clemente, D. Micheli, and M. Reini, "Experimental tests and modelization of a domestic-scale ORC (Organic Rankine Cycle)," *Energy*, vol. 58, pp. 107–116, 2013.

[259] BINE Informationsdienst, "Transforming waste heat into electricity," *Projektinfo*, vol. 13, 2011. available from http://www.bine.info/fileadmin/content/Publikationen/Englische_Infos/ProjektInfo_1311_engl_internetx.pdf.

[260] DeVeTec GmbH. http://www.devetec.de/index.php/company, last visited 11.04.2014.

[261] M. Bianchi and A. De Pascale, "Bottoming cycles for electric energy generation: Parametric investigation of available and innovative solutions for the exploitation of low and medium temperature heat sources," *Applied Energy*, vol. 88, no. 5, pp. 1500 – 1509, 2011.

[262] Pratt & Whitney Power Systems, "Model 280 PureCycle Power System." product brochure. www.pw.utc.com.

[263] M. Astolfi, M. Romano, P. Bombarda, and E. Macchi, "Binary ORC (organic Rankine cycles) power plants for the exploitation of medium–low temperature geothermal sources – part a: Thermodynamic optimization," *Energy*, vol. 66, pp. 423–434, 2014.

[264] M. Astolfi, M. Romano, P. Bombarda, and E. Macchi, "Binary ORC (organic Rankine cycles) power plants for the exploitation of medium–low temperature geothermal sources – part b: Techno-economic optimization," *Energy*, vol. 66, pp. 435–446, 2014.

[265] A. Borsukiewicz-Gozdur, "Pumping work in the organic Rankine cycle," *Applied Thermal Engineering*, vol. 51, no. 1, pp. 781–786, 2013.

[266] M. H. Dickson and M. Fanelli, *Geothermal energy: utilization and technology*. Routledge, 2013.

[267] K. Mollenhauer and H. Tschöke, eds., *Handbook of Diesel engines*. Springer, 2010.

[268] M. Villarini, E. Bocci, M. Moneti, A. Di Carlo, and A. Micangeli, "State of art of small scale solar powered ORC systems: A review of the different typologies and technology perspectives," *Energy Procedia*, vol. 45, pp. 257–267, 2014.

[269] B. White, "Waikite small geothermal power plant feasibility study," tech. rep., East Harbour Energy, 2009. available on http://www.eecabusiness.govt.nz/node/10918, last visited 17.04.2014.

[270] M. McCoy, "Regulatory issues heat up for blowing agents," *Chemical and Engineering News Online*, vol. 78, no. 44, pp. 22–23, 2000.

[271] Infinity Turbine LLC. http://www.infinityturbine.com/ORC/News/Entries/2012/5/2_Price_spikes_in_USA_for_R245fa.html, last visited 18.04.2014.

[272] Honeywell International Inc. http://www.honeywell-orc.com/tomorrows-solutions/, last visited 18.04.2014.

[273] K. Hirata, E. Ishimura, M. Kawada, T. Akazawa, and M. Iida, "D26 development of a marine heat recovery system with Stirling engine generators," in *Proceedings of the 13th International Stirling Engine Conference*, 2007.

[274] P. Lista, "The GLIMPS simulation code applied to the V160 DMA Stirling cogeneration unit," in *Proceedings of the 28th Intersociety Energy Conversion Engineering Conference*, vol. 2, pp. 683–688, 1993.

[275] G. Marinitsch, F. Biedermann, H. Carlsen, J. K. Bovin, M. Schöch, and I. Obernberger, "Development of a hot gas heat exchanger and a cleaning system for a 35kWel hermetic four cylinder Stirling engine for solid biomass fuels," in *Proceedings of the International Stirling Engine Conference*, 2005.

[276] F-Chart software, "EES - Engineering Equation Solver." http://www.fchart.com/.

[277] Turboden srl, "Turboden 200/300kw units - typical performance." data sheet, available online: http://www.turboden.eu/en/downloads/downloads.php?categoria=data%20sheets, last visited 14.04.2014.

Appendix A

Database for the West correlation

For the calculation of the West number in Section 1.2.4 the dataset shown in Table A.1 is used. It includes a large number of Stirling engines built in various arrangements and sizes which can be found in the literature.

Table A.2 is created using data sets taken from the simulation runs in Chapter 4. A mechanical efficiency of 0.9 is assumed to calculate the shaft power based on the indicated power. The first four rows represent the maximum power of the LTD at the optimum phase angle achievable at different frequencies as it can be found in Figure 4.1 (a). For each frequency the heat exchangers are optimised so that the maximum power output is obtained; it can be seen that the West numbers rise for decreasing frequencies which also corresponds to higher efficiencies. At the point of maximum power the value of the West number is close to the proposed value of 0.2.

The last three rows contain data of the maximum power of the LTD for the optimum frequencies at a phase angle of 160° for the different working fluids as seen in Figure 4.10. Despite the different fluids and frequencies the West numbers are almost identical; it seems as if the correlation works independent of the working fluid.

Table A.1: Swept volume, operating parameters, power output of selected SE. Database for the West number correlation in Figure 1.6

engine	type	gas	P/kW	f /Hz	p/MPa	V_{swept}/l	T_{hot}	T_{cold}	W_n	ref
System7	g	He	0.01	40.0	1.80	0.001	773	323	0.32	[24]
Fluidyne pump	a		0.01	0.6	0.10	2.320	633	298	0.31	[24]
Ross Yoke	a		0.03	25.0	0.10	0.069	923	350	0.35	[24]
F5 TMG	b		0.03	100.0	0.10	0.045	723	309	0.19	[24]
Karabulut	b	air	0.05	7.6	0.28	0.231	473	300	0.48	[33]
	a	air	0.06	9.3	0.55	0.098	724	323	0.31	[30]
	g	N_2	0.07	15.9	0.80	0.081	737	323	0.18	[30]
	g	He	0.10	18.4	0.90	0.081	761	323	0.19	[30]
Iwamoto	g	air	0.15	2.4	0.10	25.133	403	313	0.19	[34]
Fluidyne Pump	a		0.16	0.6	0.10	32.000	648	323	0.24	[24]
Homach TMG	b		0.17	100.0	0.20	0.135	873	353	0.15	[24]
D-60	a	air	0.19	54.4	0.27	0.060	923	323	0.45	[89]
Iwamoto	g	air	0.19	1.6	0.22	25.133	373	313	0.26	[30]
D-90	a	air	0.23	54.8	0.27	0.090	923	323	0.36	[89]
MP1002CA	b	air	0.25	25.0	1.50	0.059	973	323	0.22	[30]
102C	b		0.48	26.7	1.20	0.067	1173	288	0.37	[24]
Hirata	b	He	0.63	19.7	3.20	0.220	673	300	0.12	[273]
Takeuchi	a		0.74	3.0	0.80	10.370	408	298	0.19	[35]
Iwamoto	a	N_2	0.75	2.3	1.00	10.370	365	298	0.31	[30]
single-alpha+	b	air	0.81	11.7	0.60	2.879	553	293	0.13	[36]
RE1000	g		1.20	30.3	7.10	0.067	883	298	0.17	[24]
TDE	g		1.20	45.0	4.00	0.092	773	288	0.16	[24]
	b	He	1.24	23.5	3.80	0.133	776	323	0.25	[30]
Spike	b		1.30	63.3	1.00	0.314	983	313	0.13	[24]
proto2	b		1.75	30.2	8.20	0.133	933	308	0.11	[24]
PD-46	b	He	3.00	50.0	10.20	0.081	933	323	0.15	[30]
Melse2	a	He	3.10	16.7	4.50	0.427	858	323	0.21	[30]
Melse2	a		3.60	16.7	4.80	0.427	973	279	0.19	[24]
NS-03M	b	He	3.81	23.4	6.20	0.161	971	323	0.33	[30]

- continued on following page -

Table A.1 – continued from previous page

engine	type	gas	P/kW	f /Hz	p/MPa	V_{swept}/l	T_{hot}	T_{cold}	W_n	ref
rice husk	b		4.00	12.0	0.50	6.900	793	350	0.25	[24]
NS-03T	a	He	4.14	21.7	6.40	0.269	991	323	0.22	[30]
GPU3	b		4.20	25.0	6.80	0.120	1053	293	0.36	[24]
V-160DMA	a	He	6.27	25.0	12.50	0.226	998	356	0.19	[274]
stirling dk beta	b	N_2	8.21	16.8	7.81	0.545	945	318	0.23	[50]
GPU3	b	H_2	8.95	60.0	6.90	0.120	1019	323	0.35	[30]
double-alpha+	b	N_2	9.20	10.0	0.60	23.992	553	293	0.21	[37]
	b	He	10.40	12.5	0.60	23.992	553	293	0.19	[37]
V161 Solo-power	a	He	9.89	25.0	12.00	0.226	923	293	0.28	
V160	a		10.70	30.0	13.00	0.226	993	323	0.24	[24]
stirling dk beta	b	He	10.92	16.8	8.20	0.545	885	333	0.32	[50]
1–98	b	He	15.00	50.0	22.00	0.098	903	323	0.29	[30]
1–98	b		15.00	50.0	22.00	0.098	1123	323	0.25	[24]
stirling 1843	g		16.00	0.5	1.30	316.000	613	338	0.29	[24]
STM 4-120	a	He	20.00	30.0	9.20	0.669	1073	318	0.20	[23]
1–365	b		30.00	41.7	10.50	0.365	973	288	0.35	[24]
NS-30A	a	He	30.40	25.0	14.70	0.837	933	323	0.20	[30]
Mod1	a		37.00	33.3	11.00	0.690	1013	323	0.28	[24]
SM4D	a	He	38.46	16.9	4.60	6.809	953	333	0.15	[275]
4-95ADVENCO	a		44.00	83.3	10.00	0.539	1023	328	0.19	[23]
P40/4-95	a	H_2	45.00	66.7	15.00	0.537	1023	323	0.16	[30]
NS-30S	a	He	45.60	30.1	15.50	0.820	958	323	0.24	[30]
4-95/P40	a		52.00	66.7	15.00	0.540	1083	323	0.18	[24]
Trial	a		57.00	41.7	10.00	1.070	1023	293	0.23	[24]
4-235	b	He	68.00	41.7	11.00	1.329	903	310	0.23	[23]
4-275/P75	a		118.00	43.3	15.00	1.560	1123	293	0.20	[24]
4-215	a		125.00	75.0	20.00	1.220	1023	338	0.14	[24]
360-15	b	H_2	269.00	25.0	10.00	4.880	923	303	0.44	[23]

- end of table -

Table A.2: Swept volume, operating parameters, power output, and West number of the simulated LTD (selected values)

engine	type	gas	P/kW	f /Hz	p/MPa	V_{swept}/l	T_{hot}	T_{cold}	W_n	ref
Simulation	a	He	3.35	8.3	5.00	1.090	423	313	0.49	-
LTD	a	He	4.68	16.7	5.00	1.090	423	313	0.34	-
$\alpha = 160°$	a	He	4.95	25	5.00	1.090	423	313	0.24	-
HX optimised	a	He	4.96	33.3	5.00	1.090	423	313	0.18	-
LTD	a	H_2	7.70	30	5.00	1.090	423	313	0.32	-
$\alpha = 160°$	a	He	4.81	19.1	5.00	1.090	423	313	0.31	-
f optimised	a	N_2	2.18	8.2	5.00	1.090	423	313	0.33	-

Appendix B

Effective volume of alpha engines

In order to calculate the West number the volume amplitude is needed rather than the swept volume of the cylinders. The volumetric change in alpha engines is defined by the movement of the two pistons, as opposed to displacer engines where only one piston defines the effective volume amplitude; therefore it has to be calculated separately. Three parameters affect the total gas volume in alpha engines: the swept volume (V_{swept}) of the individual cylinders, the ratio of expansion and compression volume amplitude (k), and the phase angle between expansion and compression volume (α). The instantaneous volume in the two cylinder spaces can be calculated by

$$V_{total}(\theta) = V_{compression} + V_{expansion} \tag{B.1}$$

$$= 0.5V_{swept}(k(1+\cos\theta) + (1+\cos(\theta+\alpha))) \tag{B.2}$$

$$= 0.5V_{swept}(k(1+\cos\theta) + 1 + \cos\theta\cos\alpha - \sin\theta\sin\alpha)) \tag{B.3}$$

By finding the derivative the location of the maximum and minimum volume can be identified:

$$V'_{total}(\theta) = 0.5V_{swept}(-k\sin\theta - \cos\alpha\sin\theta - \sin\alpha\cos\theta) \tag{B.4}$$

$$= 0.5V_{swept}(-\sin\theta(k + \cos\alpha) - \sin\alpha\cos\theta) \tag{B.5}$$

$$V'_{total}(\theta) = 0 \tag{B.6}$$

$$-\sin\theta(k + \cos\alpha) = \sin\alpha\cos\theta \tag{B.7}$$

$$\tan\theta = -\frac{\sin\alpha}{k + \cos\alpha} \tag{B.8}$$

$$\theta_0 = \arctan(-\frac{\sin\alpha}{k + \cos\alpha}) \tag{B.9}$$

The volume change (ΔV) can then be found by inserting the angle found (θ_0) in Equation B.3 and subtracting the two extremes:

$$\Delta V(\alpha) = V_{max} - V_{min} \tag{B.10}$$

$$= V_{total}(\theta_0) - V_{total}(\theta_0 + \pi) \tag{B.11}$$

This volume can easily be normalised so that a factor to describe the volumetric change is gained:

$$\Delta V^*(\alpha) = \frac{\Delta V}{V_{swept}} \tag{B.12}$$

For $k = 1$ the calculation of ΔV^* can be approximated very closely using the following polynomial (α in deg) :

$$\Delta V^*(\alpha) = 1.513 \times 10^{-7}\alpha^3 - 9.234 \times 10^{-5}\alpha^2 + 6.129 \times 10^{-4}\alpha + 1.9948 \tag{B.13}$$

In Figure B.1 ΔV^* is plotted against the phase angle α; the corresponding number of cylinders for the Siemens configuration is also plotted for comparison. In Table B.1 the values for ΔV^* are given.

Table B.1: Volumetric change, maximum and minimum volume, and phase angle for various cylinder numbers in the Siemens arrangement; expansion and compression volume identical ($k = 1$)

NoC	α / deg	V^*_{max}	V^*_{min}	ΔV^*
2	0.0	2.000	0.000	2.000
3	60.0	1.866	0.134	1.732
4	90.0	1.707	0.293	1.414
5	108.0	1.588	0.412	1.176
6	120.0	1.500	0.500	1.000
7	128.6	1.434	0.566	0.868
8	135.0	1.383	0.617	0.765
9	140.0	1.342	0.658	0.684
10	144.0	1.309	0.691	0.618
11	147.3	1.282	0.718	0.563
12	150.0	1.259	0.741	0.518
13	152.3	1.239	0.761	0.479
14	154.3	1.223	0.777	0.445
15	156.0	1.208	0.792	0.416
16	157.5	1.195	0.805	0.390
17	158.8	1.184	0.816	0.367
18	160.0	1.174	0.826	0.347
19	161.1	1.165	0.835	0.329
20	162.0	1.156	0.844	0.313
21	162.9	1.149	0.851	0.298
22	163.6	1.142	0.858	0.285
23	164.3	1.136	0.864	0.272
24	165.0	1.131	0.869	0.261

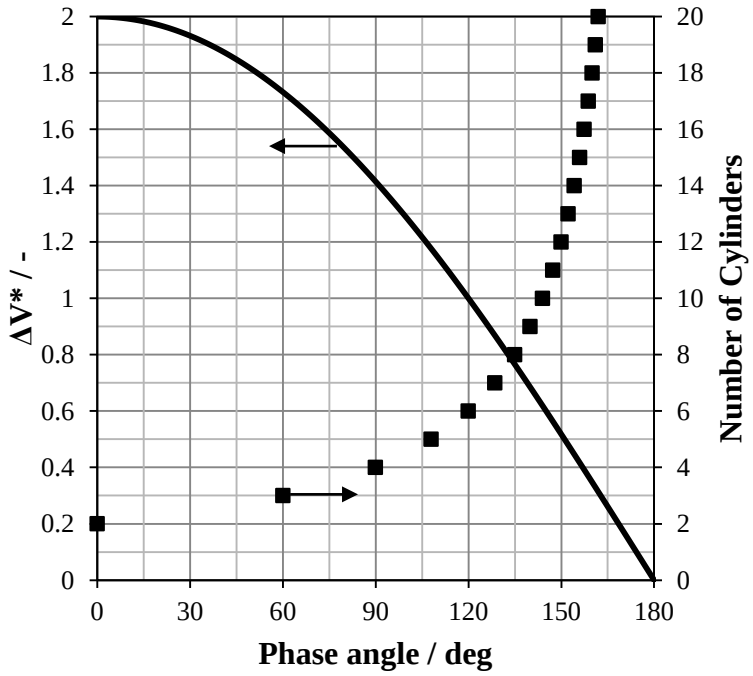

Figure B.1: Volumetric change as a function of the phase angle for alpha engines, k = 1

Appendix C

Properties of N_2, He, and H_2

Table C.1: Heat capacity for constant pressure (c_p), heat capacity for constant volume (c_v), adiabatic index (γ), density (ρ), viscosity (μ), and thermal conductivity (λ) for nitrogen, helium, and hydrogen at 100 bar for different temperatures, data from [276]

Fluid	Property	Unit	Temperature (K)				
			300	350	400	450	500
Nitrogen	c_p	kJ/(kgK)	1.196	1.146	1.12	1.107	1.101
	c_v	kJ/(kgK)	0.766	0.761	0.760	0.763	0.768
	γ	-	1.562	1.506	1.473	1.451	1.433
	ρ	$\mathrm{kg\,m^{-3}}$	111.7	93.72	81.17	71.8	64.49
100 bar	$\mu \times 10^6$	Pa s	20.05	21.89	23.73	25.49	27.18
$M = 28$	λ	W/(mK)	0.0312	0.0336	0.0362	0.0387	0.0414
Helium	c_p	kJ/(kgK)	5.187	5.185	5.185	5.185	5.185
	c_v	kJ/(kgK)	3.133	3.130	3.127	3.125	3.124
	γ	-	1.656	1.657	1.658	1.659	1.660
	ρ	$\mathrm{kg\,m^{-3}}$	15.34	13.24	11.65	10.40	9.387
100 bar	$\mu \times 10^6$	Pa s	20.26	22.44	24.54	26.58	28.56
$M = 4$	λ	W/(mK)	0.1623	0.1794	0.1960	0.2120	0.2276
Hydrogen	c_p	kJ/(kgK)	14.56	14.60	14.60	14.58	14.58
	c_v	kJ/(kgK)	10.29	10.39	10.42	10.43	10.44
	γ	-	1.415	1.405	1.400	1.398	1.396
	ρ	$\mathrm{kg\,m^{-3}}$	7.620	6.573	5.783	5.164	4.666
100 bar	$\mu \times 10^6$	Pa s	9.287	10.28	11.20	12.07	12.88
$M = 2$	λ	W/(mK)	0.1834	0.2077	0.2312	0.2538	0.2754

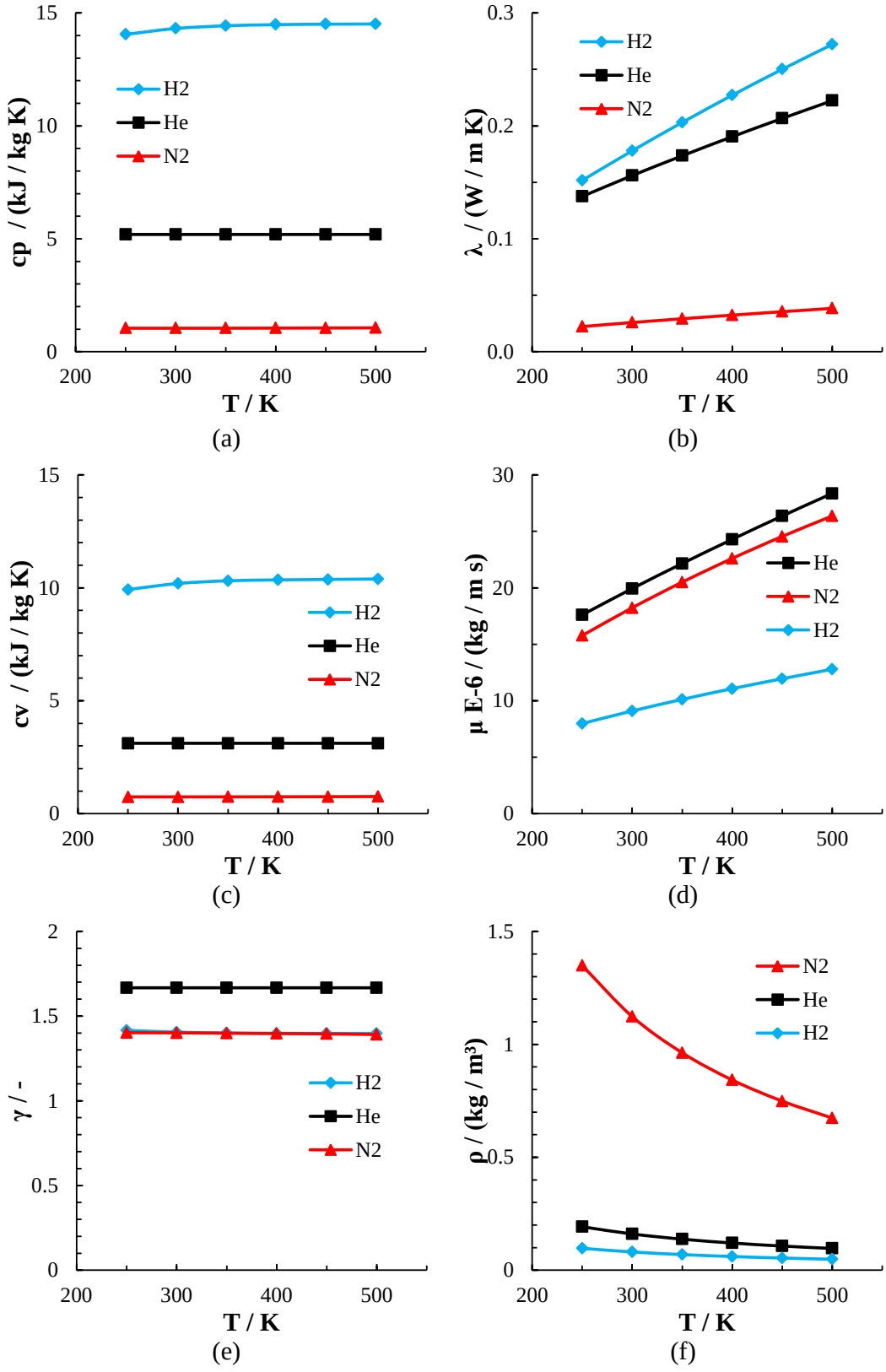

Figure C.1: Fluid properties for hydrogen, helium, nitrogen at 1 bar: (a) specific heat capacity for constant pressure (c_p), (b) thermal conductivity (λ), (c) specific heat capacity constant volume (c_v), (d) viscosity (μ), (e) adiabatic index ($\gamma = c_p/c_v$), and (f) density (ρ), EES fluid property data bases [276]

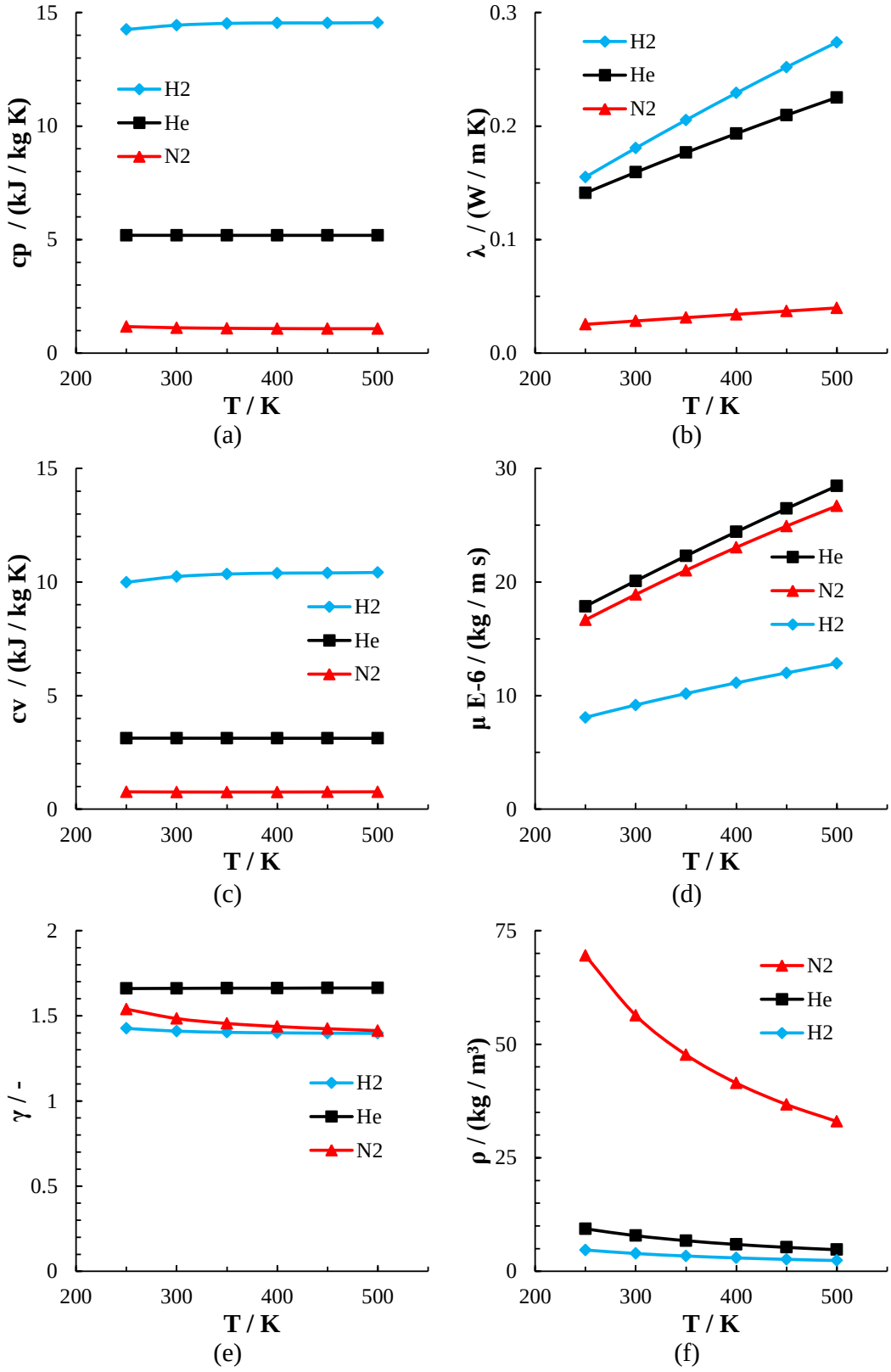

Figure C.2: Fluid properties for hydrogen, helium, nitrogen at 50 bar: (a) specific heat capacity for constant pressure (c_p), (b) thermal conductivity (λ), (c) specific heat capacity constant volume (c_v), (d) viscosity (μ), (e) adiabatic index ($\gamma = c_p/c_v$), and (f) density (ρ), EES fluid property data bases [276]

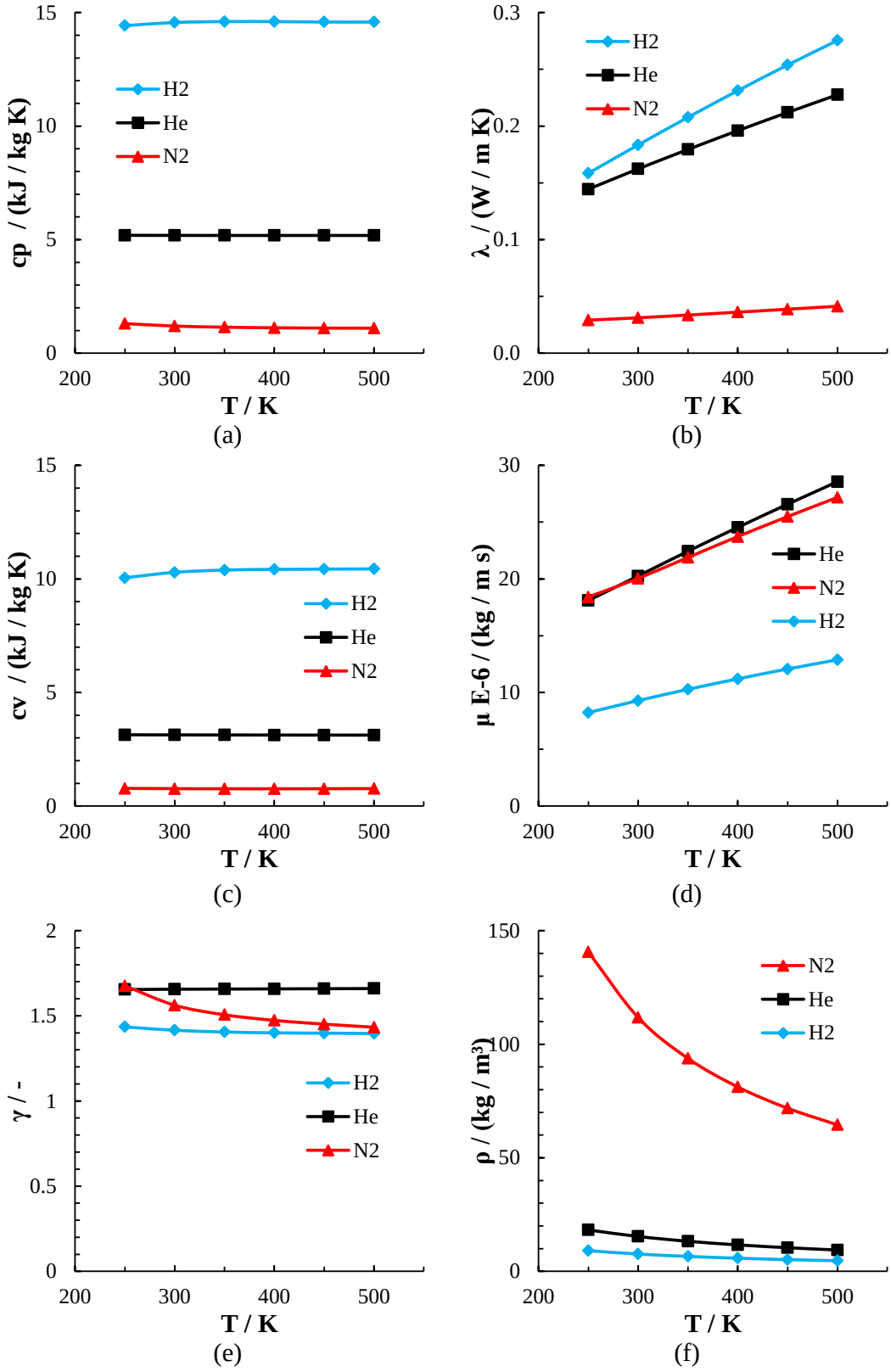

Figure C.3: Fluid properties for hydrogen, helium, nitrogen at 100 bar: (a) specific heat capacity for constant pressure (c_p), (b) thermal conductivity (λ), (c) specific heat capacity constant volume (c_v), (d) viscosity (μ), (e) adiabatic index ($\gamma = c_p/c_v$), and (f) density (ρ), EES fluid property data bases [276]

Appendix D

Data sheets for the case studies

Figure D.1: Data sheet PureCycle 250 kW ORC plants (1/2) [262]

PureCycle® Power System

Energy from a Renewable Resource

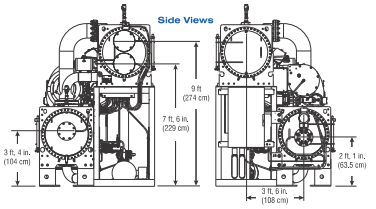

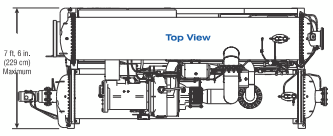

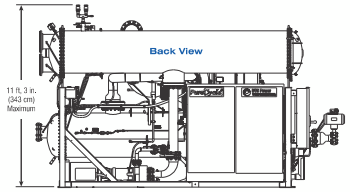

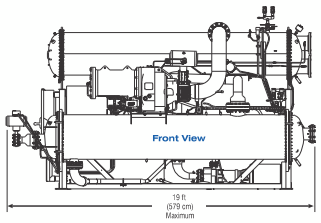

The manufacturer reserves the right to change or modify, without notice, the design or equipment specifications without incurring any obligation either with respect to equipment previously sold or in the process of construction. The manufacturer does not warrant the data on this document. Warranted specifications are documented separately.

The PureCycle® power system solution is built with the proven technology and components of commercial centrifugal chillers, ensuring product quality and reliability. This system operates with a nonflammable working fluid refrigerant called R245fa. The PureCycle® power system provides a low maintenance, cost-effective option that creates revenue, reduces process cost and supports an intelligent energy strategy.

Product Facts

Physical Data

Operating weight	33,300 lbs (15,104 kg)
Shipping weight	27,600 lbs (12,519 kg)
Dimensions (L x W x H)	19' x 7'-6" x 11'-3" (5790 x 2290 x 3430 mm)
Maximum shipping height	10'-3" (3200 mm)

Performance Characteristics

Electric power (gross)	280 kW @ 480V/3-phase/60Hz, 272 kW @ 400V/3-phase/50Hz
Electric power (net)	260 kW @ 60Hz, 252 kW @ 50Hz
Ambient operation	-22 °F to 122 °F (-30° C to 50° C)
Power factor	> 0.95 lagging
Total harmonic distortion	< 5%
Emissions	Zero (closed binary cycle)
Noise	78 dBA at 33 ft (10m)

Design Attributes

Plumbing	ASME B31.1/PED
Turbine	Radial inflow
Generator	Induction
Heat exchangers	ASME Section VIII/PED
Enclosure, electrical	NEMA 4/IP65
Design life	20 years
Lubrication	Integrated internal oil lubrication
UL/CE components	UL 1995, 984 and 1741
Transient voltage/surge suppression at utility interface	IEEE C 62.41-1980 (R1995)
Utility grid-connect protective relaying function	IEEE1547

PS-S0030.05.11

clean energy ahead
TURBODEN
A PRATT & WHITNEY POWER SYSTEMS COMPANY

Turboden
via Cernaia, 10
25124 Brescia, Italy
+39.030.3552.001
Fax: +39.030.3552.011
www.turboden.it

Pratt & Whitney
A United Technologies Company

Pratt & Whitney Power Systems
400 Main Street, M/S 191-13
East Hartford, CT 06108
1-866-769-3725
Outside USA: 1-860-565-0140
www.pw.utc.com

Figure D.2: Data sheet PureCycle 250 kW ORC plants (2/2) [262]

Turboden 200/300 kW Units - Typical Performances

		TURBODEN 2 Dual mode*		TURBODEN 3 Dual mode*		TURBODEN 3 CHP	
THERMAL INPUT		Saturated steam ~16 bar(a)	Saturated steam ~26 bar(a)	Saturated steam ~23 bar(a)	Saturated steam ~30 bar(a)	Thermal Oil	
		Max electric efficiency mode	CHP mode	Max electric efficiency mode	CHP mode	80 °C water output	90 °C water output
Saturated steam / Thermal Oil inlet temperature "HT" Loop (in)	°C	200	226	220	234	310	310
Water condensate / Thermal Oil outlet temperature "HT" Loop (out)	°C	181	209	201	216	221	227
Overall thermal power input	kW	1234	1624	1708	1971	1817	1835
Heat source flow rate**	t/h	2.2	3.1	3.2	3.8	8.4	9.0
Saturated steam / Thermal Oil inlet temperature "HT" Loop (in)	*°F*	*392*	*439*	*428*	*453*	*590*	*590*
Water condensate / Thermal Oil outlet temperature "HT" Loop (out)	*°F*	*358*	*408*	*394*	*421*	*437*	*441*
Overall thermal power input	*MMBtu/hr*	*4.21*	*5.54*	*5.83*	*6.73*	*6.21*	*6.26*
*Heat source flow rate** *	*lb/min*	*81*	*114*	*118*	*140*	*309*	*331*
THERMAL OUTPUT - Hot water							
Hot water temperature (in/out)	°C	35/55	75/95	35/55	55/75	60/80	75/90
Thermal power to the cooling water circuit	kW	1002	1402	1380	1647	1491	1505
Hot water temperature (in/out)	*°F*	*95/131*	*167/203*	*95/131*	*131/167*	*140/176*	*167/194*
Thermal power to the cooling water circuit	*MMBtu/hr*	*3.42*	*4.78*	*4.71*	*5.62*	*5.09*	*5.13*
PERFORMANCES							
Gross active electric power	kW	200	200	300	300	300	300
Captive consumption	kW	12	22	18	26	20	23
Net active electric power	kW	188	178	282	274	280	277
Gross electric efficiency	%	16.2	12.3	17.5	15.5	16.5	16.3
Electric generator		Asynchr.; 400V; 50Hz	Asynchr.; 400V; 50Hz	Asynchr.; 400V; 50Hz	Asynchr.; 400V; 50Hz	Asynchr.; 400V; 50Hz	Asynchr.; 400V; 50Hz
Biomass consumption***	Kg/h	558	735	775	880	825	830
Typical delivery time (EXW)	Months	9	9	9	9	9	9

* Dual mode: the same ORC module (fed with saturated steam) can be operated either in "max electric efficiency" mode or in "CHP" mode.

** In case of thermal oil the flow rate was calculated assuming "Therminol 66" properties.

*** Assuming a low heating value of biomass = 2.6 kWh/kg and a boiler efficiency = 0.85.

DISCLAIMER NOTE: Data provided herein are not binding and might change without prior notice.

Turboden – a Mitsubishi Heavy Industries Company

clean energy ahead

TURBODEN

a group company of MITSUBISHI HEAVY INDUSTRIES, LTD.

Turboden
via Cernaia, 10
25124 Brescia, Italy
Tel. +39.030.3552.001
Fax +39.030.3552.011
www.turboden.it

12-COM.B-6-rev.2
(August 2013)

Figure D.3: Data sheet Turboden 200 and 300 kW ORC plants [277]